UCLA
UCLA Electronic Theses and Dissertations

Title
Graphene Supercapacitors: Charging Up the Future

Permalink
https://escholarship.org/uc/item/8xv3c4p1

Author
El-Kady, Maher

Publication Date
2013

Peer reviewed|Thesis/dissertation

UNIVERSITY OF CALIFORNIA

Los Angeles

Graphene Supercapacitors: Charging Up the Future

A dissertation submitted in partial satisfaction of the requirements for the degree

Doctor of Philosophy in Chemistry

by

Maher El-Kady

2013

ABSTRACT OF THE DISSERTATION

Graphene Supercapacitors: Charging Up the Future

by

Maher El-Kady

Doctor of Philosophy in Chemistry

University of California, Los Angeles, 2013

Professor Richard B. Kaner, Chair

Batteries run just about everything portable in our lives such as smartphones, tablets, computers, etc. While we have become accustomed to the rapid improvement of portable electronics, the slow development of batteries is holding back technological progress. Thus, it is imperative to develop a new energy storage technology providing devices that are compact, reliable, and energy dense, charge quickly, and possess both long cycle life and calendar life. Using a consumer grade LightScribe DVD burner, we have developed graphene supercapacitors with high charge storage capacity while providing 20 times more power than supercapacitors currently available. Interestingly, this direct writing technique offers a way to pattern graphene precisely without using masks or cleanroom operations, thus giving the flexibility to produce supercapacitors in various sizes and architectures at low cost. The miniaturization of the electrodes to the microscale results in enhanced charge storage capacity and rate capability. In addition, by combining graphene with conducting polymers and metal oxides, this work demonstrates pseudo-capacitors and hybrid supercapacitors with enhanced charge storage capacities that rival those of thin film batteries, while they can be recharged in less than a

second. Great efforts are currently in progress between UCLA and Maxwell Technologies to move this technology from the laboratory to the industrial scale. In addition, this work describes several other applications that take advantage of the fascinating properties of graphene including lithium ion batteries and micro-batteries, sensors and catalysis.

The dissertation of Maher El-Kady is approved

Xiangfeng Duan

Paul S. Weiss

Yang Yang

Richard B. Kaner, Committee Chair

University of California, Los Angeles

2013

I dedicate this thesis to

all my family members

for their constant support and unconditional love.

I love you all!

Table of Contents

List of Figures

CHAPTER 3: LASER SCRIBING OF HIGH-PERFORMANCE AND FLEXIBLE GRAPHENE-BASED ELECTROCHEMICAL CAPACITORS

CHAPTER 4: SCALABLE FABRICATION OF HIGH-POWER GRAPHENE MICRO-SUPERCAPACTIORS FOR FLEXIBLE AND ON-CHIP ENERGY STORAGE

CHAPTER 5: RATIONAL DESIGN AND ENGINEERING OF THREE-DIMENTIONAL GRAPHENE/MnO$_2$ ELECTRODES FOR HIGH-PERFORMANCE HYBRID SUPERCAPACITORS AND MICRO-SUPERCAPACITORS

CHAPTER 6: LARGE SCALE FABRICATION OF POLYANILINE AND GRAPHENE/POLYANILINE MICRO-SUPERCAPACITORS USING LIGHTSCRIBE DVD BURNER

CHAPTER 7: SCALING UP PRODUCTION OF GRAPHENE SUPERCAPACITORS

CHAPTER 8: CONCLUSIONS AND FUTURE WORK

List of Tables

ACKNOWLEDGMENTS

The completion of my dissertation and graduate school has been a long journey. What I find most interesting about graduate school is the pleasure of finding things out. So, I wanted to share the story behind this work which I find interesting. I received Bachelor and Masters' degrees from Cairo University where my general research interests were electrochemistry, sensors, nanoscience and more importantly materials. Materials have enabled the advancement of mankind from its earliest beginning such that pre-historic ages have been classified based on the most common material of the time: Stone, Bronze and Iron Ages, Plastic and finally Silicon. I spent the first year of graduate school at UCLA reading about research trends in materials and their chemistry. I became most interested in graphene and its fascinating properties and quickly realized it is the golden material of our time. Out of the many applications for graphene, supercapacitors captured my interest only a year after the publication of the first paper in the field. The present research started with an interesting experiment that I asked my advisor to witness. I just took an LED and turned it on with a graphene supercapacitor that was pre-charged for a second. The amazing thing is that it does not stop working even after several minutes! This work was the result of many experiences I have encountered at UCLA from dozens of remarkable individuals who I also wish to acknowledge.

First I wish to thank my advisor, Professor **Richard Kaner**, Distinguished Professor of Chemistry and Distinguished Professor of Materials Science and Engineering at UCLA, for his valuable guidance throughout this research. Ric has been a great support from the first day I began working in his lab. He has always made himself available whenever I needed his help despite his busy schedule. Ric has also provided insightful discussions about my research and has given me the freedom to pursue various projects I like. There is something very special about

Ric, he is open to new ideas! I remember when I first came to the lab, I was supposed to work on conducting polymers, but it was graphene that attracted me most. I thought he will refuse my research ideas on graphene, but he did not, this was a surprise to me. It was very challenging, though, because this is the first research project on supercapacitors in the Kaner Lab. Ric is also very enthusiastic about the materials that make up our world. He has the biggest collection of materials I have ever seen. He always brings them to his classes which make his way of teaching more engaging and enjoyable than most chemistry classes at UCLA. This approach inspired me in my research about supercapacitors; I have tested a great collection of supercapacitors available from most suppliers. This helped me figure out what the real problems that must be solved to enable a new competitive technology. Thank you Ric, for all your help and support! I appreciate all your contributions of time and ideas to make this work possible.

I have to also thank **Ed Johansen** who organized a videoconference between UCLA and Cairo University a few years ago. It is because of this meeting that I got to meet Ric for the first time. I am also grateful to my former research advisor at Cairo University, Professor **Ahmed Galal**.

I must also thank the members of my PhD committee, Professors **Xiangfeng Duan**, **Paul S. Weiss** and **Yang Yang** for their helpful career advice and suggestions they made during my oral exam. Each is an authority in their field; I would like to tell them I admire their research and wish that I could work with all of them!

I am also very grateful to **Veronica Strong** for her scientific advice and many insightful discussions and suggestions. Veronica is a great mentor and is my primary resource for getting my science questions answered especially when I started working on graphene and polyaniline. She taught me various laboratory techniques in the Kaner lab. We worked together on

developing a process for producing graphene using a simple LightScribe DVD burner that is widely used by computer enthusiasts worldwide. I remember the moment when I showed her the first supercapacitor I made out of laser scribed graphene. She was very excited and enthusiastic! Our efforts finally paid off. Veronica—this work would not have been possible without your help, thanks! I wish you great success with your job at Intel.

After the publication of the first results on graphene supercapacitors, we received several offers to scale up this technology. The most promising offer came from Maxwell Technologies, the leading supplier of supercapacitors worldwide. A research team from UCLA has now been working with Maxwell engineers for the past year to achieve their target. Here, I have had the pleasure to work with a team of brilliant people. Special thanks to my friend and colleague **Lisa Wang** who has provided great support to this project. To achieve the target, Lisa and I have been working together on designing and performing experiments to keep up the progress to meet the stringent deadlines. As part of the contract between UCLA and Maxwell Technologies, a teleconference is made every two weeks to discuss updates. Before most of the teleconferences, we used to stay at school until almost midnight to achieve the project goals on time. I believe we have made great progress together and I am pretty certain this is going to pay off at the end of the day. Lisa—I am looking forward to the day when we see our graphene supercapacitors being fitted in the next generation smartphones. That would be an epic moment!

Driven by our interest to speed up the progress of the scale-up project, we asked for more help from **JeeYoun Hwang**. She joined our group two years ago as an undergraduate researcher in our lab and I had the pleasure to be her mentor. Now, she is starting her second year in graduate school after achieving exceptional grades in classes. Jee has been a great help making and testing new cells. She is highly responsible and cooperative with analyzing data. She was also involved

I am also grateful to **Mengping (Tale) Lee** who also added to my work. Coming from Fudan University of China on the UCLA-CSST program, I can always see the smile on her face that gives me the impression that everything is ok. I am surprised by her scientific background, simply, terrific! Tale just came back to UCLA for graduate school. Tale—I am sure you will do great job in the graduate school and am expecting you to set a good example for international students.

I am thankful to my colleagues and friends, **Yue (Jessica) Wang** and **Julio D'Arcy**. It was a pleasure to collaborate with them on various research projects in the Kaner Lab. Jessica & Julio—I admire your research capabilities, learned a lot by working with you. I wish the best of luck to both of you on your postgraduate studies at Stanford and MIT and looking forward to collaborating with you again in the future.

There were many people who gave interesting feedback & valuable suggestions, for which I would like to thank them: Prof. **Bruce Dunn**, **Daniel Membreno** and **Veronica Augustyn** for their help with impedance measurements and for their advice on setting up our new VMP3 multichannel potentiostat; and Prof. **George Gruner** for valuable discussions and suggestions.

I must thank Professors **Mostafa El-Sayed** and **Herbert Kaesz**, who set very good examples for me as Egyptian scholars in this department. I met Mostafa at the beginning of my graduate studies at UCLA on a very special occasion; he was the recipient of the Seaborg Medal in 2009 from the UCLA Department of Chemistry & Biochemistry. He encouraged me and shared his experiences. I also admired Herb's research and his interesting discussions during the weekly inorganic seminars. He constantly showed up to these seminars until he left us last year.

I also feel very lucky to have many good friends around. Special thanks to my friend **Thomas (Tom) Farrell**, who was always a great support to all my struggles and frustrations in my new life and studies in this country. He helped me get through the cultural differences I had as an international student. Tom, like his late father, thinks like a philosopher so I like to discuss my research with him to help me focus my ideas. Tom—cheers for being a great reliable person to whom I could always talk about my problems and excitement.

I thank all the Kaner Lab members who made the lab a friendly environment for working.

Finally, I feel very grateful to my parents who have sacrificed their lives for me, my brothers and sisters and provided unconditional love and care. I love them so much, and I would not have made it this far without them. I deeply miss my father who is not here to share this moment. He encouraged me at every stage of my personal and academic life, and longed to see this achievement come true. Dad—thank you for always supporting and believing in me!

VITA

2000-2004   Bachelor of Science, Chemistry Major
              Cairo University, Egypt
              Ranking as the top student of the 2004 chemistry graduates.

2003   Distinguished Chemistry Student Award
              Department of Chemistry, Cairo University

2004   Distinguished Chemistry Student Award
              Department of Chemistry, Cairo University

2005   The highest honor for a chemistry graduate from the Faculty of Science,
              Cairo University with six distinguished student awards in various fields.

2005   Shield of the Egyptian Syndicate of Scientific Professions

2005-2008   Lecturer of Chemistry at Cairo University

2007-2008   The award of distinguished teaching for the academic years 2007 and 2008
              Department of Chemistry, Cairo University

2005-2008   Master of Science in Physical Chemistry
              Cairo University, Egypt

2008   Full Ph.D. fellowship from the Egyptian Ministry of Higher Education,
              General Missions Program.

2009   The Best M.S. Thesis Award from the Faculty of Science Cairo University.
              The Faculty of Science at Cairo University includes 10 departments: the
              Departments of Chemistry, Physics, Mathematics, Zoology, Botany,
              Entomology, Astronomy and Meteorology, Biophysics, Geophysics and
              Geology.

2009   Invited by the Lindau Nobel Laureates Meeting Council (after passing its
              selection criteria) to participate as a young researcher in the 59th Lindau
              Nobel Laureates Meeting dedicated to chemistry, Lindau, Germany.

2009	Featured in a short movie (Nanotechnology: Use and misuse) with the 1996 chemistry Nobel laureate Prof. Sir Harold Kroto in a series of films by the Nature Publishing Group in Lindau Nobel Laureates Meeting. Available online at nature.com: http://www.nature.com/video/lindau2009/index.html
2009	Was invited by the **DFG** (German Research Foundation) to visit various research institutions in Germany. The program consisted of visits to institutions in Munich, Berlin, Frankfurt and Bonn. July, 4-10, 2009.
2009-2010	Teaching Assistant University of California, Los Angeles Los Angeles, CA
2009-present	Research Assistant University of California, Los Angeles Los Angeles, CA
2012	A recipient (among others) of the 2012 **Award for Excellence in Research** from the Ministry of Higher Education of Egypt, Program of Continuous and Qualifying for Accreditation in HEI.
2012	**Cairo University Presidential Award for Excellence in Research.** The award was presented by Prof. Gamal Esmat, Vice President of Cairo University for Graduate Studies and Research Affairs, in a ceremony held at the UCLA Faculty Center in May 2012 and in the presence of a delegate from the Egyptian Embassy in Washington, Joseph Rudnick, Dean of the UCLA School of Letters and Sciences.
2012	One of two recipients of the 2012 Herbert Newby McCoy Award from UCLA Department of Chemistry & Biochemistry "for the student or faculty member in the Chemistry Department of the University of California at Los Angeles making the greatest contribution of the year to the science of chemistry"
2013	Featured with Prof. Richard B. Kaner in a three-minute movie entitled "the Super Supercapacitor" for the Sun Dance film festival by the videographer Brian Davis on ideas that could change the world. This video has gone "viral" receiving over 2 million views since it was posted on the internet earlier this year

PUBLICATIONS

Publications, Peer-reviewed Journals:

- Maher F. El-Kady and Richard B. Kaner "Graphene Supercapacitors", *Nano Today* (**Invited Review**), in preparation (2013).

- Maher F. El-Kady, Veronica A. Strong, Richard B. Kaner "Graphene Supercapacitors: Charging up the future", *Energy & Environmental Science* (**Invited Review**), in preparation (2013).

- Maher F. El-Kady, Richard B. Kaner "Teeny-Tiny, But Super, Capacitors", *IEEE Spectrum* (**Invited Feature Article**), in preparation (2013).

- Maher F. El-Kady, Richard B. Kaner *et al.* "Large Scale Fabrication of Polyaniline and Graphene/Polyaniline Supercapacitors and Micro-Supercapacitors Using a LightScribe DVD burner", In preparation (2013).

- Maher F. El-Kady, Richard B. Kaner *et al.* "Rational Design and Engineering of Three-Dimensional Hybrid Supercapacitors and Micro-Supercapacitor Based on Graphene and Nanostructured Metal Oxide Frameworks", In preparation (2013).

- Julio M. D'Arcy, Maher F. El-Kady, Paula T. Hammond and Richard B. Kaner "Evaporative Vapor Phase Polymerization of High Aspect Ratio Nanofibrilar Poly(3,4-Ethylenedioxythiophene) for Symmetric Supercapacitors", submitted (2013).

- Maher F. El-Kady, Richard B. Kaner "Scalable Fabrication of High Power Graphene Micro-Supercapacitors for Flexible and On-Chip Energy Storage", *Nature Communications*, 4:1475, DOI: 10.1038/ncomms2446 (2013). Highlighted as the Feature/Cover Article. The work also attracted significant attention on various web news outlets and radio stations. It was highlighted in US Today, National Geographic and around the internet.

- Maher F. El-Kady, Veronica Strong, Sergey Dubin, Richard B. Kaner "Direct Laser Scribing of High-Performance and Flexible Graphene-Based Electrochemical Capacitors", *Science* 335, 1326-1330 (2012). This work attracted significant attention and was **highlighted** in AAAS news, a perspective in *Science*, Scientific American, National Geographic, US Today, Optics Society of America, Nature Middle East, MIT technology review, Chemistry World (Royal Society of Chemistry), Chemistry Views (Wiley-VCH), Materials Today, Nano Energy (Elsevier). It was also highlighted around the internet.

- Veronica Strong, Sergey Dubin, Maher F. El-Kady, Andrew Lech, Bruce H. Weiller, Richard B. Kaner "Pattering and Electronic Tuning of Laser Scribed Graphene for Flexible All-Carbon Devices, *ACS Nano* 6, 1395-1403 (2012).

- Giacomo Mariani, Yue Wang, Ping-Show Wong, Andrew Lech, Chung-Hong Hung, Joshua Shapiro, Sergey Prikhodko, Maher El-Kady, Richard B. Kaner and Diana L. Huffaker "Three-Dimensional Core-Shell Hybrid Solar Cells via Controlled in Situ Materials Engineering" *Nano Letters* 12, 3581-3586 (2012).

- Nada F. Atta and Maher F. El-Kady "Novel poly(3-methythiophene)/Pd, Pt nanoparticles sensor: Synthesis, Characterization and its application to the simultaneous analysis of dopamine and ascorbic acid in biological fluids", *Sensors and Actuators B:Chemical 145, 2010, 299-310.*

- Nada F. Atta, Maher F. El-Kady and Ahmed Galal "Simultaneous determination of catecholamine neurotransmitters, uric acid and ascorbic acid at physiological levels using poly(N-methylpyrrole)/Pd nanoclusters sensor", *Analytical Biochemistry 400, 2010, 78-88.*

- Nada F. Atta, Maher F. El-Kady, Ahmed Galal, "Palladium nanoclusters coated polyfuran as a novel sensor for catecholamine neurotransmitters and paracetamol", *Sensors and Actuators B: Chemical*, 141 (2), 2009, 566-574.

- Nada F. Atta, Maher F. El-Kady, "Poly(3-methylthiophene)/ Palladium sub-micro modified sensor electrode, Part II: Voltammetric and EIS studies, and analysis of catecholamine neurotransmitters, ascorbic acid and acetaminophen, *Talanta*, 79 (3), 2009, 639-647.

Publications, Book Chapters:

- Nada F. Atta, Ahmed Galal and Maher F. El-Kady "Chemical Sensors and Biosensors based on conducting polymer thin films", a book chapter in an edited book "Polymer Films: Properties, Performance and Applications" by NOVA publishers, New York, USA. Click here for a link to the book at the Publisher Webpage.

Presentations:

- Maher El-Kady, Veronica Strong, Sergey Dubin and Richard Kaner "Graphene Supercapacitors and Micro-Supercapacitors for Flexible and On-Chip Energy Storage with Ultrahigh Power" Materials Research Society Meeting, San Francisco, California, April 2013 (**Oral Presentation**).

- <u>Maher El-Kady</u> and Richard Kaner "The Promise of Laser Scribed Graphene Supercapacitors" to be presented at the Annual CAFE Electric Aircraft Symposium (EAS VII), Santa Rosa, California, April 2013 (**Oral Presentation**).

- <u>Maher El-Kady</u>, Veronica Strong, Sergey Dubin, Jonathan Wassei, Jaime Torres and Richard B. Kaner "Synthesis and Patterning of Laser Converted Graphene for Flexible Energy Storage Devices" 221st Electrochemical Society Meeting, Seattle, Washington May 2012 (**Oral Presentation**).

- <u>Maher El-Kady</u>, Veronica Strong, Sergey Dubin, and Richard B. Kaner "Laser Printing of Flexible Graphene-Based Supercapacitors with Ultrahigh Power and Energy Densities" 243th ACS meeting, San Diego, California, March 2012 (**Poster Presentation**).

Patents Pending:

- "Capacitor with electrodes made of an interconnected corrugated carbon-based network", United States Patent Application PCT/US13/29022, Filed March 5, 2013. Applicant: the Regents of the University of California. Inventors: Maher F. El-Kady, Veronica A. Strong, Richard B. Kaner.

- "Interconnected corrugated carbon-based network", United States Patent Application PCT/US12/71407, Filed December 21, 2012. Applicant: the Regents of the University of California. Inventors: Veronica A. Strong, Maher F. El-Kady, Richard B. Kaner.

CHAPTER 1

Overview, Motivation and Scope of The Dissertation

1.1 THESIS OVERVIEW

Every day we use batteries and supercapacitors to run our portable electronics that keeps us away from the electrical grid. They are also essential for renewable energy production from sun and wind as well as the development of electric vehicles and hybrid electric vehicles (1). Thus, it is fair to say that batteries and supercapacitors have become the lifeblood of our society. Any incremental improvement in performance enhances freedom and mobility (2). Supercapacitors are experiencing increasingly broader use, both replacing batteries in some cases, and in others complementing their performance. In a few situations supercapacitors have been an enabling technology (3). A recent report by the US Department of Energy assigns equal importance to supercapacitors and batteries for future energy storage systems (4). Moreover, articles on supercapacitors appearing in business and popular magazines show increasing interest by the general public in this topic (5-7).

Basically, almost everywhere you see next generation electronic and power technology you see supercapacitors being fitted or planned because of superior performance, cost-over-life and fit-and-forget (8). The number of developers and manufacturers of supercapacitors is rising rapidly, having doubled from 40 to 80 in just the last few years (9). The average market growth rate of supercapacitors over the past decade is 25% and most analysts predict continued rapid growth over the next 10 years (10). Since supercapacitors are used for an increasing number of

purposes in electric vehicles, mobile phones, energy harvesting, renewable energy and other products of the future, this market has considerable upside potential, Figure 1.1 (8).
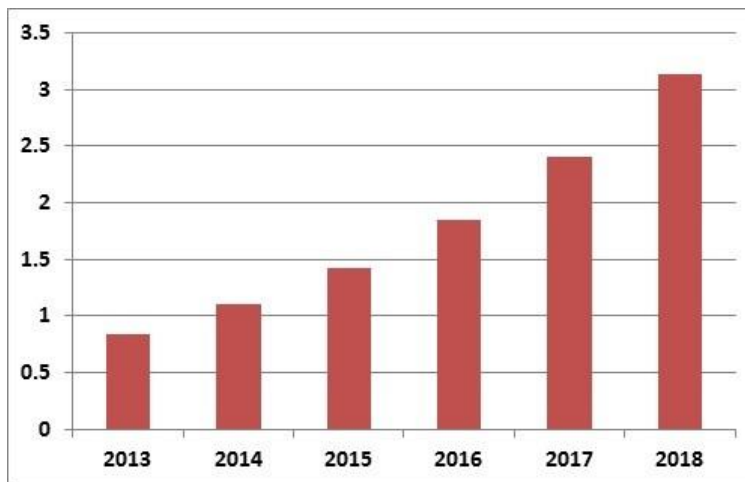
Figure 1.1: Global supercapacitor market ($ billions). Source: IDTechEx research report "Electrochemical Double Layer Capacitors: Supercapacitors 2013-2023" www.IDTechEx.com/EDLC

However, we need to improve their performance substantially to meet the higher requirements of future systems by developing new materials and advancing our understanding of the electrochemical interfaces at the nanoscale (5). Specifically, supercapacitors that store higher amounts of charge, while also being capable of rapid charging and discharging are needed. Over the past few years, researchers at several companies and institutions around the world have been racing to achieve this target.

In an attempt to improve the performance of supercapacitors, the present study investigates a large number of alternative electrode materials including graphene, conducting polymers and metal oxides and their hybrids. Graphene—a one atom thick layer of graphitic carbon—has garnered attention recently because of its interesting electrical conductivity and surface area. Graphene can offer a surface area of up to 2630 m^2/g; a single sheet of this material

sufficient in size to cover an entire football field, would weigh about one-quarter of a gram. This surface area is large enough to store massive amounts of charge to bridge the gap between the current supercapacitors and high energy density batteries, while at the same time being able to be charged very quickly. Until recently, though, graphene-based supercapacitors have been expensive to produce, and their energy densities have fallen far below of what's theoretically possible (11).

To solve these problems, we used a consumer grade LightScribe DVD burner to produce graphene electrodes (LSG) on a large scale and at low cost. These graphene electrodes have interesting surface areas, and electrical and mechanical properties that can be used for making supercapacitors with high charge storage capacity that are 20 times more powerful than those available in the market. These supercapacitors can be integrated directly on-chip to provide power for next generation electronics. Furthermore, LSG electrodes with their high electrical conductivity and porous structure, serve as excellent scaffolds for nanostructured pseudo-capacitive materials such as conducting polymers and metal oxides. The unique structure of these hybrid electrodes is shown to achieve considerably higher charge storage capacity than pure graphene. Throughout this work, we have developed new device architectures and solid-state electrolytes that can be considered a leap ahead of current state-of-the-art supercapacitors. The energy density and power density of our graphene-based supercapacitors are superior to those of commercially available carbon-based supercapacitors, pseudo-capacitors and hybrid supercapacitors. Considering the simplicity of the device architecture and scalability of the process, these graphene-based supercapacitors hold promise for commercial applications.

1.2 MOTIVATION AND OBJECTIVES

The main objective of this study is to develop new materials, electrolytes and device architectures that enable supercapacitors with improved performance compared to current technology. Specifically, there is a need for designing supercapacitors with increased energy density and power density to meet growing demands of power-hungry gadgets and to find new markets for supercapacitors. The new supercapacitors should be manufactured using scalable techniques and the materials should be of low cost. Once successful, a working program will be developed to move this technology from the laboratory to the industrial scale.

The size of the supercapacitor is another important factor that defines its end use. Supercapacitors miniaturized to the microscale—known as micro-supercapacitors—have recently garnered attention due to the current miniaturization trend with portable electronics. The interest in smaller electronics has spurred the miniaturization of different technologies; however, the lack of a battery or a supercapacitor with the appropriate size often limits the miniaturization of the entire system. Although critical improvements have been achieved over the past few years, the progress is marginal compared with the vast advancements in microelectronics (2). Hence, it is highly desirable to develop a reliable technique for the scalable fabrication of micro-supercapacitors. This technique should be compatible with current manufacturing protocols used for electronic devices.

To achieve these goals, the supercapacitors developed should meet the following requirements that are also summarized in Figure 1.2:

1. Capacitance: While existing double layer supercapacitors can charge and discharge much faster than batteries, their low energy density have limited their wide adoption in various

markets. Since the energy density is proportional to the capacitance and the voltage squared, strategies aimed at improving both of them are of particular importance (12). Various research efforts are focused on designing new materials to increase the capacitance of the electrodes. Activated carbons are widely used, but their low specific capacitance has limited the energy density of state-of-the-art commercially available supercapacitors. This has inspired us to explore alternative electrode materials. Graphene, conducting polymers and metal oxides and their hybrids are particularly interesting because of their high electronic conductivity, large surface area and high theoretical specific capacitance.

2. Voltage: The majority of supercapacitors currently available in the market are symmetric double layer capacitors (EDLC) featuring activated carbon and an organic electrolyte that provides a cell voltage as high as 2.7 V. Because the energy density is proportional to the voltage squared ($E = \frac{1}{2} CV^2$), large efforts of the current study have been directed at the design of highly conducting, stable electrolytes with a wider voltage window. Ionic liquids are particularly interesting because of their wide electrochemical stability window which can be as large as 6.0 V (13). Another research direction of this dissertation involves the design of asymmetric supercapacitors combining different positive and negative electrodes. The difference in the chemical potential between both electrodes results in a higher operating voltage window (14,15).

3. Power: High power density is the major advantage that supercapacitors offer compared to batteries. The electrodes developed in this study were specially designed to satisfy the critical features for high power: high surface area, high electronic conductivity, large and interconnected pores, facilitated electron and ion transport.

4. Safety: There are growing environmental concerns about the disposal of current batteries containing toxic and flammable materials. Hence, there is an urgent need for the development of new electrodes and electrolytes that are safe and non-flammable. In this study, environmentally friendly electrode materials—carbon-based—were developed. Improved organic electrolytes such as ionic liquids are widely researched nowadays because of their high thermal stability. Ultimately, neutral aqueous-based electrolytes would be the best solution for environmentally benign supercapacitors. These systems are likely to gain market share because they have improved safety and often improved performance in certain aspects as well.

5. Scalable: Commercially viable devices should be produced through inexpensive and scalable techniques. Cost-to-benefit ratio is the main factor in the energy storage industry. For example, although RuO_2 based supercapacitors demonstrate high specific capacitance, their ultrahigh cost limits their use to military and space applications (16). In this dissertation, huge efforts have been devoted to the development of graphene electrodes that only need an inexpensive infrared laser and graphite oxide precursor which is already produced at the ton scale at low cost (17).

6. Flexibility: Flexible energy storage devices have received great interest in many emerging multifunctional gadgets, such as electronic paper, collapsible displays and other personal multimedia devices (18). This study has aimed to design flexible electrodes with stable electrical and electrochemical response under different bending and twisting conditions.

7. All-solid-state: Electrolytes are essential components for supercapacitors and batteries. For safety considerations, a solid-state electrolyte is superior to its liquid counterpart since robust encapsulation is needed to prevent leakage of a liquid electrolyte. This inspired us to develop

simplified and low-cost methods to fabricate solid-state supercapacitors that are highly desirable for portable electronics.

8. Size: It is highly desirable to develop new techniques for the fabrication of not only regular size supercapacitors, but also micro-supercapacitors. To meet the growing demands of smaller portable electronics, numerous efforts in the current study have been devoted at developing micro-supercapacitors using simple and scalable techniques.

9. On-Chip integration: Current trends for developing miniaturized electronic devices place emphasis on achieving performance levels generally associated with integrated circuits. The developed techniques should, thus, be compatible with current manufacturing protocols for electronic devices.
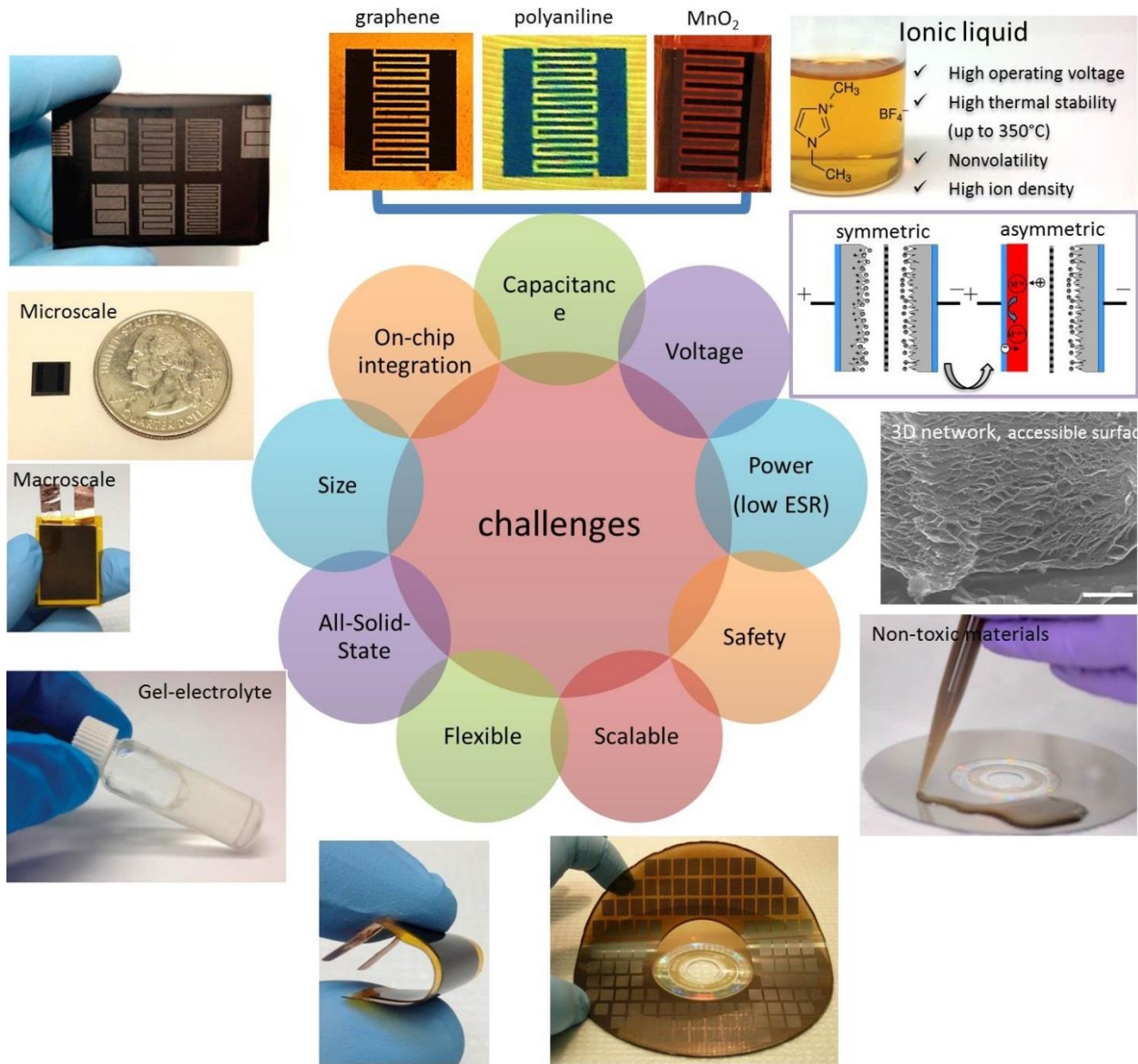
Figure 1.2: Challenges for the next generation of supercapacitors.

1.3 SCOPE OF THE DISSERTATION

First, it is necessary to understand the background and applications of supercapacitors. This is the subject of the second chapter of this dissertation. Why are supercapacitors important? What should then be done so the supercapacitor market will continue to grow in the future?

The major objective of this dissertation is to develop high-performance supercapacitors for a variety of applications. To achieve this target, three approaches have been proposed. This includes the design and fabrication of supercapacitors with (i) high power density, (ii) high energy density and (iii) hybrid systems. Here, the supercapacitors are designed for macro-scale energy storage and as a micro-power source for the growing industry of miniaturized electronics.

Once the properties of supercapacitors are presented, in the second part of the dissertation I discuss the research achievements of this work. In Chapter 3, I describe the development of flexible and lightweight graphene supercapacitors by the direct laser reduction of graphite oxide films using a consumer grade DVD burner. Unlike commercial supercapacitors, our devices show ultrahigh energy density approaching those of batteries, but still maintain the high power density and excellent cycle stability of supercapacitors. Interestingly, we have demonstrated flexible and all-solid-state supercapacitors whose performance is unaffected by extreme bending conditions which holds great promise as an energy storage system for flexible electronics.

While the demand for ever-smaller electronic devices has spurred the miniaturization of a variety of technologies, one area has lagged behind in this downsizing revolution: energy-storage units, such as batteries and capacitors. Here, we made smaller versions of graphene supercapacitors, called micro-supercapacitors, which is the focus of Chapter 4. Unlike the previous methods reported in the literature, this technique potentially scales up the production of

micro-supercapacitors to industrial levels, which could lay the foundation for new micro-power sources for miniaturized flexible and portable electronics.

Chapter 5 is devoted to the rational design of hybrid supercapacitors using three-dimensional electrodes based on graphene and metal oxides. These hybrid systems achieve extremely high energy density values exceeding those of commercial available electric double layer capacitors, pseudo-capacitors and hybrid supercapacitors, while providing one order of magnitude higher power density.

Since the specific capacitance of the conducting polymer polyaniline is generally higher than graphene, it is more suitable when high energy density in a limited space is required. This is the core idea of Chapter 6 of this dissertation. We demonstrate for the first time a simple, yet versatile technique for the direct fabrication of high-performance polyaniline micro-pseudo-capacitors with ultrahigh area-normalized capacitance. Furthermore, by combining graphene with nanostructured polyaniline to produce hybrid supercapacitors, the areal energy density and power density is further enhanced.

Turning the graphene supercapacitor work into a viable commercial product could make people's lives better. Here, I will discuss the efforts we have made to move this technology from the laboratory to the industrial level in Chapter 7.

The last chapter of this dissertation is devoted to conclusions and future work. In this final chapter, I will conclude by describing the progress made towards the goal of achieving high-performance supercapacitors for a variety of applications. The research presented in this thesis appears to have raised more questions than it has answered. Therefore, I will suggest some

future research directions that could provide the next steps on the way to practical energy storage devices.
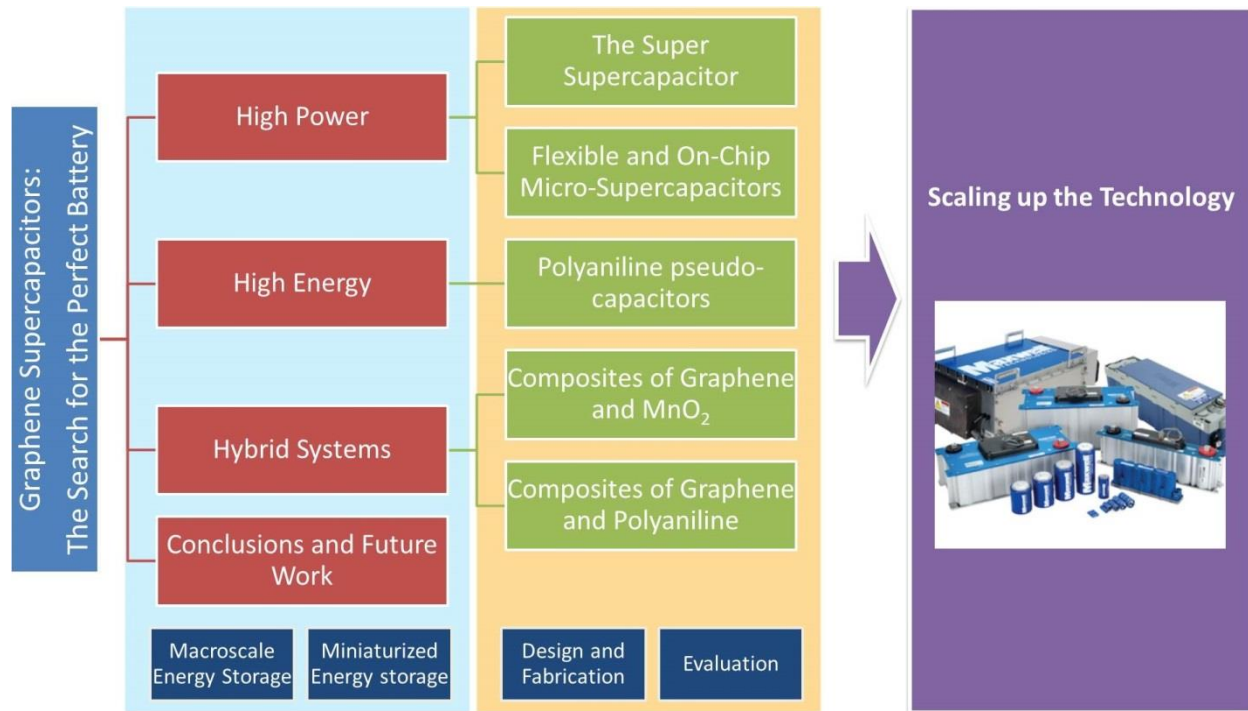
Figure 1.3: Flowchart showing the research plan of the dissertation.

BIBLIOGRPAHY

[1] Yang, Z.; Zhang, J.; Kintner-Meyer, M. C. W.; Lu, X.; Choi, D.; Lemmon, J. P.; Liu, J. Chem. Rev. 2011, 111 (5), 3577–3613.

[2] Isidor Buchmann, Batteries in a Potable World, A Handbook on Rechargeable Batteries for Non-engineers, Cadex Electronics Inc., 3rd edition, 2011.

[3] John R. Miller and Andrew F. Burke, The Electrochemical Society Interface, Spring 2008, 53-57.

[4] US Department of Energy. *Basic Research Needs for Electrical Energy Storage* <www.sc.doe.gov/bes/reports/abstracts.html#EES2007> (2007)

[5] Simon, P.; Gogotsi, Y. Nat. Mater. 2008, 7, 845.

[6] David LaGesse, Supercapacitors Amp Up as an Alternative to Batteries, National Geographic, August 20, 2013.
http://news.nationalgeographic.com/news/energy/2013/08/130821-supercapacitors/

[7] Tyler Wells Lynch, Reviewed.com: In search of a better battery, USA TODAY July 17, 2013.

http://www.usatoday.com/story/tech/2013/07/17/reviewed-better-battery-column/2509507/

[8] Dr Peter Harrop and Dr Victor Zhitomirsky, Electrochemical Double Layer Capacitors: Supercapacitors 2013-2023, Business Report IDTechEx, July 2013.
http://www.idtechex.com/research/reports/electrochemical-double-layer-capacitors-supercapacitors-2013-2023-000318.asp

[9] http://www.idtechex.com/research/articles/change-of-leadership-of-the-global-market-value-of-supercapacitors-00005344.asp

[10] http://www.nesscap.com/images/news/Nesscapcatalogue_2012.pdf

[11] Yi Huang, Jiajie Liang , and Yongsheng Chen, *Small* 8, 1805–1834 (2012).

[12] Katsuhiko Naoi and Patrice Simon, The Electrochemical Society Interface, pp 34-37, Spring 2008.

[13] J. F. Wishart, Energy Environ. Sci. 2, 956-961 (2009).

[14] Katsuhiko Naoi, Syuichi Ishimoto, Jun-ichi Miyamoto and Wako Naoi , Energy Environ. Sci., 2012, 5, 9363–9373.

[15] Jeffrey W. Long , Daniel Bélanger , Thierry Brousse , Wataru Sugimoto , Megan B. Sassin , and Olivier Crosnier, MRS Bulletin 36, 513-522 (2011).

[16] Andrew Burke, Journal of Power Sources 91, 37–50 (2000).

[17] M. Segal, Selling graphene by the ton. *Nature Nanotechnology* 4, 612 (2009).

[18] Leif Nyholm, Gustav Nyström, Albert Mihranyan, and Maria Strømme. *Adv. Mater.* 23, 3751–3769 (2011).

CHAPTER 2

Introduction to Supercapacitors

2.1 How energy storage has changed our lives

The battery is our steady travel companion that allows us to carry out our activities disconnected from home and office. Cell phones, laptop computers, MP3 players, cameras, and calculators are unplugged because they are powered by batteries. Batteries have affected various aspects of our lives, think of all the things that needs batteries to work—the number of applications is just too large to be listed here. What follows is a brief survey of some of the applications, especially those that require some specialized batteries (1):

- Portable consumer devices: mobile power for an unplugged society, power tools.

- Medical devices: life-sustaining and life-enhancing medical devices, including pacemakers, defibrillators, hearing aids, pain management devices, and drug pumps.

- Electric vehicles: The environmental concerns over the use of fossil fuels has spurred great interest in electric and hybrid-electric vehicles powered by batteries.

- Large-scale energy storage: Batteries are widely used to store electrical energy during times when production (from power plants) exceeds consumption and the stores are used at times when consumption exceeds production.

- Space: Lithium ion batteries are used in the two Mars Exploration Rovers.

- Millitary batteries: Batteries are also used for powering electronics for the military, such as GPS, night vision and advanced weapons. So critical were batteries according to reliable reports, that the second gulf war in 2003 was nearly halted due to the lack of

batteries at the front line, it was described a "near term disaster". What saved the day was fast thinking that saw additional batteries airlifted into the theater of operations and a quick end to the ground fighting (2).

- Electric Aircraft: is an aircraft that runs on electric motors rather than internal combustion engines, with electricity coming from solar cells or batteries. In 2011, the *eGenius* electric aircraft completed the first manned 250 miles flight completely powered by batteries (3).

Figure 2.1: Range of devices that are powered by batteries/supercapacitors.

2.2 Energy and Power:

Energy and power are often used to describe the characteristics of any energy storage device. If the energy storage device is used in an electric vehicle, power density shows how fast one can go, and the energy density shows how far one can go on a single charge (4). Capacitors put out enormous power, but store only tiny amounts of energy, similar to the behavior of the water cup in Figure 2.2. Batteries store a fair amount of charge, but charge and discharge slowly, similar to the large water bottle in Figure 2.2. Supercapacitors offer a unique combination of high power and high energy properties, bridging the gap between batteries and capacitors.

Figure 2.2: Energy versus power, adapted from reference (5).

2.3 What is a supercapacitor?

Traditional capacitors are made of two metal plates separated by a thin insulating layer. The capacitor stores charge electrostatically in an electric field and the amount of charge is measured by its capacitance, C, which is a function of the area of the metal plates, A, and the spacing between them, d. For typical capacitors, $d \approx 1$ µm and $A < 1$ m^2 (see Figure 2.3). So, in order to increase the amount of charge stored, one needs to minimize d and maximize A and that is what

a supercapacitor does. A supercapacitor consists of two electrodes separated by an ion permeable separator to prevent short circuits between the electrodes and the cell is impregnated with a liquid electrolyte (4). As voltage is applied to a supercapacitor, ions from the electrolyte diffuse into the pores of the electrode of opposite charge. Charge accumulates at the interface between the electrodes and the electrolyte, forming two charged layers (known as electric double layers) with an extremely small separation distance on the order of 1 nm. The current supercapacitor technology uses activated carbon as the active electrode material since this material is electrically conductive and exhibits extremely large surface area on the order of 1000-2000 m^2/g, meaning that high capacitance values can be achieved in a small space. For instance, comparing a capacitor and a supercapacitor of similar volume shown in Figure 2.3, the capacitor stores only 0.003 F, whereas the supercapacitor stores >10,000 times more charge – about 50 F.
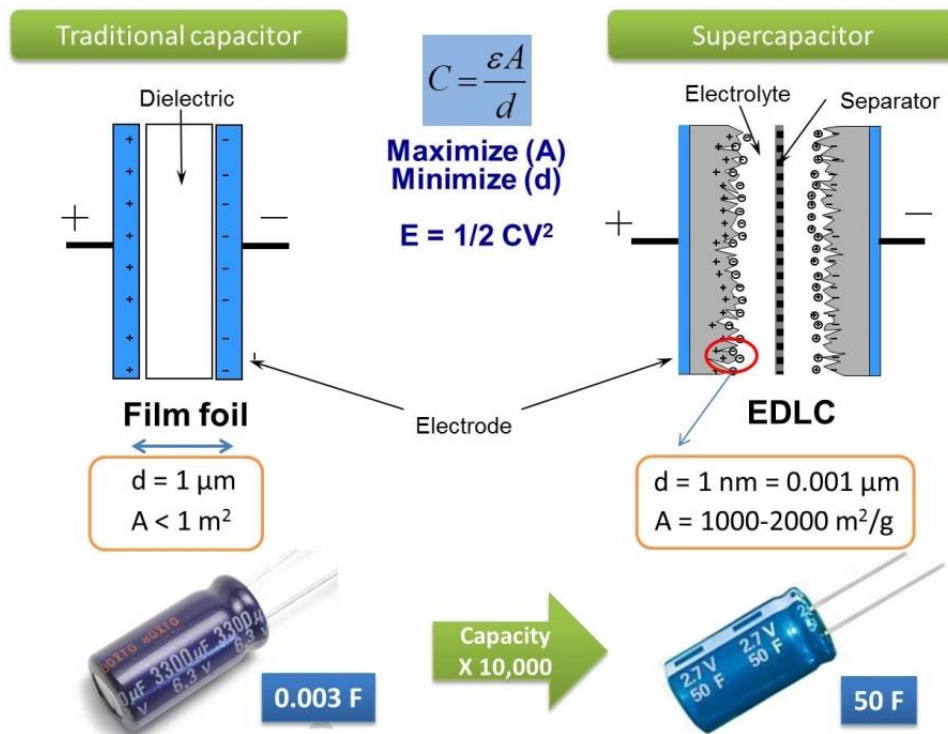
Figure 2.3: Schematic diagram showing the structure of a traditional capacitor and an electric double layer supercapacitor.

Supercapacitors versus batteries: It is important to understand the basic differences between supercapacitors and rechargeable (secondary) batteries in the way they function. Generally, a battery consists of a positive electrode (cathode), a negative electrode (anode) and an electrolyte that allows ions to move from anode to cathode during discharge and return during recharge, Figure 2.4 (6). The voltage developed across the battery terminals varies according to the type of battery and the chemistry involved between the electrodes and electrolyte. Electrochemical reactions typical of rechargeable batteries and their operating voltages are shown in Figure 2.4. The fundamental difference between batteries and supercapacitors is that the former store energy in the bulk of chemical reactants capable of generating charge, whereas the latter store energy directly as surface charge. Battery discharge rates and therefore power performance is then limited by the reaction kinetics as well as the mass transport, while such limitations do not apply to supercapacitors constructed with two activated carbon electrodes, thereby allowing exceptionally high power capability during both discharge and charge (7).
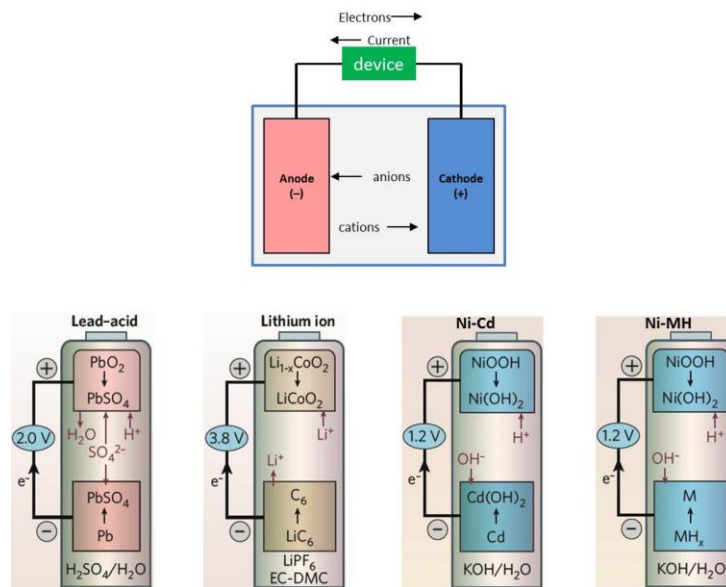
Figure 2.4: Schematic diagram showing the mechanism of operation of chemical batteries with examples. The schematic shown in the bottom is reproduced from reference (79).

18

Another fundamental difference between the two technologies is the cycle life; while batteries can be operated for ~1000 cycles only, due to volume changes during charge and discharge, supercapacitors can be charged and discharged virtually an unlimited number of cycles (7-9). The main shortcoming of supercapacitors, though, is low energy density, 5-7 Wh/kg compared to 20-150 Wh/kg for batteries (8,9). Hence, there is a growing interest by chemists and researchers in other fields to improve the energy density of supercapacitors as a step forward towards ultimate energy storage.

2.4 Supercapacitor performance characteristics

Supercapacitors have several advantages over conventional energy storage devices (10):

- ✓ Supercapacitors perform mid-way between conventional capacitors and batteries. They offer higher energy density than conventional capacitors and higher power density than batteries, Figure 2.5.

- ✓ Fast charge and discharge capability: supercapacitors can be charged in seconds, compared to hours for batteries and milliseconds for capacitors.

- ✓ Supercapacitors store charge in a highly reversible process. Typical rechargeable batteries last only for a few hundreds of charge/discharge cycles, whereas supercapacitors can be used up to a million cycles (Figure 2.6).

- ✓ Supercapacitors can be operated under extreme working conditions. For example, supercapacitors can be used at temperatures as low as −40 °C, where batteries cannot function properly.

- ✓ Environmentally friendly—no heavy metals or disposal issues as is common for conventional batteries.

- ✓ Maintenance free—providing superior cost-over-life, and fit-and-forget.
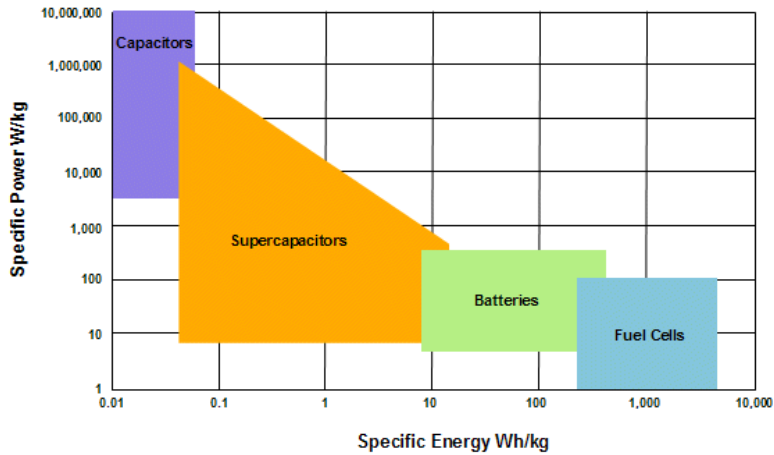
Figure 2.5: Specific power against specific energy, also called a Ragone plot, for capacitors, batteries, supercapacitors and fuel cells (78).
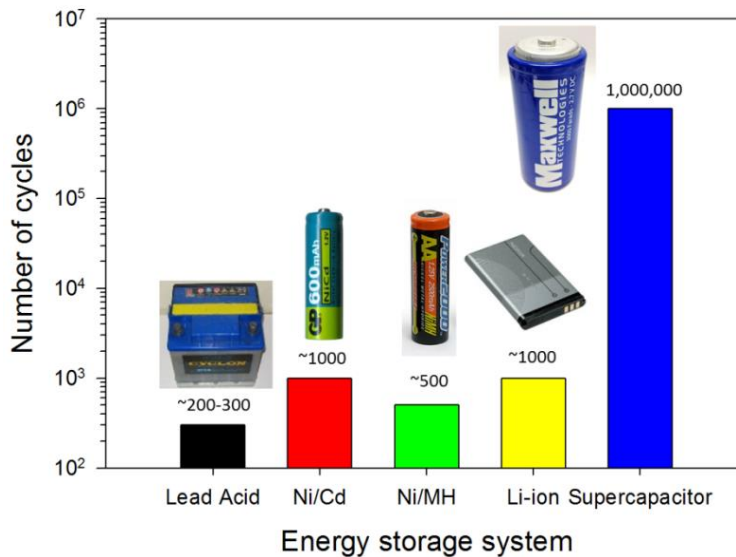
Figure 2.6: Cycling life of supercapacitors compared with typical rechargeable batteries including lead acid, Ni/Cd, Ni/MH and Li-ion batteries.

2.5 Applications of supercapacitors

Supercapacitors store and discharge energy very quickly and are being used in thousands of different applications around us, some of these applications are described here.

2.5.1 Industrial Applications

The supercapacitors initially introduced to the market in 1978 by NEC were mainly used as backup power devices for volatile clock chips and complementary metal-oxide-semiconductor computer memories (11). Today, supercapacitors are widely used in uninterruptible power supplies (UPS) that are typically used to protect hardware such as computers, data centers, telecommunication equipment and other electrical equipment where an unexpected power disruption could cause injuries, fatalities, serious business disruption or data loss (12). They are also the sole power source for low energy applications such as automated meter reading (AMR) equipment or for event notifications in industrial electronics (13). Furthermore, supercapacitors complement a primary energy source like an internal combustion engine, fuel cell or battery, which cannot repeatedly provide quick bursts of power. This combination reduces the cost per cycle, saves on replacement and maintenance costs, enables the battery to be downsized, and extends battery life (14).

2.5.2 Transportation

Heavy Hybrid Vehicles: Supercapacitors are among the most promising of the energy storage technologies currently in use or being considered for use in heavy hybrid vehicles. They are particularly well suited for city transit buses (Figure 2.7a) with stop-and-go driving; in trash trucks, which can experience as many as a thousand start/stop cycles during a day; and in delivery trucks, which operate on similar drive cycles (11).

Engine Start Modules using supercapacitors (shown in Figure 2.7b) can replace the traditional lead acid starter battery and deliver reliable, quick-burst power at ignition—even after loading in hot or cold temperature extremes (15).

Energy recovery: a primary challenge facing current transport vehicles is to reduce greenhouse gas emissions and energy consumption. Supercapacitors can provide a solution to this problem by capturing and storing energy from regenerative braking which can be used immediately or saved for later use. Fleet vehicles, long-haul trucks, and other heavy-transportation vehicles such as trains, light rail, trams and metros all benefit from the adoption of a hybrid power train approach with the use of supercapacitors (16). For example, supercapacitors enable the electric trams in southern Germany (Figure 2.7c) to use 30% less energy than their equivalents in other regions (17). Other examples include industrial cranes and fork lifts (18).

Next Stop, Supercapacitor Buses: Recently, China has been experimenting with new buses that run entirely on carbon-based supercapacitors. Unlike a conventional trolley bus that has to continually touch an overhead power line, supercapacitor buses take big sips of electricity every three to five miles at designated charging stations (19). So, while people are getting on and off the bus at bus stops, the supercapacitors can be fully recharged within a couple minutes, Figure 2.7d.
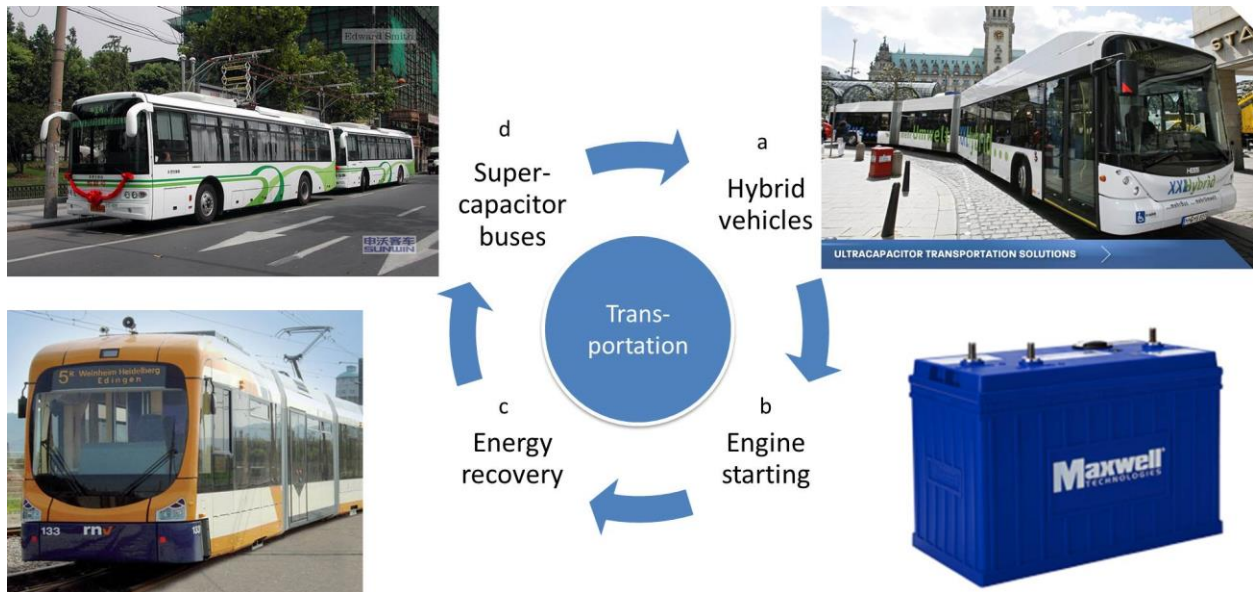
Figure 2.7: Applications of supercapacitors in transportation. (a) Hybrid city-transit bus, adapted from reference (16). (b) Engine Starting Module, adapted from (15). (c) Electric trams, Mannheim, Germany, adapted from reference (17). (d) Supercapacitor buses, Shanghai, China, adapted from reference (20).

2.5.3 Consumer Electronics:

Mobile phones: Your mobile phones may have a better sound and flash system that works at 10 times the normal distance because a supercapacitor has taken over these functions from a conventional capacitor. For example, Figure 2.8a shows a SonyEricsson K800 pictured from inside featuring two bulky electrolytic capacitors that precludes a thin form factor of the phone camera. A supercapacitor can be smaller and more powerful (Figure 2.8a, bottom picture) (21). In another example, Figure 2.8b shows two pictures that were taken in a dark room to compare with a standard battery-powered LED flash in a current camera phone and another one modified with a supercapacitor (21).

Power tools: Coleman™ introduced a cordless screwdriver powered by supercapacitors that takes only in 90 seconds for a recharge (22). This is very advantageous to most conventional cordless screwdrivers using batteries that can take up 3 to 5 hours to recharge, Figure 8c.

23

Toys: Recently, supercapacitors found their way into toys (Figure 2.8d). Using a supercapacitor instead of a battery, a toy car can accelerate almost instantly to racing speeds. Combined with the ability of supercapacitors to be charged very quickly and recharged 100,000's of times, this application appears to be interesting (23).

Figure 2.8: Applications of supercapacitors in consumer electronics. (a,b) Camera flash, pictures adapted from (21). (c) Cordless screwdriver, picture adapted from reference (22). (d) Toys, picture adapted from reference (23).

2.5.4 Energy Harvesting

Energy harvesting is the process by which ambient energy is captured and converted directly into electricity for small and mid-sized devices, such as autonomous wireless sensor nodes, consumer electronics and vehicles (24). The generated energy should be consumed immediately or it will be lost. Because of its rapid charging, a supercapacitor is often combined with the energy harvester to store this energy. The following are a few examples of this application:

The World's First Energy-Generating Revolving Door located at Natuurcafe La Port in the Netherlands is used to produce electricity for a train station coffee shop (25). The door uses a generator that is driven by the energy applied when people pass through, Figure 2.9a. Supercapacitors store the generated energy and provide a power supply for the ceiling's LED lights. A large display inside the railway station shows how much energy is being generated by the revolving door as a service to curious patrons (25).

The Forever Flashlight uses no batteries or bulbs. Instead it uses Faraday's principle of magnetic induction and a bright LED to produce light without batteries. The flashlight is shaken by hand for about 30 seconds to recharge a supercapacitor and it will then provide about 5-7 minutes of light (26), Figure 2.9b.

Figure 2.9: Typical applications of supercapacitors for energy harvesting: (a) World's first energy-generating revolving door, Netherlands, adapted from reference (25). (b) A mechanically powered flashlight, adapted from reference (27). (c) Wireless power modules, adapted from (28). (d) A stand-alone power source for a street light, adapted from reference (29).

Wireless Power Modules combine an energy-harvester with a supercapacitor to create a perpetual, battery-free power source. The supercapacitor stores the harvested energy and provides peak transmission power over wireless networks such as the wireless sensors commonly used in security, environmental and condition-monitoring systems (28). Shown in Figure 2.9c are two examples for energy-harvesting modules that convert energy from radio-frequency waves (left) and unused mechanical vibrations (right).

Street lights: Sado City, in Japan's Niigata Prefecture, has street lamps that lights up LEDs at night time with energy generated by solar cells and stored in supercapacitors, Figure 2.9d. This stand-alone power source ensures high durability and stable performance under various climates, from areas that exceeds 40 degrees Celsius in summer to areas that plunge to sub-zero in winter (29).

2.5.5 Grid Storage: As renewable energy sources grow in use, grid stability becomes an increasingly important issue. The variability in wind and solar output creates instability on the grid. This variability also results in poor utilization of these resources by 30-50% (30). Supercapacitors can help combat these challenges by providing energy storage for firming the output of renewable installations which increases grid stability. As of June 2012, Maxwell Technologies has installed power of >30 GW for the grid market and this use is still growing (30).

2.5.6 Aircraft: In 2005, Diehl Luftfahrt Elektronik GmbH, a leading producer of aerospace systems and controls, selected supercapacitors to power emergency actuation systems for doors and evacuation slides in passenger aircraft, including the new Airbus 380 jumbo jet (31).

2.1.7 Medical: Supercapacitors are advantageous when extremely fast discharging is required. They are used in defibrillators where they can deliver a "lethal" 500 joules of energy providing the burst of power required to shock the heart (32). Low ESR supercapacitors are also used in DC motors for infusion, pumps and monitoring devices (33).

2.1.8 Military: The ability of supercapacitors to provide high power bursts offer solutions to a variety of power challenges for the military. Some of the earliest uses were motor startup (cold diesel engine start) for large engines in tanks and submarines (34). Evans' hybrid supercapacitors based on a ruthenium oxide cathode, shows a frequency response similar to an electrolytic capacitor while at the same time offering an energy content of about a factor of 10 higher than a comparable aluminum electrolytic capacitor of the same size (35). This makes them perfectly suited for Defense and Aerospace applications requiring high power such as power interruption buffers, filtering and high current pulse generation. Other applications that benefit from the high power of supercapacitors include GPS guided missiles and projectiles, laser power supplies, Unmanned Aerial Vehicles, radar and high power discharges for naval warfare (36).

2.6 Capacitive Energy Storage Mechanisms

Depending on the charge storage mechanism, supercapacitors can be classified into three major types: electric double layer capacitors (EDLCs), pseudo-capacitors or hybrid capacitors as shown in Table 2.1 (37,38).

EDLC materials store charge mainly in an electrochemical double-layer formed at the interface between the electrode and the electrolyte, rather than storing them in the bulk of the capacitive material, Figure 2.10a. Therefore, the capacitance predominantly depends on the

surface area accessible to the electrolyte ions. The important factors influencing their electrochemical performance are specific surface area, pore-size distribution, pore shape and structure, electrical conductivity, and surface functionality (39). Among these, the pore size can have a considerable impact on the electrochemical performance of the electrode. According to Largeot *et al.*, the pore size of electrode materials that yielded maximum double-layer capacitance was very close to the ion size of the electrolyte (with respect to an ionic liquid electrolyte), and both larger and smaller pores led to a significant drop in capacitance (38,40).

Pseudo-capacitors store charge mainly via fast and reversible redox (Faradaic) reactions happening near the surface of conducting polymers or metal oxides, Figure 2.10b. The introduction of these redox reactions has drastically increased the charge storage performance (4,38). Typically, pseudo-capacitors can increase the capacitance value by as much as an order of magnitude over that of EDLCs. However, because of the nature of the redox reactions, pseudo-capacitors generally have poor cycling stability.

Hybrid systems offer an attractive alternative to conventional pseudo-capacitors or EDLCs by combining a battery-like electrode (energy source) with a capacitor-like electrode (power source) in the same cell (4). Further, by designing electrolytes for optimum performance in such hybrid configurations, the critical need for high-voltage operation may be achieved without compromising stability or long-term cyclability. Three types of hybrid capacitors are identified as shown in Table 2.1 and discussed in the following section (41).

	EDLC	Pseudocapacitor	Hybrid capacitors
Storage mechanism	Electrochemical double layer, Physical separation of charges	Faradaic reactions (Redox reactions)	EDLC-pseudocapacitance hybrid 3 designs • composite hybrids • Asymmetric hybrids • Battery-type hybrid

Electrode material	Carbon materials	Oxides and polymers	• Composite: composite of carbon and either an oxide or a polymer
			• Asymmetric:
			  ▪ positive electrode: pseudocapacitor
			  ▪ Negative electrode: carbon
			• Battery-type:
			  ▪ Positive electrode: Li-insertion
			  ▪ Negative electrode: carbon

Specific capacitance	~ 200 F/g in aqueous KOH ~ 120 F/g in organic electrolytes (<50 F/cm^3)* *typical values for activated carbon	~ 200 – 1200 F/g in aqueous electrolytes ~ 6000 F/cm^3 (MnO$_2$) ~4200 F/cm^3 (RuO$_2$)	Intermediate between EDLC and pseudocapacitors
Cycling performance	Up to million cycles	<10,000 cycles	~10,000
Operating voltage	2.3-2.7 V	~ 1 V (symmetric structure)	Composite: <1 V Asymmetric: 1-2 V depending on materials Battery-type: 2.3-4V

Table 2.1: Summary of the charge storage mechanisms of supercapacitors
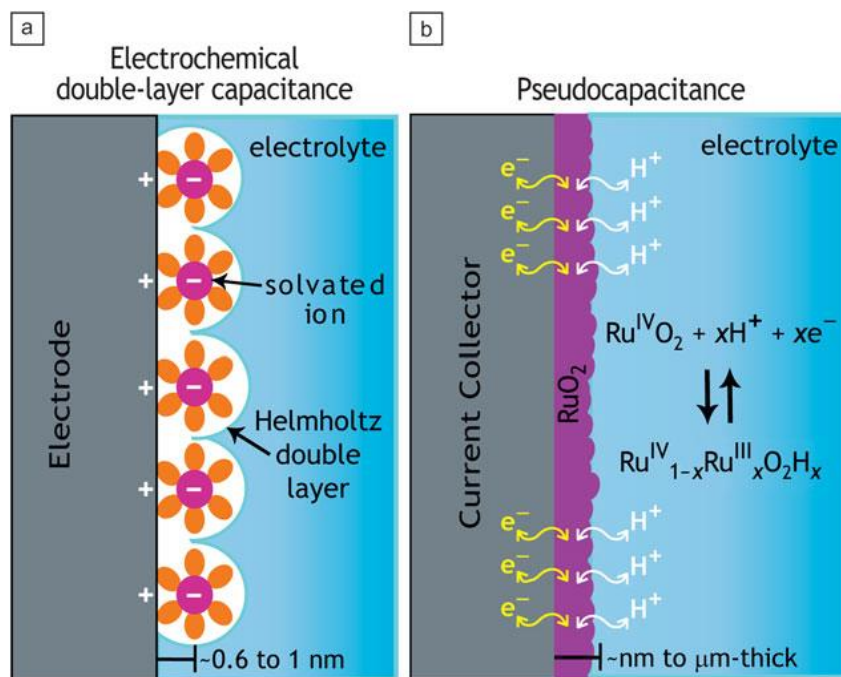
Figure 2.10. Schematic diagram showing charge storage via the process of either (a) electrochemical double-layer capacitance or (b) pseudo-capacitance. Adapted from reference (51).

2.7 Materials for Supercapacitors

2.7.1 Materials for Electric Double Layer Capacitors

The key to reaching high capacitance by charging the double layer is in using high specific surface area (SSA) and electronically conducting electrodes. Graphitic carbon satisfies all the requirements for this application, including high conductivity, electrochemical stability and open porosity (4). A wide range of high surface area carbon materials have been tested including activated carbon, carbon nanotubes, templated carbons, carbide-derived carbons, onion-like carbon, carbon nanofibers and graphene (37), see Table 2.2. Among these, activated carbons are the most widely used materials in the majority of supercapacitors currently available in the market due to lower cost, easy processing and manufacturing, high surface area and chemical stability.

Activated carbons (AC) are prepared by creating a three-dimensional porous network in the bulk of carbon materials through an activation process. This process consists of controlled oxidation of bulk carbon precursor using various activation techniques, such as oxidation in water vapor, KOH or CO_2 (37). Various carbon precursors have been used including carbonaceous materials derived from wood, coal, nutshells, etc. Depending on the activation process as well as the carbon precursor, ACs with surface areas of over 2000 m^2/g can be achieved. The porous structures of these ACs have a broad pore size distribution consisting of micropores (<2 nm), mesopores (2–50 nm) and macropores (>50 nm), which are responsible for the high SSA of ACs (38). However, the specific capacitance does not increase linearly with increasing the specific surface area of the electrode. This is because not all micropores in the electrode are necessarily accessible to electrolyte ions, resulting in limited capacitance of only

60-120 F/g (39). In addition, the presence of oxygen-containing groups on the surface of ACs from the activation process can reduce its electrical conductivity and power performance. Although ACs are widely used in today's supercapacitors, their applications are still limited to only niche markets due to their limited energy density and rate capability (38). Conway suggested that the development of new dense carbon materials with controlled and interconnected pore structures, high electrical conductivity and high surface area easily accessible to the electrolyte could effectively improve the energy and power performance of EDLCs (39,10).

In the past two decades, considerable efforts have been made with the aim of developing such carbon material. For instance, onion-like carbons are zero-dimensional quasi-spherical nanoparticles consisting of concentric graphitic shells that are few nanometers in diameter (42). They are usually prepared by annealing nano-diamond powders in vacuum or argon at 1800 ℃. They offer SSA up to 500–600 m^2/g fully accessible to ion adsorption and a high electrical conductivity resulting in high power (37, 42-44), but a limited capacitance of about 30 F/g.

Carbon nanotubes (CNTs), which are one-dimensional materials, have been extensively studied for EDLC applications within the past decade (45). They are usually the materials of choice for high power applications because of their high electrical conductivity and readily accessible surface area (4). The energy density is, however, a concern due to their relatively small specific surface area (generally <500 m^2/g) as compared to ACs (38).

Carbide-derived carbon (CDC) is a class of carbon materials produced by selectively etching metals from metal carbides using chlorine at elevated temperatures (46). This method allows for the synthesis of microporous carbons with SSAs of 1000-3000 m^2/g with narrow pore

size distributions (47). It is also possible to control the pore size within 0.6 to 1.1 by properly selecting the metal carbide precursor, the chlorination and carbonization temperatures. A volumetric capacitance of up to 180 F/cm^3 have been achieved; however, this value was found to decrease significantly as the film thickness was increased (46).

The template carbonization method has been shown to be an efficient protocol for producing mesoporous carbon materials with large surface areas and pore volumes (48). In general, templated carbons are produced by the infiltration of a carbon precursor into the pores of the template, followed by a carbonization treatment and finally the removal of the template to leave behind a porous carbon structure (38). In contrast with ACs, the templated carbons offer narrow pore size distributions and ordered straight pore channels that allow for improved ionic transport. Therefore, supercapacitors based on these materials demonstrate higher power density than those built with ACs (38). Nevertheless, this method involves complicated and time-consuming procedures for the removal of the template, which excludes them from further consideration for industrial applications. Therefore, it is both urgent and crucial to develop simple and efficient methods for the preparation of new materials for high-performance supercapacitors.

Other carbons are also used in supercapacitors. The general rules for the selection are a high and accessible specific surface area with good electrical conductivity. For example, single-walled carbon nanohorns, with a conical structure rather than the typical tubular structure of CNTs, have been used for high-power supercapacitors, but they have limited capacitance (49). Also, they are presently produced only in small quantities and mainly used for research purposes. Carbon aerogels have also been used, but their mass density is too low for achieving energy

dense electrodes. Recently, graphene has attracted significant interest for building EDLCs, as discussed in Section 2.8.
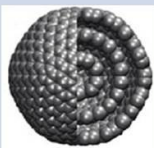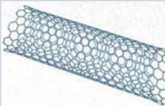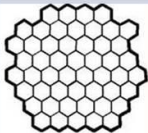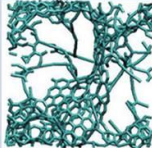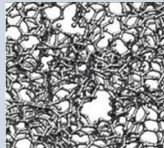
Material	Carbon onions	Carbon nanotubes	Graphene	Activated carbon	Carbide derived carbon	Templated carbon
Dimensionality	0-D	1-D	2-D	3-D	3-D	3-D
Specific surface area (m^2/g)	<500	120-500	2600, theoretical	1000-3500	1000-2000	500-3000
Conductivity	High	High	High	Low	Moderate	Low
Density (g/cm^3)	-	0.6	0.01-1.5	0.4-0.7	0.5-0.7	0.5-1
Aqueous electrolyte	-	50-100 F/g	100-220	<200	170-220	120-135
	-	<60 F/cm^3	<255	<80	<120	<200
Organic electrolyte	-	<60 F/g	80-276	<100	100-120	60-140
	-	<30 F/cm^3	<261	<50	<70	<100
Structure						

Table 2.2. Different carbon structures used in EDLCs, reproduced from references (37) and (38).

2.7.2 Materials for pseudo-capacitors

Materials exhibiting redox behavior for use as electrodes in pseudo-capacitors include transition metal oxides and conducting polymers. Figure 2.11 summarizes the capacitive performance of the most commonly studied metal oxides and conducting polymers (50).

Metal oxides that can be used for pseudo-capacitor applications are required to (i) be electronically conductive, (ii) exist in two or more oxidation states over a continuous potential range without irreversible phase/structure changes, (ii) the protons can freely intercalate into the oxide lattice on reduction (out of the lattice on oxidation), allowing facile interconversion of O_2

$\leftrightarrow 2OH^-$ (39). Ruthenium oxide, RuO_2, is widely studied because it is conductive and has three distinct oxidation states accessible within 1.2 V (4). Its capacitive behavior can be ascribed to a series of fast, reversible electron-transfer reactions that are coupled with adsorption of protons at or near the electrode surface.

$$Ru^{IV}O_2 + xH^+ + xe^- \leftrightarrow Ru^{IV}_{1-x}Ru^{III}_xO_2H_x$$
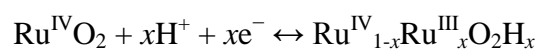
Specific capacitance of more than 720 F/g has been reported, determined by factors such as the degree of crystallinity, particle size, and electrode architecture (51). However, the prohibitive cost of ruthenium has limited its use to the military and space applications (52). Less expensive oxides of manganese, iron, vanadium, nickel and cobalt have also been tested in aqueous electrolytes. Among these, manganese oxide is most promising because of its high theoretical capacitance of 1380 F/g that promises high energy density supercapacitors (53,54). Although promising, none of these materials is in commercial use; they are produced on the lab-scale only.

Another type of supercapacitor showing high pseudo-capacitance uses conducting polymer electrodes. Many kinds of conducting polymers (polyaniline, polypyrrole, polythiophene and their derivatives) have been tested and have shown high gravimetric and volumetric pseudo-capacitance in various nonaqueous electrolytes at operating voltages of about 3 V (4,38). When used as electrode materials, conducting polymers suffer from poor stability during cycling. However, supercapacitors using polyacene electrodes provide up to 10,000 cycles with stable capacitive behavior (55). Since these Faradaic processes are generally slow, pseudo-capacitors suffer from relatively low power density compared to EDLCs. Research efforts with conducting polymers for supercapacitor applications are nowadays directed towards hybrid systems.

2.7.3 Materials for hybrid supercapacitors

Asymmetric supercapacitors have been, so far, the most successful hybrid supercapacitors in the market. Hybrid supercapacitors based on pseudo-capacitive positive electrodes e.g. PbO_2 and $NiOOH$ with carbon negative electrodes in aqueous electrolytes were initially developed in Russia (53,56,57). This asymmetric configuration can extend the operating voltage window of aqueous electrolytes beyond the thermodynamic limit of water (~1.2 V). Since carbon shifts the hydrogen evolution towards potentials below the nominal thermodynamic value, when coupled with pseudo-capacitive metal oxides possessing high oxygen over-potential, the resulting electrochemical stability windows can be widened to ca. 2 V (56). The energy density of these devices can be as high as 20 Wh/kg, nearly that of a high power lead-acid battery, but with much higher cycle life (11). Obviously, this energy density is significantly higher than EDLCs, but the charge/discharge characteristics of these hybrid systems are very non-ideal (non-linear) (53). Promising asymmetric configurations with linear charge/discharge and large operating voltage windows based on MnO_2 or V_2O_5 and carbon electrodes are being developed in research labs nowadays (38,39).

Lithium ion capacitors (LIC) are another emerging hybrid capacitor technology which involves the combination of a lithium insertion battery-type positive electrode and carbon negative electrode. Usually, the battery-type electrode is pre-doped with lithium ions, which lowers the potential of the positive electrode and allows high output voltage of up to 3.8-4 V (59,60). Various battery-type electrodes have been developed and commercialized including graphite, which is the state of the art anode material in current lithium ion batteries, and nanostructured lithium titanate, $Li_4Ti_5O_{12}$ (4). LICs can provide energy densities of up to ca. 15 Wh/kg which is more than twice the energy density of EDLCs (60).
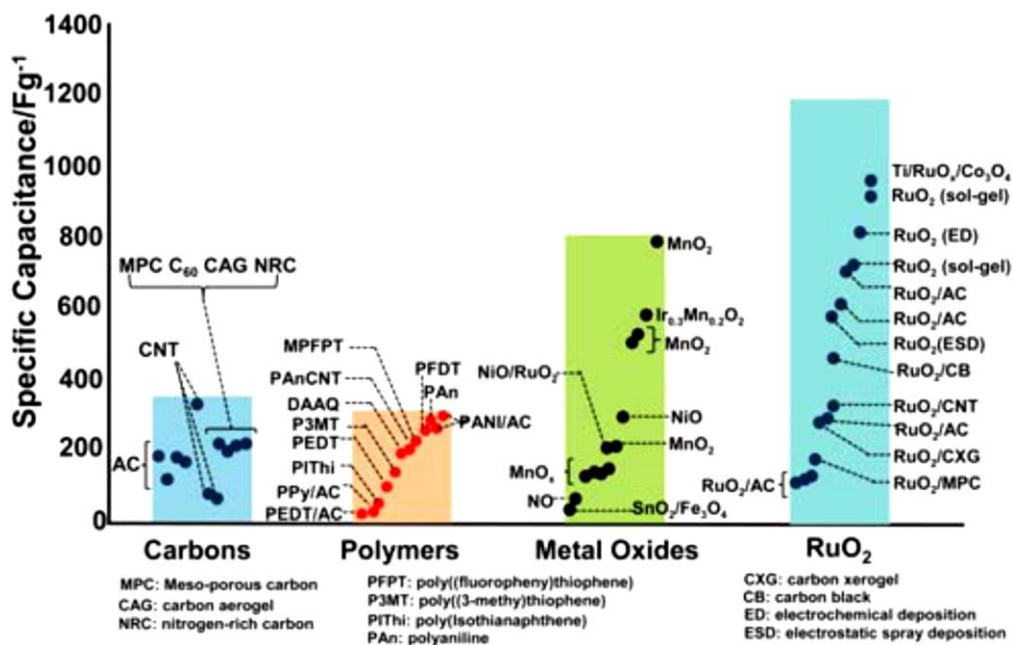
Figure 2.11: Electrochemical performance of the most commonly studied pseudo-capacitive materials, adapted from reference (58).

2.8 Graphene: Potential candidate for high-performance supercapacitors

Ever since it was discovered in 2004, graphene has been hailed as a natural wonder of the materials world destined to transform our lives in the 21st century (61). Graphene is attractive because it possesses many extraordinary characteristics that are a direct consequence of its unique atomic structure. Graphene can be visualized as an atomic scale chicken wire and is the basic building block for graphitic materials of all other dimensionalities (Figure 2.12). It can be wrapped up into 0D fullerenes, rolled into 1D nanotubes or stacked into 3D graphite (62).

Scientists have developed a myriad of techniques for the synthesis of graphene which can be classified as bottom-up and top-down approaches. The most common techniques are summarized here; however, a detailed description of the synthetic routes to graphene can be found elsewhere (63).
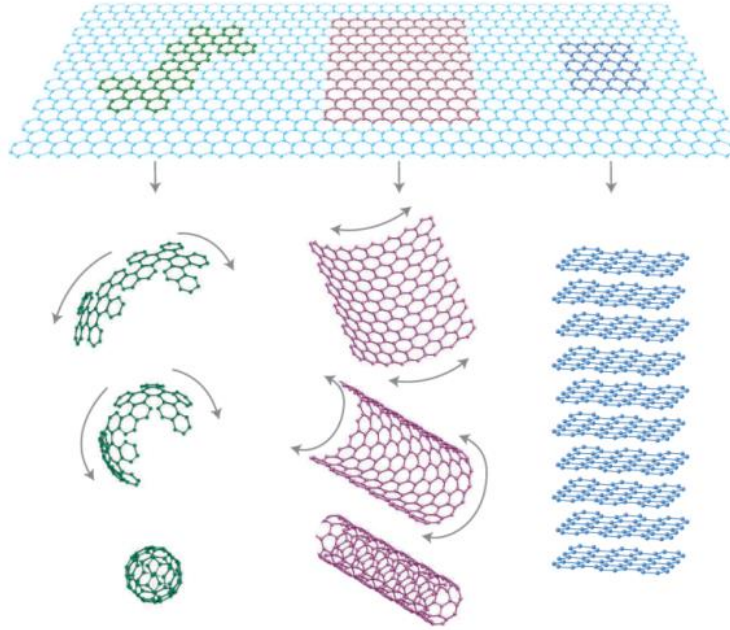
Figure 2.12. Graphene, the mother of all graphitic carbons of all dimensionalities. Adapted from reference (62).

In the bottom-up approach, graphene is grown at the atomic scale and built up atom-by-atom to the desired final size. For example, chemical vapor deposition (CVD) can be used to grow graphene using a hydrocarbon gas as the carbon source and copper foil as the catalyst inside a CVD chamber at high temperature. This graphene can be transferred onto other substrates for further processing in devices (61), Figure 2.13.

In the top down approach, mainly graphite is used as the precursor which can be seen as a stack of graphene sheets connected together through weak van der walls interactions. So the challenge is to peel off the sheets down to a single layer. Surprisingly enough, the method that was used for making the first samples of graphene involved using Scotch tape, which led to the Nobel Prize in physics a few years later. The middle image of Figure 2.13 displays a donation by Andre Geim and Konstantin Novoselov to the Nobel Museum in Stockholm, showing that with just a lump of graphite and Scotch tape, it is possible to make one of the world's best transistors

based on graphene. Although these two techniques provide high quality graphene for transistor applications, it does not supply enough graphene to build a supercapacitor.

As chemists we use chemicals, instead of Scotch tape, to do the exfoliation of graphite. This introduces oxygen groups to the planes of graphene to form what we call graphene oxide which can then be deoxygenated back to graphene. The reduction of graphene oxide to a graphene-like material can be achieved through a variety of routes such as: chemical reduction using hydrazine, thermal deoxygenation or laser scribing (61, 64).
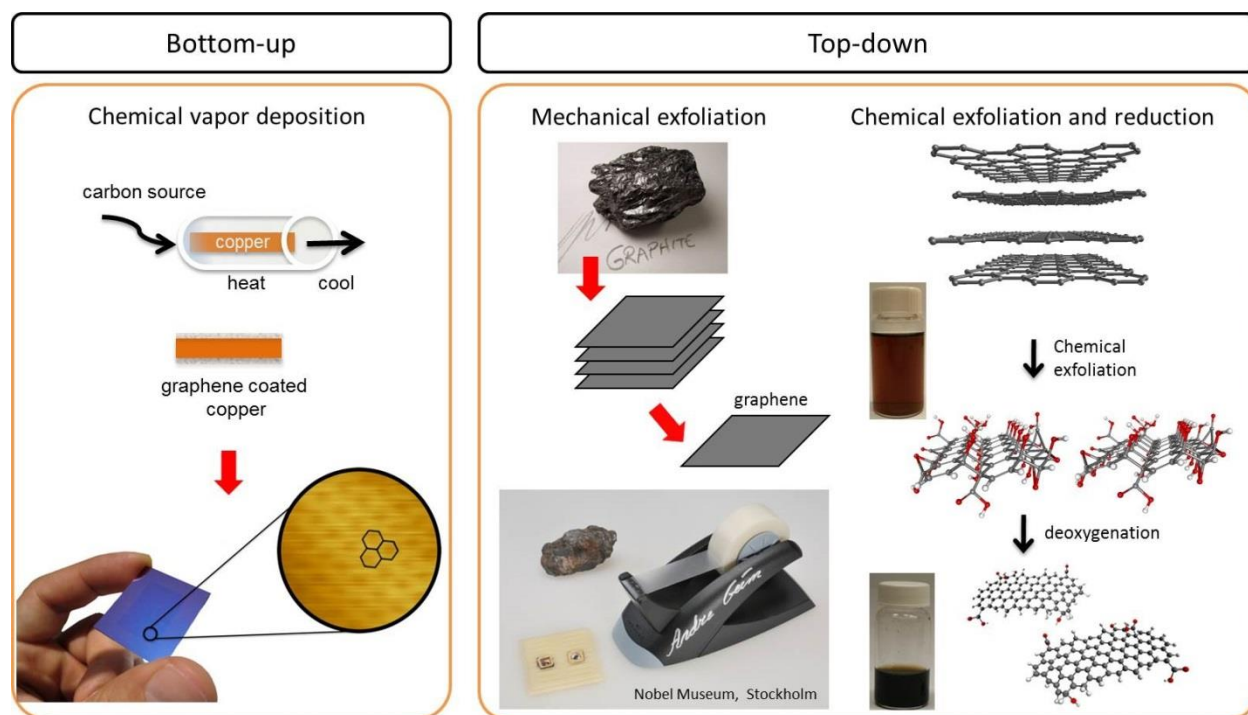
Figure 2.13: General approaches for the synthesis of graphene. Reproduced from references (61 and 64).

Graphene has attracted great interest during the past few years for EDLC applications. As a 2D material, graphene can potentially combine fully accessible high SSA and high conductivity. In traditional supercapacitors made of activated carbon, most of the surface area resides in the micropores of the carbon; thus, this is unlikely to contribute significantly to the

charge storage, especially at a high rate (65, 66), see Figure 2.14. This results in a poor frequency response, with the energy stored in these carbon electrode materials released only at a slow rate. Graphene, on the other hand, with its two-dimensional sheet-like structure possesses a large open surface area that is readily accessible to electrolyte with a small diffusion barrier. Graphene thus has the potential for making supercapacitors with power densities that surpass any other form of activated carbon. Furthermore, the high surface area of graphene based materials promises extremely high energy density.
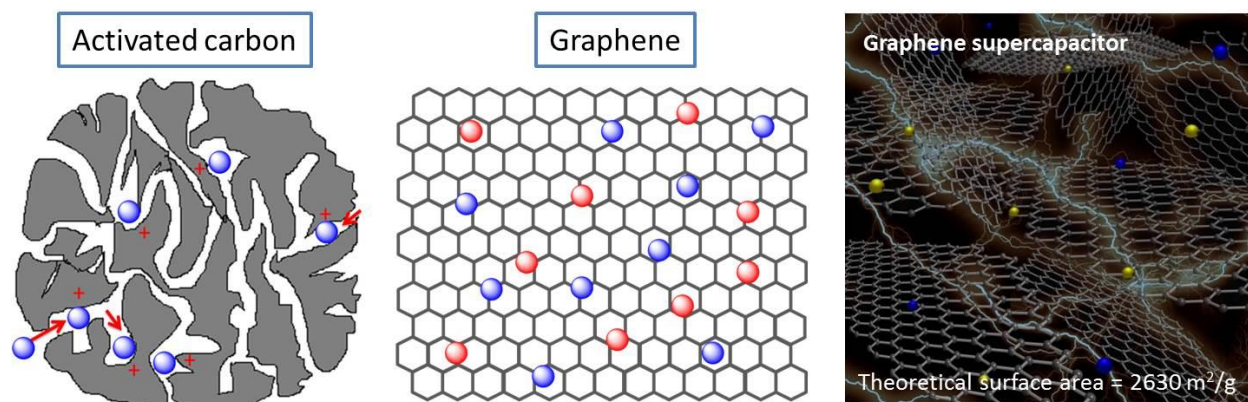
Figure 2.14: An explanation of the main differences between activated carbon and graphene in supercapacitors.

2.9 Miniaturization of energy storage units

Nowadays, smartphones and many other mobile devices are increasingly becoming an essential part of human life as the most effective and convenient communication tools not bound by time and place (67). The public has become accustomed to the rapid progress in this mobile technology over the past few decades. For example, what you can do nowadays with your smartphone that fits into your pocket was not possible with the most bulky computers a few decades ago. These developments are due in part to the ongoing exponential increase in computer processing power, doubling approximately every 2 years for the past several decades.

This pattern is usually called Moore's Law and is named after Gordon Moore, a cofounder of Intel. This prediction became a self-fulfilling prophecy that emerged as one of the driving principles of the semiconductor industry over the past 50 years. For decades, chipmakers could speed up their microprocessors simply by shrinking the transistors and packing more of them onto a chip. This changed from around 1000 transistors per die in the early 1970's to around 4 billion nowadays (Figure 2.15a). This trend explains why we are getting smaller and more efficient electronics over time. However, one area has lagged behind in this miniaturization trend—that is the energy storage units such as batteries and capacitors (68).

Batteries have been around for over 200 years and they power a huge number of consumer electronics from mobile phones to electric vehicles. However, the slow development of this technology is holding back technological progress (69,70). Shown in Figure 2.15b is the miniaturization trend of the most widely used rechargeable batteries, reflected by the increase in the energy density over time. The energy density of Ni-Cd and Ni-MH saturated a few years ago, meaning that they approached the theoretical limit. The energy density of Li-ion batteries, which is the preferred technology for mobile electronics, doubled in the past 10 years and is approaching its theoretical capacity soon. Actually, had batteries improved at the same rate as transistors did, a heavy duty car battery would be the size of a red blood cell (Figure 2.15c)! Unfortunately, such batteries do not exist; there is no Moore's law for batteries (68). In fact, looking at today's electronics one will find that the energy storage units are the most bulky components, e.g. consider capacitors in a mid-2000's computer motherboard and the iPhone battery shown in Figure 2.15d,e.

In recent years, there has been major progress on implantable biomedical systems such as cardiac pacemakers. Nevertheless, these devices remain mostly limited, in part due to the

40

constraints of bulky power supplies (69). In addition, the rapid growth of miniaturized electronics such as non-volatile memory, micro-sensors and actuators, hearing aids, RFID tags, and micro-electromechanical systems has spurred the development of rechargeable power sources with an appropriate size (67). The reduction in size and improvement in capability of microsystems is presently limited by the specific and gravimetric properties, and the overall sizes of on-board power supplies (70-72). Indeed, power supplies often comprise up to ten times the mass of the other elements of the system, combined (70).

2.10 Micropower sources

Several kinds of micron-sized power sources such as micro-batteries, micro-fuel cells, and energy harvesters have been developed in recent years (70-74). Among these, Li-ion micro-batteries were developed in the early 2000s and are now the most widely researched for use as integrated micro-power sources (70). The structure of micro-batteries is very similar to those of conventional batteries except that the thickness of the electrodes and other components are in the micro-meter range (75). However, batteries have some drawbacks such as limited lifetime which could be a major problem when they have to be embedded in permanent structures, such as biomedical implants, active radio frequency identification tags and embedded micro-sensors where no maintenance or replacement is possible. Also, micro-batteries suffer from low power density that is not enough for many applications (73). For example, the energy generated by energy harvester micro-systems lasts only for a few seconds, which is too short to recharge batteries. Microscale supercapacitors offer a fast charge, higher number of cycles and longer life time than micro-batteries. They can also be coupled with micro-batteries or energy harvesting micro-systems to provide peak power (73).
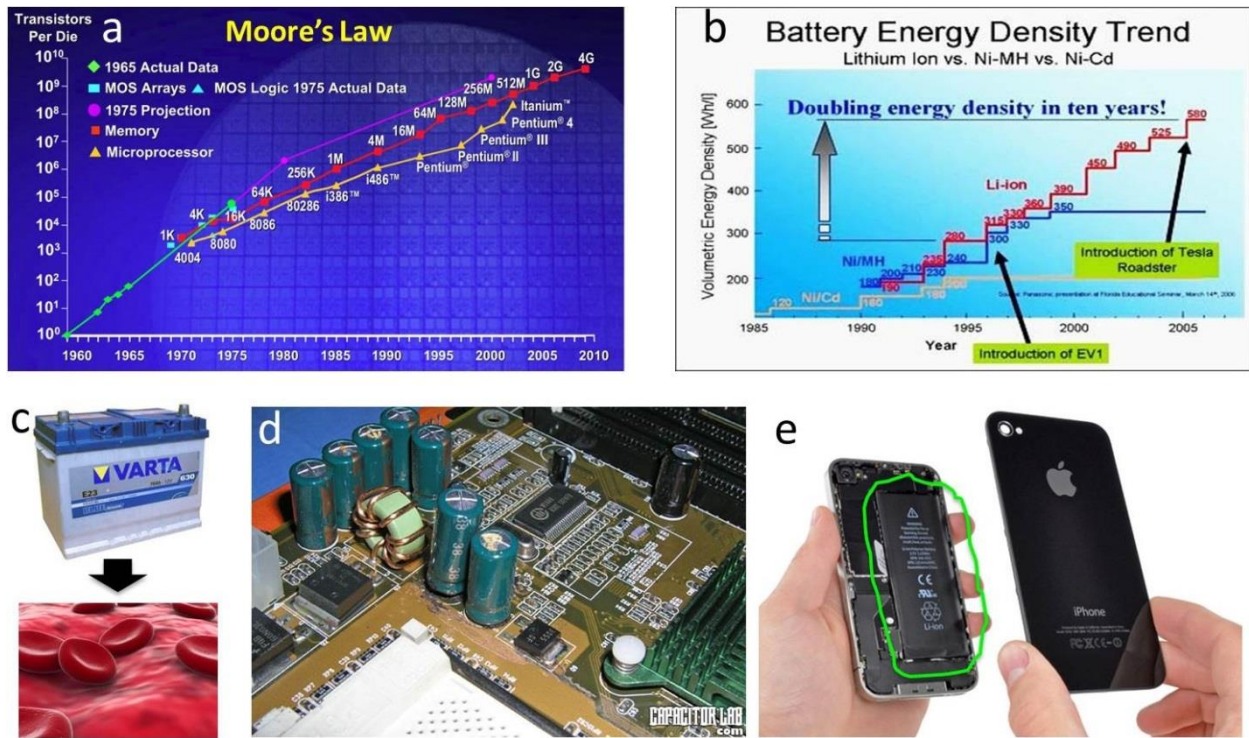
Figure 2.15: Miniaturization trend in semiconductor electronics vs. batteries. Pictures adapted from reference (76).

2.10.1 Micro-Supercapacitors

What is a micro-supercapacitor? A micro-supercapacitor can be defined through the following example. The motherboard of today's computers is supported by a small battery that is used to keep up the configuration settings of the CMOS when the system power is turned off. Typically, the CMOS battery is a CR2032 lithium coin cell and can last two to ten years, depending on the type of motherboard, ambient temperature and the length of time that the system is powered off. Supercapacitors can also be made in the CR2032 coin cell parts in which the electrodes are stacked like the slices of bread on a sandwich. While this design is functional, it is not compatible with integrated circuits and, of course, limits the shrinking of the system. Moreover, additional electrical connections are required to extract the energy from the CMOS battery which means more interconnect routing problems (Figure 2.16, top left). In order to solve these problems, the battery or the supercapacitor should be integrated directly on-chip. It turns out that

the current semiconductor industry uses planar processes to build individual components of integrated circuits. For example, Figure 2.16 shows the structure of MOSFET which is the basic component of computer chips: all the parts are in the same plane. Thus, to integrate a supercapacitor directly onto a chip, one needs to have both electrodes (positive and negative) placed side-by-side in the same plane in an interdigitated pattern as shown in Figure 2.16 (bottom right). This new structure is called a micro-supercapacitor and it is compatible with current integrated circuits. However, the integration of micro-supercapacitors with electronic circuits is challenging. This is because the necessary energy-storage components scale down poorly in size and are not well suited to the planar geometries of most integrated fabrication processes. Progress in micro-fabrication techniques has enabled a number of methods for fabricating micro-supercapacitors (46). However, they are still produced in research labs at high cost.
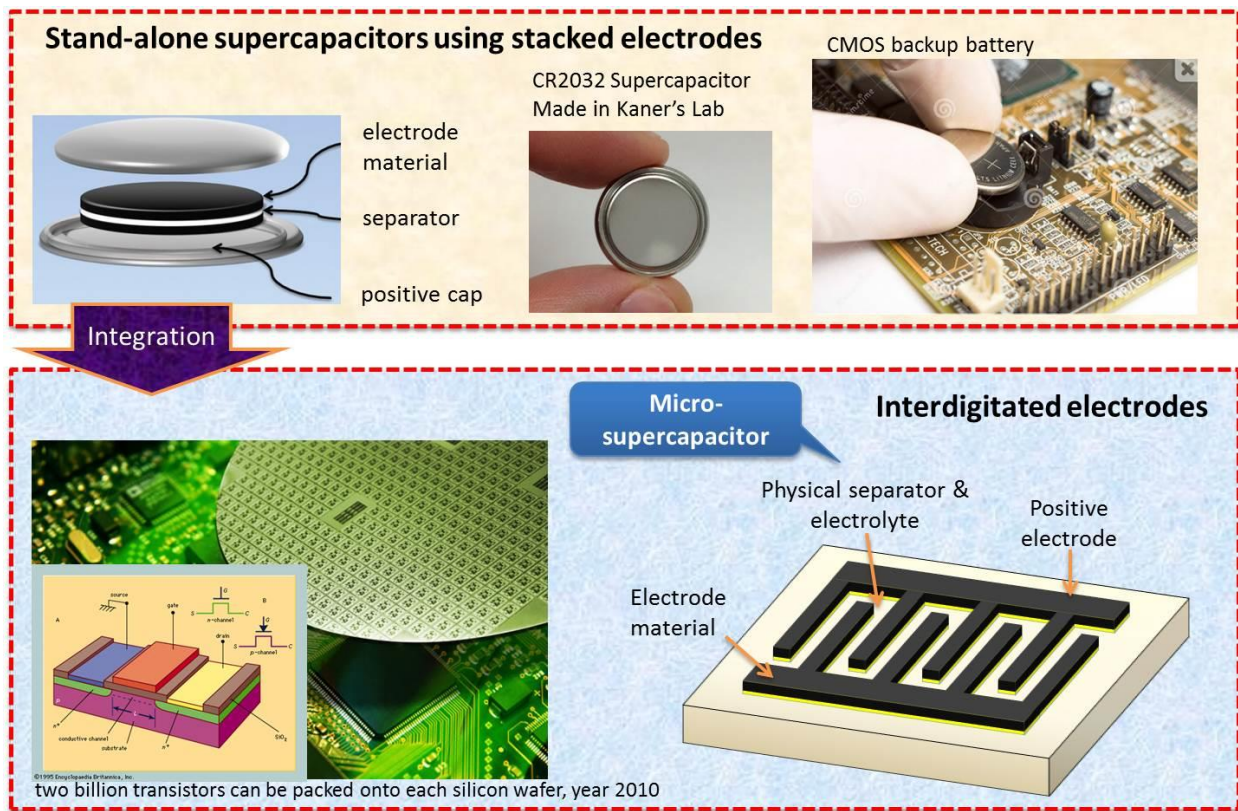
Figure 2.16: Differences between a supercapacitor and a micro-supercapacitor. Pictures adapted from reference (77).

43

BIBLIOGRAPHY

[1] Michael Root, The Tab Battery Book: An In-Depth Guide to Construction, Design, and Use. McGraw-Hill, New York, 2011.

[2] Henry Schlesinger, The Battery: How Portable Power Sparked A Technological Revolution. HarperCollins Publisher, New York, 2010.

[3] http://cafefoundation.org/v2/ea_main.php

[4] P. Simon, Y. Gogotsi, *Nature Materials* 7, 845-854 (2008)

[5] http://www.maxwell.com/

[6] Thomas Reddy, ed. Linden's Handbook of Batteries, Mc-Grow Hill, New York, 2010.

[7] J.R. Miller, P. Simon, *The Electrochemical Society Interface*, Spring 2008, 31-32

[8] D. S. Su, R. Schlögl, ChemSusChem 3, 136 (2010).

[9] J. R. Miller, P. Simon, Science 321, 651 (2008).

[10] B. E. Conway, Electrochemical Supercapacitors, Kluwer Academic/ Plenum Press, New York, 1999.

[11] John R. Miller and Andrew F. Burke. *The Electrochemical Society Interface, pp* 53-57, Spring 2008.

[12] http://www.maxwell.com/products/ultracapacitors/industries/ups-systems

[13]http://www.maxwell.com/products/ultracapacitors/docs/200904_casestudy_smartsync.pdf#search="automated meter read"

[14] http://www.maxwell.com/

[15] http://www.maxwell.com/products/ultracapacitors/products/engine-start-module

[16] http://www.maxwell.com/products/ultracapacitors/industries/transportation

[17] Philip Ball, MRS Bulletin 37, 802-803 (2012).

[18] John R. Miller, Patrice Simon. *Science* 321, 651-652 (2008).

[19] http://www.technologyreview.com/news/415773/next-stop-ultracapacitor-buses/

[20] http://www.flickr.com/photos/shanghai_sunwin_bus_corporation/6730978683/

[21] http://www.cap-xx.com/news/photogallery.htm

[22] http://www.popularmechanics.com/technology/gadgets/4223118

[23] http://www.sciencewiz.com/

[24] http://www.idtechex.com/research/reports/energy-harvesting-and-storage-for-electronic-devices-2012-2022-forecasts-technologies-players-000316.asp

[25] http://cleantechnica.com/2008/12/10/netherlands-train-station-features-worlds-first-energy-generating-revolving-door/

[26] http://www.amazon.com/Shake-Flashlight--Batteries--Simply-Recharge/dp/B000637LTY/ref=sr_1_15?ie=UTF8&qid=1378178072&sr=8-15&keywords=flashlight+mechanical#productDetails

[27] http://emergencyplanahead.com/shop/emergency-real-shake-flashlight/

[28] http://www.cap-xx.com/news/photogallery.htm

[29] http://www.chemi-con.co.jp/e/company/pdf/20100330-1.pdf

[30] http://www.maxwell.com/products/ultracapacitors/industries/grid-storage

[31] http://www.maxwell.com/ultracapacitors/ and http://www.prnewswire.com/news-releases/diehl-selects-maxwell-technologies-boostcapr-ultracapacitors-to-power-emergency-actuation-systems-for-aircraft-doors-and-slides-54295762.html

[32] http://www.qmed.com/mpmn/article/opinion-ultra-capacitors-offer-medical-equipment-powerful-reliable-alternative-batterie and http://www.yec.com.tw/dir-super/super-capacitor-supplier-list-list/super-capacitor-supplier-list-list-17/

[33] http://www.bt2000.co.uk/supercapacitors.html

[34] http://www.cantecsystems.com/

[35] http://www.evanscap.com/pdf/Hybrid_Caps_COTS.pdf and http://www.evanscap.com/pdf/Product_Overview.pdf

[36] http://www.tecategroup.com/ultracapacitors-supercapacitors/military-applications.php

[37] P. Simon, Y. Gogotsi, Capacitive Energy Storage in Nanostructured Carbon-Electrolyte Systems, Accounts of Chemical Research 45, 1094–1103 (2013).

[38] Li Li Zhang and X. S. Zhao, Carbon-based materials as supercapacitor electrodes, Chem. Soc. Rev., 2009, 38, 2520–2531

[39] Guoping Wang, Lei Zhang and Jiujun Zhang, A review of electrode materials for electrochemical supercapacitors, Chem. Soc. Rev., 2012, 41, 797–828

[40] C. Largeot, C. Portet, J. Chmiola, P. Taberna, Y. Gogotsi and P. Simon, *J. Am. Chem. Soc.*, 2008, **130**, 2730

[41] M. Zhi, C. Xiang, J. Li, M. Li, N. Wu, Nanoscale 5, 72 (2013)

[42] Portet, C.; Yushin, G.; Gogotsi, Y. Carbon 2007, 45 (13), 2511–2518.

[43] Zhang, L. L.; Zhou, R.; Zhao, X. S.; J. Mater. Chem. 2010, 20 (29), 5983–5992.

[44] David Pech, Magali Brunet, Hugo Durou, Peihua Huang, Vadym Mochalin, Yury Gogotsi, Pierre-Louis Taberna and Patrice Simon, Nature Nanotechnology 5, 651-654 (2010).

[45] Zhai, Y.; Dou, Y.; Zhao, D.; Fulvio, P. F.;Mayes, R. T.; Dai, S. Adv. Mater. 2011, 23 (42), 4828–4850

[46] John Chmiola, Celine Largeot, Pierre-Louis Taberna, Patrice Simon, Yury Gogotsi, Science 328, 480-483 (2010).

[47] Presser, V.; Heon, M.; Gogotsi, Y. Adv. Funct. Mater. 2011, 21 (5), 810–833.

[48] Nishihara, H.; Kyotani, T.Templated nanocarbons for energy storage Adv. Mater. 2012, 24, 4473

[49] Yang, C. M.; Kim, Y. J.; Endo, M.; Kanoh, H.; Yudasaka, M.; Iijima, S.; Kaneko, K. J. Am. Chem. Soc. 2007, 129 (1), 20–21.

[50] K. Naoi and P. Simon, Electrochem. Soc. Interf. 17 (2008) 34–37.

[51] J.W. Long, D. Belanger, T. Brousse, W. Sugimoto, M.B. Sassin, O. Crosnier, MRS Bulletin 36 (2011) 513.

[52] A. Burke, J. Power Sources, 2000, 91, 37.

[53] Weifeng Wei, Xinwei Cui, Weixing Chen and Douglas G. Ivey, Chem. Soc. Rev., 2011, 40, 1697–1721.

[54] Megan B. Sassin, Christopher N. Chervin, Debra R. Rolison, and Jeffrey W. Long, Accounts of Chemical Research 46, 1062-1074 (2013).

[55] Taiyo Yuden, Shoe Electronics Ltd, http://www.t-yuden.com/

[56] Xin Zhao, Beatriz Mendoza Sanchez, Peter J. Dobson and Patrick S. Grant, Nanoscale, 2011, 3, 839-855.

[57] Y. M. Vol'fkovich and T. M. Serdyuk, Russ. J. Electrochem., 2002, 38(9), 935.

[58] Katsuhiko Naoi and Patrice Simon, Electrochemical Society Interface 17, pp 34-37 (Spring 2008).

[59] Katsuhiko Naoi, Syuichi Ishimoto, Jun-ichi Miyamoto and Wako Naoi, Energy Environ. Sci., 2012, 5, 9363

[60] K. Naoi, W Naoi, S. Aoyag, J.-I. Miyamoto, T. Kamino, Accounts of Chemical Research 46, 1075-1083 (2013).

[61] J.K. Wassei, R.B. Kaner, *Acc. Chem. Res.*, Article ASAP, DOI: 10.1021/ar300184v

[62] A.K. Geim and K.S. Novoselov Nature Materials 6, 183-191 (2007)

[63] Y. Zhu, S. Murali, W. Cai, X. Li, J.W. Suk, J.R. Potts, R.S. Ruoff, *Adv. Mater.* 15, 3906-3924 (2010)

[64] Tung, V.C., Allen, M.J., Yang, Y., Kaner, R.B. *Nature Nanotech.* 4, 25 (2009).

[65] Du, C., Pan, N. Journal of Power Sources 160, 1487–1494 (2006).

[66] Merlet, C., Rotenberg, B., Madden, P. A., Taberna, P.-L., Simon, P., Gogotsi, Y. & Salanne, M. Nature Materials 11, 306-310 (2012).

[67] N. Fernando, S.W. Loke, W. Rahayu, Future Generation Computer Systems 29, 84-106 (2013).

[68] Fred Schlachter, PNAS 110, 5273 (2013).

[69] David C. Bock, Amy C. Marschilok, Kenneth J. Takeuchi, Esther S. Takeuchi, Electrochimica Acta 84 (2012) 155– 164

[70] Timothy S. Arthur *et al.,* MRS Bulletin 36, 523-531 (2011).

[71] K. A. Cook-Chennault, N. Thambi, A.M. Sastry, Smart Mater. Struct. 17 (2008) 043001.

[72] F. Albano, Y. Lin, D. Blaauw, D. Sylvester, K. Wise, a Sastry, *J. Power Sources* 185 (2008) 1524-1532.

[73] Majid Beidaghi and Chunlei Wang, Proc. of SPIE Vol. 7679 76791G-1

[74] R.J.M. Vullers, R. van Schaijk, I. Doms, C. Van Hoof, R. Mertens, Solid-State Electronics 53 (2009) 684–693

[75] J. Oudenhoven, L. Baggetto, P. Notten, Adv. Energy Mater. 1, 10-33 (2011).

[76] a: http://www.cmg.org/measureit/issues/mit41/m_41_2.html

b: http://www.kk.org/thetechnium/archives/2009/07/was_moores_law.php
c: http://www.ebay.co.uk/itm/Varta-Mazda-RX8-Petrol-Heavy-Duty-Car-Battery-Upgrade-/370461838544, http://www.fi.edu/learn/heart/blood/red.html
d: http://www.greenlinecomputers.com/?p=56
e: http://diy-battery.com/where-is-the-battery-on-the-iphone-4/
[77]Top right: http://www.makeuseof.com/tag/why-does-my-motherboard-have-a-battery/

Top left: http://www.mp-i.fr/wp-content/uploads/2012/11/20121030_Brunet_MP-Innov_Toulouse.pdf
Bottom left: http://www.zdnet.com/after-silicon-what-will-power-computing-for-the-next-10-years-and-beyond-3040153697/
[78] http://www.cap-xx.com/resources/reviews/pwr-v-enrgy.htm

[79] M. Armand, J.-M. Tarascon. Nature 451, 652-657 (2008).

CHAPTER 3

Laser Scribing of High-Performance and Flexible Graphene-Based Electrochemical Capacitors

3.1 ABSTRACT

Although electrochemical capacitors (ECs), also known as supercapacitors or ultracapacitors, charge and discharge faster than batteries, they are still limited by low energy densities and slow rate capabilities. We used a standard LightScribe DVD optical drive to do the direct laser reduction of graphite oxide films to graphene. The produced films are mechanically robust, show high electrical conductivity (1738 siemens per meter) and specific surface area (1520 square meters per gram), and can thus be used directly as EC electrodes without the need for binders or current collectors, as is the case for conventional ECs. Devices made with these electrodes exhibit ultrahigh energy density values in different electrolytes while maintaining the high power density and excellent cycle stability of ECs. Moreover, these ECs maintain excellent electrochemical attributes under high mechanical stress and thus hold promise for high-power, flexible electronics.

3.2 INTRODUCTION

Batteries and electrochemical capacitors (ECs) stand at opposite ends of the spectrum in terms of their power and energy densities (1). Batteries store energy through electrochemical reactions and can exhibit high energy densities (on the order of 20 to 150 Wh/kg), whereas ECs, which

store charge in electrochemical double layers (EDLs), can only achieve values of 4 to 5 Wh/kg (2-4). However, because ion flow is faster than redox reactions ECs can deliver much higher power densities. ECs are also generally maintenance free and display a longer shelf and cycle life, so they are often favored in many electronic applications (2-4).

An EC that combines the power performance of capacitors with the high energy density of batteries would represent a major advance in energy storage technology (5, 6), but this requires an electrode with higher and more accessible surface area than that of conventional EC electrodes while maintaining high conductivity. Graphene-based materials are attractive in this regard because of their mechanical and electrical properties as well as exceptionally high surface area. Recently, the intrinsic capacitance of single-layer graphene was reported to be ~21 $\mu F/cm^2$; this value now sets the upper limit for EDL capacitance for all carbon-based materials (7). Thus, ECs based on graphene materials could, in principle, achieve an EDL capacitance as high as ~550 F/g if their entire surface area could be used.

Currently, graphene-based materials derived from graphite oxide (GO) can be manufactured on the ton scale at low cost, making them potentially cost-effective materials for charge storage devices (8). Although these graphene-based materials have shown excellent power density and life-cycle stability, their specific capacitance (130 F/g in aqueous potassium hydroxide and 99 F/g in an organic electrolyte) still falls far below the theoretical value of 550 F/g calculated for single-layer graphene (9). A variety of other graphene-based materials derived from GO have also been used, yet the values of specific capacitance, energy density, and power density have remained lower than expected (10-13)—an effect often attributed to the restacking of graphene sheets during its processing as a result of the strong sheet-to-sheet van der Waals interactions. This reduction in the specific surface area of graphene accounts for the overall low

49

capacitance. In addition, these ECs exhibited relatively low charge/discharge rates, which precludes their use for high-power applications. Recently, EC devices composed of curved graphene (14), activated graphene (15), and solvated graphene (16) have demonstrated enhanced performance in terms of energy density. However, further improvements in energy density are needed that do not sacrifice high power density. In particular, the production of mechanically robust graphene electrodes with large thickness (~10 μm or higher) and high surface-to-volume ratio in a binder free process would result in high power and high energy density ECs (5).

3.3 RESULTS AND DISCUSSION

Here, we present a strategy for the production of graphene-based ECs through a simple all-solid-state approach that avoids the restacking of graphene sheets. The process is schematically illustrated in Figure 3.1. Initially, a thin film of GO dispersed in water was drop-cast onto a flexible substrate (see Appendix, Figure 3S.1). Irradiation of the film with an infrared laser inside an inexpensive commercially available LightScribe CD/DVD optical drive, as discussed in (17), reduces the GO to laser-scribed graphene (LSG), as indicated by the change in film color from golden brown to black. Analysis of cross sections of the film with scanning electron microscopy showed that the initially stacked GO sheets were converted into well-exfoliated LSG sheets through laser irradiation (Figure 3.1E and Figure 3S.2). The resulting LSG films showed excellent conductivity (1738 S/m) as opposed to 10 to 100 S/m for activated carbons, the state-of-the-art material used in commercial devices (18). Additionally, LSG shows excellent mechanical flexibility with only ~1% change in the electrical resistance of the film after 1000 bending cycles (Figure 3S.3). Thus, LSG can be directly used as EC electrodes without the need for any additional binders or conductive additives. More importantly, these properties allow LSG

50

to act as both the active material and current collector in the EC. The combination of both functions in a single layer leads to a simplified and lightweight architecture. Thus, a device can be readily made by sandwiching an ion porous separator [Celgard 3501 (Celgard, Charlotte, NC)] between two identical LSG electrodes. The devices are super-thin with a total thickness of <100 μm, making them potentially useful in microdevice applications (Figure 3S.4) (19). Other devices can be made by putting LSG on porous substrates such as a nitrocellulose membrane or photocopy paper or on conductive aluminum foil, which is often used in commercial devices (figures. 3S.1 and 3S.7). Therefore, LSG electrochemical capacitors (LSG-ECs) can be readily made into different designs, including stacked and spirally wound structures to target different applications.
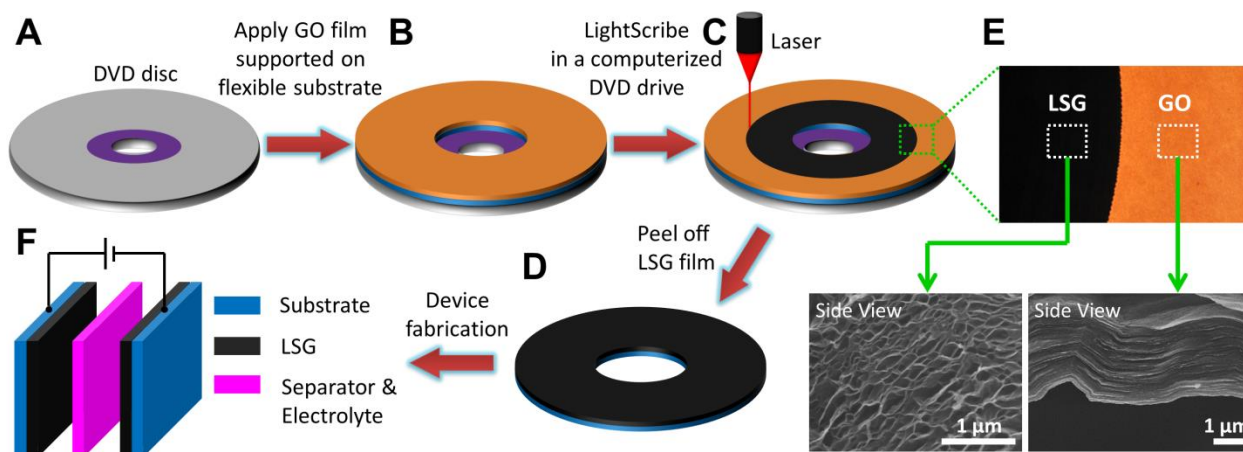
Figure 3.1: Schematic illustration of the fabrication of laser-scribed graphene-based electrochemical capacitors. (**A** to **D**) A GO film supported on a flexible substrate is placed on top of a LightScribe-enabled DVD media disc, and a computer image is then laser-irradiated on the GO film in a computerized LightScribe DVD drive. (**E**) As shown in the photograph, the GO film changes from golden brown color to black as it reduced to laser-scribed graphene. The low-power infrared laser changes the stacked GO sheets immediately into well-exfoliated few-layered LSG film, as shown in the cross-sectional SEM images. (**F**) A symmetric EC is constructed from two identical LSG electrodes, ion-porous separator, and electrolyte.

The LSG electrodes we have fabricated satisfy the critical features for high-performance ECs. First, the large and accessible specific surface area of the LSG (1520 m^2/g compared with 1000 to 2000 m^2/g for a typical activated carbon material) results in a sizeable charge storage capacity and accounts for the high areal and volumetric stack capacitances observed. Second, the LightScribe laser causes the simultaneous reduction and exfoliation of GO sheets and produces an open network of LSG (Figure 3.1). This structure prevents the agglomeration of graphene sheets, which has been a major barrier in achieving the full potential of graphene-based ECs. The network structure of LSG has open pores, which helps facilitate the electrolyte accessibility to the electrode surfaces. This offers an opportunity to optimize the ionic diffusion in LSG electrodes, which is crucial for charging the EDL, and generates high-power ECs. Last, LSG possesses excellent electronic conductivity, which is another key factor for achieving high power. These three properties taken together and optimized could, in theory, produce landmark performances in EC electrodes. Working with these properties, three-dimensional composite electrodes have been successfully used to make batteries with relatively high energy density and fast charge/discharge rates (20). Although activated carbons can provide high surface area, the difficulty of controlling their pore structure and pore size distribution has so far limited the energy densities and rate capabilities of commercial ECs (21).

In order to demonstrate the superior performance of LSG electrodes for electrochemical energy storage, we assembled symmetric LSG-ECs using polyethylene terephthalate (PET) as a thin flexible substrate and an aqueous electrolyte of 1.0 M H_3PO_4. The EC performance was analyzed through both cyclic voltammetry (CV) and galvanostatic charge/discharge (CC) experiments, as shown in Figure 3.2. In comparison with GO, the LSG-EC shows an enhanced electrochemical performance with a nearly rectangular CV shape at a scan rate of 1000 mV/s,

which is indicative of nearly ideal capacitive behavior (Figure 3.2A) even though no metal current collector, binders, or electroactive additives were used, as is the case in commercial ECs. Additionally, the LSG-EC is robust enough to be charged and discharged over a wide range of scan rates (100 to 10,000 mV/s) and still maintain its nearly ideal rectangular CV shape (figures 3S.5 to 3S.7). Figure 3.2B shows the nearly triangular shape of the CC curves obtained at a high current density of 10 A/g of LSG per electrode (abbreviated 10 A/$g_{LSG/electrode}$). This is indicative of the formation of an efficient EDL and fast ion transport within the LSG electrodes. In addition, these CC curves show only a small voltage drop of 0.018 V at the start of the discharge curve, indicating a device with a low equivalent series resistance (ESR). We measured the specific capacitance from CC curves over a wide range of charge/discharge current densities. Here, the areal and volumetric capacitance of the stack (this includes the flexible substrate, the current collector, the active material, and the separator) were calculated and compared with a commercial activated-carbon EC (AC-EC) tested under the same dynamic conditions. Although the AC-EC shows a slightly higher volumetric capacitance at low charge/discharge rates, its capacitance falls off quickly at higher rates, whereas the LSG-EC continues to provide high capacitance even when operated at very high rates (Figure 3.2C and Figure 3S.8). In addition, the areal capacitance of the LSG-EC was calculated to be 3.67 mF/cm^2 [and 4.04 mF/cm^2 in 1.0 M H$_2$SO$_4$ (figures 3S.5 to 3S.7)] at 1 A/$g_{LSG/electrode}$. The device also shows a very high rate capability while still maintaining a capacitance of more than 1.84 mF/cm^2, even when the EC is operated at an ultrafast charge/discharge rate of 1000 A/$g_{LSG/electrode}$. This is comparable with values reported in the literature for microdevices and thin-film ECs at much lower current charge/discharge rates (0.4 to 2 mF/cm^2) (5, 13). As is shown in Figure 3S.6, these ECs can be efficiently charged/discharged on the 0.1-s time scale. Additionally, the LSG-EC retained 96.5% of its initial capacitance after 10,000 cycles (Figure 3.2D).
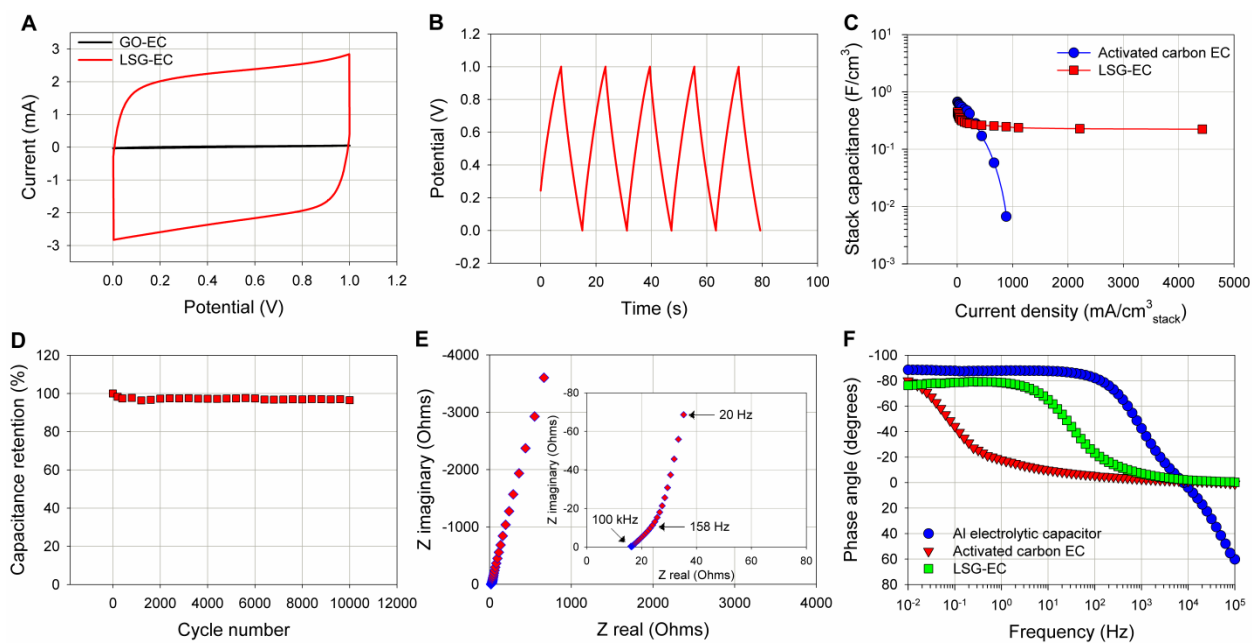
Figure 3.2: Evaluation of the performance of an LSG electrochemical capacitor in aqueous 1.0 M H_3PO_4 solution. (**A**) Cyclic voltammetry of LSG- and GO-ECs at a scan rate of 1000 mV/s. A rectangular CV shape is observed for the LSG-EC, indicating an efficient double-layer formation. (**B**) Galvanostatic charge/discharge (CC) curves of an LSG-EC measured at a high current density of 10 A/$g_{LSG/electrode}$. (**C**) The volumetric stack capacitance of an LSG-EC is calculated from the CC curves at different charge/discharge current densities. Data obtained from a commercial activated carbon EC are shown for comparison. As can be seen, an LSG-EC can sustain ultrahigh current density operation, indicating the potential for ultrahigh-power delivery. (**D**) The LSG-EC shows excellent cyclic stability and retains >96.5% of its initial response after 10,000 cycles. (**E**) Complex plane plot of the impedance of a LSG-EC, with a magnification for the high-frequency region in the inset. (**F**) Impedance phase angle versus frequency for a LSG-EC and a commercial activated carbon EC. The -45° phase angle occurs at ~30 Hz for the LSG-EC and at ~0.1 Hz with the commercial EC.

Electrochemical impedance spectroscopy (EIS) confirmed the fast ion transport within the LSG electrodes. A complex plan plot of the impedance data of the LSG-EC is shown in Figure 3.2E with an expanded view provided in the inset. The device displays a pure capacitive behavior, even at high frequencies of up to ~158 Hz. The series resistance of the device is estimated to be ~16 ohms. This value can be attributed to the contact resistance of the device with the external circuit that could be reduced by using current collectors. The dependence of the phase angle on the frequency for the LSG-EC, AC-EC, and an aluminum electrolytic capacitor is shown in Figure 3.2F. For frequencies up to 10 Hz, the phase angle of the LSG-EC is close to $-90°$, which suggests that the device functionality is close to that of an ideal capacitor. The characteristic frequency f_0 for a phase angle of $-45°$ is 30 Hz for the LSG-EC. This frequency marks the point at which the resistive and capacitive impedances are equal (22). The corresponding time constant τ_0 ($=1/f_0$) equals 33 ms compared with 10 s for the conventional AC-EC and 1 ms for the aluminum electrolytic capacitor. This rapid frequency response of the LSG-EC can be accounted for by the large and accessible surface area of the LSG, whose exposed flat sheets enhance the ion transport rate in the device (23). This is consistent with results reported recently for an EC made from vertically oriented graphene nanosheets grown directly on metal current collectors (24-26) and carbon nanotube electrodes made with an electrophoretic deposition technique (27, 28).

The future development of multifunctional flexible electronics such as roll-up displays, photovoltaic cells, and even wearable devices presents new challenges for designing and fabricating lightweight, flexible energy storage devices (29). Commercially available ECs consist of a separator sandwiched between two electrodes with liquid electrolyte, which is then either spirally wound and packaged into a cylindrical container or stacked into a button cell (3).

Unfortunately, these device architectures not only suffer from the possible harmful leakage of electrolytes, but their design makes it difficult to use them for practical flexible electronics. We replaced the liquid electrolyte with poly(vinyl alcohol) (PVA)-H_3PO_4 polymer gelled electrolyte, which also acts as the separator (Figure 3.3A, device structure). This electrolyte reduced the device thickness and weight compared with phosphoric acid and simplified the fabrication process because it does not require any special packaging materials. As demonstrated in Figure 3.3B, at any given charge/discharge rate the specific capacitance values for the all-solid-state device were comparable with those obtained with an aqueous electrolyte. The high-rate performance of this device can be accounted for by the porous structure of the LSG electrodes, which can effectively absorb the gelled electrolyte and act as an electrolyte reservoir to facilitate ion transport and minimize the diffusion distance to the interior surfaces (30). Another key factor is that LSG electrodes are binder free—thus, enabling a reduction in interfacial resistance and enhancing the electrochemical reaction rate. The device performance was completely stable over 4 months of testing (Figure 3.3C). As with the aqueous LSG-EC, the flexible all-solid-state LSG-EC maintains its excellent cycling stability: >97% of the initial capacitance was maintained even after 10,000 cycles (Figure 3S.10).
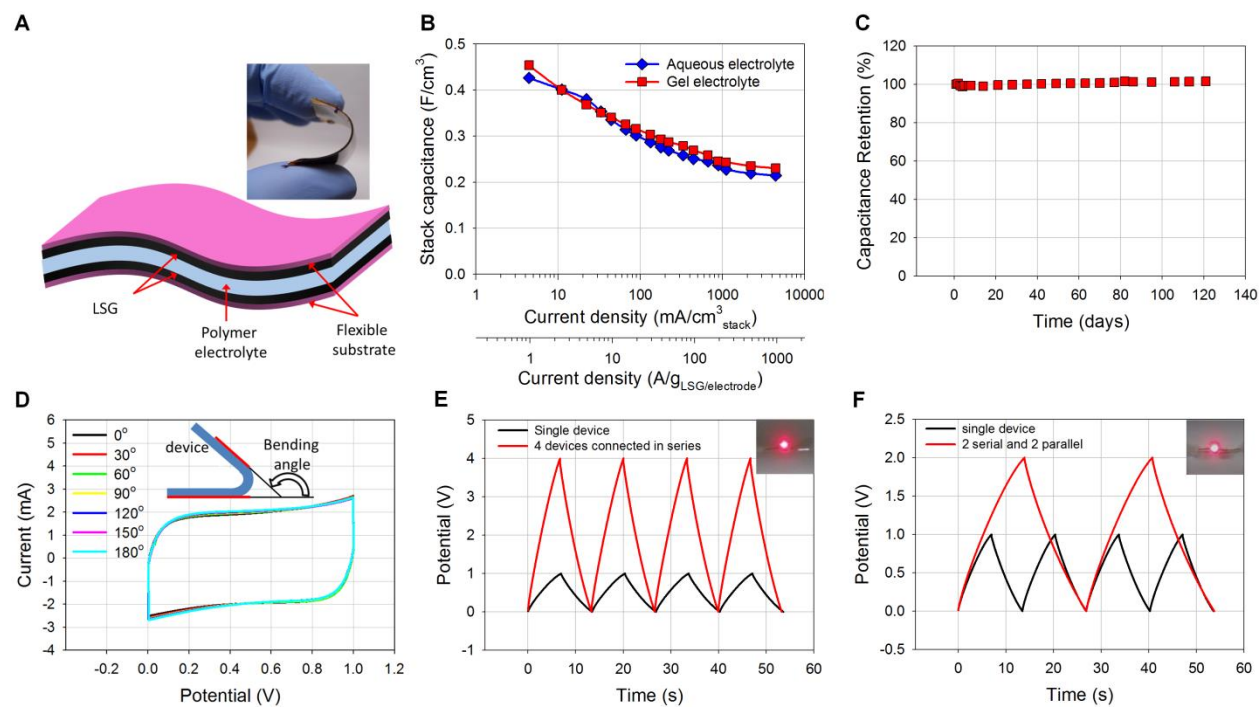
Figure 3.3: Design and fabrication of a flexible, all-solid-state LSG electrochemical capacitor. (**A**) A schematic diagram of the all-solid-state LSG-EC illustrates that the gelled electrolyte can serve as both the electrolyte and separator. (Inset) A digital photograph showing the flexibility of the device. (**B**) A comparison between performances of LSG-EC using gelled versus aqueous electrolytes. Both devices show similar capacitance values at all the tested charge/discharge current densities. (**C**) A shelf-life test shows excellent stability for over 4 months without any obvious degradation. (**D**) Bending the device has almost no effect on its performance, as seen in these CVs collected at a scan rate of 1000 mV/s. Galvanostatic charge/discharge curves for four tandem ECs connected (**E**) in series, and (**F**) in a combination of series and parallel. A single device is shown for comparison. Both the tandem devices and the single device were operated at the same constant current charge/discharge. The serial connection extends the output voltage to 4 V (versus 1 V for a single device), whereas the output voltage and current can both be doubled with the serial-parallel connection. (Insets) The glow of an LED when powered by tandem LSG-ECs.

In order to evaluate under real conditions the potential of this all-solid-state LSG-EC for flexible energy storage, a device was placed under constant mechanical stress and its performance analyzed. The CV performance of this device when tested under different bending conditions is shown in Figure 3.3D. The bending had almost no effect on the capacitive behavior; it can be bent arbitrarily without degrading performance. Moreover, the stability of the device was tested for more than 1000 cycles while in the bent state, with only ~5% change in the device capacitance (Figure 3S.11). This performance durability can be attributed to the high mechanical flexibility of the electrodes along with the interpenetrating network structure between the LSG electrodes and the gelled electrolyte. The electrolyte solidifies during the device assembly and acts like a glue that holds all the device components together, improving the mechanical integrity and increasing its cycle life even when tested under extreme bending conditions. Because this remarkable performance has yet to be realized in commercial devices, these ECs may be ideal for next-generation flexible, portable electronics.

Portable equipment often require cells packaged either in series, in parallel, or in combinations of the two in order to meet energy and power requirements. For example, laptop batteries commonly have four 3.6-V lithium ion cells connected in series to achieve a voltage of 14.4 V, and two in parallel to increase the capacity from 2400 mAh to 4800 mAh (31). Thus, it would be of interest to develop an EC that could exhibit control over the operating voltage and current by using tandem serial and parallel assemblies with minimal energy losses. The performances of a set of tandem LSG-EC were evaluated by assembling four devices both in series and in parallel configurations. Compared with a single EC, which operates at 1.0 V, the tandem series ECs exhibited a 4.0-V charge/discharge voltage window (Figure 3.3E). In the parallel assembly, the output current increased by a factor of 4, and thus the discharge time was

four times that of a single device when operated at the same current density (figures 3S.12 to 3S.14). As expected, when the four ECs were combined two in series and two in parallel, both the output voltage and the runtime (capacitive current) increased by a factor of 2 under the same charge/discharge current (Figure 3.3F). As with the single devices, the tandem devices show essentially perfect triangular CC curves with a miniscule voltage drop, which again indicates excellent capacitive properties with minimal internal resistance. Thus, when used in tandem, the LSG-ECs undergo minimal energy losses. As a demonstration, a tandem EC's ability to light a red light-emitting diode (LED) that operates at a minimum voltage of 2 V is shown in the Figure 3.3, E and F, insets.

We also examined an organic electrolyte, which would allow the operation of the devices at higher voltages, thus achieving higher energy densities. In this case, tetraethylammonium tetrafluoroborate dissolved in acetonitrile was used because this is the most common organic electrolyte used in commercial devices (3). As shown in Figure 3.4, the LSG-EC again exhibits enhanced performance and rate capabilities when compared with the commercial AC-EC; this is consistent with the data acquired in the aqueous and gelled electrolytes. Furthermore, the LSG-EC can be operated over a wider voltage window of 3 V. This EC offers a specific capacitance of up to 4.82 mF/cm^2 (265 F/$g_{LSG/electrode}$) and retains a capacitance of 2.07 mF/cm^2 when operated at the ultrahigh current density of 1000 A/$g_{LSG/electrode}$ (Figure 3S.15).
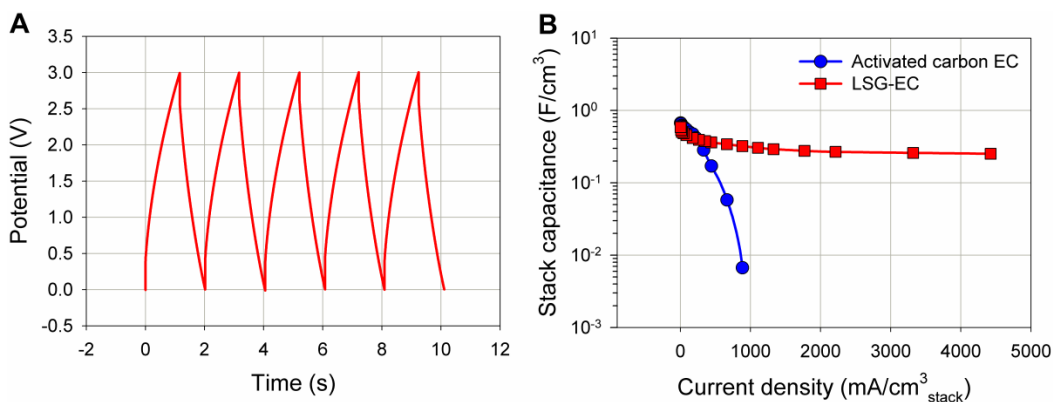
Figure 3.4: The performance of a LSG electrochemical capacitor using an organic electrolyte of 1.0 M tetraethylammonium tetrafluoroborate dissolved in acetonitrile. (**A**) Galvanostatic charge/discharge curves of the device when operated at an ultrahigh current density of 250 A/$g_{LSG/electrode}$, showing near symmetric triangular shapes. (**B**) Stack capacitance values calculated from galvanostatic curves as a function of the applied charge/discharge current density showing the high rate performance possible with a LSG-EC versus that of an activated carbon EC.

Recently, room-temperature ionic liquids have been intensively studied as an attractive alternative to conventional electrolytes for ECs because of their high ion density, good thermal stability, and nonvolatility, as well as their wider potential window when compared with organic electrolytes (14, 32). We fabricated an LSG-EC using the ionic liquid 1-ethyl-3-methylimidazolium tetrafluoroborate (EMIMBF$_4$) that exhibited a specific capacitance as high as 5.02 mF/cm^2 (276 F/$g_{LSG/electrode}$) and at a wider potential window of 4 V (Figure 3S.16). A prototype LSG-EC was made and encapsulated in the EMIMBF$_4$ electrolyte, charged at a constant potential of 3.5 V, and used to light up a red LED for ~24 min (movie 3S.1).

In order to demonstrate the overall performance of the LSG-ECs using various electrolytes, a Ragone plot is shown in Figure 3.5 comparing the performance of LSG-ECs with different energy storage devices designed for high-power microelectronics. This includes a commercial 2.75 V/44 mF AC-EC and a 500-μAh thin-film lithium battery and a 3 V/300 μF

aluminum electrolytic capacitor, all tested under the same dynamic conditions (Appendix, section 3.5.8). The plot shows the volumetric energy density and power density of the stack for all the devices tested. The LSG-EC can exhibit energy densities of up to 1.36 mWh/cm^3, a value that is approximately two times higher than that of the AC-EC. Additionally, LSG-ECs can deliver a power density of ~20 W/cm^3, which is 20 times higher than that of the AC-EC and three-orders of magnitude higher than that of the 500-µAh thin-film lithium battery. Although the electrolytic capacitor delivers ultrahigh power, it has an energy density that is three orders of magnitude lower than the LSG-EC.
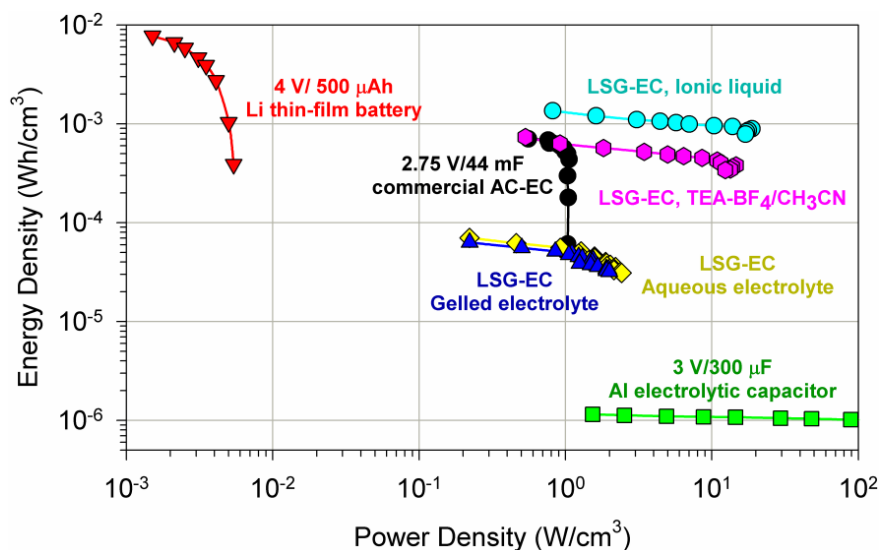
Figure 3.5: Energy and power densities of LSG-ECs compared with commercially available AC-EC, aluminum electrolytic capacitors, and a lithium thin-film battery. The LSG-ECs exhibit electrochemical energy storage with both ultrahigh power and energy densities. [The data for the Li thin-film battery are reproduced from (5) with permission from Nature Publishing Group]

3.4 CONCLUSIONS

We have fabricated graphene ECs with an unusually high power density and energy density using a consumer grade LightScribe DVD burner. Because of the simplicity of the device architecture and the availability of the graphite oxide precursor, which is already manufactured on the ton scale, these LSG-ECs hold promise for commercial applications.

3.5 MATERIALS AND METHODS

3.5.1 Synthesis of Laser Scribed Graphene (LSG) electrodes: GO was synthesized from high purity graphite powder using a modified Hummer's method as reported previously (33). Dispersions of GO in water (3.7 mg/mL) were then used to make GO films on various substrates, including polyethylene terephthalate (PET), nitrocellulose membrane (with 0.4 μm pore size), aluminum foil, and regular Xerox paper, among others. GO films were made by either drop-casting or vacuum filtering GO dispersions onto substrates that were previously cut to the size of a CD/DVD media disc. The films were then allowed to dry for 24 hours under ambient conditions (Figure S1). These films were affixed on top of a LightScribe enabled DVD media disc and moved into the DVD optical drive for laser treatment. LightScribe is a direct labeling technology that patterns text and graphics onto the surface of a CD/DVD disc. LightScribe DVD drives are commercially available for ~ $20 and the LightScribing process is completely controlled by a standard desktop computer. The drive uses a laser (optimum power output = 5 mW, wavelength = 788 nm) to pattern a computer-generated image onto a light sensitive dye that changes color when hit with the laser; here, we use the GO film instead. The images are patterned in concentric circles, moving outward from the center of the disc as shown

schematically in Figure 3.1. The laser irradiation process results in the removal of oxygen species and the re-establishment of the sp^2 carbons. This causes a change in the conductivity of the film from the insulating graphite oxide, with a typical resistance of >20 MΩ/sq to highly conducting laser scribed graphene. We have shown that the number of times a film is laser-treated results in a significant and controllable change in conductivity (17). The electrodes used in the fabrication of the electrochemical capacitors are laser irradiated 6 times reaching an excellent conductivity of 1738 S/m. The laser irradiation process takes about 20 min per cycle. The produced laser scribed graphene (LSG) possesses very low oxygen content (only 3.5%) (17) that contributes to the very high cycling stability of the electrochemical capacitor. The thickness of the LSG layer, as measured from cross-sectional SEM and profilometry, was found to be ~7.6 µm (Figure S2). In the actual device, the area made accessible to the electrolyte was 1 cm^2, which corresponds to a mass of 36.3 µg of the active material (LSG) per electrode or 72.8 µg for the device.

3.5.2 Electromechanical properties of laser scribed graphene electrodes: Flexible electronics have impacted our life in several ways, including flexible transistors, sensors, displays, etc. They are made possible by using flexible, mechanically robust and highly conducting electrodes. Nowadays, there is a great interest in using graphene films as flexible electrodes in these devices because of its excellent electrical, mechanical and optical properties (34). Here, we have investigated the electromechanical properties of the LSG electrodes to explore their potential for flexible devices. Figure S3A shows the change in the resistance of an LSG electrode as a function of its bending radius. The electrical resistance shows a small decrease (2.8%) upon bending and this change is completely reversible by straightening the electrode back to its original flat state. Interestingly, the electrical resistance of the electrodes fluctuated up and down

with only ~1% change after 1000 repeated bending cycles, Figure S3B. Thus, LSG electrodes hold promise for other flexible electronics besides the electrochemical capacitors discussed in this paper.

3.5.3 Measurement of the specific surface area of laser scribed graphene: The surface area for the LSG was calculated to be ~1520 m^2/g using the methylene blue adsorption method. Methylene blue is a common dye probe used to determine the surface area of graphitic materials, with each molecule of adsorbed methylene blue representing 1.35 nm^2 of surface area (35-38). The surface area was calculated by adding a known mass of LSG into a standard concentration of methylene blue in DI water. LSG was stirred in the methylene blue solution continuously at a rate of 300 rpm for a total of 24 hr to reach maximum adsorption. The mixture was then allowed to settle and further centrifuged to remove any suspended material. The methylene blue concentration was determined by analyzing the supernatant through UV-vis spectroscopy at a wavelength of 665 nm and compared to the initial standard concentration of methylene blue prior to interacting with LSG.

3.5.4 Fabrication of LSG electrochemical capacitors: A simple device architecture has been employed to make the LSG electrochemical capacitors. Two LSG films serve as both electrodes and current collectors in a symmetric two-electrode cell configuration. LSG films made on various substrates are flexible and mechanically robust and thus can be directly used as electrochemical capacitor electrodes without any additional binders or conductive additives. Additionally, the high conductivity of the LSG films enables the construction of devices without the need for metallic current collector electrodes used in commercial electrochemical capacitors. In a typical device, an ion-porous separator [Celgard® 3501, (Celgard, Charlotte, NC)] was sandwiched between two identical pieces of LGC films (area, ~2 cm^2) in a layered structure (see

Figure 3.1). This layered assembly was wrapped with Kapton tape and then dipped in the electrolyte. To evaluate the electrochemical capacitor performance, the device was connected to an electrochemical workstation using alligator clips. Electrode edges were lightly painted with conducting silver paint to ensure good electrical contact between the LSG films and the alligator clips. The dimensions of the device and volume are shown in Figure S4. Celgard® 3501 separators were generously supplied by Celgard, LLC Corporate Headquarters in Charlotte, NC, USA.

3.5.5 Fabrication of all-solid-state flexible LSG electrochemical capacitors: All solid-state devices were assembled by pouring the polymer gelled electrolyte (100 µL electrolyte/1 cm^2 of the electrode) slowly onto the LSG electrodes. This assembly was left under ambient conditions for 5 hours to ensure that the electrolyte completely wets the electrode and to allow for evaporation of any excess water. Two electrodes were then assembled face-to-face and left overnight until the electrolyte solidified. This results in mechanically robust devices with the polymer electrolyte acting as both the electrolyte and the ion-porous separator. The solidified polymer electrolyte simplifies the device architecture and helps maintain the electrodes in closer proximity.

3.5.6 Preparation of the polymer gelled electrolyte: The gelled electrolyte was prepared according to the method described in reference (39). Briefly, polyvinyl alcohol (PVA) (molecular weight 89,000-98,000, 99% hydrolyzed, Sigma-Aldrich) powder was mixed with water (1 g PVA/10 g H$_2$O). The mixture was heated at ~90 °C under constant stirring until the solution turned clear. After cooling under ambient conditions, 0.8 g of concentrated phosphoric acid solution (85% solution in water, Fisher Scientific) was added and the solution was stirred thoroughly.

3.5.7 Characterization of the electrochemical capacitors: The performance of our prototype electrochemical capacitors were evaluated by cyclic voltammetry (CV), galvanostatic charge/discharge (CC) curves using a VersaSTAT3 electrochemical workstation (Princeton Applied Research, USA). The electrochemical capacitor performances were evaluated in various electrolytes including aqueous and organic electrolytes as well as ionic liquids. Two different aqueous electrolytes were used, 1.0 M H_3PO_4 and 1.0 M H_2SO_4 (Sigma-Aldrich). The organic electrolyte consisted of 1.0 M tetraethylammonium tetrafluoroborate (Simga-Aldrich) in dry acetonitrile (Sigma-Aldrich). The ionic liquid, 1-ethyl-3-methylimidazolium tetrafluoroborate ($EMIMBF_4$) was obtained from Sigma-Aldrich and was used without further treatment. Electrochemical impedance spectroscopy (EIS) was carried out on a Solartron electrochemical workstation (Solartron Analytical, Oak Ridge, TN). EIS experiments were carried out at open circuit potential with a sinusoidal signal with amplitude of 10 mV over a frequency range of 100 kHz to 10 mHz. The sheet resistance and conductivity values were calculated from two-point probe measurements and the film thicknesses. The morphologies of GO and LSG were imaged using scanning electron microscopy (JEOL 6700, Philips XL 30). The film thicknesses of each layer in the device (e.g., the penetration depth of the laser into the GO layer, LSG layer, gelled polymer layer, etc.) were measured on a Dektak 6 profilometer and using cross-sectional scanning electron microscopy. The device dimensions are summarized in Figure S4.

3.5.8 Characterization of commercial capacitors: A commercially available activated carbon electrochemical capacitor, PANASONIC EECS0HD223H Supercap 5.5 V, 22 mF was used. It consists of two electrochemical capacitors connected in series. A single device was separated from this serial assembly for characterization. An aluminum electrolytic capacitor, Mouser

Electronics, 75-TE1066-E3, 3V/300μF was also tested. All the devices were characterized under the same dynamic conditions as the LSG-EC.

3.5.9 Tandem electrochemical capacitors: To be useful as energy storage devices in vehicles and peak-load applications, tandem electrochemical capacitors are usually assembled in series, in parallel or in combinations of the two. By choosing different tandem electrochemical capacitor assemblies, it is possible to control and improve the output potential and current (capacitance) so that the energy and power requirements can be met. Tandem LSG electrochemical capacitors were made simply by wiring four devices together in series, in parallel and in series-parallel combinations and characterized as shown in Figures S12-S14.

3.5.10 Calculations: The capacitance of each device was calculated from the galvanostatic (CC) curves at different current densities using the formula:

$$C_{device} = i/(-dV/dt) \qquad (1)$$

Where i is the current applied (in amps, A), and dV/dt is the slope of the discharge curve (in volts per second, V/s). Specific capacitances were calculated based on the area or the volume of the device stack according to the following formulae:

$$Areal\ capacitance = C_{device}/A \qquad (2)$$

$$Volumetric\ stack\ capacitance = C_{device}/V \qquad (3)$$

Where A and V refer to the area (cm^2) and the volume (cm^3) of the device, respectively. It is worth mentioning that the volumetric capacitances were calculated taking into account the volume of the device stack. This includes the active material, the flexible substrate (or the current collector) and the separator with electrolyte. For the device testing, we did not include

67

the packaging. The area and volume of the device used in the calculations can be found in Figure S4.

The electrochemical performance of each device reported in Figure 3.5 is based on the volume of the stack and measured under the same dynamic conditions from galvanostatic curves. The power of each device was calculated from the galvanostatic curves at different charge/discharge current densities using the formula given in Equation (4):

$$P = (\Delta E)^2/4R_{ESR}V \qquad (4)$$

where P is the power (W/cm^3), ΔE is the operating voltage window (measured in volts and obtained from the discharge curve excluding the IR drop) and V is the volume of the stack as indicated earlier (in cm^3). R_{ESR} is the internal resistance of the device which can be estimated from the voltage drop at the beginning of the discharge, V_{drop}, at a constant current density (i) using the formula $R_{ESR} = V_{drop}/2i$.

The energy density of the device was obtained from the formula given in Equation (5):

$$E = C_V \times (\Delta E)^2/(2 \times 3600) \qquad (5)$$

where E is the energy density in Wh/cm^3, C_V is the volumetric stack capacitance obtained from Equation (3) in F/cm^3 and ΔE is the operating voltage window in volts.
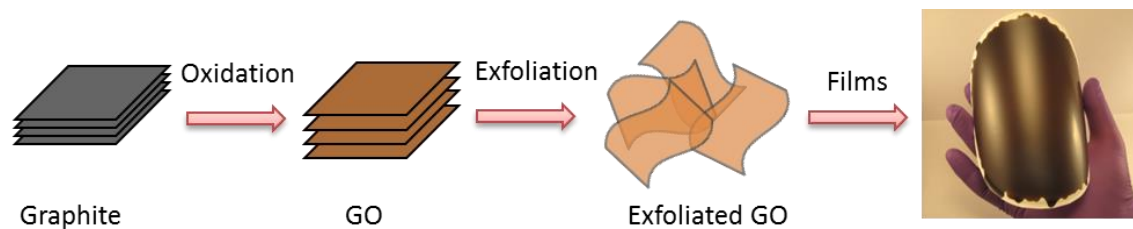
Figure 3S.1. Schematic illustration of the preparation of GO films: (A) The GO precursor is made by oxidation of graphite using a modified Hummer's method and then dispersed in water by ultrasonication. GO films are coated onto various flexible substrates such as polyethylene terephthalate, aluminum foil, a porous nitrocellulose membrane (shown in the photograph) or regular photocopy paper.
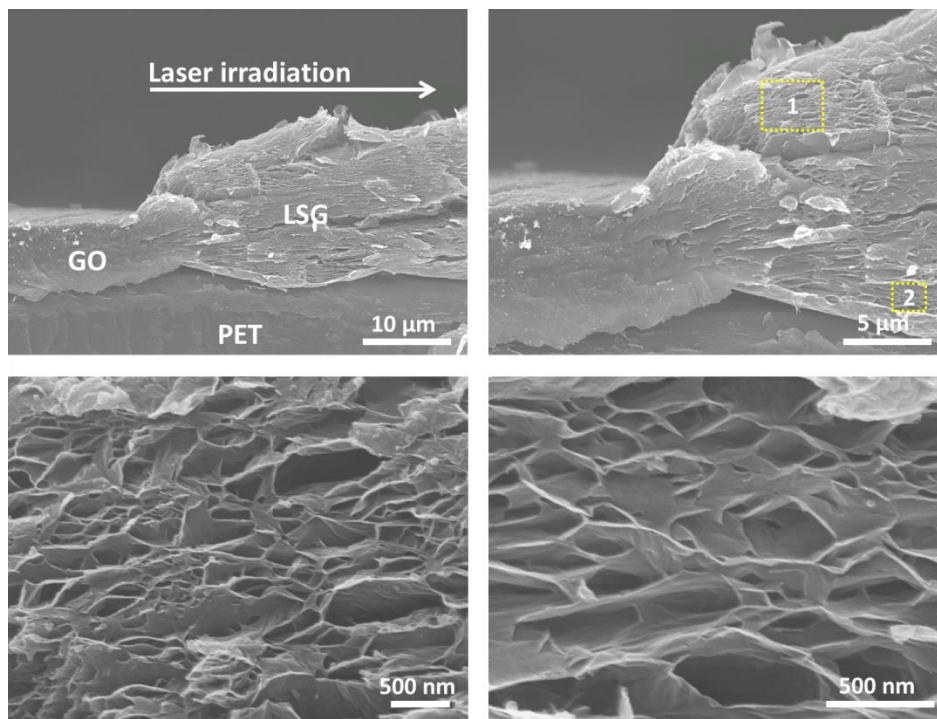
Figure 3S.2: Laser scribing of graphene from graphite oxide film on a polyethylene terephthalate (PET) flexible support. (A) A cross-sectional SEM image of the film at the interface between GO and LSG. As the LightScribe laser converts GO into LSG, a substantial expansion of the film is observed. (B) A zoomed-in view of the interface region. (C) and (D) show expanded views of the locations 1 and 2, respectively. The laser penetrates all the way into the film producing the expanded LSG network. The LSG electrode possesses a significant thickness and shows potential for electrochemical capacitors with high power and energy densities.
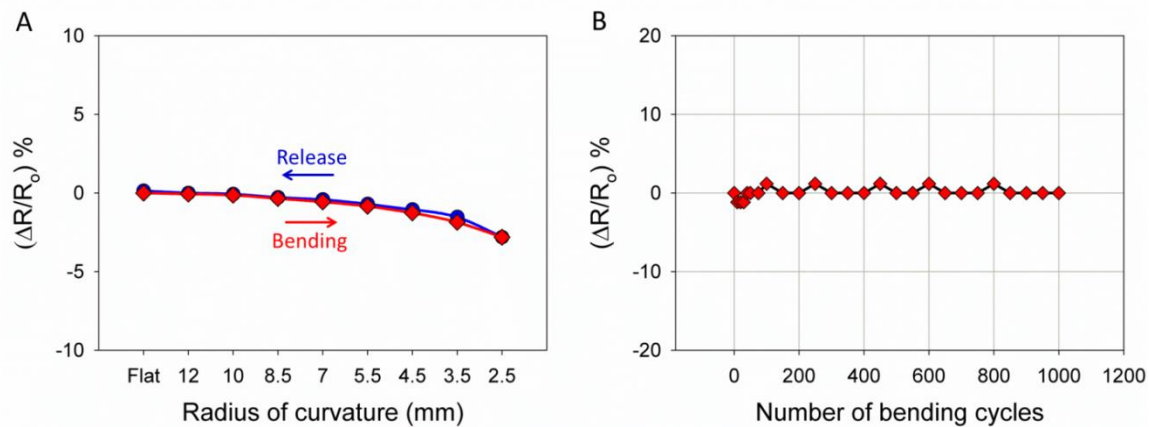
Figure 3S.3. Electromechanical properties of LSG electrodes made on polyethylene terephthalate (PET) flexible supports. (A) The electrical resistance change of an LSG electrode as a function of the bending radius. The electrode shows a decrease in the electrical resistance of ~2.8% and this change is completely reversible by flattening back the electrode to its original flat state. (B) The resistance change of an LSG electrode under repeated bending cycles for a bend radius of 5 mm. Only a slight change in resistance of ~1% can be observed after 1000 repeated bending cycles.
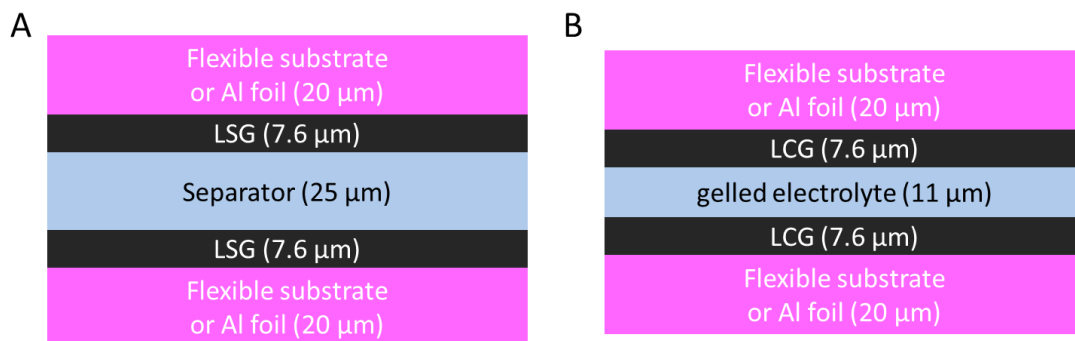
Figure 3S.4: Schematic diagrams showing cross-sections of the electrochemical capacitors with their device dimensions. (A) Two LSG electrodes are supported on a flexible substrate or an Al foil current collector and separated with an organic ion-porous separator [Celgard® 3501 (Celgard, Charlotte, NC)]. The electrolyte wets the LSG layer and the separator. This design of the electrochemical capacitor was tested in a variety of electrolytes including aqueous, organic and ionic liquid electrolytes. The device effective thickness is 82.2 µm, with an active area of 1 cm^2 and a volume of 8.22×10^{-3} cm^3. (B) In an all solid-state device, the organic separator is replaced with a gelled electrolyte that has a thickness of 11 µm and thus the device thickness becomes 68.2 µm with a volume of 6.82×10^{-3} cm^3.
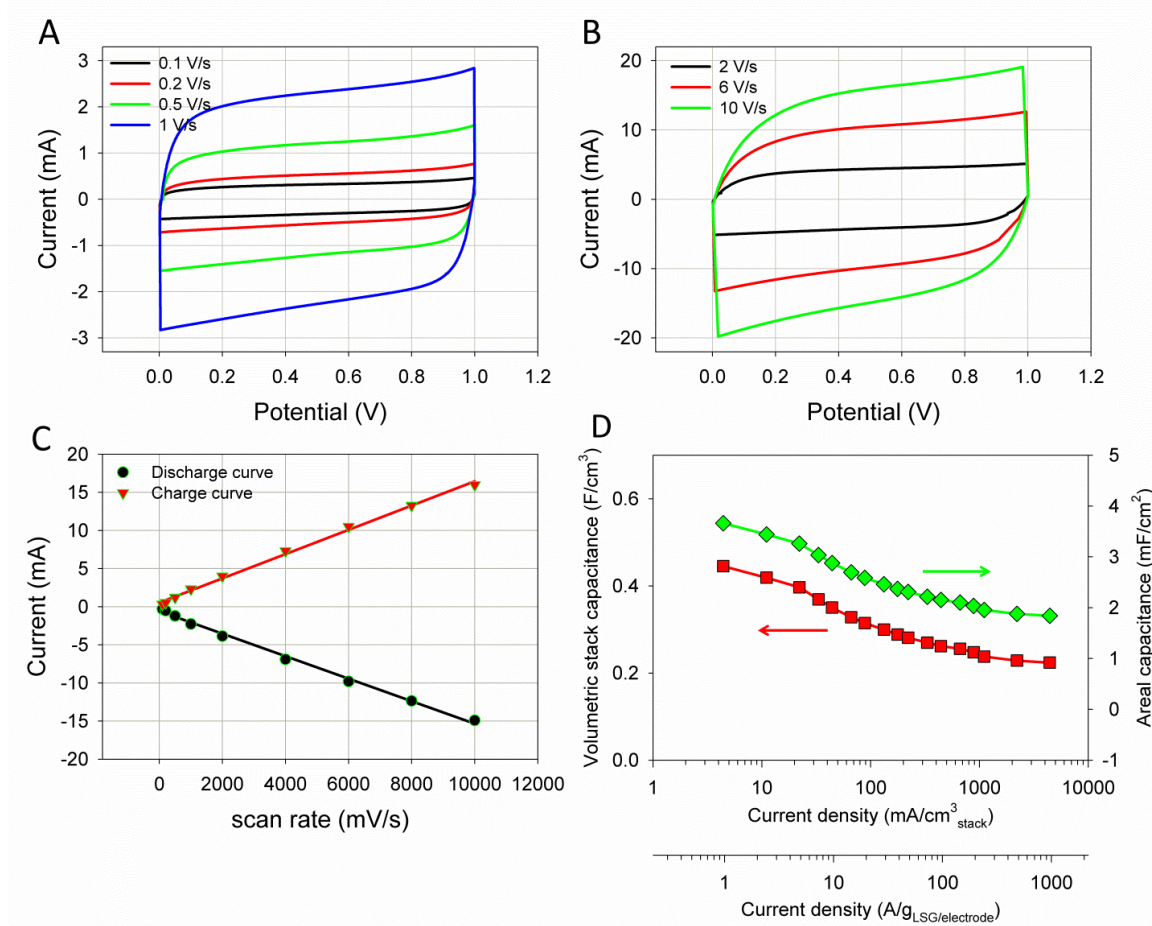
Figure 3S.5: Performance of an LSG electrochemical capacitor over a wide range of scan rates: cyclic voltammetry profiles of an LSG electrochemical capacitor in aqueous 1.0 M H_3PO_4 at different scan rates: (A) 100 mV/s to 1000 mV/s; and (B) 2000 mV/s to 10,000 mV/s. (C) The dependence of the capacitive current (extracted from the CV profiles at 0.5 V for the charge and discharge curves) on the applied scan rate. A linear relationship is observed with R^2 = 0.997 and 0.996 for the charge and discharge curves, respectively. (D) The specific capacitance of the device calculated from the galvanostatic curves as a function of the charge/discharge current density. The specific capacitance data are presented on the basis of the area of the device or the volume of the entire device stack (Figure S4). Note that the current density shown is based on the volume of the whole stack or the mass of the LSG in one electrode. The areal capacitance of the LSG-EC was calculated to be 3.67 mF/cm^2 at 1 A/g$_{LSG/electrode}$. This translates to a gravimetric capacitance of 202 F/g$_{LSG/electrode}$.
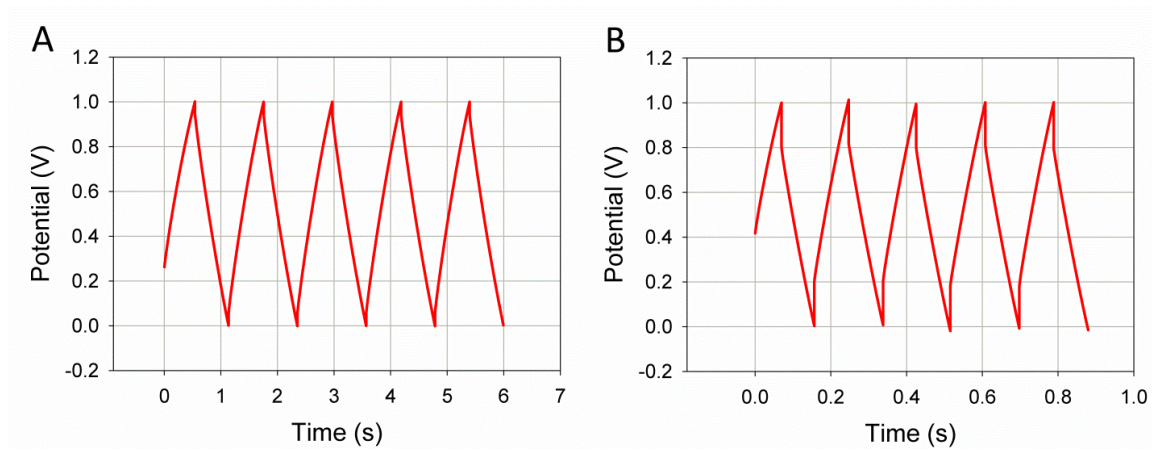
Figure 3S.6: Capability of an LSG electrochemical capacitor for ultrafast charging and discharging in the sub-second time scale as tested in aqueous 1.0 M H_3PO_4: galvanostatic charge/discharge curves obtained at ultrahigh current densities of (A) 100 A/g; and (B) 500 A/g (based on the mass of the LSG per electrode). As can be seen in B, the device can be efficiently charged/discharged multiple times in less than a second.
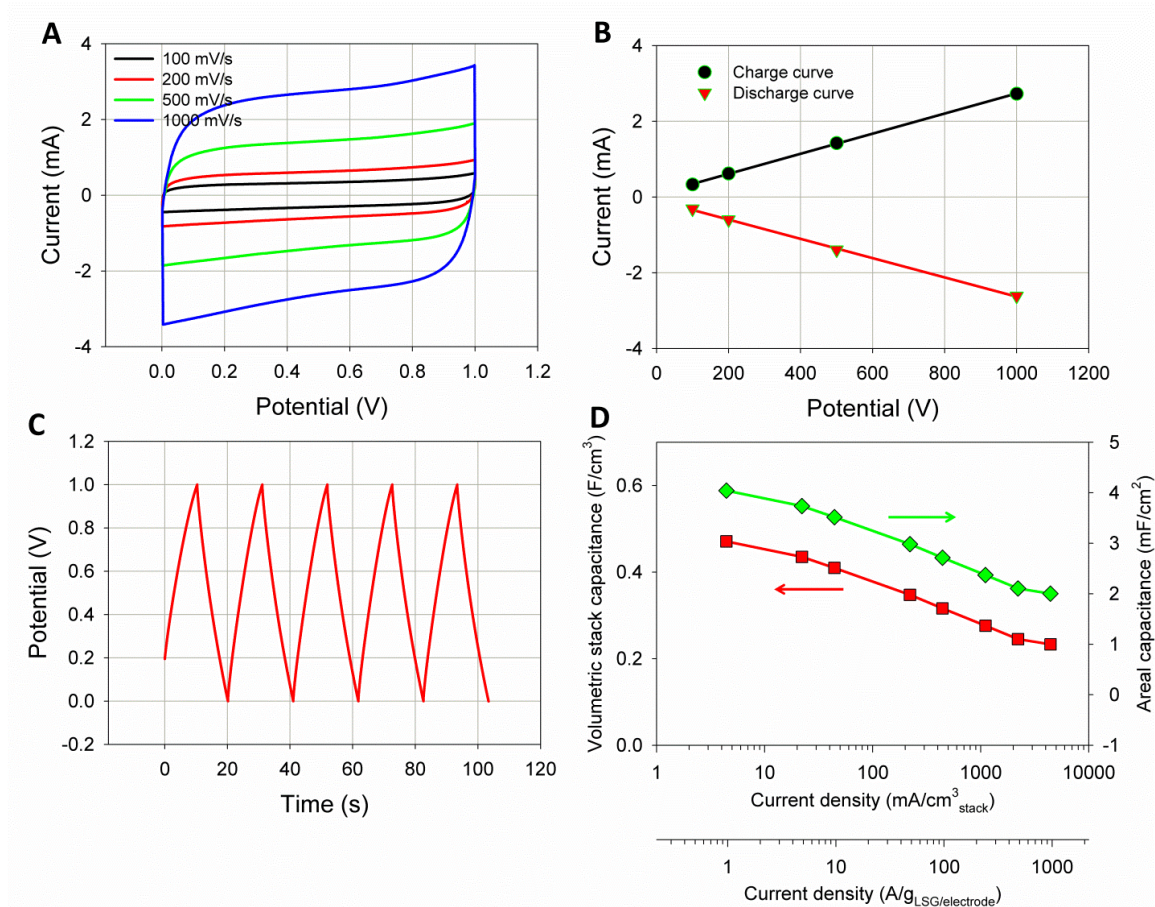
Figure 3S.7: Performance of an LSG electrochemical capacitor in aqueous 1.0 M H_2SO_4: (A) Nearly rectangular CV profiles are observed at increasing potential scan rates from 100 to 1000 mV/s. (B) A linear relationship is obtained between the capacitive current (extracted from the CV profiles at 0.5 V for the charge and discharge segments) and the scan rate with $R^2 = 0.9998$ for both curves. This trend confirms the formation of a pure electrostatic double layer. (C) Galvanostatic curves obtained at 10 A/$g_{LSG/electrode}$; the device exhibits a voltage drop of only 0.014 V at the beginning of the discharge curve. This corresponds with a low internal resistance for the device. (D) Specific capacitance (areal and volumetric) as a function of the charge/discharge current density. The device shows an areal capacitance of 4.04 mF/cm^2 at 1 A/$g_{LSG/electrode}$ which translates to a gravimetric capacitance of 222 F/$g_{LSG/electrode}$.
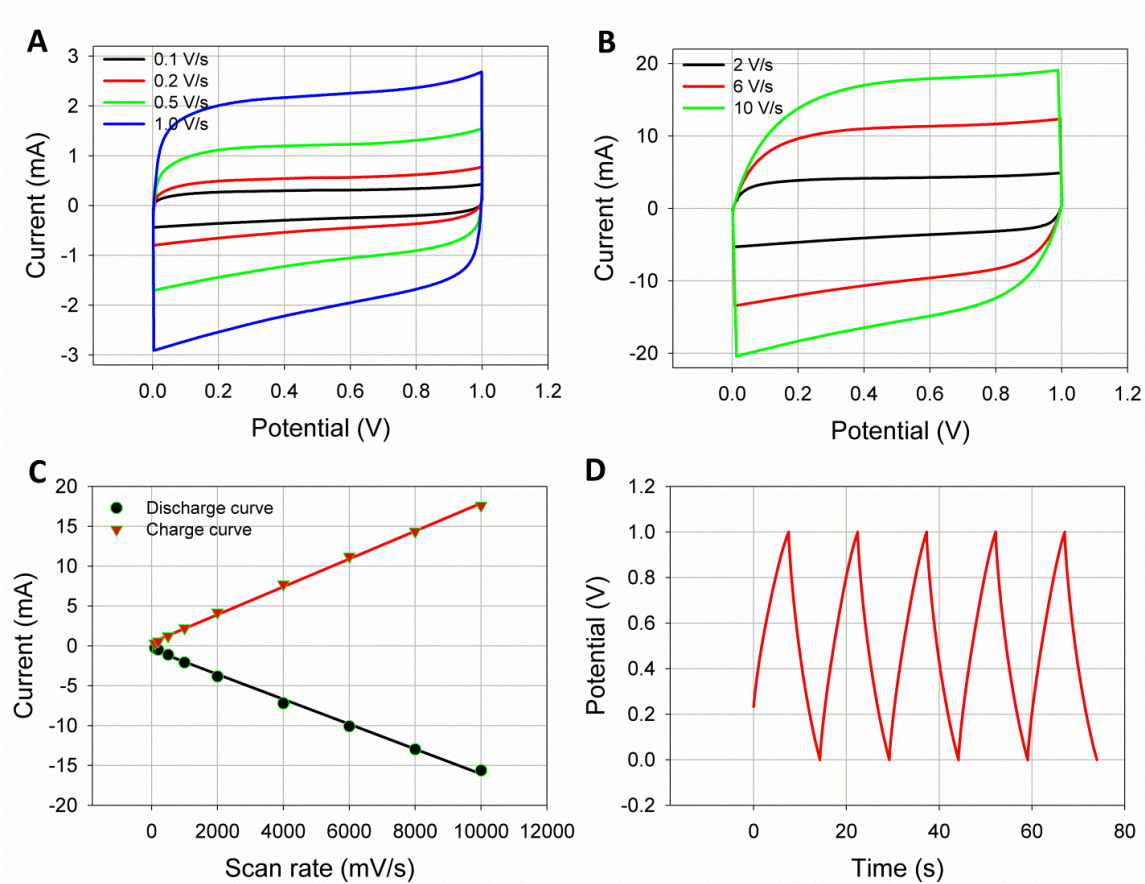
Figure 3S.8: Performance of an LSG electrochemical capacitor when supported on a nitrocellulose membrane in aqueous 1.0 M H_3PO_4: (A) CV profiles at different scan rates (A) from 100 to 1000 mV/s and (B) from 2,000 to 10,000 mV/s. Nearly rectangular CV profiles are obtained at all the scan rates; (C) A linear relationship is observed between the capacitive current (extracted from the CV profiles at 0.5 V for the charge and discharge segments) and the scan rate with $R^2 = 0.9985$ and 0.9970 for the charge and discharge curves, respectively. (D) Galvanostatic curves obtained at 10 A/$g_{LSG/electrode}$; the device exhibits a voltage drop of only 0.019 V at the beginning of the discharge curve. This corresponds to a very low internal resistance for the device. These data show that an LSG can be made on different substrates and still maintain its high performance.
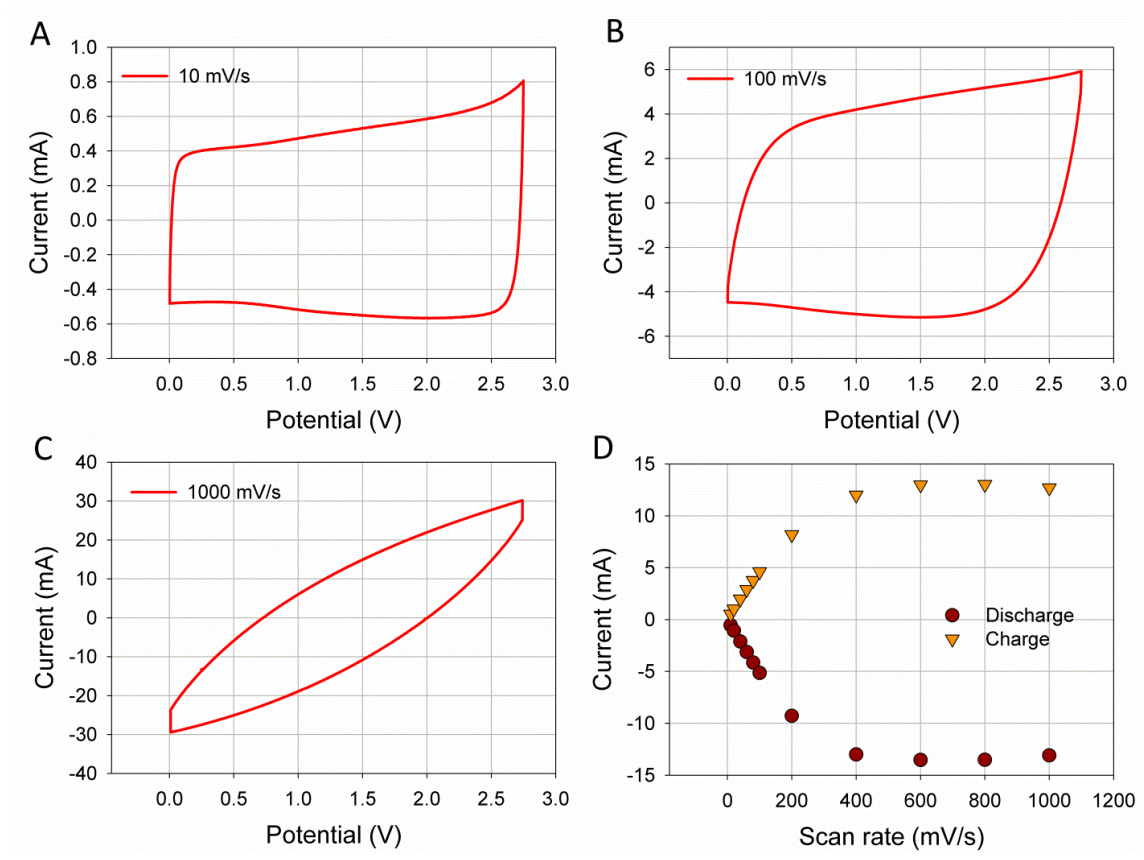
Figure 3S.9: Electrochemical characterization of the performance of a commercially available activated carbon electrochemical capacitor: CV profiles of the device shown in a potential window of 2.75 V at different scan rates of (A) 10 mV/s (B) 100 mV/s and (C) 1000 mV/s. In contrast to the LSG electrochemical capacitors, this commercial device exhibits the desired rectangular CV shape only at slow scan rates, 10 to 100 mV/s; (D) Dependence of the capacitive current (extracted from the CV profiles at 1.375 V) on the potential scan rate. A linear relationship is observed only between 10-100 mV/s, indicating the limited rate performance of this activated carbon electrochemical capacitor.
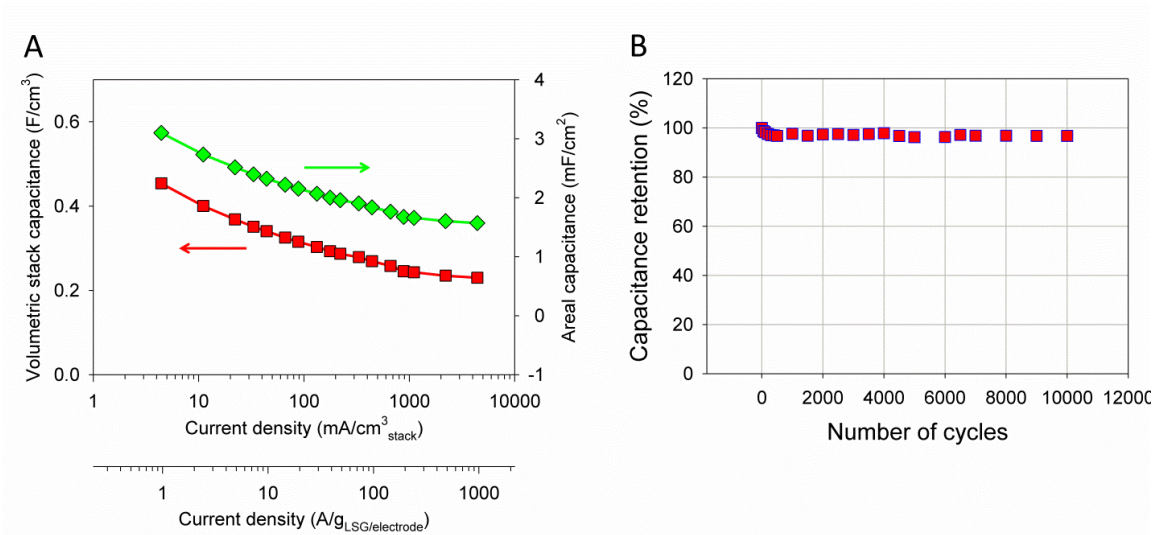
Figure 3S.10: Characterization of an all-solid state LSG electrochemical capacitor: (A) Areal and volumetric capacitance of the device as a function of the current density. (B) Cycling stability of an all solid-state LSG electrochemical capacitor: the device loses only about 3% of its capacitance after 10,000 cycles indicating very good cycling stability.
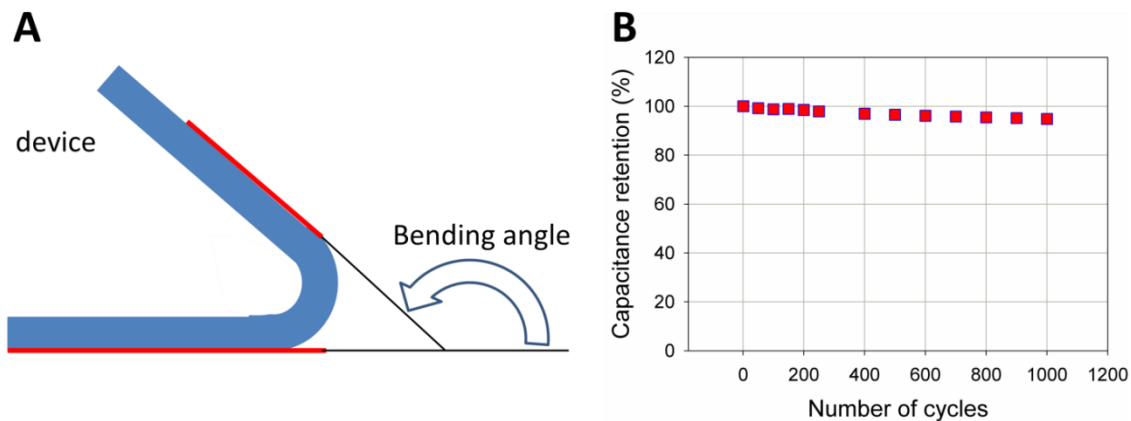
Figure 3S.11: Capability of an all solid-state LSG electrochemical capacitor for charge/discharge under bending conditions. (A) A schematic diagram showing the device under stress and defining the bend angle. (B) The device can be bent arbitrarily without any obvious decrease in performance compared to its planar state. The device retains about 95% of the initial capacitance after 1000 cycles when tested under the bent state (applying a bend angle = 150°).
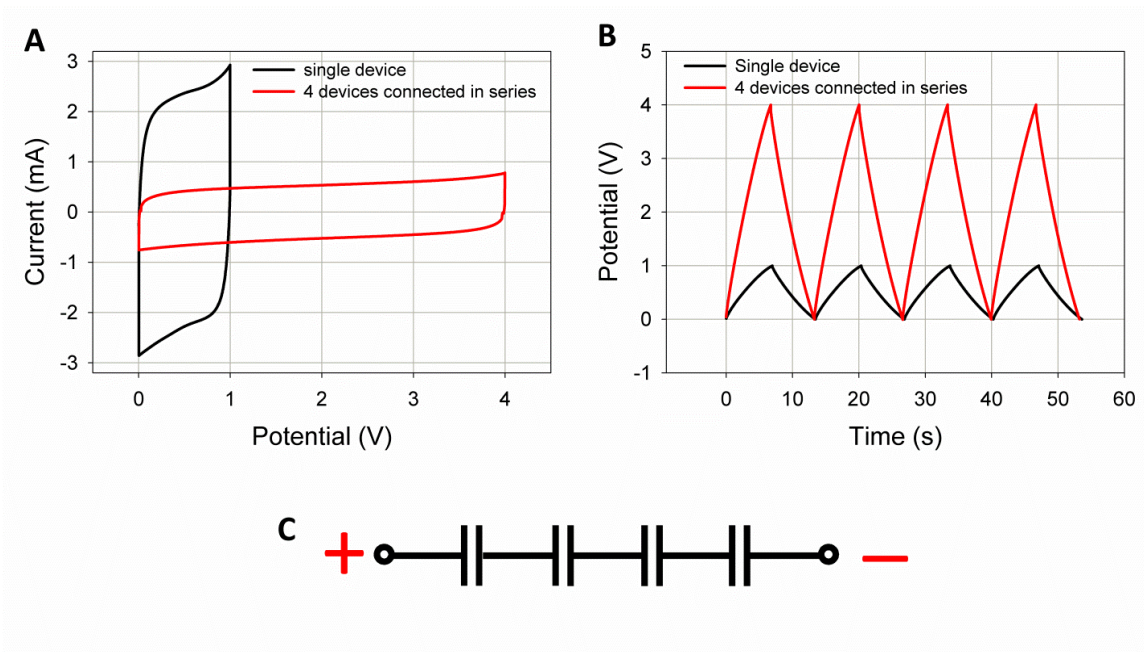
Figure 3S.12: Increasing the output voltage via tandem serial electrochemical capacitors: portable equipment needing higher voltages use device packs with two or more devices connected in series. Adding electrochemical capacitors together in a serial string increases the voltage, while the current remains the same. Here, the performance of an all solid-state electrochemical capacitor pack with 4 devices connected in series was tested. (A) Cyclic voltammetry at 1000 mV/s shows that the voltage is extended to 4 volts (vs. 1 volt for a single device), while the produced current (represented by the area under the curve) is essentially the same for the single device and for the cell pack; (B) Galvanostatic charge/discharge curves for a single device and for the cell pack were all operated under the same constant current conditions. As can be seen, at the same charge/discharge current, the voltage is extended from 1 volt for a single device to 4 volts for a cell pack. Interestingly, a very low voltage drop is observed in the CC curves of the device pack indicating low internal resistance. This helps optimize the useful energy that can be drawn from the device.
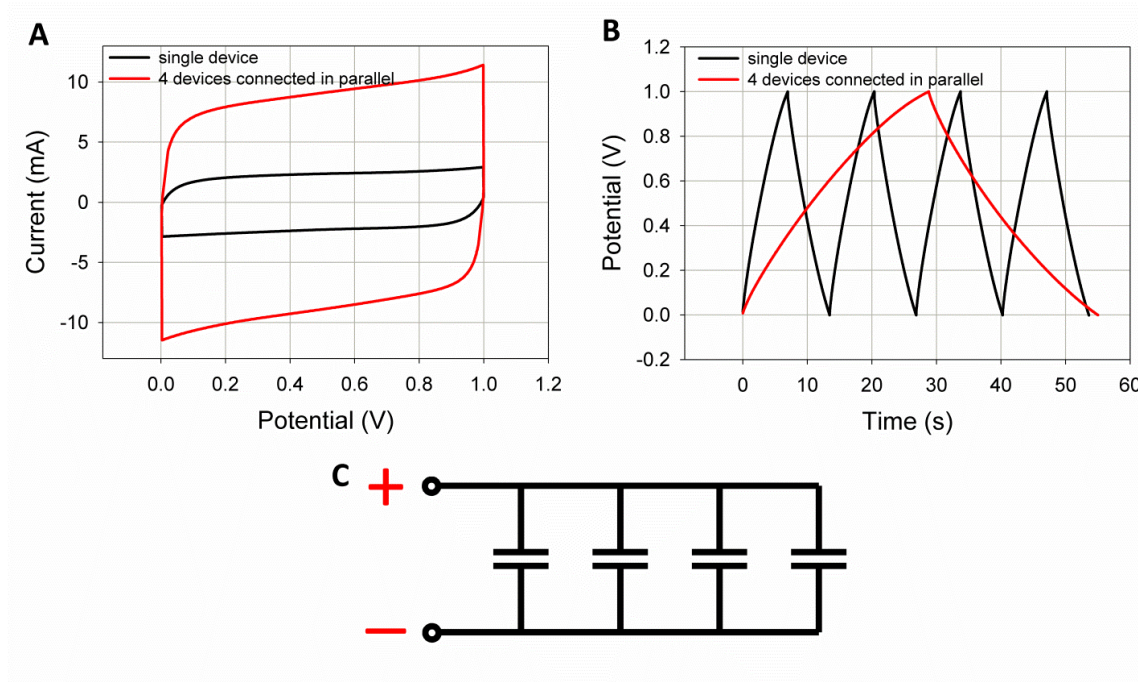
Figure 3S.13: Increasing the output current via tandem parallel electrochemical capacitors: If higher operating currents are needed, two or more cells can be connected in parallel. Putting electrochemical capacitors together in parallel enhances the output current, while the operating voltage remains the same. Here, the performance of an all solid-state electrochemical capacitor pack with 4 devices connected in parallel was tested; (A) Cyclic voltammetry at 1000 mV/s shows that the capacitive current increases by a factor of 4; (B) Galvanostatic charge/discharge curves for the single device and for the cell pack were all operated under the same constant current conditions. Clearly, the runtime of the electrochemical capacitor pack (and thus the ampere-hour rating) increases by a factor of 4 under the same charge/discharge current.
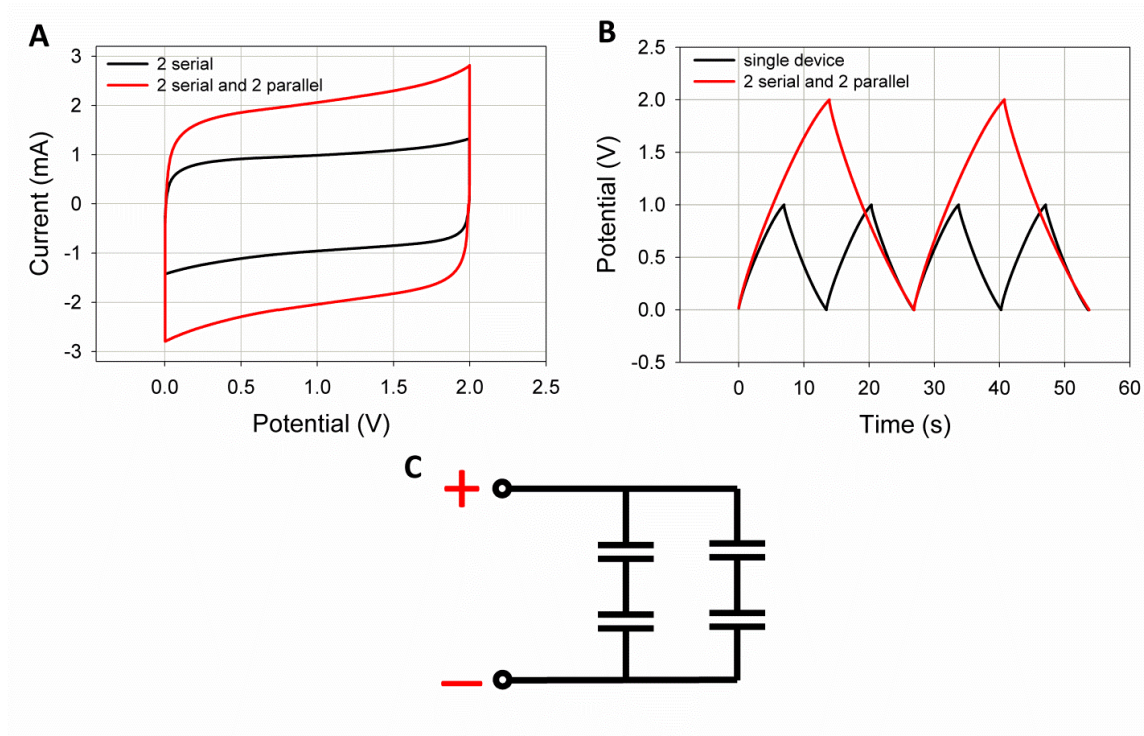
Figure 3S.14: Increasing the output voltage and current via tandem serial/parallel electrochemical capacitors: In a serial/parallel design, the electrochemical capacitors are connected in a way that produces both the required voltage and current. Here, the performance of an all solid-state electrochemical capacitor pack with 4 devices connected in serial/parallel as shown in C was tested: (A) Cyclic voltammetry at 1000 mV/s shows that both the output voltage and current increase by a factor of 2; (B) Galvanostatic charge/discharge curves for a single device and for the cell pack were all operated under the same constant current conditions. Clearly, both the output voltage and the runtime of the electrochemical capacitor pack increases by a factor of two under the same charge/discharge current.
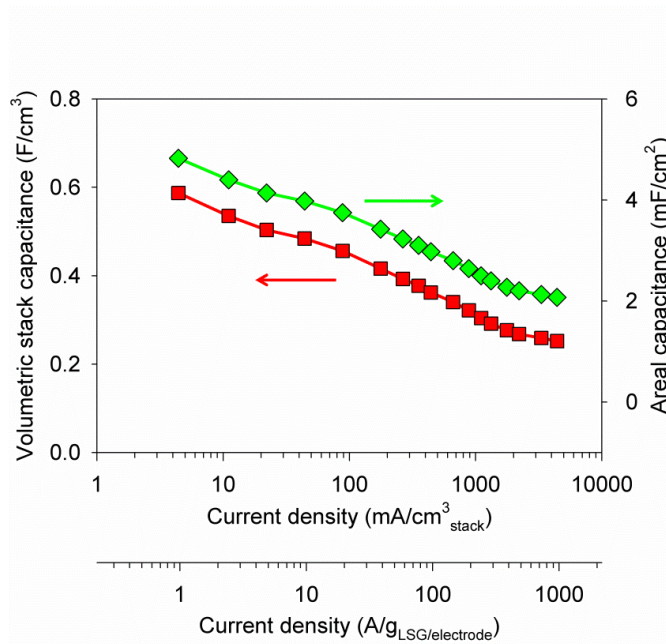
Figure 3S.15: The performance of an LSG electrochemical capacitor in an organic electrolyte of 1.0 M tetraethylammonium tetrafluoroborate (TEA-BF$_4$) in acetonitrile: The capacitance was calculated from the galvanostatic curves and represented in terms of the area or the volume of the device stack.
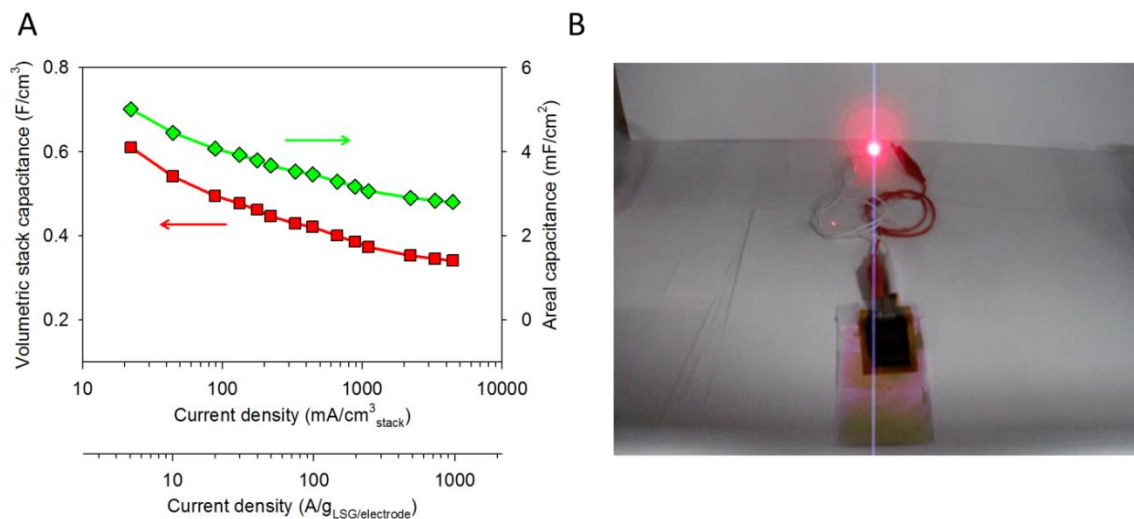
Figure 3S.16: Performance of an LSG electrochemical capacitor in the ionic liquid 1-ethyl-3-methylimidazolium tetrafluoroborate (EMIMBF$_4$). (A) Specific capacitance as calculated from the galvanostatic curves at different charge/discharge current densities. The electrochemical capacitor exhibits a high rate performance with a specific capacitance as high as ~5 mF/cm^2 (276 F/g based on the weight of the LSG on one electrode). (B) This charged electrochemical capacitor is used to light up a red light emitting diode.

Movie 3S.1

In this movie an LSG electrochemical capacitor is packaged in the ionic liquid 1-ethyl-3-methylimidazolium tetrafluoroborate (EMIMBF$_4$). After charging the electrochemical capacitor at a constant potential of 3.5 V, it is used to light up a red light emitting diode (with a minimum operating potential of 2 V) for about 24 minutes.

BIBLIOGRAPHY

1. C. Liu, F. Li, L.-P. Ma, H.-M. Cheng, Advanced materials for energy storage. *Adv. Energy Mater.* **22**, E28 (2010).

2. D. S. Su, R. Schlögl, Nanostructured carbon and carbon nanocomposites for electrochemical energy storage applications. *ChemSusChem* **3**, 136 (2010).

3. P. Simon, Y. Gogotsi, Materials for electrochemical capacitors. *Nat. Mater.* **7**, 845 (2008).

4. J. R. Miller, P. Simon, Materials science. Electrochemical capacitors for energy management. *Science* **321**, 651 (2008).

5. D. Pech *et al.*, Ultrahigh-power micrometre-sized supercapacitors based on onion-like carbon. *Nat. Nanotechnol.* **5**, 651 (2010).

6. J. Chmiola, C. Largeot, P. L. Taberna, P. Simon, Y. Gogotsi, Monolithic carbide-derived carbon films for micro-supercapacitors. *Science* **328**, 480 (2010).

7. J. Xia, F. Chen, J. Li, N. Tao, Measurement of the quantum capacitance of graphene. *Nat. Nanotechnol.* **4**, 505 (2009).

8. M. Segal, Selling graphene by the ton. *Nat. Nanotechnol.* **4**, 612 (2009).

9. M. D. Stoller, S. Park, Y. Zhu, J. An, R. S. Ruoff, Graphene-based ultracapacitors. *Nano Lett.* **8**, 3498 (2008).

10. Y. Wang *et al.*, Supercapacitor devices based on graphene materials. *J. Phys. Chem. C* **113**, 13103 (2009).

11. Z. Weng *et al.*, Graphene-cellulose paper flexible supercapacitors. *Adv. Energy Mater.* **1**, 917 (2011).

12. Y. Zhu *et al.*, Exfoliation of graphite oxide in propylene carbonate and thermal reduction of the resulting graphene oxide platelets. *ACS Nano* **4**, 1227 (2010).

13. W. Gao *et al*., Direct laser writing of micro-supercapacitors on hydrated graphite oxide films. *Nat. Nanotechnol.* **6**, 496 (2011).

14. C. G. Liu, Z. Yu, D. Neff, A. Zhamu, B. Z. Jang, Graphene-based supercapacitor with an ultrahigh energy density. *Nano Lett.* **10**, 4863 (2010).

15. Y. Zhu *et al*., Carbon-based supercapacitors produced by activation of graphene. *Science* **332**, 1537 (2011).

16. X. Yang, J. Zhu, L. Qiu, D. Li, Bioinspired effective prevention of restacking in multilayered graphene films: Towards the next generation of high-performance supercapacitors. *Adv. Mater. (Deerfield Beach Fla.)* **23**, 2833 (2011).

17. V. Strong *et al*., Patterning and electronic tuning of laser scribed graphene for flexible all carbon devices. *ACS Nano* 120215095449007 (2012).

18. R. Chandrasekaran, Y. Soneda, J. Yamashita, M. Kodama, H. Hatori, Preparation and electrochemical performance of activated carbon thin films with polyethylene oxide-salt addition for electrochemical capacitor applications. *J. Solid State Electrochem.* **12**, 1349 (2008).

19. S. W. Lee, B. M. Gallant, H. R. Byon, P. T. Hammond, Y. Shao-Horn, Energy. *Energy Environ. Sci.* **4**, 1972 (2011).

20. H. Zhang, X. Yu, P. V. Braun, Three-dimensional bicontinuous ultrafast-charge and -discharge bulk battery electrodes. *Nat. Nanotechnol.* **6**, 277 (2011).

21. L. L. Zhang, X. S. Zhao, Carbon-based materials as supercapacitor electrodes. *Chem. Soc. Rev.* **38**, 2520 (2009).

22. P. L. Taberna, P. Simon, J. F. Fauvarque, Electrochemical characteristics and impedance spectroscopy studies of carbon-carbon supercapacitors. *J. Electrochem. Soc.* **150**, A292 (2003).

23. Y. Shim, Y. J. Jung, H. J. Kim, Graphene-Based Supercapacitors: A computer simulation study. *J. Phys. Chem. C* **115** 23574 (2011).

24. X. Zhao *et al*., Carbon nanosheets as the electrode material in supercapacitors. *J. Power Sources* **194**, 1208 (2009).

25. J. R. Miller, R. A. Outlaw, B. C. Holloway, Graphene double-layer capacitor with ac line filtering performance. *Science* **329**, 1637 (2010).

26. J. R. Miller, R. A. Outlaw, B. C. Holloway, Graphene electric double layer capacitor with ultra-high-power performance. *Electrochim. Acta* **56**, 10443 (2011).

27. C. Du, N. Pan, Supercapacitors using carbon nanotubes films by electrophoretic deposition. *J. Power Sources* **160**, 1487 (2006).

28. C. Du, N. Pan, High power density supercapacitor electrodes of carbon nanotube films by electrophoretic deposition. *Nanotechnology* **17**, 5314 (2006).

29. H. Nishide, K. Oyaizu, Toward flexible batteries. *Science* **319**, 737 (2008).

30. D. W. Wang, F. Li, M. Liu, G. Q. Lu, H.-M. Cheng, 3D Aperiodic hierarchical porous graphitic carbon material for high-rate electrochemical capacitive energy storage. *Angew. Chem. Int. Ed.* **47**, 373 (2008).

31. D. Andrea, *Battery Management Systems for Large Lithium Ion Battery Packs* (Artech House, Norwood, MA, 2010).

32. J. F. Wishart, *Energy Environ. Sci.* **2**, 956 (2009).

33. N. I. Kovtyukhova *et al*., Layer-by-layer assembly of ultrathin composite films from micronsized graphite oxide sheets and polycations. *Chem. Mater.* **11**, 771 (1999).

34. Y. Zhu, Z. Sun, Z. Yan, Z. Jin, J. M. Tour, Rational design of hybrid graphene films for high performance transparent electrodes. *ACS Nano* **5**, 6472 (2011) and references therein.

35. P. T. Hang, G. W. Brindley, Methylene blue absorption by clay minerals. Determination of

surface areas and cation exchange capacities (Clay-Organic Studies XVIII). *Clays Clay Miner.* **18**, 203 (1970).

36. M. J. McAllister *et al*., Single sheet functionalized graphene by oxidation and thermal expansion of graphite. *Chem. Mater.* **19**, 4396 (2007).

37. R. S. Rubino, E. S. Takeuchi, The study of irreversible capacity in lithium-ion anodes prepared with thermally oxidized graphite. *J. Power Sources* **81**, 373 (1999).

38. M. Choucair, P. Thordarson, J. A. Stride, Gram-scale production of graphene based on solvothermal synthesis and sonication. *Nat. Nanotechnol.* **4**, 30 (2009).

39. M. Kaempgen, C. K. Chan, J. Ma, Y. Cui, G. Gruner, Printable thin film supercapacitors using single-walled carbon nanotubes. *Nano Lett.* **9**, 1872 (2009).

CHAPTER 4

Scalable Fabrication of High-Power Graphene Micro-Supercapacitors for Flexible and On-Chip Energy Storage

4.1 ABSTRACT

The rapid development of miniaturized electronic devices has increased the demand for compact on-chip energy storage. Microscale supercapacitors have great potential to complement or replace batteries and electrolytic capacitors in a variety of applications. However, conventional micro-fabrication techniques have proven to be cumbersome in building cost-effective micro-devices, thus limiting their widespread application. Here, we demonstrate a scalable fabrication of graphene micro-supercapacitors over large areas by the direct laser writing on graphite oxide films using a standard LightScribe DVD burner. More than 100 micro-supercapacitors can be produced on a single disc in 30 minutes or less. The devices are built on flexible substrates for flexible electronics and on-chip uses that can be integrated with MEMS or CMOS in a single chip. Remarkably, miniaturizing the devices to the microscale results in enhanced charge storage capacity and rate capability. These micro-supercapacitors demonstrate a power density of ~200 W/cm^3 which is among the highest values achieved for any supercapacitor.

4.2 INTRODUCTION

The current trend with portable electronics lies in continuous miniaturization, while enhancing the functionality and reliability of existing components. However, the integration of energy storage units—i.e. batteries and supercapacitors—with electronic circuits is challenging, and

90

often limits the miniaturization of the entire system. This is because the necessary energy storage components scale down poorly in size and are not well suited to the planar geometries of most integrated fabrication processes. Progress in micro-fabrication technology has enabled on-chip micro-supercapacitors in an interdigitated planar form in contrast to the conventional sandwich structure; the latter being incompatible with integrated circuits [1]. Among the most desirable properties of a micro-supercapacitor, high power density, high rate capability and especially high frequency response are crucial for future applications [2,3]. From a materials perspective, carbon is earth abundant and inexpensive; hence, many nanostructured carbon-based materials have been studied for use in electric double layer (EDL) micro-supercapacitors including activated carbons [4], carbon nanotubes [5], carbide derived carbons [1, 6] and onion-like carbon [2]. In addition, transition metal oxides such as ruthenium oxide [7], manganese oxide [8] and conducting polymers such as polypyrrole [9] and polyaniline [10] have been used as materials for pseudo-capacitive micro-supercapacitors. Among all the previous examples, only onion-like carbon has produced a micro-supercapacitor with ultrahigh power handling with a RC time constant of only 26 ms [2]. However, the high temperature processing of onion-like carbon and the scalability problems of the fabrication technique limit the potential of these devices.

Graphene, a 2D carbon sheet with monoatomic layer thickness offers great potential for energy storage [11-13]. With its high theoretical surface area (2630 m^2/g) and electrical conductivity, graphene could produce supercapacitors with ultrahigh power. We [11] and others [13-15] have developed thin film graphene supercapacitors that demonstrated high power performance with superior frequency response. Although promising, the sandwich structure of these supercapacitors limits their integration into electronic circuits. Yoo *et al.* observed a dramatic increase in the specific capacitance of graphene supercapacitors when made in a planar

91

structure [16]. Later, this research group developed a process for the direct writing of planar graphene micro-supercapacitors through the laser reduction and pattering of hydrated graphite oxide (GO) films [17]. Having discovered that hydrated GO is simultaneously a good ionic conductor and an electrical insulator; they used hydrated GO as both the separator and electrolyte to simplify the fabrication of the device. Although this fabrication technique is promising, the poor frequency response and the large internal resistance (6.5 kΩ) of the as-made devices are not adequate for practical applications. Most recently, Beidaghi *et al.* reported graphene/CNT composite micro-supercapacitors using a combination of micro-fabrication techniques and electrostatic spray deposition [3]. They measured a high volumetric capacitance with an RC time constant as low as 4.8 ms. However, all the fabrication methods reported so far involve conventional lithographic techniques or employ masks for the definition of patterns on substrates. Unfortunately, these methods are awkward for building cost-effective devices for commercial applications. Therefore the challenge is to develop a simple, inexpensive high-throughput lithographic technique that does not require masks, additional processing or sophisticated operation while producing high-performance micro-devices.

In consideration of the problems described above, we report on the direct fabrication of interdigitated graphene micro-supercapacitors using a consumer grade LightScribe DVD burner. This process is readily scalable and the devices can be fabricated on large substrates at a fraction of the cost of traditional micro-fabrication methods. The produced devices are extremely thin, all-solid-state and completely flexible. We also describe the first experimental demonstration of an all-solid-state micro-supercapacitor using an ionogel electrolyte that allows the operation of the device at a voltage window of 2.5 V compared with 1 V for traditional hydrogel-polymer electrolytes. Recently, considerable efforts have been made for the fabrication of flexible micro-

92

supercapacitors for the emerging electronics industry. However, none of these configurations have been shown to be suitable for flexible energy storage. The micro-supercapacitors demonstrated here show exceptional electrochemical stability under different bending and twisting conditions. These microscale supercapacitors can also be fabricated on-chip for the next generation of CMOS applications. Moreover, by varying the dimensions of the interdigitated micro-electrodes, it is possible to control the energy and power handling of these devices. These supercapacitors exhibit ultrahigh power of ~200 W/cm^3 and excellent frequency response with an RC time constant of only 19 ms.

4.3 RESULTS AND DISCUSSION

Fabrication of Laser Scribed Graphene Micro-Supercapacitors. LightScribe is a direct-to-disc labeling technology that burns text and graphics onto the surface of a CD or DVD using a laser inside the drive [18]. To make these labels, the surface of the disc is coated with a reactive dye that changes color on exposure to the laser light. Instead of printing on this specialized coating, our approach is to coat the disc with a film of graphite oxide (GO), which then can be directly printed upon. The process is schematically illustrated in **Figure 4.1**. Circuits designed on a computer can be patterned onto the DVD disc which is now coated with a film of GO. We [19] and others [20] originally found an unusual photo-thermal effect in which GO absorbs high intensity light and is converted into graphene. By using the precision of a laser, the drive renders the computer-designed pattern onto the GO film to produce the desired graphene circuits [21]. In this way, interdigitated graphene electrodes can be readily LightScribed on the disc as shown in **Figure 4.1a**. This form of graphene is called laser scribed graphene (LSG). With its nearly insulating properties, GO serves as a good separator between the positive and negative graphene

93
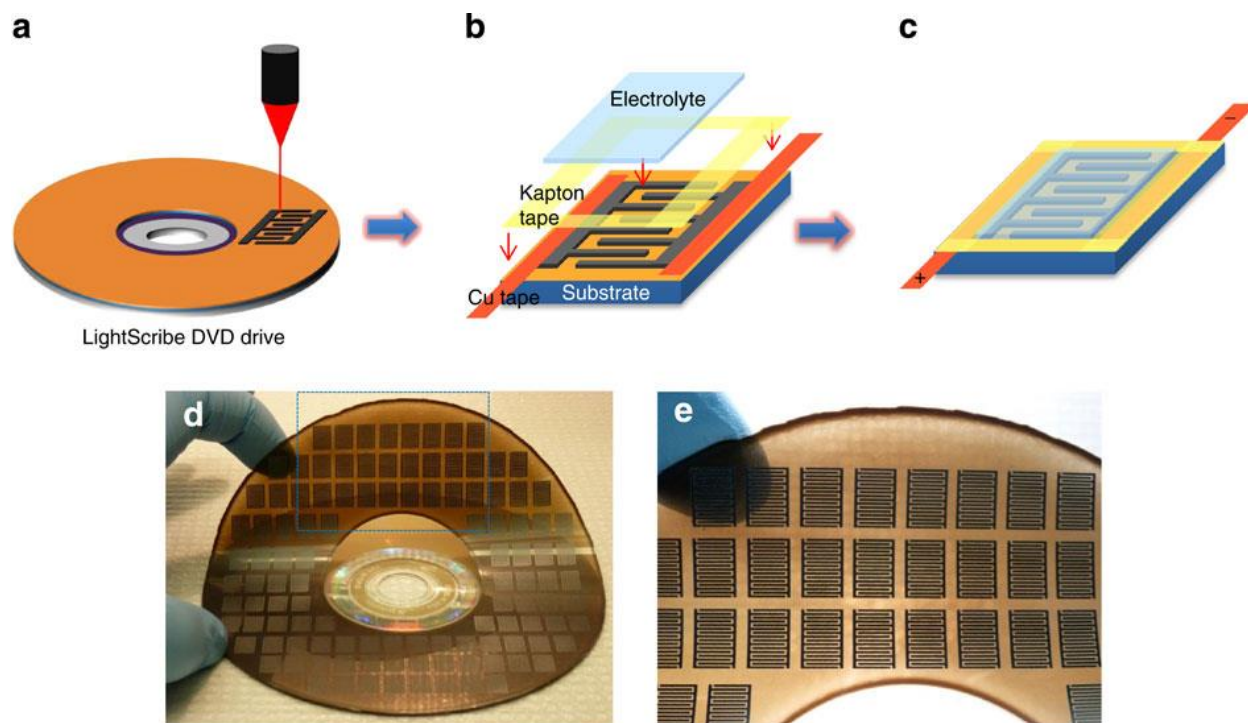
Figure 4.1: Fabrication of laser scribed graphene micro-supercapacitors (LSG-MSC). (a-c) Schematic diagram showing the fabrication process for an LSG micro-supercapacitor. A graphite oxide film supported on a poly(ethylene-terephthalate) (PET) sheet is placed on a DVD media disc. The disc is inserted into a LightScribe DVD drive and a computer designed circuit is etched onto the film. The laser inside the drive converts the golden brown graphite oxide (GO) into black laser scribed graphene (LSG) at precise locations to produce interdigitated graphene circuits. Copper tape is applied along the edges to improve the electrical contacts and the interdigitated area is defined by polyimide (Kapton) tape. An electrolyte overcoat is then added to create a planar micro-supercapacitor. **(d,e)** This technique has the potential for the direct writing of micro-devices with high areal density. More than 100 micro-devices can be produced on a single run. The micro-devices are completely flexible and can be produced on virtually any substrate.

94

interdigitated electrodes [17]. These graphene circuits can thus be directly used as planar micro-supercapacitors after receiving an electrolyte overcoat, **Figure 4.1b-c**. Unlike conventional micro-fabrication methods, this direct "writing" technique does not require masks, expensive materials, post-processing or clean room operations. Furthermore, the technique is cost effective and readily scalable. For example, using the design we chose for this work, 112 micro-supercapacitors can be produced on a single piece of GO deposited on DVD disc, **Figure 4.1d** (see also Appendix**, Figure 4S.1**). Interdigitated electrodes can be precisely patterned with a lateral spatial resolution of ~20 μm using Lightscribe, **Figure 4S.2**. This technique is thus appropriate for the fabrication of high-resolution micro-supercapacitors taking into account that the interdigitated electrodes made with conventional micro-fabrication techniques are usually on the order of ~100 μm (with the exception of references [1,6]).

Characterization of LSG micro-devices. The laser scribing process is associated with significant changes in the optical properties, the electrical properties and the structure of the film. For example, GO changes from a golden brown color to black; a direct impact of the reduction of GO into graphene. **Figure 4.2a** shows a photograph of the as-prepared LSG micro-supercapacitors. A micro-device was constructed with 16 interdigitated microelectrodes; 8 positive and 8 negative electrodes. An optical microscope image shows a well-defined pattern with no short circuits between the microelectrodes, **Figure 4.2b**. **Figure 4.2c** shows the expansion of the film when treated with the laser, thus enabling full access to the electrode surface that is essential for charging the electrodes (see also **Figure 4S.3**). Analysis of the cross-section of the micro-device reveals a thickness of 7.6 μm. For comparison, I–V tests were carried out for both GO and LSG as shown in **Figures 4.2d** and **4.2e**, respectively. The GO film exhibits nonlinear and slightly asymmetric behavior with a differential conductivity value ranging from

8.07×10^{-4}—5.42×10^{-3} S/m depending on the gate voltage. Reducing GO within the DVD burner results in a linear I-V curve associated with a significant increase in the film conductivity to 2.35×10^3 S/m as calculated for the LSG, **Figure 4.2f**. Because of its high electrical conductivity and exceptionally high surface area of over 1500 m^2/g, LSG can serve as both the electrode material and current collector [11]. This simplifies the fabrication process and results in cost-effective micro-supercapacitors.
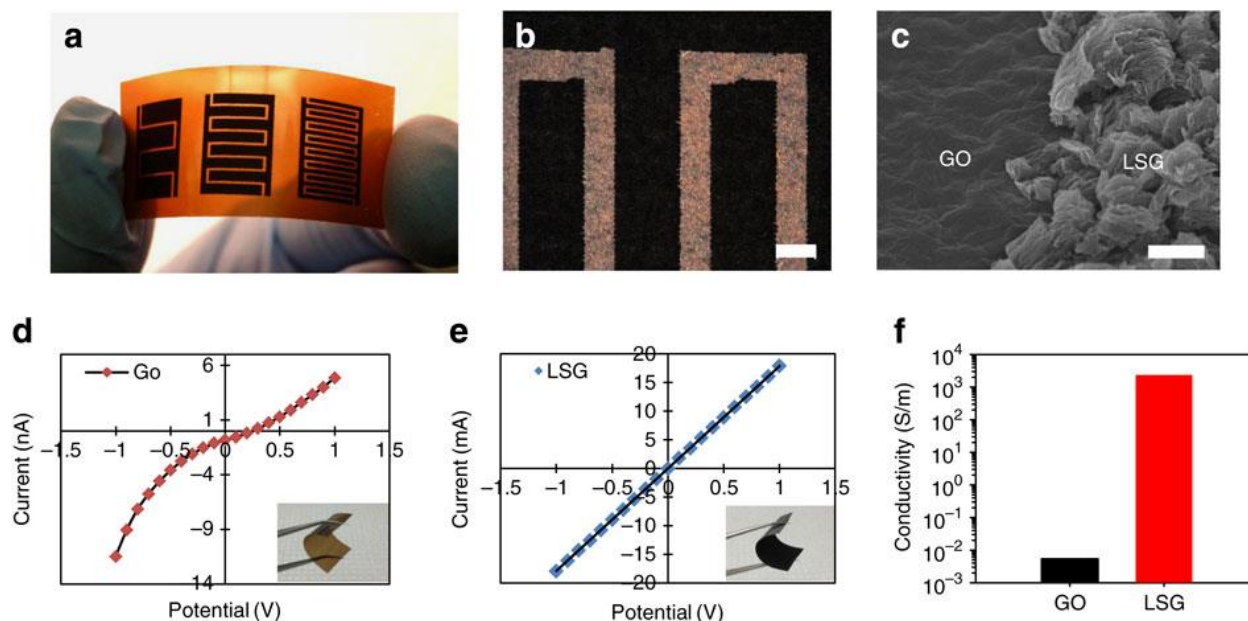
Figure 4.2: Characterization of LSG micro-devices. (a) A digital photograph of the laser scribed micro-devices with 4 (LSG-MSC$_4$), 8 (LSG-MSC$_8$) and 16 interdigitated electrodes (LSG-MSC$_{16}$); **(b)** An optical microscope image of LSG-MSC$_{16}$ shows interdigitated fingers with 150-µm spacings. The dark area corresponds to LSG and the light area is GO. Scale bar = 200µm; **(c)** A tilted view (45°) SEM image shows the direct reduction and expansion of the GO film after exposure to the laser beam. Scale bar = 10µm; **(d)** and **(e)** show the I-V curves of GO and LSG, respectively. LSG exhibits a current enhanced by about 6 orders of magnitude confirming the change from nearly insulating GO to conducting LSG. **(f)** A comparison of electrical conductivity values for GO and LSG.

Evaluation of the performance of LSG micro-supercapacitors. In order to understand the role of the micro-scale architecture of the device on its electrochemical properties, different configurations were designed and tested. Micro-supercapacitors with 4 (MSC4), 8 (MSC8), and 16 (MSC16) interdigitated microelectrodes were constructed and their electrochemical performance at 1,000, 5,000 and 10,000 mV/s tested, as shown in **Figure 4.3 a–c**. Here, a hydrogel-polymer electrolyte, poly(vinyl alcohol) (PVA)-H_2SO_4, was used to fabricate the all-solid-state LSG micro-supercapacitors (LSG-MSC). A sandwich-type LSG supercapacitor was also tested for comparison (**Figure 4S.4**). The cyclic voltammetry (CV) profiles are all rectangular in shape confirming the formation of an efficient electrochemical double layer (EDL) capacitor and fast charge propagation within the electrodes. Even at an ultrafast scan rate of 10,000 mV/s, the CV remains rectangular in shape indicating the high power capability of this micro-supercapacitor (see also **Figure 4S.5**). Recently, it has been shown that the volumetric and areal capacitances give a more accurate picture of the true performance of a supercapacitor compared with gravimetric values [22,23]. This is even more relevant in the case of micro-devices since the mass of the active material is very small. Therefore, we have calculated the specific capacitance of the micro-devices based on the volume of the stack. This includes the combined volume of the active material, current collector and the gap between the electrodes. The stack capacitances of the different micro-supercapacitors as a function of the scan rate are shown in **Figure 4.3d**. Interestingly, the micro-devices show higher capacitance when using the interdigitated structure as opposed to the sandwich structure. Furthermore, the more interdigitated electrodes per unit area, the more power and energy can be extracted from the micro-devices. This can be explained by the unique porous network structure of the LSG electrodes that helps minimize the pathway for ion diffusion from the electrolyte to the electrode material. Moreover, the micro-scale architecture of the devices result in a significant reduction of

97

the mean ionic diffusion pathway between two microelectrodes. This effect becomes even more pronounced when increasing the number of interdigitated electrodes per unit area (see also **Figures 4S.6-8**). This allows for maximizing the available electrochemical surface area and results in the increased capacitance and the fast charge/discharge rates observed with the micro-devices. These conclusions are confirmed by the galvanostatic charge/discharge curves, **Figure 4.3e**. Note that all the micro-devices, regardless of whether they possess 4, 8 or 16 interdigitated electrodes, show nearly ideal triangular charge/discharge curves obtained at an ultrahigh current density of 1.684×10^4 mA/cm^3. The voltage drop at the beginning of each discharge curve, known as the *iR* drop, is a measure of the overall resistance of the device and since its value is proportional to the discharge current, the small *iR* drop shown in **Figure 4.3e** at a high discharge current indicates a very low resistance for all of the micro-supercapacitors tested. The *iR* drop gradually decreases from LSG-MSC(4) through LSG-MSC(16), thus confirming the increase of power density of the micro-devices with an increasing number of interdigitated electrodes per unit area. **Figure 4.3f** shows the volumetric capacitance of the stack as a function of the current density for the LSG micro-supercapacitor for both the interdigitated and sandwich structures. For comparison, the data for a commercial activated carbon supercapacitor obtained under the same dynamic conditions are also shown. Not only does the activated carbon supercapacitor exhibit lower capacitance, but its performance falls off very quickly at higher charge/discharge rates because of the limited diffusion of ions in the inner porous network of the activated carbon [11,24]. The surface of the LSG, on the other hand, is highly accessible to the electrolyte with very little impediment to ion transport, thus providing high capacitance even when operated at ultrahigh charge/discharge rates (see **Figure 4S.9** for more details). For example, LSG-MSC(16) exhibits a stack capacitance of 3.05 F/cm^3 at 16.8 mA/cm^3 and maintains 60% of this value when operated at an ultrahigh current density of 1.84×10^4 mA/cm^3, **Figure 4.3f**.
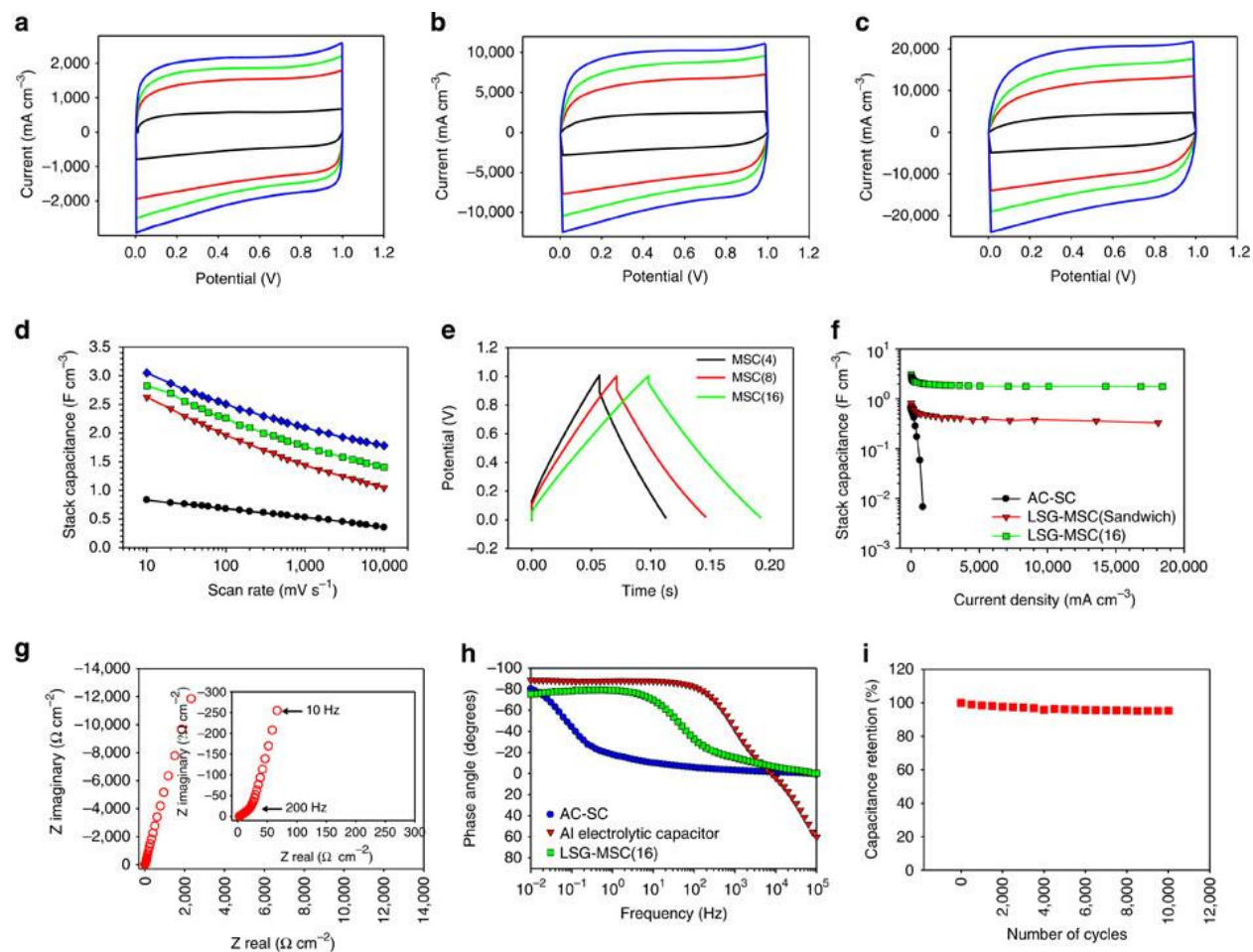
Figure 4.3: Electrochemical performance of the LSG micro-supercapacitors in PVA-H$_2$SO$_4$ gelled electrolyte.
CV profiles of LSG-MSC in sandwich and interdigitated structures with 4, 8 and 16 electrodes at scan rates of **(a)** 1,000 mV/s, **(b)** 5,000 mV/s and **(c)** 10,000 mV/s. **(d)** Evolution of the specific capacitance of the different supercapacitors as a function of the scan rate. Symbol key for (a-d): Sandwich (black), MSC(4) (red), MSC(8) (green), and MSC(16) (blue). **(e)** Galvanostatic charge/discharge curves of micro-supercapacitors based on interdigitated structures with 4, 8 and 16 electrodes, all operated at an ultrahigh current density of 1.68×10^4 mA/cm^3. **(f)** Volumetric stack capacitance of LSG micro-supercapacitors in the sandwich and interdigitated structures as calculated from the charge/discharge curves at different current densities. Data for a commercial activated carbon supercapacitor (AC-SC) are shown for comparison. **(g)** Complex plane plot of the impedance of a LSG-MSC(16) with a magnification of the high-frequency region is provided in the inset. **(h)** Impedance phase angle versus frequency for LSG-MSC(16) compared to commercial AC-SC and aluminum electrolytic capacitors. **(i)** The LSG-MSC(16) shows excellent stability losing only about 4% of its initial capacitance over 10,000 cycles.

99

This is equivalent to the operation of the device at ~1100 $A/g_{LSG/electrode}$ which is about 3 orders of magnitude higher than the normal discharge current densities used for testing traditional supercapacitors [2,3]. This corresponds to an areal capacitance that varies only slightly from 2.32 mF/cm^2 at 16.8 mA/cm^3 to 1.35 mF/cm^2 at 1.84×10^4 mA/cm^3. This is superior to the values reported in the literature for EDLC micro-supercapacitors with typical capacitance values of 0.4-2 mF/cm^2 collected at much lower charge/discharge rates [2,4,25].

Electrochemical impedance spectroscopy further confirms the superior power performance of the LSG micro-supercapacitors. The complex-plane plot of the impedance of LSG-MSC(16) shows pure capacitive behavior even at high frequencies (200 Hz) thanks to the highly accessible surface of the LSG, **Figure 4.3g**. The equivalent series resistance (ESR) obtained from the intercept of the plot on the real axis is only 3.6 Ω/cm^2, made manifest by the good ionic conductivity of the electrolyte and the low internal resistance of the microelectrodes. Remarkably, the LSG micro-supercapacitor shows superior frequency response with an extremely small relaxation time, **Figure 4.3h**. Data from a commercial AC supercapacitor and an aluminum electrolytic capacitor are included for comparison. The RC time constant of LSG-MSC(16) was calculated to be 19 ms in comparison with 10,000 ms for the commercial activated carbon supercapacitor and 1.1 ms for the electrolytic capacitor (**Table 4S.1**). This extremely small time constant for the LSG-MSC(16) is very promising compared with previously reported values for planar micro-supercapacitors: activated carbon (700 ms) [2], onion-like carbon (26 ms) [2], and graphene/CNT composite (4.8 ms) [3]. Furthermore, the LSG supercapacitors show excellent cycling stability retaining 96% of the initial performance after 10,000 charge/discharge cycles.
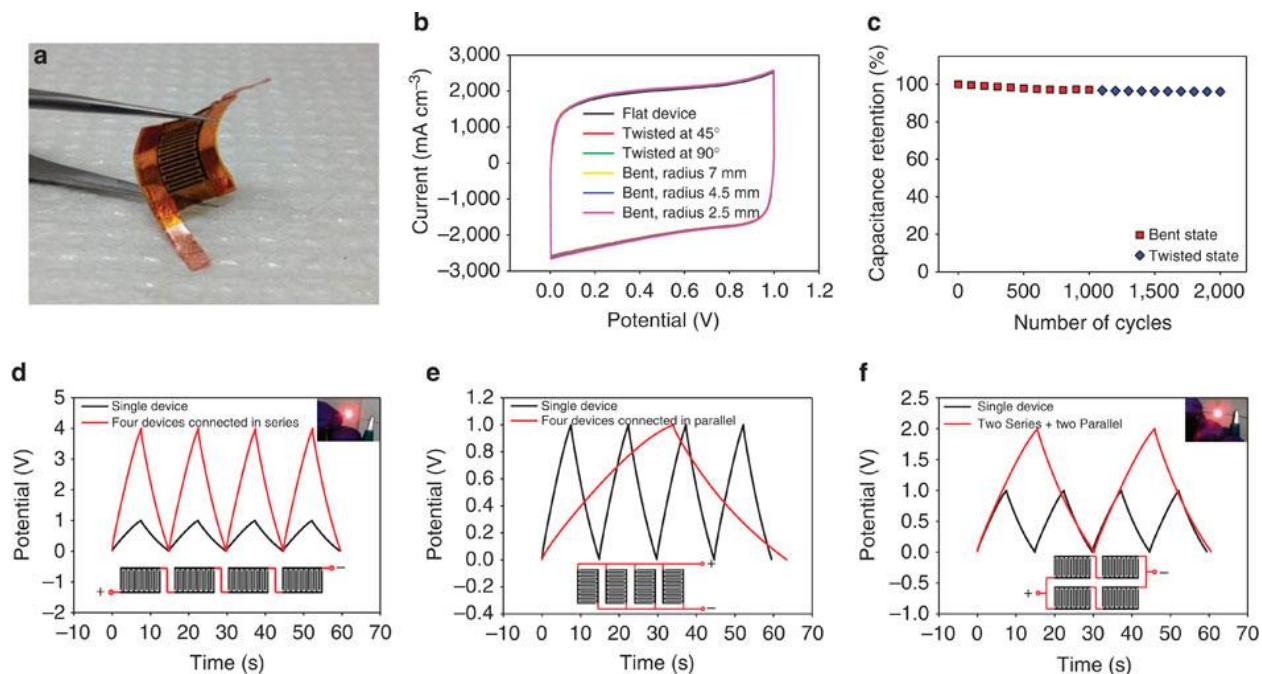
Figure 4.4: Behavior of LSG-MSC under mechanical stress and in series/parallel combinations. (a) A photograph of LSG-MSC(16) bent with a tweezers demonstrates the flexibility of the micro-device; **(b)** Bending/twisting the device has almost no effect on its performance as can be seen from these CVs collected under different bending and twisting conditions at 1,000 mV/s; **(c)** Performance durability of the micro-device when tested under bending and twisting conditions. The device retains ~97% of its initial capacitance after 1,000 cycles under the bent state followed by another 1,000 cycles under the twisted state. Galvanostatic charge/discharge curves for four tandem micro-supercapacitors connected; **(d)** in series, **(e)** in parallel, and **(f)** in a combination of series and parallel. A single device is shown for comparison. Both the tandem devices and the single device were operated at the same charge/discharge current. (Insets) the tandem micro-supercapacitor can be used to power an light emitting diode (LED) bulb.

Bendable and Twistable LSG micro-supercapacitors. Flexible electronics have recently attracted much attention because of their potential in providing cost-efficient solutions to large-area applications such as roll-up displays and TVs, *e*-paper, smart sensors, transparent RFIDs and even wearable electronics [26]. However, the fabrication of micro-supercapacitors on flexible substrates using current micro-fabrication techniques does not appear to be feasible.

101

Attempts to fabricate micro-supercapacitors on flexible substrates using a number of printing and electrochemical techniques have also been reported [27-28]. However, none of these configurations have been shown to be suitable for flexible energy-storage devices. In fact, the performance durability of these devices has not been examined under any strain conditions such as bending or twisting. LSG micro-supercapacitors are highly flexible and can be bent and twisted without affecting the structural integrity of the device, **Figure 4.4a** (see also Appendix, Discussion). To prove the durability of LSG micro-supercapacitors for flexible energy storage, we tested their electrochemical performance under constant strain. **Figure 4.4b** shows the CV performance of the micro-supercapacitor with different bending and twisting conditions at 1,000 mV/s. The micro-supercapacitor shows exceptional electrochemical stability regardless of the degree of bending or twisting, indicating excellent mechanical stability. The flexibility endurance of the device was tested while keeping the device under the bent or twisted state, **Figure 4.4c**. Remarkably, the capacitance was reversibly maintained with 97% retention of the initial capacitance after 2,000 cycles. This superior performance makes LSG-MSC promising for flexible micro-electronics.

In general, the total energy that can be stored in a single supercapacitor is too low for most practical applications. Thus, depending on the application, supercapacitors need to be connected together in series and/or parallel combinations, just as batteries are, to form a "bank" with a specific voltage and capacitance rating. The adaptability of LSG micro-supercapacitors for serial/parallel combinations is demonstrated by connecting four devices together both in series and in parallel configurations, **Figure 4.4d-f**. The tandem LSG micro-supercapacitors exhibit a very good control over the operating voltage window and capacity, thus enabling them to be considered for practical applications. Like the individual micro-supercapacitors, the tandem

102

devices exhibit essentially ideal triangular charge/discharge curves with a minute voltage drop, which again indicates excellent capacitive properties with minimal internal resistance. It is worth noting that this exceptional performance has been achieved without using a voltage balance which is often needed with series connections to prevent any cell from going into over-voltage.

Ionogels – devices with high energy and power densities. Previous research attempts to design supercapacitors in the all-solid-state form have focused mainly on using aqueous hydrogel-polymer electrolytes. Unfortunately, the operating voltage range of these devices barely exceeds 1 V, making them non-functional for many applications. Unlike water-based electrolytes, ionic liquids (IL) provide an attractive alternative to these conventional electrolytes owing to their wide electrochemical window and high ionic conductivity as well as good thermal stability and non-volatility [29]. These interesting properties of ILs can be hybridized with another solid component (e.g. polymer, silica, etc.) to form gel-like electrolytes called ionogels [30]. The combination of a solid matrix with ILs preserve the main properties of ILs, while allowing easy shaping of the device without having the intrinsic leakage problems of liquid electrolytes that limit their flexible operation. Although promising, the integration of ionogels into all-solid-state micro-supercapacitors has not yet been demonstrated. Here, we mixed together fumed silica (FS) nano-powder with the ionic liquid, 1-butyl-3-methylimidazolium bis(trifluoromethylsulfonyl)imide to form a clear viscous (FS-IL) ionogel, **Figure 4.5a** (see also **Figure 4S.10**). The ionogel was integrated into an all-solid-state device and its electrochemical performance is shown in **Figure 4S.11**.
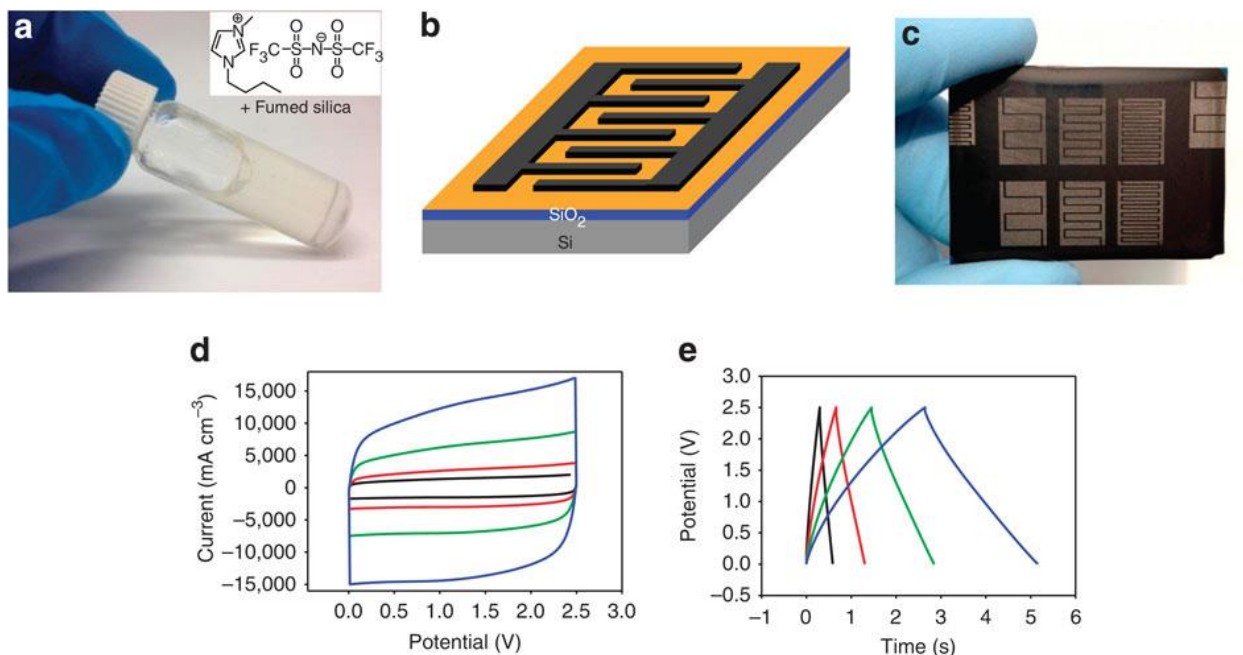
Figure 4.5: Fabrication and characterization of LSG micro-supercapacitors on a chip. LightScribe can be used to produce LSG micro-supercapacitors directly on a chip that contains integrated circuits, which they can then power; **(a)** An ionogel electrolyte was employed in the assembly of the device. It is prepared by mixing together the ionic liquid, 1-buty-3-methylimidazolium bis(trifluoromethylsulfonyl)imide with fumed silica nanopowder. **(b)** Schematic of the device; **(c)** Photograph of the micro-devices; **(d)** CV profile of LSG-MSC(16) at various scan rates, from low to high: 1000 (black), 2000 (red), 5000 (green), and 10000 (blue) mV/s; **(e)** Galvanostatic charge/discharge curves of LSG-MSC(16) collected at different current densities, 1.06×10^4 (black), 5.05×10^3 (red), 2.42×10^3 (green), and 1.38×10^3 (blue) mA/cm^3.

Interestingly, the device demonstrates ultrahigh charge/discharge rates comparable to those with PVA-H_2SO_4 hydrogel electrolyte, but the device can now be operated at a larger potential window of 2.5 V, **Figures 4S.11 and 4S.12**. The almost ideal CV profiles and triangular charge/discharge curves at ultrafast charge/discharge rates verify good EDLC behavior. The LSG-MSC(16) achieved a stack capacitance of 2.35 F/cm^3 at a current density of 16.8 mA/cm^3. When operated at an ultrafast charge/discharge current density of 1.84×10^4 mA/cm^3, the capacitance of the device drops only slightly to 1.40 F/cm^3. Since the energy density increases with the square of the operating potential window, the micro-supercapacitor employing a FS-IL ionogel promises an order of magnitude higher energy density. Furthermore, the high thermal stability of ionic liquids eliminates the fire hazards associated with commercial supercapacitors. Finally, the micro-supercapacitor shows excellent cycling stability; the capacitance remains unchanged after more than 30,000 charge/discharge cycles.

Direct fabrication of a LSG-MSC on a chip. Current trends for developing miniaturized electronic devices place emphasis on achieving performance levels generally associated with integrated circuits. Here we demonstrate an on-chip micro-supercapacitor that can be integrated with MEMS devices and CMOS in a single chip using the LightScribe direct writing technique. The structure of the device is schematically illustrated in **Figure 4.5b**; with an ionogel used as the electrolyte. The device was fabricated using the same process described earlier except for the plastic substrate which has been replaced with an oxidized silicon wafer, **Figure 4.5c**. **Figure 4.5d-e** show that the device reveals superior electrochemical performance with ultrahigh power, comparable to that demonstrated on the flexible substrate. This technique may thus present a low-cost and scalable solution for on-chip self-powered systems.

Low leakage current and slow self-discharge rate. Charged supercapacitors, like charged batteries, are in a state of high free energy relative to that of the discharged state, so there is a thermodynamic driving force for them to self-discharge [31]. The self-discharge behavior of supercapacitors is a matter of major practical significance in their operation and the types of function they may be required to fulfill. During self-discharge, a small amount of leakage current will cause the voltage decay of a charged supercapacitor over time. The leakage current can be measured by applying a rated DC voltage to the supercapacitor and measuring the current required to maintain that voltage. Typically, this is done using the voltage at which the supercapacitor is operated, V_{max}. The results are presented in **Figure 4.6a** which also include the data for two commercially available supercapacitors, all tested under the same dynamic conditions. The results show that the LSG micro-supercapacitor exhibits an ultra-small leakage current of <150 nA after 12 hours compared to ~5 µA for both of the commercial supercapacitors. With its low leakage current, LSG micro-supercapacitors could be integrated with energy harvesters to create efficient self-powered systems.

The self-discharge curves obtained immediately after pre-charging to V_{max} in the previous test are shown in **Figure 4.6b**. Basically, the voltage difference between the two terminals of the supercapacitor is recorded on open circuit as a function of time. Normally, most supercapacitors are operated in the range of V_{max} to approximately $½V_{max}$ [32]. Thus the time required for the voltage across the supercapacitor to change from V_{max} to $½V_{max}$ was measured for all of the tested supercapacitors. The results show that the LSG micro-supercapacitor self-discharges in 13 hours, a value comparable to those of commercial supercapacitors with self-discharge rates of 8 hours and 21 hours. This fine performance for the LSG micro-supercapacitors shows promise for practical applications.
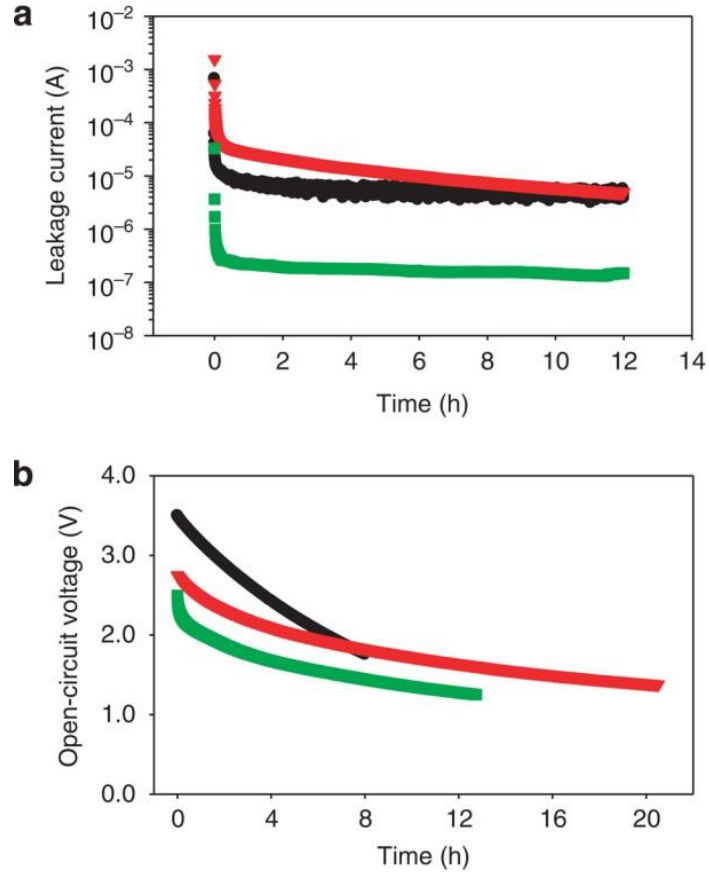
Figure 4.6: Testing the self-discharge rate of LSG micro-supercapacitors. (a) Leakage current measurement of an LSG micro-supercapacitor (with 16 interdigitated electrodes) and two commercially available supercapacitors. A DC voltage (the voltage at which the supercapacitor is operated, V_{max}) was applied across the capacitor, the current required to retain that voltage was measured over a period of 12 hours; (b) Self-discharge curves of the respective supercapacitors obtained immediately after pre-charging to V_{max} in the previous test. This involves measuring the open-circuit voltage across the supercapacitors between V_{max} and ½V_{max} versus the course of time. This involves 3.5 V/25 mF commercial supercapacitor (black), 2.75 V/ 44 mF commercial supercapacitor (red), and LSG micro-supercapacitor assembled using ionogel electrolyte (green).

Figure 4.7 shows a Ragone plot comparing the performance of LSG micro-supercapacitors with different energy storage devices designed for high-power microelectronics. The plot shows the volumetric energy density and power density of the stack for all the devices tested. It reveals a significant increase in the supercapacitor performance when scaling down the electrode dimensions to the micro-scale. For example, the interdigitated micro-supercapacitors deliver more energy and power than their sandwich counterparts both in the hydrogel-polymer and ionogel electrolytes. Remarkably, compared with the AC supercapacitor, the LSG micro-device exhibits 3 times more energy and ~200 times more power. Furthermore, the LSG micro-supercapacitors demonstrate power densities comparable to those of the aluminum electrolytic capacitor, while providing more than 3 orders of magnitude higher energy density. Although Li-ion batteries can provide high energy density, they have limited power performance that is 4 orders of magnitude lower than the LSG-MSC. This superior energy and power performance of the LSG micro-supercapacitors should enable them to compete with micro-batteries and electrolytic capacitors in a variety of applications. See also a comparison between LSG micro-supercapacitors and the state-of-the-art ultrahigh power micro-supercapacitors reported in the literature, Supplementary Table S2. Further miniaturization of the width of the micro-electrodes and the space between them would reduce the ionic diffusion pathway, thus leading to micro-supercapacitors with even higher power density.

4.4 CONCLUSIONS

The single-step fabrication technique described here obviates the need for time-consuming and labor-intensive lithography, while enhancing the yield of the process and the functionality of the micro-devices produced.
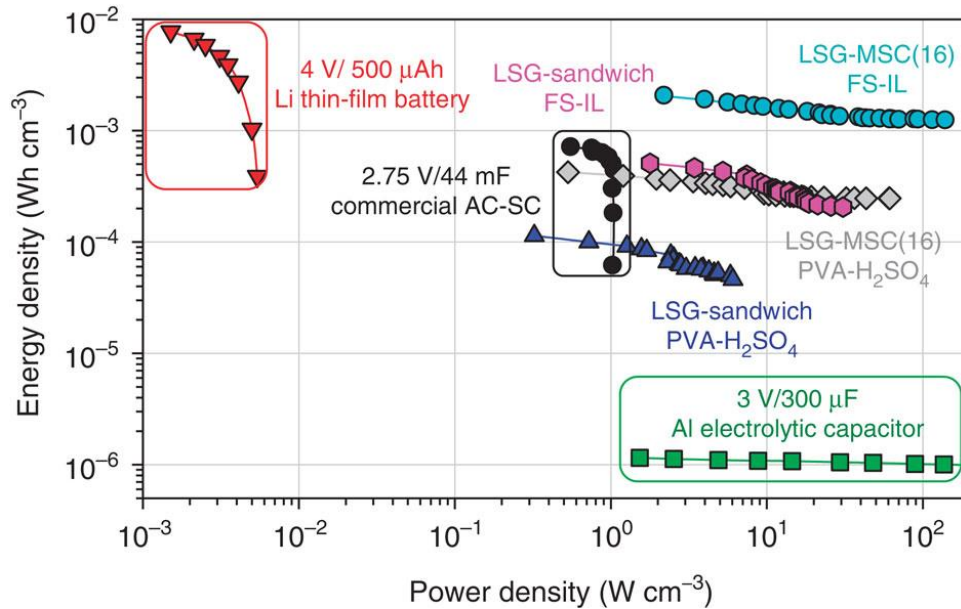
Figure 4.7: Energy and power densities of LSG-MSCs compared with commercially available energy storage systems. LSG-MSCs exhibit ultrahigh power and energy densities compared with a commercially available activated carbon supercapacitor (AC-SC), an aluminum electrolytic capacitor and a lithium thin-film battery. LSG micro-devices can deliver ultrahigh power density comparable to those of aluminum electrolytic capacitor, while providing three orders of magnitude higher energy density. Data for the Li battery are reproduced from reference [2].

Remarkably, this technique allows for the fabrication of micro-devices without the use of organic binders, conductive additives or polymer separators that are often needed in commercial supercapacitors, thus leading to improved performance because of the ease with which ions can access the active material. The combination of the microscale design of the device with LSG whose surface is fully accessible to electrolyte ions is responsible for the high power/energy performance of the LSG micro-supercapacitors. They combine the power density of electrolytic capacitors with the energy density of micro-batteries that could have a significant impact on high-power microelectronics. These findings also provide a solution to microscale energy storage in numerous areas where electrolytic capacitors cannot provide sufficient volumetric energy

density. Furthermore, LSG micro-supercapacitors show excellent cycling stability. This is very important when compared with micro-batteries whose finite life-time could be a major problem when they have to be embedded in permanent structures such as biomedical implants, active radio frequency identification (RFID) tags and embedded micro-sensors where no maintenance or replacement is possible. Since these micro-supercapacitors can be directly integrated on-chip, they may help to better extract the energy from solar, mechanical, and thermal sources and thus make more efficient self-powered systems [33]. They could also be fabricated on the backside of solar cells in both portable devices and rooftop installations, to store power generated during the day for use after sundown and thus may help to provide electricity around the clock where connection to the grid is not possible. Other applications could arise which take advantage of the flexible nature of the substrates, such as electronics embedded into clothing, large-area flexible displays, and roll-up portable displays [23, 34].

4.5 MATERIALS AND METHODS

Fabrication of LSG Micro-Supercapacitors (LSG-MSC). LSG-MSCs were produced by the direct writing of graphene patterns on graphite oxide (GO) films using a consumer grade LightScribe DVD burner. Briefly, GO was synthesized using a modified Hummer's method [35] and aqueous dispersions of GO with the appropriate concentration (2.7 mg/mL) were made. A sheet of plastic, polyethylene terephthalate (PET), was glued to the surface of a LightScribe DVD media disc. 16 mL of GO solution was then drop-cast on PET and allowed to dry overnight under ambient conditions. The GO-coated DVD disc was then inserted into the DVD optical drive for laser patterning. Interdigitated micro-patterns designed using regular computer software were directly LightScribed onto the GO film. This LightScribing process converts the golden brown insulating GO into black highly conducting LSG patterns at precise locations. With the laser precision, the drive renders the computer-designed patterns onto the GO film to produce the graphene micro-patterns in about 20 minutes.

The LSG micro-patterns were directly used as micro-supercapacitors after receiving an electrolyte overcoat. Here, LSG serves as both the active electrode material and the current collector. For electrochemical characterization of the micro-devices, copper tape was applied to the electrode edges to ensure good electrical contact between the LSG devices and the electrochemical workstation. For better current collection, the copper tape was glued to the electrodes using silver paint. The interdigitated area is defined with polyimide (Kapton) tape to protect the contact pad from the electrolyte. The electrolyte was drop-cast on the active interdigitated electrode area, left under ambient conditions for 3 hours to ensure that the electrolyte completely wets the electrode and to allow for evaporation of any excess water.

LSG micro-devices can be made on virtually any substrate. For example, we made devices on silicon wafers to demonstrate the potential of the technique for the direct fabrication of LSG-MSCs for the next generation of CMOS applications. Si/SiO$_2$ (500 nm) wafers of the appropriate size were glued to the surface of the DVD media disc and coated with a GO solution as previously described and then LightScribed in the drive to produce the micro-devices.

Characterization and measurements. The microstructures of GO and LSG micro-devices were investigated by means of field-emission scanning electron microscopy (JEOL 6700) and optical microscopy (Zeiss Axiotech 100). Electrical measurements (I-V curves) were carried out on a VersaSTAT3 electrochemical workstation (using a two electrode setup) by measuring the current produced at different gate voltages (from -1 to +1) with a potentiostatic technique. To prevent the graphene network from being damaged by the probes, two contact electrodes were first made by carefully painting a layer of silver (SPI supplies, Pennsylvania, USA) on the LSG film. Ten measurements were performed on different areas of the film to ensure reproducibility. The thicknesses of the different components of the device were measured using cross-sectional scanning electron microscopy and a Dektak 6 profilometer. Conductivity values were calculated from the slopes of the I-V curves and the thickness of each film.

The electrochemical performances of the LSG micro-supercapacitors were investigated by cyclic voltammetry (CV), galvanostatic charge/discharge tests (CC) and electrochemical impedance spectroscopy (EIS). Cyclic voltammetry and charge/discharge testing were performed on a VersaSTAT3 electrochemical workstation (Princeton Applied Research, USA). EIS measurements were carried out on a Solartron electrochemical workstation (Solartron Analytical, Oak Ridge, TN) over a frequency range of 100 kHz to 10 MHz with an amplitude of 10 mV at the open circuit potential. The characterization experiments of the devices using PVA-H$_2$SO$_4$

were performed in air, while those made with ionogel electrolyte were fully characterized in an argon-filled glove bag. All experiments were performed at room temperature. Calculations of the specific capacitance and the energy and power densities are discussed in detail in the Appendix.

SUPPLEMENTARY DISCUSSION

Key points to be addressed to achieve flexible energy storage. Flexible electronics fabricated on bendable substrates (e.g. plastic) have great potential for novel applications in consumer flexible electronics such as flexible displays, e-paper and smart labels. Compared with silicon technologies, flexible electronics offer not only ease of manufacturing and low cost, but lightweight and mechanical flexibility. Thus, flexible electronics are expected to impact our daily lives in significant ways in the near future. However, achieving high efficiency miniaturized energy storage devices that are compatible with flexible and wearable electronics is still a major challenge. This requires all the essential components of the device (electrodes, electrolytes and separator) to be integrated into an all-solid-state unit with a compact, flexible design. Unfortunately, EDLC micro-supercapacitors reported in literature so far generally employ liquid electrolytes that limit their flexible operation. This requires the development of new gelled electrolytes in which the properties of liquid electrolytes are hybridized with those of another solid component which could be organic (e.g. low molecular weight gelator or a polymer) or inorganic (e.g. carbon nanotube, silica, etc.). The properties of the gelled electrolyte are expected to derive both from those of the liquid electrolyte and those of the component forming the solid-like network. The gelled electrolyte improves the mechanical integrity of the device by acting like a glue that holds all the device components together. Furthermore, the leakage of liquid electrolytes could deteriorate the electronic components on which it is integrated. The gelled electrolyte can thus be used to prepare all-solid-state devices that can be safely integrated into electronic circuits. Another key point that must be addressed to achieve flexible energy storage is

the development of new electrode materials with appropriate electrical and mechanical properties. LSG electrodes are promising in this respect; they can be bent thousands of times without suffering any noticeable damage to their electrical properties [11]. The combination of LSG electrodes with an appropriate gelled electrolyte in a single device explains its excellent electrochemical stability under mechanical stress.

On the self-discharge of LSG micro-supercapacitors. Self-discharge curves provide important information for the detailed analysis of the mechanisms of self-discharge of supercapacitors [31, 36-38]. B. Conway suggested that the degree of self-discharge in a supercapacitor depends on the chemistry and electrochemistry of the system, the type and purity of reagents and electrolyte, and significantly, the temperature [34]. It is noteworthy that the self-discharge rate of LSG micro-supercapacitor is rapid in the initial state. This is possibly because of slow faradaic reactions occurring at imperfections on the surface of the electrode material. LSG has remnant oxygen containing groups from the graphite oxide precursor (hydroxyl, epoxy, carboxylic, etc.) that are plausible reaction sites [21]. Another possibility for the rapid self-discharge in the initial stage could be the separator material, graphite oxide. The chemical and electrical properties of graphite oxide are different from those of the conventional polymer separators used in commercial supercapacitors. Note that all measurements for the LSG micro-supercapacitors were carried out on the unpackaged device, meaning that the actual charge retaining time could be longer. Further optimization of the device architecture and fabrication may result in better charge retention. In conclusion, graphite oxide can be used as a separator in supercapacitors with self-discharge rates comparable to those of commercially available supercapacitors. This confirms the previous results reported by Gao *et al.* [17]. However, it would be good to see a detailed study on the self-discharge behavior of graphene supercapacitors. Understanding the mechanisms of self-

discharge is required to better control and or even prevent the self-discharge of graphene supercapacitors, thus extending their life and practical applications.

SUPPLEMENTARY METHODS

Preparation of the hydrogel-polymer electrolyte, PVA-H$_2$SO$_4$. Polyvinyl alcohol (PVA) (molecular weight 89,000-98,000, 99% hydrolyzed, Sigma-Aldrich) powder was mixed with water (1 g PVA/10 g H$_2$O). The mixture was heated at ~90 °C under constant stirring until the solution turned clear. After cooling under ambient conditions, 0.8 g of concentrated sulfuric acid solution (98% solution in water, Sigma-Aldrich) was added and the solution was stirred thoroughly.

Preparation of the ionogel electrolyte, FS-IL. The FS-IL ionogel was prepared by mixing fumed (FS) silica nano-powder (average particle size = 7 nm, Sigma-Aldrich) with the ionic liquid (IL) 1-butyl-3-methylimidazolium bis(trifluoromethylsulfonyl)imide ([BMIM][NTf$_2$]). In a typical synthesis, 0.03 g of FS was mixed with 1.0 g of [BMIM][NTf$_2$] in an argon-filled glove bag. This mixture was magnetically stirred for 5 hours inside the glove bag to produce the ionogel as a clear viscous solution, see **Figure S10**.

Characterization of commercial energy storage devices designed for high-power micro-electronics. The best way to understand the superior performance of LSG micro-supercapacitors is to compare their performance data with those of commercially available energy storage devices designed for high power micro-electronics. This includes an activated carbon supercapacitor (5.5 V, 22 mF) and an aluminum electrolytic capacitor (3 V, 300 µF) and a lithium thin-film battery (4 V/ 500 µAh). The activated carbon supercapacitor consists of two devices connected in series. A single supercapacitor was separated from this assembly for testing

116

(rendering the device as 2.75 V, 44 mF). All the devices were characterized under the same dynamic conditions as the LSG-MSC.

Calculations. The capacitance of each device was calculated from the galvanostatic (CC) curves at different current densities using the formula:

$$C_{device} = i/(-dV/dt) \qquad (1)$$

where i is the current applied (in amps, A), and dV/dt is the slope of the discharge curve (in volts per second, V/s). Specific capacitances were calculated based on the area or the volume of the device stack according to the following formulae:

$$Areal\ capacitance = C_{device}/A \qquad (2)$$

$$Volumetric\ stack\ capacitance = C_{device}/V \qquad (3)$$

Where A and V refer to the area (cm^2) and the volume (cm^3) of the device, respectively. The stack capacitances (F/cm^3) were calculated taking into account the volume of the device stack. This includes the active material, the current collector and the separator with electrolyte, and for all the devices tested it did not include the packaging. In case of the micro-devices, the volume was calculated by multiplying the entire projected surface area of the device (40.28 mm^2 which includes the area of the microelectrodes and the gaps between them) into the thickness of the LSG which acts as both the active material and the current collector.

The electrochemical performance of each device reported in **Figure 6** is based on the volume of the stack. The power of each device was calculated from the galvanostatic curves at different charge/discharge current densities using the formula given in Equation (4):

$$P = (\Delta E)^2/4R_{ESR}V \qquad\qquad (4)$$

where P is the power (W/cm^3), ΔE is the operating voltage window (measured in volts and obtained from the discharge curve excluding the IR drop) and V is the volume of the stack as indicated earlier (in cm^3). R_{ESR} is the internal resistance of the device that can be estimated from the voltage drop at the beginning of the discharge, V_{drop}, at a constant current density (i) using the formula $R_{ESR} = V_{drop}/2i$.

The energy density of the device was obtained from the formula given in Equation (5):

$$E = C_V \times (\Delta E)^2/(2 \times 3600) \qquad\qquad (5)$$

where E is the energy density in Wh/cm^3, C_V is the volumetric stack capacitance obtained from Equation (3) in F/cm^3 and ΔE is the operating voltage window in volts.

The specific capacitance was also calculated from cyclic voltammetry by integrating the discharge current (i) vs. potential (E) plots using the following equation:

$$\text{Volumetric stack capacitance} = \int i\ dE/vV\Delta E \qquad\qquad (6)$$

where v is the scan rate (V/s), V is the volume of the micro-device (cm^3) and ΔE is the operating potential window (1 V for PVA-H$_2$SO$_4$ and 2.5 V for FS-IL).
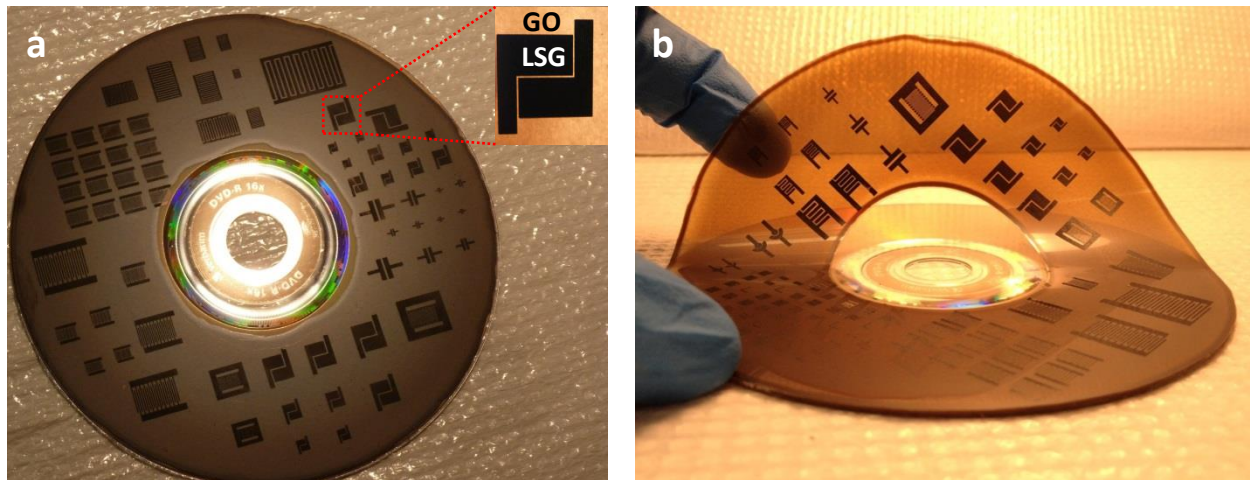
Figure 4S.1 | LightScribe is a scalable technique for the production of high-performance LSG micro-supercapacitors. (a) Various micro-devices with different sizes and shapes can be produced on a single run. **(b)** The devices are completely flexible and can be produced on virtually any substrate. Here, a transparency sheet made from polyethylene terephthalate (PET) is used, but other substrates such as membranes, paper, textiles and Si/SiO$_2$ wafers can also be used.
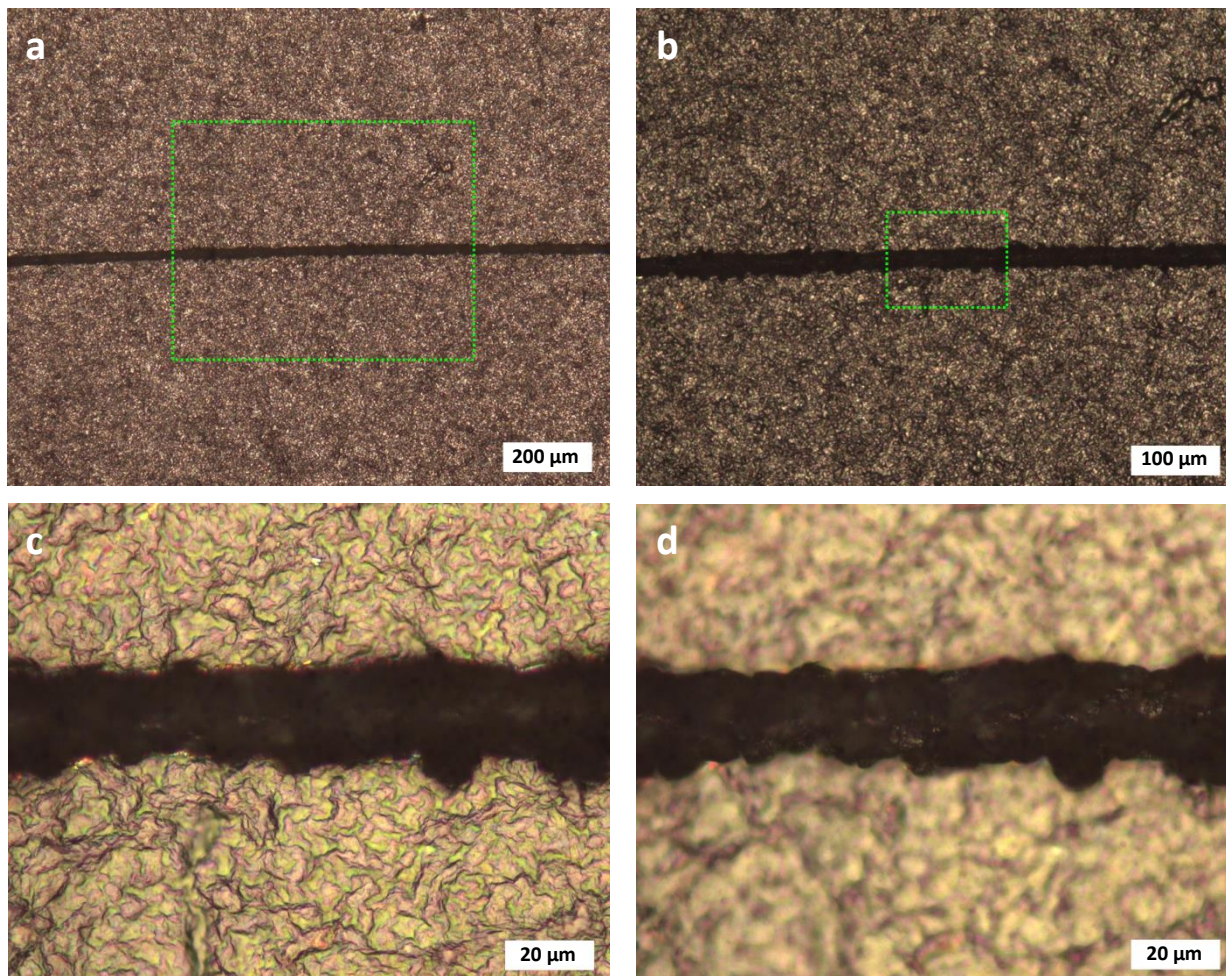
Figure 4S.2 | Laser Scribing of a LSG micro-pattern on graphite oxide film with a spatial resolution of 20 μm.

(a) An optical microscope image of an LSG individual micro-electrode that was LightScribed on a film of graphite oxide. **(b)** A zoomed-in view of the pattern. SEM characterization indicates that the height of the LSG micro-pattern is higher than the rest of the film (see Figure 2c). **(c)** A magnified view of the micro-pattern, with the GO layer focused on in the image. **(d)** A magnified view of the micro-pattern, focusing on the LSG micro-electrode. The images show that the LightScribe produces LSG micro-patterns with a spatial resolution of ~20 microns.
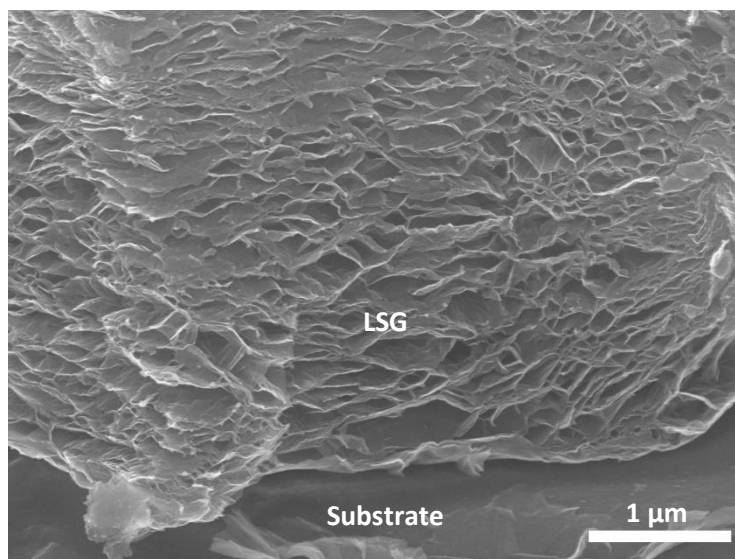
Figure 4S.3 | Microscopic analysis of graphene LSG micro-electrodes: Microscopic analysis using SEM illustrates the fundamental differences between GO and LSG. A side view SEM image of the LSG film on a PET substrate shows the expansion of the film after treatment with the laser inside the DVD burner. In our previous study [11] we showed that the GO film has its sheets stacked together making them inaccessible to the electrolyte ions; whereas, the laser treatment of GO results in the formation of a three-dimensional network of graphene with highly accessible surface area.
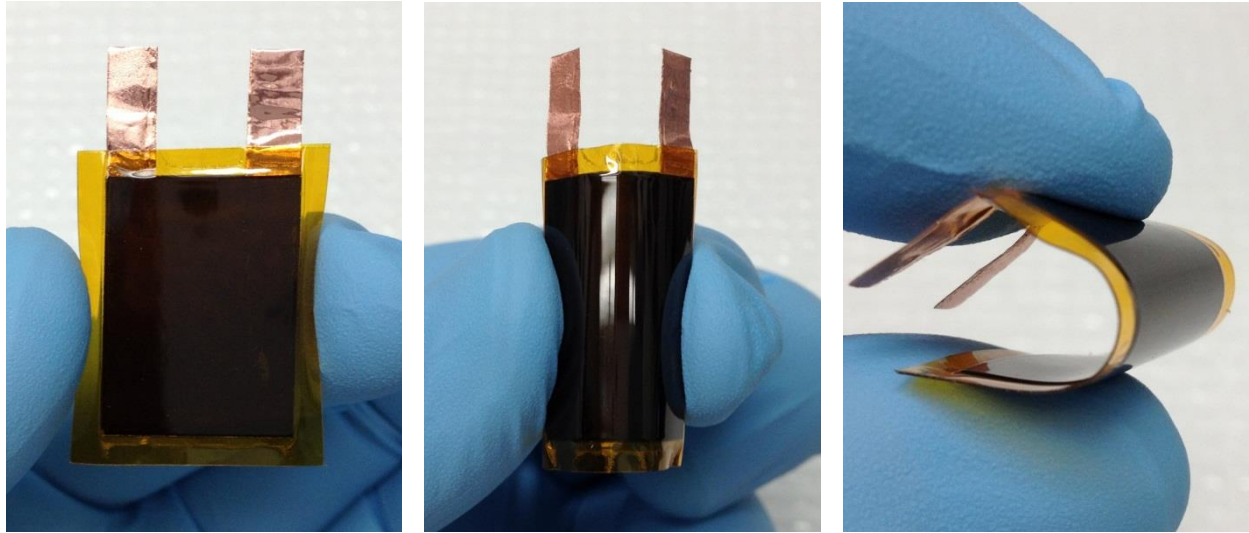
Figure 4S.4 | Sandwich type LSG supercapacitors. LSG supercapacitors can be produced in the sandwich structure by assembling together two graphene electrodes with a small amount of gelled electrolyte which also acts as the separator. Copper tape is used to make electrical contact with the potentiostat and the whole device is then packaged with polyimide (Kapton) tape.
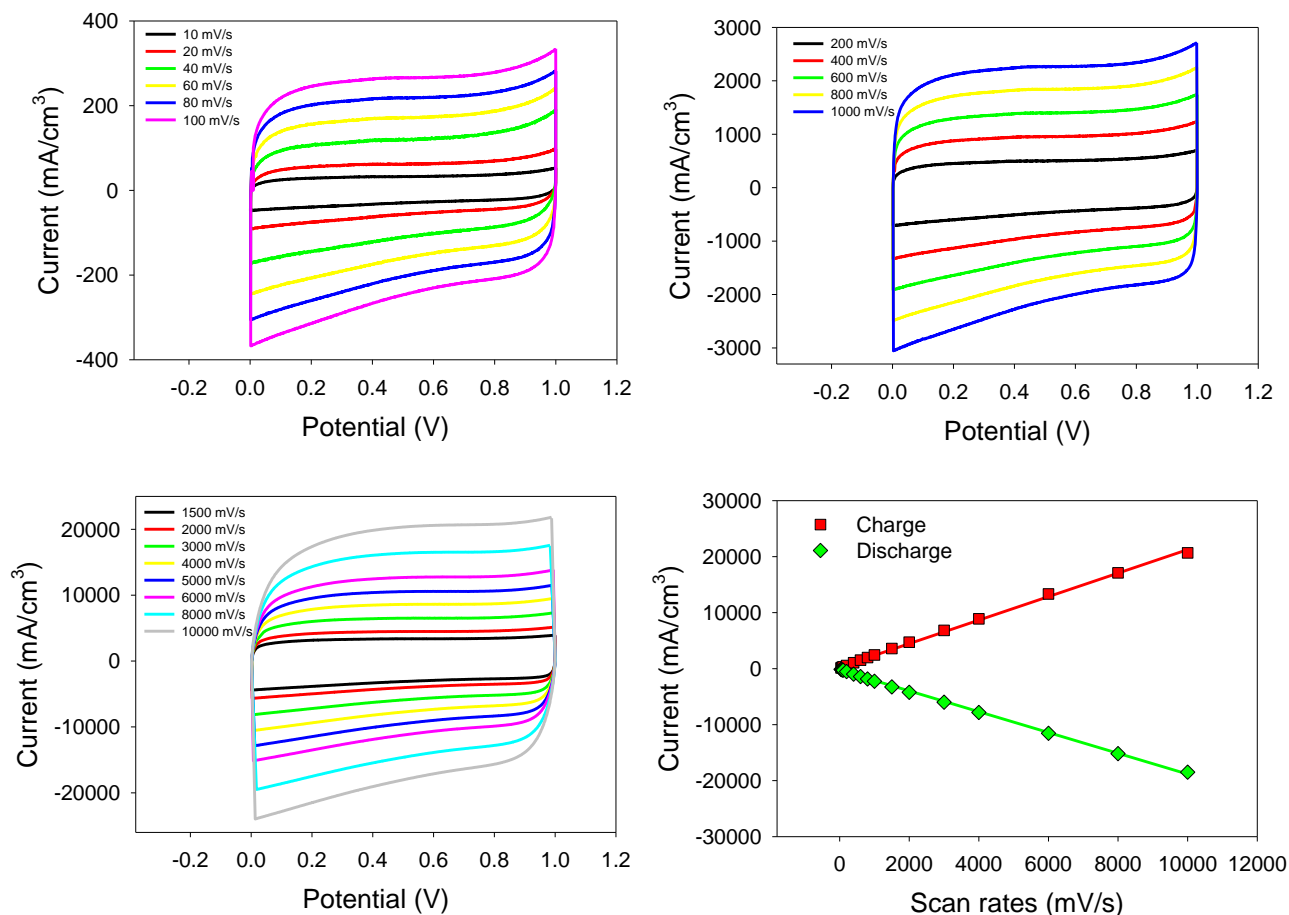
Figure 4S.5 | Electrochemical performance of an LSG micro-supercapacitor with 16 interdigitated electrodes in PVA-H₂SO₄ gelled electrolyte. CV profiles of the device at different scan rates of **(a)** 10 to 100 mV/s; **(b)** 100 to 1,000 mV/s; **(c)** 1,500 to 10,000 mV/s. The CV profiles are rectangular in shape over a wide range of scan rates confirming the formation of an efficient EDL and fast charge propagation within the electrodes. **(d)** Dependence of the capacitive current (extracted from the CV profiles at 0.5 V) on the applied scan rate between 10 to 10,000 mV/s. A linear relationship is observed over the entire range of studied scan rates.

123

Sandwich (conventional) structure
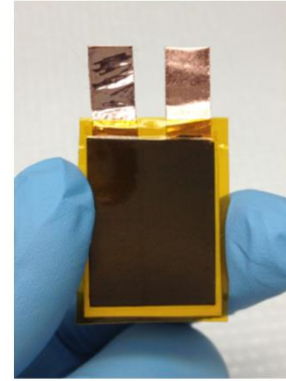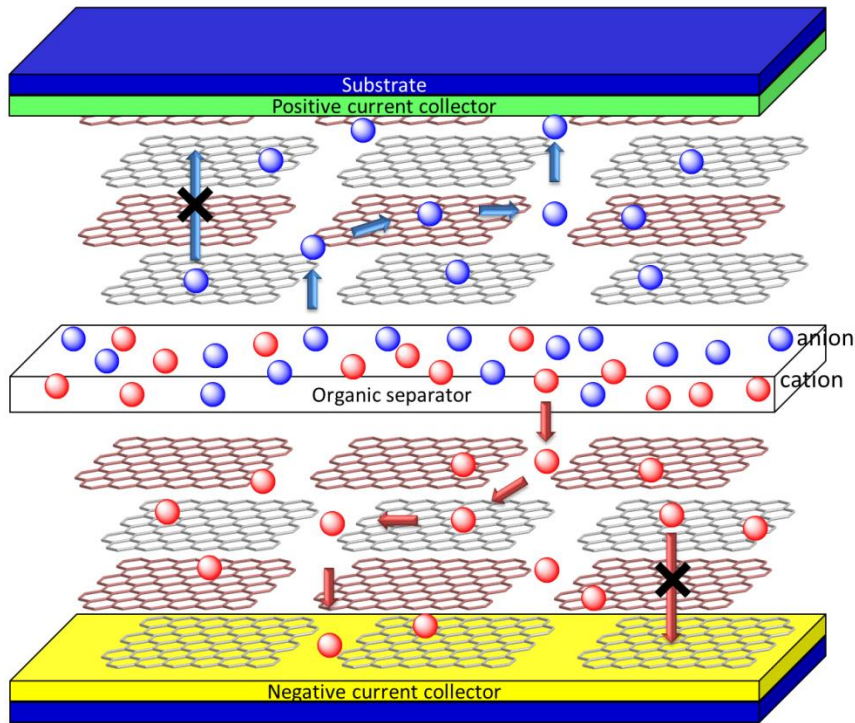
Interdigital (planar) structure
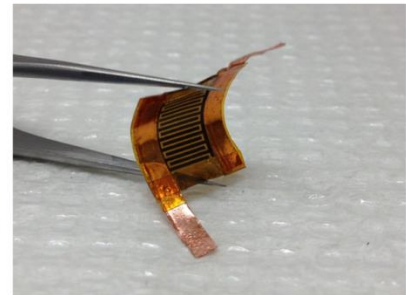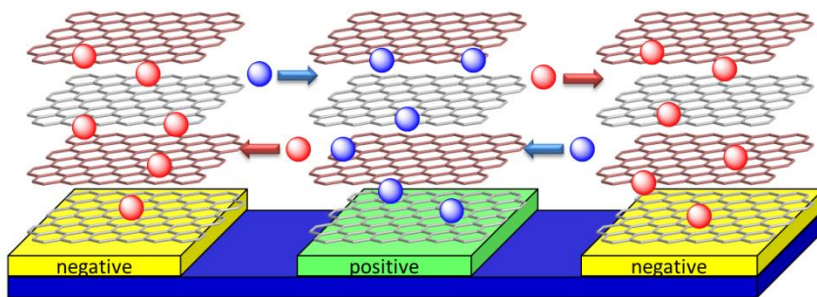
Figure 4S.6 | Schematic illustration of the differences between the electrochemical properties of LSG supercapacitors in the sandwich and interdigitated structures. There have been two main types of micro-supercapacitors which differ by structure; the conventional sandwich structure in which two thin film electrodes are combined together to form the supercapacitor stack (top figure). The other structure consists of interdigitated micro-electrodes designed in a planar configuration (bottom figure). In comparison, interdigitated micro-supercapacitors have several advantages over the conventional stacked design. First, having both electrodes in the same plane is compatible with on-chip integration. Second, the travelling distance of the ions in the electrolyte, a major performance factor in supercapacitors, can be well controlled and shortened while eliminating the necessity of a

separator, which is indispensable in the sandwich-type supercapacitors to prevent electrical shorting [16]. Third, the interdigitated structure can potentially be extended to three dimensions, which allows more materials loaded per unit area while leaving the mean ionic diffusion path unaffected. This architecture thus has the potential to achieve high power density and high energy density in a small footprint [39,40]. Using laser scribed graphene (LSG) as the active electrode material provides even more advantages to the interdigitated structure. This is because of its extremely high electrical conductivity, surface area and accessibility to the electrolyte ions (see the main paper for details). In short, designing the interdigitated structure with LSG can more fully exploit the advantages of planar micro-supercapacitors.
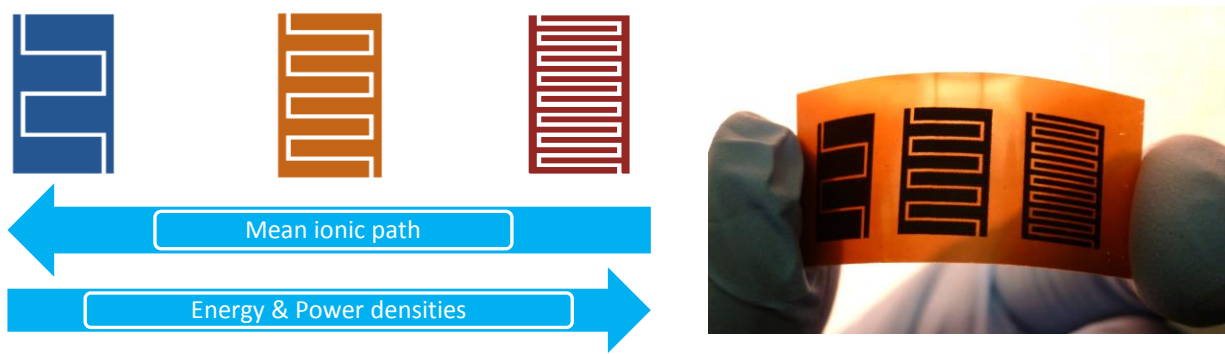
Figure 4S.7 | Dependence of the electrochemical properties of the micro-devices on design parameters. In order to understand the role of the micro-scale architecture of the device on the electrochemical properties, different configurations were designed and tested. As shown in Figure S7, devices with 4, 8 and 16 micro-electrodes were made. The average migration distance is proportional to the width of the micro-electrodes (called 'w' in Figure S8) and that of the space between them (i). Thus, the migration distance decreases from MSC(4) through MSC(16). The reduction of the mean ionic diffusion path lowers the electrolyte resistance between micro-electrodes, thus reducing ion transport limitations. Hence, the more interdigitated electrodes per unit area, the more power that can be extracted from the micro-device. What is really interesting about the laser scribing technique is that w and l can be readily adjusted using the interdigitated electrodes so that the average migration distance of ions can be well controlled.

	4 wires	8 wires	16 wires
Width, w (µm)	1770	810	330
Length, l (µm)	4800	4800	4800
Interspace, i (µm)	150	150	150
Edge, e (µm)	200	200	200
Total surface area (mm^2)	40.28	40.28	40.28
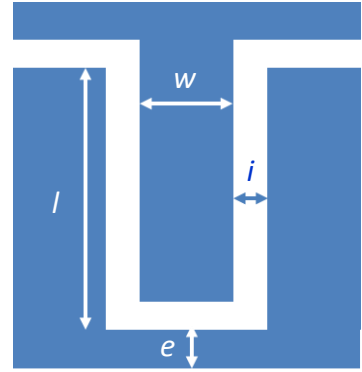
Figure 4S.8 | Dimensions of the micro-supercapacitors produced with 4, 8 and 16 interdigitated electrodes.

The table shows the dimensions of the micro-supercapacitors designed with 4, 8 and 16 interdigitated electrodes.
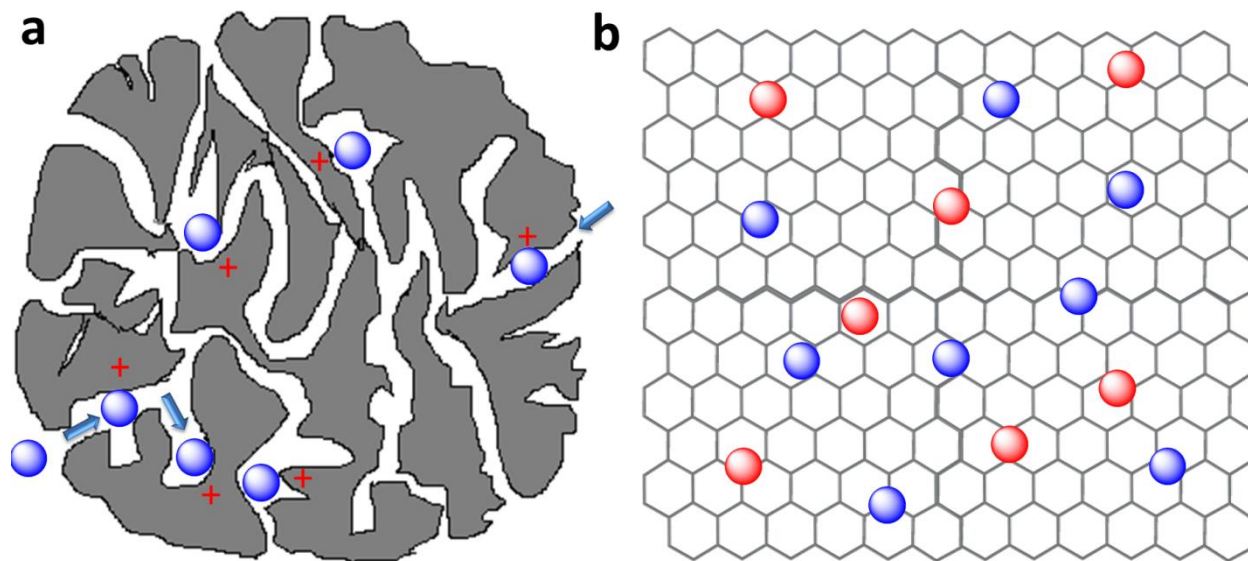
Figure 4S.9 | Explanation of the main differences between activated carbon and graphene in supercapacitors. In traditional supercapacitors made of activated carbon, most of the surface area resides in the micropores of the carbon; thus, this is unlikely to contribute significantly to the charge storage, especially at a high rate [41,42]. This results in a poor frequency response, with the energy stored in these carbon electrode materials released only at slow rate. Graphene, on the other hand, with its two-dimensional sheet-like structure possesses a large open surface area that is readily accessible to electrolyte with a small diffusion barrier. Graphene has thus the potential for making supercapacitors with power densities that surpass any other form of activated carbon.

The superior frequency response achieved with LSG micro-devices is due to the excellent electrolyte access to the graphene surfaces through its interconnected pores as shown in **Figure S3**. The micro-scale design of the device improves the rate capability through the reduction of the ion transport pathways. In addition, the LSG forms a highly conductive network, thus reducing the internal resistance of the microelectrodes.
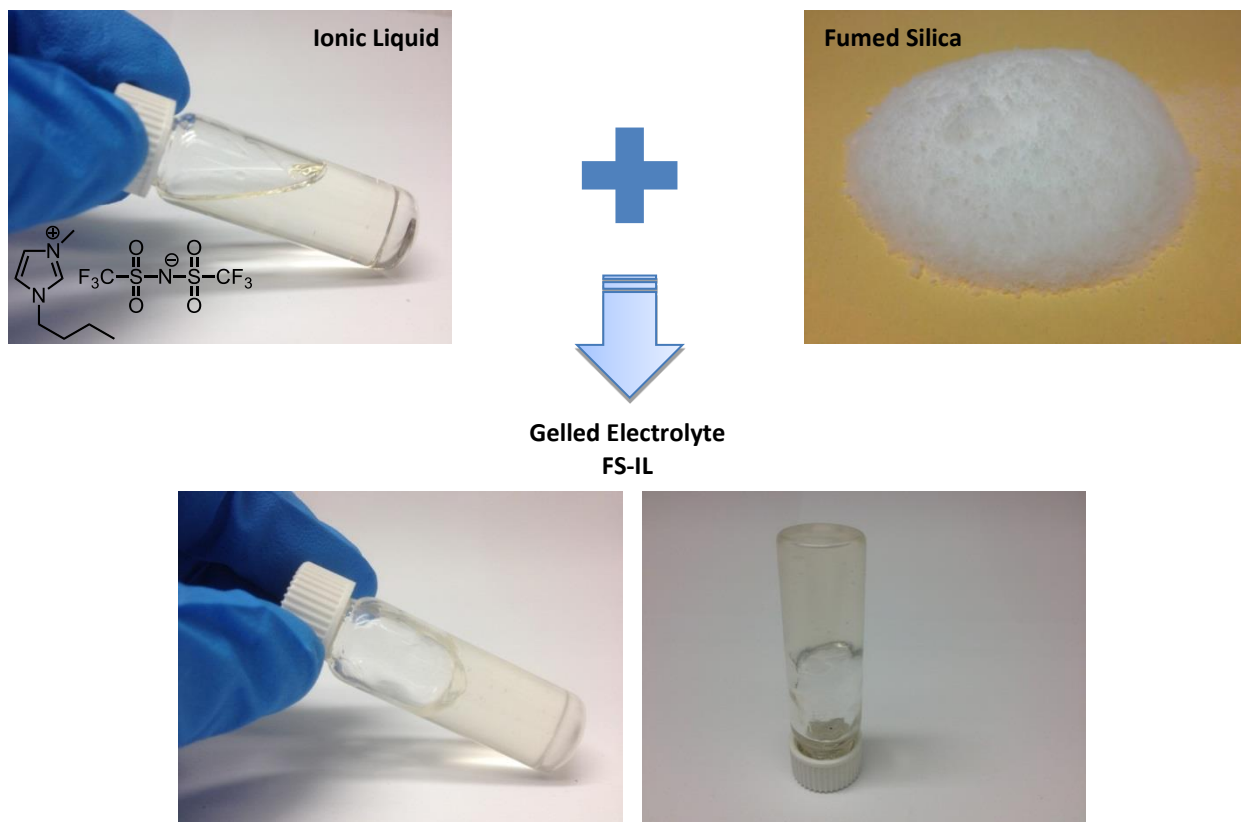
Figure 4S.10 | Preparation of ionogel based on ionic liquid and fumed silica. The ionogel was prepared by mixing together fumed silica nanopowder (average particle size 7 nm) with the ionic liquid (1-butyl-3-methylimidazolium bis(trifluoromethylsulfonyl)imide ([BMIM][NTf$_2$])) (0.03 g FS/1.0 g ([BMIM][NTf$_2$]). This mixture was stirred under an Ar atmosphere for 5 hours to produce a clear viscous ionogel (FS-IL). This ionogel was used as an electrolyte for the fabrication of all-solid-state micro-supercapacitors that are capable of providing 2.5 V compared with 1 V for traditional hydrogel-polymer electrolytes. These micro-supercapacitors thus have the potential to increase the energy density by one order of magnitude.
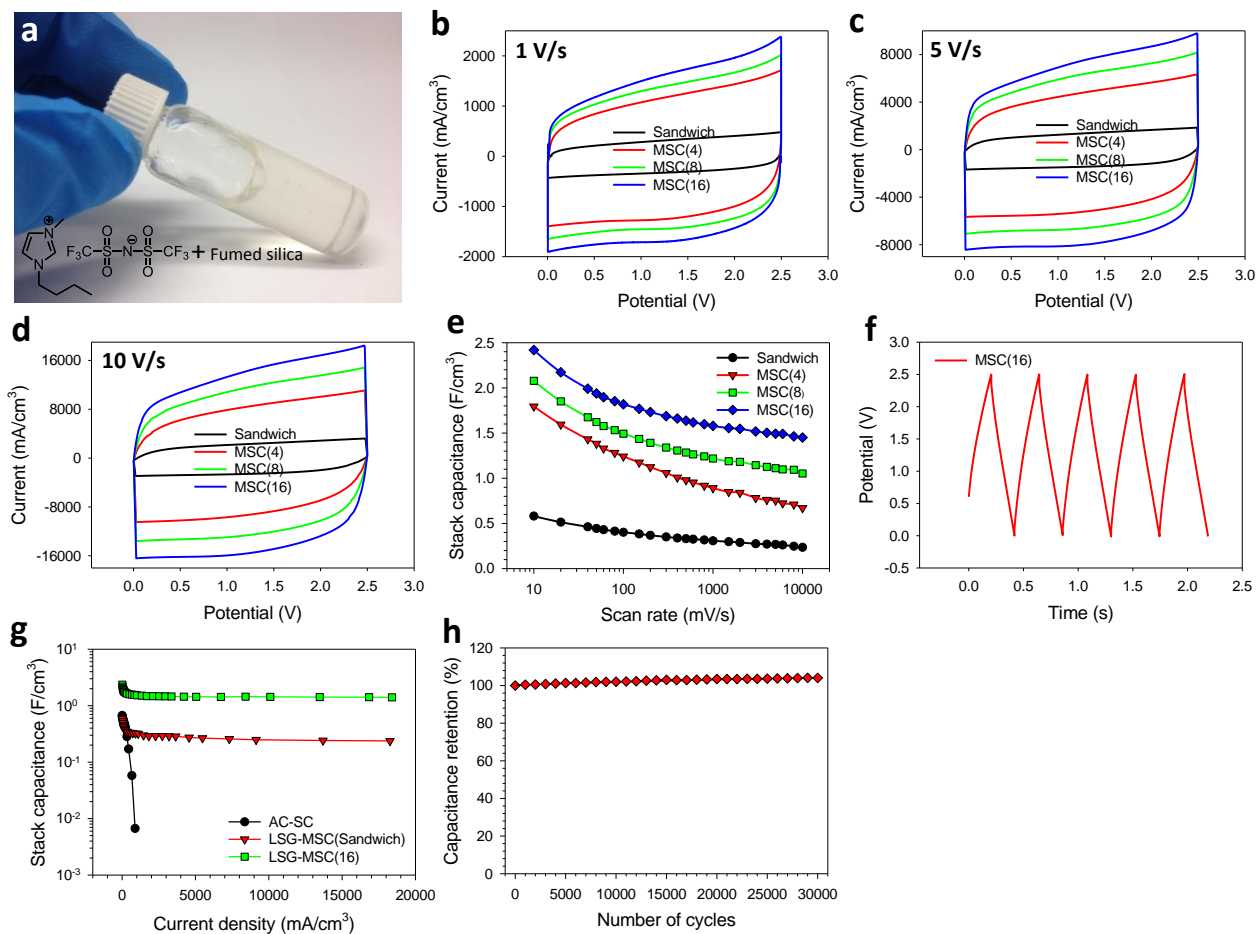
Figure 4S.11 | Ionogel electrolyte based on an ionic liquid and fumed silica is promising for high energy/high power density all-solid-state micro-supercapacitors. (a) The ionogel is prepared by mixing fumed silica nano-powder with the ionic liquid, 1-butyl-3-methylimidazolium bis(trifluoromethylsulfonyl)imide ([BMIM][NTf$_2$]). CV profiles of LSG-MSC in the sandwich and interdigitated structures with 4, 8 and 16 electrodes at scan rates of **(b)** 1,000 mV/s, **(c)** 5,000 mV/s and **(d)** 10,000 mV/s. **(e)** The stack capacitance of the different supercapacitors as a function of the scan rate. **(f)** Galvanostatic charge/discharge curves of LSG-MSC(16) at an ultrahigh current density of 1.6×10^4 mA/cm^3. **(g)** Volumetric stack capacitance of LSG micro-supercapacitors as calculated from the charge/discharge curves at different current densities. The micro-devices exhibit superior electrochemical performance comparable to that achieved with the PVA-H$_2$SO$_4$; **(h)** The micro-supercapacitor shows excellent cycling stability; the capacitance remains unchanged after 30,000 cycles of charge/discharge at a high current density of 1×10^3 mA/cm^3.

130
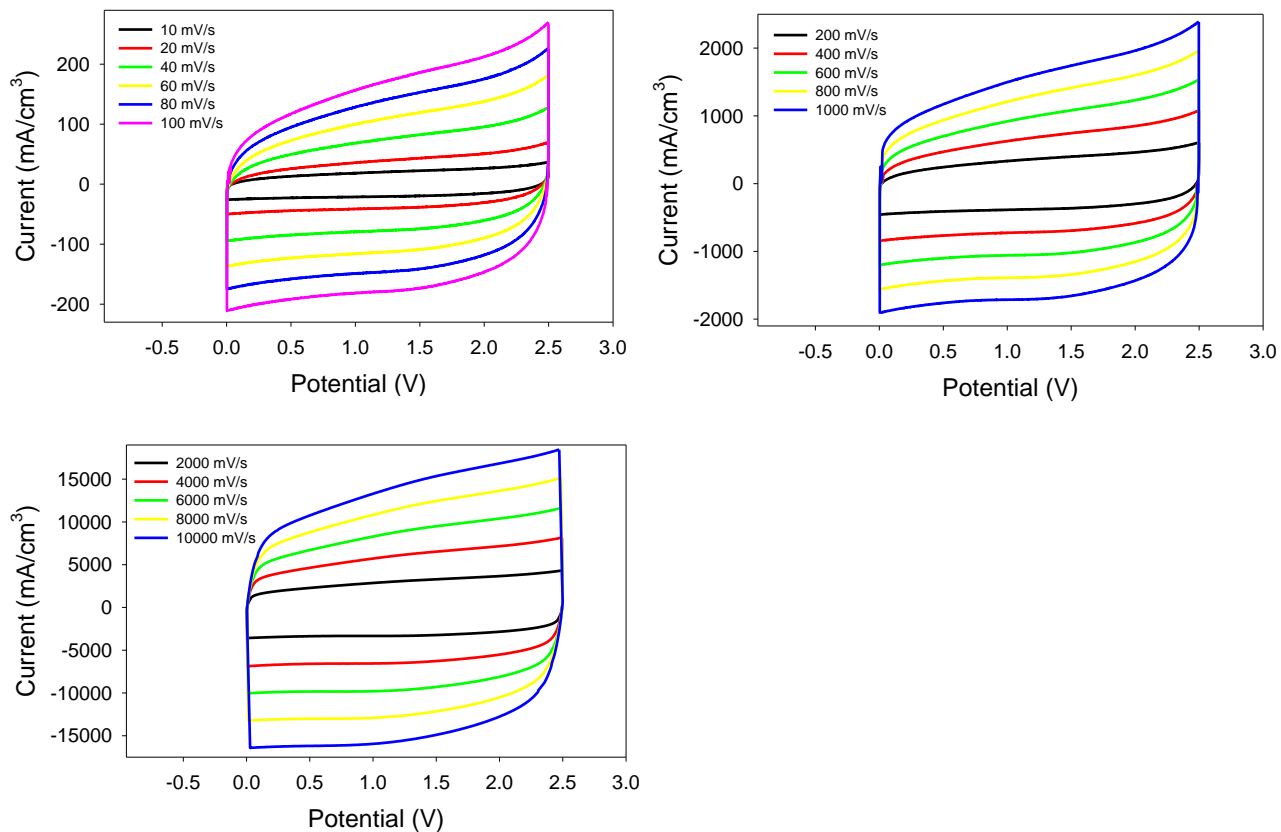
Figure 4S.12 | Electrochemical performance of LSG micro-supercapacitor with 16 interdigitated electrodes in a FS-IL gelled electrolyte. CV profiles of the device shown in a potential window of 2.5 V at different scan rates of (a) from 10 to 100 mV/s (b) from 200 to 1,000 mV/s and (c) from 2,000 to 10,000 mV/s.

	Activated carbon	LSG-MSC(16)	electrolytic capacitor
Freq. at -45° (Hz)	0.1	30	900
Time const. (ms)	10,000	19	1.1

Table 4S.1 | Electrochemical Impedance Spectroscopy (EIS) parameters for the different capacitors. The characteristic frequency f_o for a phase angle of -45° as obtained from the phase angle versus frequency plot for an activated carbon micro-supercapacitor, an interdigitated LSG micro-supercapacitor and an aluminum electrolytic capacitor. The frequency at -45° marks the point at which the resistive and capacitive impedances are equal; this is known as the characteristic frequency (f_o) of the device. The corresponding time constant is the time required to discharge the device with an efficiency of 63.2% and can be calculated using the formula ($1/f_o$). It takes approximately 5 time constants to effectively remove 99.7% of the stored energy.

Electrode material	Electrolyte	Operating voltage (V)	Energy density (mWh/cm³)	Power density W/cm³	Time constant (ms)	Ref
onion-like carbon	1M TEABF₄ in PC	3	~1.59 at 1 V/s*	~250*	26	2
rGO/CNT	3M KCl	1	0.68 at 1 V/s	77	4.8	3
LSG	Ionogel	2.5	2.1 at 0.01 V/s 1.37 at 1 V/s	141	19	This work

*these numbers were estimated from figures in the papers.

Table 4.S2. Comparison of the performance of LSG micro-supercapacitors with the state-of-the-art ultrahigh power micro-supercapacitors reported in the literature. Pech *et al.*[2] and Beidaghi *et al.*[3] presented planar micro-supercapacitors with the highest power density and the best frequency response reported thus far. **Table S2** shows that the LSG micro-supercapacitor can provide ultrahigh power with excellent frequency response that compares very well with the results reported in references [2,3]. Unfortunately, these micro-supercapacitors were produced using conventional micro-fabrication methods that require expensive and complex lithographic tools, thus limiting their potential for practical applications. Laser scribing, on the other hand, is a simple, one-step, scalable process that can be carried out using an inexpensive set-up. LightScribe is now commercially available at low cost for use with personal computers. LSG micro-supercapacitors are therefore promising for commercial applications. Furthermore, they can be made on flexible substrates that could have a significant impact on embedded flexible electronics. In addition, LSG micro-supercapacitors use gel electrolytes, making them all solid-state and thus they can be integrated safely into electronic circuits.

BIBLIOGRAPHY

[1] Chmiola, J., Largeot, C., Taberna, P.-L., Simon, P. & Gogotsi, Y. Monolithic carbide-derived carbon films for micro-supercapacitors. *Science* 328, 480-483 (2010).

[2] Pech, D., Brunet, M., Durou, H., Huang, P., Mochalin, V., Gogotsi, Y., Taberna, P.-L. & Simon, P. Ultrahigh-power micrometre-sized supercapacitors based on onion-like carbon. *Nature Nanotechnology* 5, 651-654 (2010).

[3] Beidaghi, M., Wang, C. Micro-Supercapacitors Based on Interdigital Electrodes of Reduced Graphene Oxide and Carbon Nanotube Composites with Ultra high Power Handling Performance. *Advanced Functional Materials* 22, 4501-4510 (2012).

[4] Pech, D., Brunet, M., Taberna, P.-L., Simon, P., Fabre, N., Mesnilgrente, F., Conédéra, V., Durou, H. Elaboration of a microstructured inkjet-printed carbon electrochemical capacitor. *J. Power Sources* 195, 1266-1269 (2010).

[5] Chen, W., Beidaghi, M., Penmatsa, V., Bechtold, K., Kumari, L., Li, W.Z. & Wang, C. Integration of carbon nanotube to C-MEMS for on-chip supercapacitors. *IEEE Transactions on Nanotechnology* 9, 734-740 (2010).

[6] Heon, M., Lofland, S., Applegate, J., Nolte, R., Cortes, E., Hettinger, J. D., Taberna, P.-L., Simon,P., Huang, P., Brunet, M. & Gogotsi, Y. Continuous carbide-derived carbon films with high volumetric capacitance. *Energy Environ. Sci.* 4, 135-138 (2011).

[7] Liu, C.-C., Tsai, D.-S., Susanti, D., Yeh, W.-C., Huang, Y.-S., Liu, F.-J. Planar ultracapacitors of miniature interdigital electrode loaded with hydrous RuO_2 and RuO_2 nanorods. *Electrochimica Acta* 55, 5768-5774 (2010).

[8] Xue, M., Xie, Z., Zhang, L., Ma, X., Wu, X., Guo, Y., Song, W., Li, Z. & Cao, T. Microfluidic etching for fabrication of flexible and all-solid-state micro supercapacitor based on MnO_2 nanoparticles. *Nanoscale* 3, 2703-2708 (2011).

[9] Beidaghi, M., Wang, C., Micro-Supercapacitors based on three dimensional interdigital polypyrrole/C-MEMS electrodes. *Electrochim. Acta* 56, 9508-9514 (2011).

[10] Wang, K., Zou, W., Quan, B., Yu, A., Wu, H., Jiang, P., Wei, P. An All-Solid-State Flexible Micro-supercapacitor on a Chip. *Adv. Energy Mater.* 1, 1068–1072 (2011).

[11] El-Kady, M. F., Strong, V., Dubin, S., Kaner, R. B. Laser Scribing of High-Performance and Flexible Graphene-Based Electrochemical Capacitors. *Science* 335, 1326-1330 (2012).

[12] Zhu, Y., Murali, S., Stoller, M. D., Ganesh, K. J., Cai, W., Ferreira, P. J., Pirkle, A., Wallace, R. M., Cychosz, K. A., Thommes, M., Su, D., Stach, E. A., Ruoff, R. S. Carbon-Based Supercapacitors Produced by Activation of Graphene. Science 332, 1537-1541 (2011).

[13] Miller, J. R., Outlaw, R. A., Holloway, B.C. Graphene double-layer capacitor with ac line-filtering performance. *Science* 329, 1637-1639 (2010).

[14] Miller, J.R., Outlaw, R.A., Holloway, B.C. Graphene electric double layer capacitor with ultra-high-power performance. *Electrochimica Acta* 56, 10443-10449 (2011).

[15] Sheng, K., Sun, Y., Li, C., Yuan, W. & Shi, G. Ultrahigh-rate supercapacitors based on electrochemically reduced graphene oxide for ac line-filtering, *Scientific Reports* 2, 247 (2012).

[16] Yoo, J. J., Balakrishnan, K., Huang, J., Meunier, V., Sumpter, B. G., Srivastava, A., Conway, M., Reddy, A. L. M., Yu, J., Vajtai, R. & Ajayan, P. M. Ultrathin Planar Graphene Supercapacitors. *Nano Lett.* 11, 1423–1427 (2011).

[17] Gao, W., Singh, N., Song, L., Liu, Z., Reddy, A. L. M., Ci, L., Vajtai, R., Zhang, Q., Wei, B. & Ajayan, P. M. Direct laser writing of micro-supercapacitors on hydrated graphite oxide films. *Nature Nanotechnology* 6, 496-500 (2011).

[18] Stinson, D. G.; Maguire, M. LightScribe Direct Disc Labeling, International Symposium on Optical Memory and Optical Data Storage, Optics Society of America, Hawaii, July 2005.

[19] Gilje, S., Dubin, S., Badakhshan, A., Farrar, J., Danczyk, S. A. & Kaner, R.B. Photothermal Deoxygenation of Graphene Oxide for Patterning and Distributed Ignition Applications. *Adv. Mater.* 22, 419–423 (2010).

[20] Cote, L. J., Cruz-Silva, R. & Huang, J. Flash reduction and patterning of graphite oxide and its polymer composite. *J. Am. Chem. Soc.* 131, 11027–11032 (2009).

[21] Strong, V., Dubin, S., El-Kady, M. F., Lech, A., Wang, Y., Weiller, B. H. & Kaner, R. B. Patterning and electronics tuning of laser scribed graphene for flexible all-carbon devices. *ACS Nano* 6, 1395-1403 (2012).

[22] Gogotsi, Y., Simon, P., True performance metrics in electrochemical energy storage. *Science* 334, 917-918 (2011).

[23] Miller, J. R. Valuing reversible energy storage. *Science* 335, 1312-1313 (2012).

[24] Zhang, L. L., Zhao, X. S. Carbon-based materials as supercapacitor electrodes. *Chem. Soc. Rev.* 38, 2520-2531 (2009).

[25] In, H. J., Kumar, S., Shao-Horn, Y. & Barbastathis, G. Origami fabrication of nanostructured, three-dimensional devices: electrochemical capacitors with carbon electrodes. *Appl. Phys. Lett.* 88, 0831041 (2006).

[26] Park, S., Wang, G., Cho, B., Kim, Y., Song, S., Ji, Y., Yoon, M.-H. & Lee, T. Flexible molecular-scale electronic devices. *Nature Nanotechnology* 7, 438-442 (2012)

[27] Xue, M., Li, F., Zhu, J., Song, H., Zhang, M. & Cao, T. Structure-based enhanced capacitance: In situ growth of highly ordered polyaniline nanorods on reduced graphene oxide patterns. *Adv. Funct. Mater.* 22, 1284–1290 (2012).

[28] Sung, J.-H., Kim, S.-J., Jeong, S.-H., Kim, E.-H., Lee, K.-H. Flexible Micro-supercapacitors. *J. Power Sources* 162, 1467-1470 (2006).

[29] Wishart, J.F. Energy applications of ionic liquids. *Energy Environ. Sci.* 2, 956-961 (2009).

[30] Bideau, J. L., Viau, L. & Vioux, A. Ionogels, ionic liquid based hybrid materials, *Chem. Soc. Rev.* 40, 907–925 (2011).

[31] Conway, B.E. *Electrochemical Supercapacitors: Scientific Fundamentals and Technological Applications*, (Kluwer Academic Press/Plenum Publishers) New York, NY, 1999, pp. 557-596.

[32] Stoller, M. D. & Ruoff, R. S. Best practice methods for determining an electrode material's performance for ultracapacitors. *Energy & Environmental Science* 3, 1294-1301 (2010).

[33] Wang, Z. L. Self-Powered Nanosensors and Nanosystems. *Adv. Mater.* 24, 280–285 (2012).

[34] Nishide, H., Oyaizu, K. Towards flexible batteries. *Science* 319, 737-738 (2008).

[35] Kovtyukhova, N. I. *et al.*, Layer-by-layer assembly of ultrathin composite films from micron-sized graphite oxide sheets and polycations. *Chem. Mater.* 11, 771-778 (1999).

[36] Ricketts, B. W., Ton-That, C. Self-discharge of carbon-based supercapacitors with organic electrolytes. *Journal of Power Sources* 89, 64-69 (2000).

[37] Zhang, Q., Rong, J., Ma, D. & Wei, B. The governing self-discharge processes in activated carbon fabric-based supercapacitors with different organic electrolytes. *Energy & Environmental Science* 4, 4152-4259 (2011).

[38] Kowal, J., Avaroglu, E., Chamekh, F., Senfelds, A., Thien, T., Wijaya, D. & Sauer, D. U. Detailed analysis of the self-discharge of supercapacitors. *Journal of Power Sources* 196, 573-579 (2011).

[39] Arthur, T. S., Bates, D. J., Cirigliano, N., Johnson, D. C., Malati, P., Mosby, J. M., Perre, E., Rawls, M. T., Prieto, A. L. & Bruce Dunn. Three-dimensional electrodes and battery architectures. *MRS Bulletin* 36, 523-531 (2011).

[40] Shen, C., Wang, X., Zhang, W. & Kang, F. A high-performance three-dimensional micro supercapacitor based on self-supporting composite materials. *Journal of Power Sources* 196, 10465-10471 (2011).

[41] Du, C., Pan, N. Supercapacitors using carbon nanotubes films by electrophoretic deposition. *Journal of Power Sources* 160, 1487–1494 (2006).

[42] Merlet, C., Rotenberg, B., Madden, P. A., Taberna, P.-L., Simon, P., Gogotsi, Y. & Salanne, M. On the molecular origin of supercapacitance in nanoporous carbon electrodes. *Nature Materials* 11, 306-310 (2012).

CHAPTER 5

Rational Design and Engineering of Three-Dimensional Graphene/MnO$_2$ Electrodes for High-Performance Hybrid Supercapacitors and Micro-Supercapacitors

5.1 ABSTRACT

Supercapacitors have been playing an important role in the progress of hybrid and electric vehicles, consumer electronics, military and space applications. There is a growing demand in developing hybrid supercapacitor systems to overcome the energy density limitations of the current generation of carbon-based supercapacitors. Here, we demonstrate 3D hybrid supercapacitors and micro-supercapacitors by rationally designing the electrode microstructure, combination of materials, and proper choice of electrolytes that operate at high voltages. By choosing a 3D graphene support structure with high conductivity, suitable porosity, and high specific surface area and further doping with nanostructured MnO$_2$, ultrahigh volumetric capacitance of over 300 F/cm^3 can be achieved. This corresponds to a specific capacitance of the constituent MnO$_2$ of 1029 F/g, which is close to the theoretical value of 1380 F/g. The energy density of the full device is between 0.1-16.2 mWh/cm^3 depending on the configuration, which is superior to those of commercially available double layer capacitors, pseudo-capacitors and hybrid supercapacitors tested under the same conditions.

5.2 INTRODUCTION

As a result of the rapidly growing energy needs of modern life, the development of high performance energy storage devices has gained significant attention. Supercapacitors are promising energy storage devices with properties intermediate between those of batteries and traditional capacitors, but they are being improved more rapidly than either (1). Over the past couple of decades, supercapacitors have become key components of our everyday life and are currently replacing batteries and capacitors in an increasing number of applications. Their high power density and excellent low temperature performance have made them the technology of choice for back-up power, cold starting, camera flash, regenerative braking and hybrid electric vehicles (2). The future growth of this technology depends on further improvements of the energy density, power density, calendar and cycle life and cost of production.

According to the charge storage mechanism, supercapacitors are classified as electric double layer capacitors (EDLCs) or pseudo-capacitors (3,4). In EDLCs, charge is stored through rapid adsorption/desorption of electrolyte ions on high-surface-area carbon materials, whereas pseudo-capacitors store charge via fast and reversible Faradaic reactions near the surface of metal oxides or conducting polymers. The majority of supercapacitors currently available in the market are symmetric EDLCs featuring activated carbon electrodes and organic electrolytes that provide cell voltages as high as 2.7 V (2-5). Although commercial EDLCs exhibit high power density and excellent cycle life, they suffer from low energy density because of the limited capacitance of carbon-based electrodes. The specific pseudo-capacitance of Faradaic electrodes (typically 300-1000 F/g) exceeds that of carbon-based EDLCs, however, their performance tend to degrade quickly up on cycling (2-4).

Studies in the past few years have demonstrated an attractive alternative to conventional EDLCs and pseudo-capacitors by using hybrid systems. Utilizing both Faradaic and non-Faradaic processes to store charge, hybrid capacitors can achieve energy and power densities greater than EDLCs without sacrificing the cycling stability and affordability that have so far limited the success of pseudo-capacitors (6,7). Several combinations of materials, such as RuO_2 (8), Co_3O_4 (9), NiO (10), V_2O_5 (11), $Ni(OH)_2$ (12), and MnO_2 (13) have been studied for preparing hybrid supercapacitors. Among these, MnO_2-based systems are particularly attractive as MnO_2 is an earth abundant and environmentally friendly material with a high theoretical specific capacitance of 1380 F/g (14). However, the poor ionic (10^{-13} S/cm) and electronic (10^{-5}-10^{-6} S/cm) conductivity of pristine MnO_2 often limits its electrochemical performance. Recent reports show that some high-performance results can be achieved only from ultrathin MnO_2 films that are a few tens of nanometers in thickness (15). Nevertheless, the thickness and the area-normalized capacitance of these electrodes are not adequate for most applications. A promising approach to realizing practical applications of MnO_2 is to incorporate nanostructured MnO_2 on highly conductive support materials with high surface area such as nickel foam (16), activated carbon (17), carbon foam (18), carbon fabric (19), conducting polymers (20), carbon nanotubes (21-22) and graphene (23-26). Although promising specific capacitances of 148 – 410 F/g have been achieved, such values were obtained only under slow charge/discharge rates and they were found to decrease rapidly as the discharge rate was increased. Moreover, many of these materials have low packaging density with large pore volume, meaning that a huge amount of electrolyte is needed to build the device, which adds to the mass of the device without adding any capacitance (27). Accordingly, the energy density and power density of these systems struggle on the device level. To solve these critical problems, we have developed promising hybrid electrodes based on three-dimensional graphene doped with MnO_2 nanoflowers. By

rationally designing the structure of the graphene substrate to achieve high conductivity, suitable porosity, and high specific surface area, one may expect to not only achieve a high gravimetric capacitance, but also to improve the volumetric capacitance (26). Furthermore, the high surface area nanostructured MnO_2 provides more active sites for the Faradaic reactions and shortens the ion diffusion pathways that are crucial for realizing its full pseudo-capacitance.

Portable electronic devices are becoming increasingly small and flexible which pose new challenges for the design of rechargeable micro-power sources of appropriate size (28-29). Several kinds of micron-sized power sources such as micro-batteries, micro-fuel cells, and energy harvesters have been developed in recent years (30). However, for applications that require high power, there is a need for miniaturized supercapacitors known as micro-supercapacitors (30). Since the size of these systems is often determined by the power supply, the micro-supercapacitor should be able to store a large amount of charge per footprint area of the device (31). While great efforts have been made for the fabrication of macro-scale hybrid supercapacitors, there are only a few studies on the design and integration of hybrid materials into micro-supercapacitors (32-34). This is likely due to complicated micro-fabrication techniques that are often involved in building 3D micro-electrodes with micro-meter separations (32). Here, we present a simple, yet versatile technique for the fabrication of 3D hybrid micro-supercapacitors based on graphene and MnO_2. These micro-devices enable an ultrahigh areal capacitance of over 60 mF/cm^2 and energy density of 16 mWh/cm^3.

5.3 RESULTS AND DISCUSSION

Rational design of high-performance hybrid supercapacitors. In designing supercapacitor electrodes, special efforts are made to ensure that they are capable of providing high energy density and high power density. This requires optimization of the preparation conditions to facilitate ionic and electronic transport within the electrodes [35] as illustrated in Figure 5.1. However, this is very challenging especially with metal oxide pseudo-capacitors because of the low electrical conductivity and long ionic diffusion pathways of conventional metal oxide films. Thus, in conventional compact MnO_2 thick film electrodes, only the top layer is exposed to the electrolyte, meaning that a limited amount of the active material is involved in charge storage, Fig. 5.1A. To solve these problems, various approaches have been explored in the literature. For example, the electrochemical utilization of electrodes was improved by using nanostructured MnO_2 such as nanoparticles, nanorods, nanowires and nanoflowers [36-37]. The porous structure of these electrodes maximizes the area of active material that is exposed to the electrolyte and thus available to discharge compared to a solid electrode surface, Fig. 5.1B. Although this system exhibits higher energy density, it still suffers from the inherently low electrical conductivity of MnO_2 leading to low power output. To improve the electrical conductivity of MnO_2 film, conductive materials such as carbon powder, carbon nanotubes and graphene have been introduced into nanostructured MnO_2 electrodes [38]. However, the electronic charge carriers must move through small inter-particle contact areas which exhibit additional resistance resulting in poor electron transport from the electrode material to the current collector, Fig. 5.1C. An ideal electrode would be obtained by growing MnO_2 nanostructures onto a 3D interconnected macro-porous graphene framework with high electrical conductivity and high surface area, Fig. 5.1D.
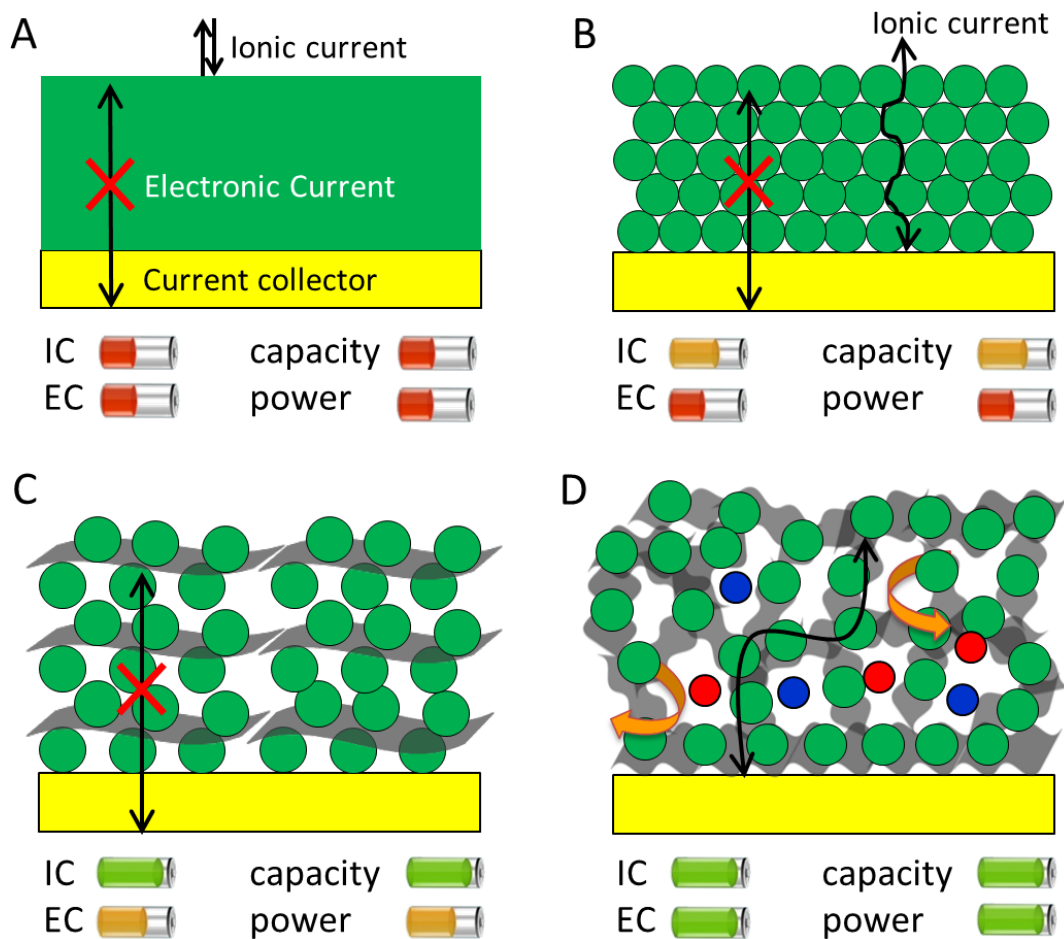
Figure 5.1: Rational design of high energy/high power hybrid supercapacitor electrodes. Improving the ionic current (IC) and electronic current (EC) within the electrode is the key. Different approaches have been explored including (A) Compact thick films of metal oxide (here, MnO_2), (B) Nanostructured metal oxide films. (C) Addition of conductive materials to the nanostructured metal oxide. (D) Growing nanostructured metal oxide on 3D interconnected graphene networks with high surface area and high electronic conductivity.

In this structure, the conducting graphene framework acts as a 3D current collector to provide

In this structure, the conducting graphene framework acts as a 3D current collector to provide electron "superhighways" for charge storage and delivery and the nanostructured MnO_2 enables fast, reversible Faradaic reactions with short ionic diffusion pathways. Another interesting feature of this structure is that each MnO_2 nanoparticle is electrically connected to the current collector so that all the nanoparticles contribute to capacity with almost no "dead" mass.

Synthesis and characterization of 3D macroporous LSG/MnO₂ electrodes. To experimentally realize energy dense and high power supercapacitor electrodes, we integrated a highly conductive and high surface area 3D laser scribed graphene (LSG) framework with MnO_2 as schematically illustrated in Fig. 5.2A. The 3D LSG framework was produced from the laser scribing of GO films following our previously reported method [35], upon which the color changes from golden brown to black. The LSG framework was subsequently coated *in situ* with MnO_2 using an electrochemical deposition technique as described in the Methods section, Figure 5.2B. This *in situ* growth technique enables MnO_2 to be strongly anchored onto the graphene framework, thus enabling reduced contact resistance and better electrochemical utilization of MnO_2. Note in Fig. 5.2B that the graphene electrode turns darker in color after electro-deposition, a visual indication of the loading of MnO_2. It is well accepted that the conductivity and mass loading of the active materials have a significant impact on the electrochemical behavior of supercapacitor electrodes. Here, the mass loading of MnO_2 is controlled by adjusting the deposition current and deposition time. Fig. 5.2C shows that the MnO_2 loading changes almost linearly with the deposition time at an applied current of 0.25 mA/cm^2 and an average deposition rate estimated to be ~6 µg/min.
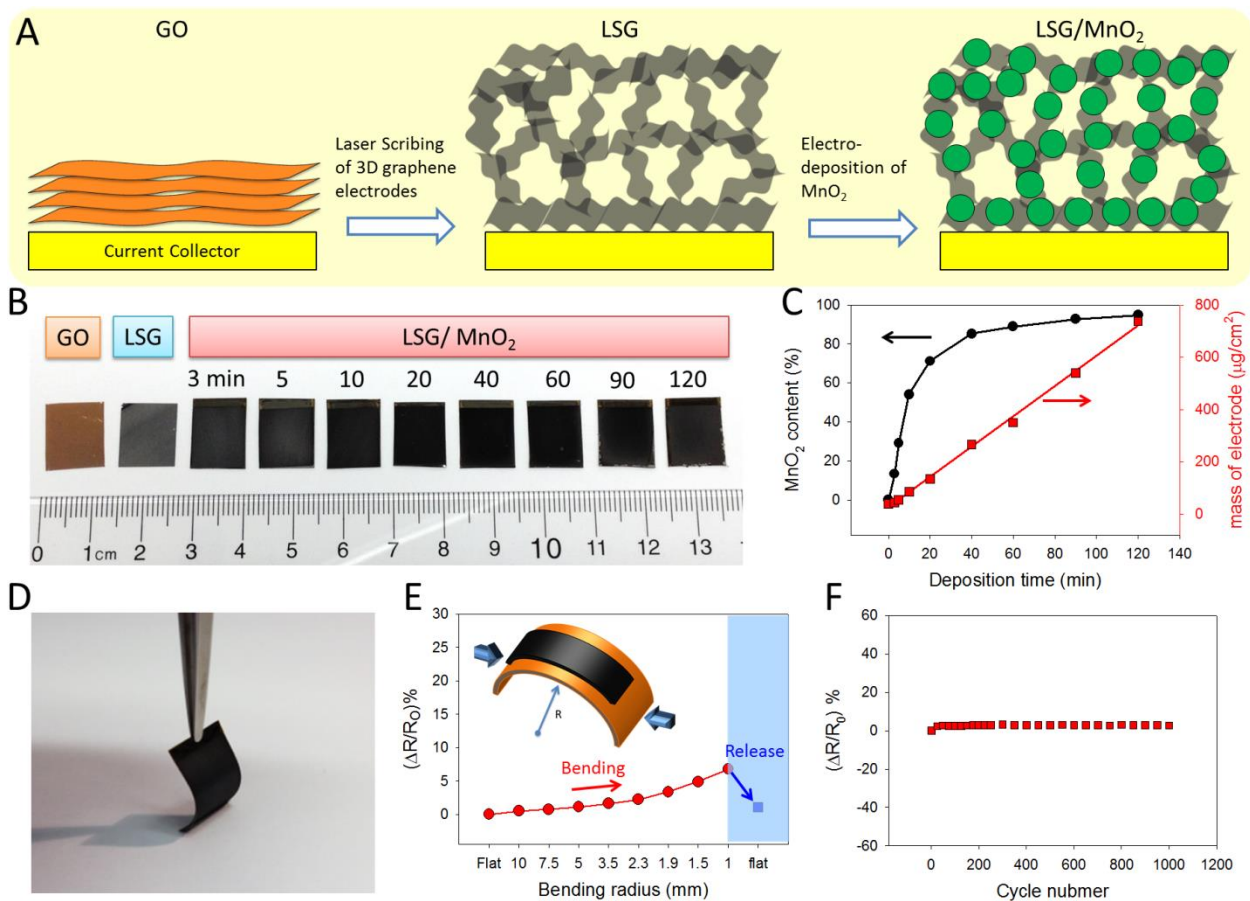
Figure 5.2: Fabrication and characterization of LSG/MnO$_2$ electrodes. (A) A schematic diagram showing the fabrication procedure of LSG/MnO$_2$ electrodes. (B) Digital photographs showing a GO film before and after it has been laser scribed to form LSG. LSG is then loaded with MnO$_2$ whose amount can be controlled by adjusting the deposition time from 3 min to 120 min. (C) Mass loading of MnO$_2$ versus deposition time. (D) Photograph showing the flexibility of a LSG/MnO$_2$ electrode. (E) Variation of the resistance of a LSG/MnO$_2$ electrode as a function of bending radius. (F) The resistance change of a LSG/MnO$_2$ electrode under repeated bending cycles for a bend radius of 5 mm.

146

In addition to interesting electrical properties, the LSG/MnO$_2$ electrodes are monolithic and demonstrate superb mechanical integrity under large mechanical deformation. Fig. 5.2D shows that a LSG/MnO$_2$ electrode can be bent significantly without damage. We evaluated the foldability of LSG/MnO$_2$ electrodes by measuring their electrical resistance under successive bending cycles. The resistance varies only slightly up to a bending radius of 1.0 mm (approximate tensile strain of 11.7%) and can be completely recover after straightening, Fig. 5.2E. Notably, after 1000 cycles of bending and straightening at a bend radius of 5.0 mm, the resistance increases by only about 2.8%, Fig. 5.2F. These measurements demonstrate the excellent electro-mechanical properties of LSG/MnO$_2$ electrodes, which is highly desirable for applications in flexible and wearable electronics.
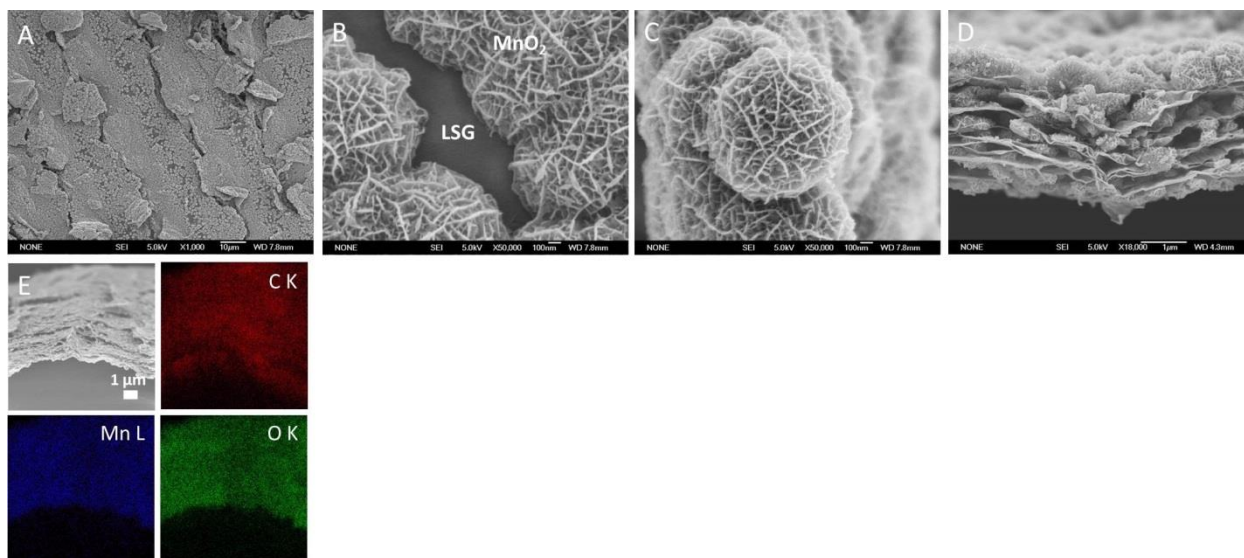
Figure 5.3: Morphological and structural characterization of LSG/MnO$_2$ electrodes. (A and B) SEM images of a LSG/MnO$_2$ electrode at low and high magnification. (C) SEM image showing the nanoflower morphology of electrodeposited MnO$_2$. (D) Cross-sectional SEM image of LSG/MnO$_2$. (E) EDS elemental mapping of C (red), Mn (blue) and O (green).

The evolution of morphology corresponding to different deposition times was examined by scanning electron microscopy, Fig. 5.3A-D. The SEM micrographs show the general morphology and detailed microstructure of a typical sample prepared by 60 minutes of deposition. MnO_2 has been uniformly coated onto the surface of graphene throughout the entire film. Moreover, the electrodeposited MnO_2 particles show a nanoflower-shaped hierarchical architecture with a clear interface between MnO_2 and the graphene substrate, which is consistent with previous studies (23). Closer inspection of the MnO_2 nanoflowers shows that they are made up of hundreds of ultrathin nanoflakes that are 10-20 nm thick. These nanoflakes are interconnected together to form mesoporous MnO_2 with large accessible surface area, thus offering numerous electroactive sites available to the electrolyte which promotes fast surface Faradaic reactions.

The 3D structure of LSG/MnO_2 electrodes was further analyzed using cross-sectional SEM, Fig. 5.3D. The 3D porous structure of LSG is preserved after the deposition of MnO_2 without any agglomerations. The graphene surface has been uniformly coated with MnO_2 over the entire cross-section. In addition, energy-dispersive X-ray spectroscopy (EDS) provides elemental maps of C, O and Mn, which confirms that a homogeneous coating of MnO_2 throughout the 3D macroporous framework has been created. As a control for comparison purposes, the electrodeposition of MnO_2 was carried out on chemically converted graphene (CCG) and gold substrates. Unlike the LSG framework, the electrodeposition of MnO_2 occurs only on the top surface of the CCG (figure not shown), whereas a thick and compact film of MnO_2 is deposited on gold, which is typical of structure A shown in Fig. 5.1. In addition, both the CCG/MnO_2 and Au/MnO_2 electrodes showed poor mechanical properties compared to LSG/MnO_2.

XPS was successfully used for better understanding of the chemical composition and the oxidation state of Mn in LSG/MnO$_2$ electrodes. The Mn 2p, Mn 3s and O 1s spectra are presented in Fig. 5.3 H-J (not shown). The peaks of Mn 2p$_{3/2}$ and Mn 2p$_{1/2}$ are located at 642.1 and 653.9 eV respectively, with a spin energy separation of 11.8 eV, which is in good agreement with the reported data of Mn 2p states previously reported [21-26]. Toupin *et al.* showed that the peak separation of the Mn 3s doublet is related to the oxidation state of Mn in manganese oxides, where reference samples of MnO, Mn$_3$O$_4$, Mn$_2$O$_3$ and MnO$_2$ showed a separation of 5.79, 5.50, 5.41 and 4.78 eV, respectively [39]. The as-prepared LSG/MnO$_2$ showed a separation energy of 4.8 eV for the Mn 3s doublet (Fig. 3H, not shown), suggesting that the oxide is MnO$_2$ which was further confirmed from the O 1s spectrum.

Assembly and electrochemical performance of symmetric LSG/MnO$_2$ supercapacitors. In order to test the electrochemical performance of LSG/MnO$_2$ macroporous frameworks, a supercapacitor pouch cell was assembled from two symmetric electrodes separated by a Celgard 3501 ion porous separator and impregnated with 1.0 M Na$_2$SO$_4$ electrolyte, Fig. 5.4A. The cells were tested by cyclic voltammetry (CV) over a wide range of scan rates from 1 mV/s—1000 mV/s. As an example, consider the LSG/MnO$_2$ sample with a deposition time of 3 minutes, the supercapacitor shows nearly rectangular CV profiles up to a scan rate as high as 1000 mV/s, indicating excellent charge storage characteristics and ultrafast response time for the electrodes, Fig. 5.4B. The capacitances of the devices made with different deposition times were calculated from CV profiles and presented in Fig. 5.4C. Note that the capacitance was calculated using the total volume of the cell stack, rather than a single electrode. This includes the volume of the current collector, the active material, the separator and electrolyte.
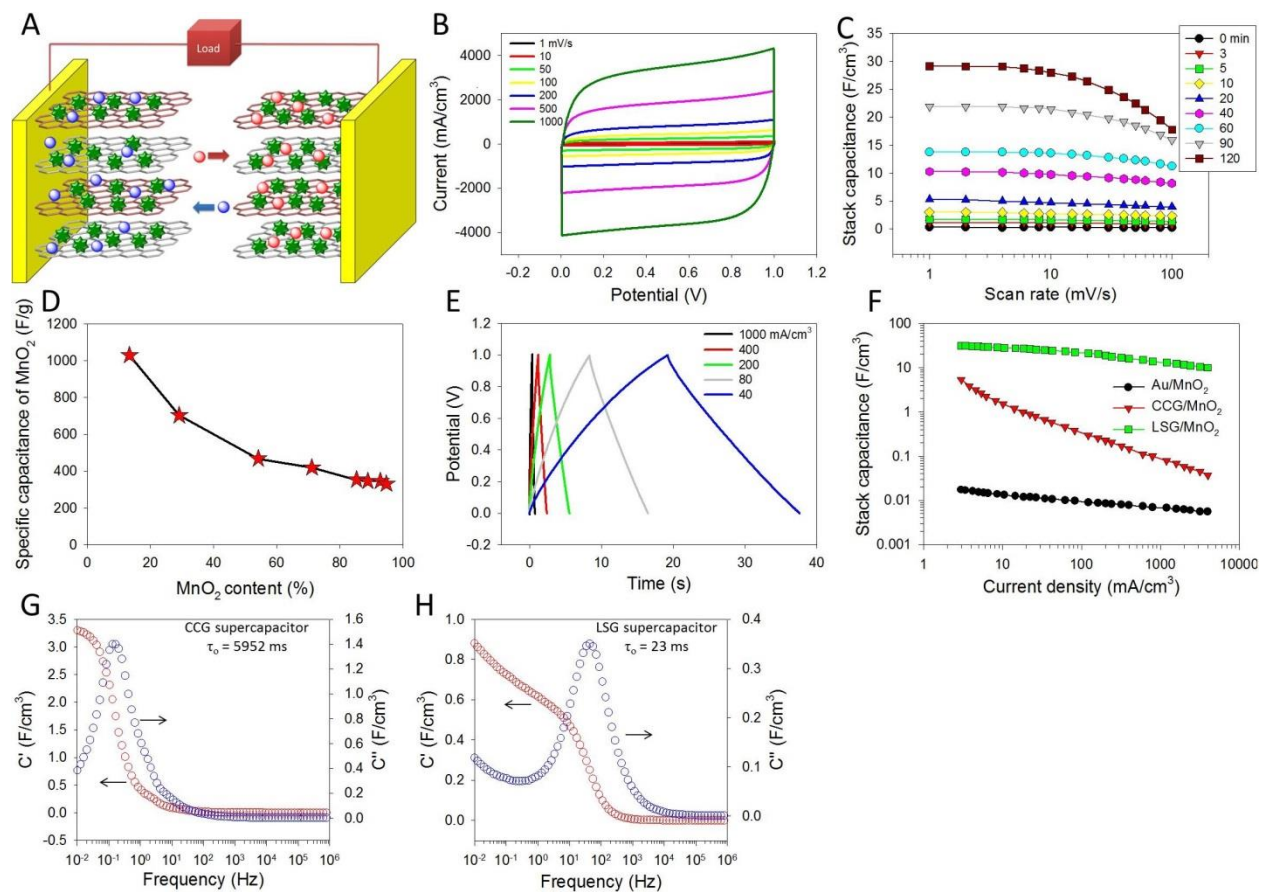
Figure 5.4: Electrochemical performance of LSG/MnO₂ symmetric supercapacitors. (A) A photograph of the device. (B) Cyclic voltammetry profiles for a LSG/MnO₂ (3 min) supercapacitor at different scan rates. (C) Evolution of the stack capacitance of LSG with various mass loadings of MnO₂ as a function of scan rate. (D) Specific capacitance due to MnO₂ only as a function of the loadings measured at a scan rate of 1 mV/s. (E) Charge/discharge curves of a LSG/MnO₂ (3 min) supercapacitor at different current densities. (F) The change of stack capacitance of a LSG/MnO₂ (120 min) supercapacitor with current density. Data for CCG/MnO₂ and Au/MnO₂ supercapacitors are presented for comparison. (G-H) Progression of the real part (C') and imaginary part (C") of the stack capacitance of CCG (G) and LSG (H) as a function of frequency.

We observe that the capacitance depends strongly on the loading amount of the pseudo-capacitive MnO_2 and increases significantly with deposition time from 0-120 min. For example, a stack capacitance of up to 30 F/cm^3 at 10 mV/s can be achieved with the sample at 120 min deposition time. This translates to a volumetric capacitance of ~300 F/cm^3 when calculated based on the volume of the active material only. This value is much higher than the capacitance of bare LSG (12 F/cm^3) and activated MEGO (60 F/cm^3), indicating that the volumetric capacitance of graphene based electrodes can be significantly improved by incorporating pseudo-capacitive materials. Furthermore, this value is higher than some of the best values reported previously for MnO_2 based supercapacitors: 130 F/cm^3 for graphene/MnO_2/CNT (40), 246 F/cm^3 for CNT/MnO_2 (41), 108 F/cm^3 for meso-porous carbon/MnO_2 (42) and 90 F/cm^3 for ultra-porous carbon/MnO_2 (18).

This unprecedented performance can be understood by separating the contribution of the MnO_2 nanoflowers to the average capacitance of the LSG/MnO_2 electrodes. The specific capacitance contributed by MnO_2 alone was calculated by subtracting the charge of the bare LSG framework according to the equation $C_{s,MnO2} = (Q_{LSG/MnO2} - Q_{LSG})/(\Delta V \times m_{MnO2})$ [15]. Here Q is the voltammetric charge, ΔV is the operating potential window and m is the mass. The specific capacitance of MnO_2 depends on the mass of the active material reaching a maximum value of 1029 F/g which is about 75% of the theoretical capacitance at a mass loading of 13% of MnO_2, Fig. 5.4D (see Appendix 1, SI for a further explanation). This remarkable performance can be attributed to the electrode microstructure that facilitates the transport of ions and electrons and provides abundant surfaces for charge-transfer reactions, ensuring a greater utilization of the active materials.

In order to demonstrate the superior properties of LSG/MnO$_2$ macro-porous electrodes, CCG/MnO$_2$ and Au/MnO$_2$ symmetric supercapacitors were built as well, and their electrochemical performance was tested under the same dynamic conditions, Fig. 5.4F. Not only does the CCG/MnO$_2$ exhibit lower capacitance, but its performance falls off very quickly at higher charge/discharge rates. This can be attributed to the restacking of graphene sheets during the fabrication of the CCG electrodes, resulting in a significant reduction in the surface area and eventually closing most of the porosity [43]. In addition, the Au/MnO$_2$ supercapacitor shows extremely low capacitance because of the limited surface area and structural properties as can be seen in Fig. 5.1. LSG/MnO$_2$, on the other hand, shows a stack capacitance of 31 F/cm^3 that is more than four times higher than CCG/MnO$_2$ and about three orders of magnitude higher than Au/MnO$_2$. The enhanced capacitance and rate capability of the LSG/MnO$_2$ further confirms its optimized structure which synergizes the effects of both effective ion migration and high electroactive surface area, thus enabling high and reversible capacitive behavior even at high charge/discharge rates.

Construction of asymmetric supercapacitors. Asymmetric supercapacitors (ASCs) make use of positive and negative electrode materials of different types that can be charged/discharged in well-separated potential windows in the same electrolyte. They have attracted attention because they offer high capacity via a Faradaic reaction at the positive electrode and maintain fast charge/discharge due to the EDL mechanism at the negative electrode. Moreover, the asymmetric configuration can extend the operating voltage window of aqueous electrolytes beyond the thermodynamic limit of water (about 1.2 V), leading to significantly higher specific energy than symmetric supercapacitors using aqueous electrolytes.
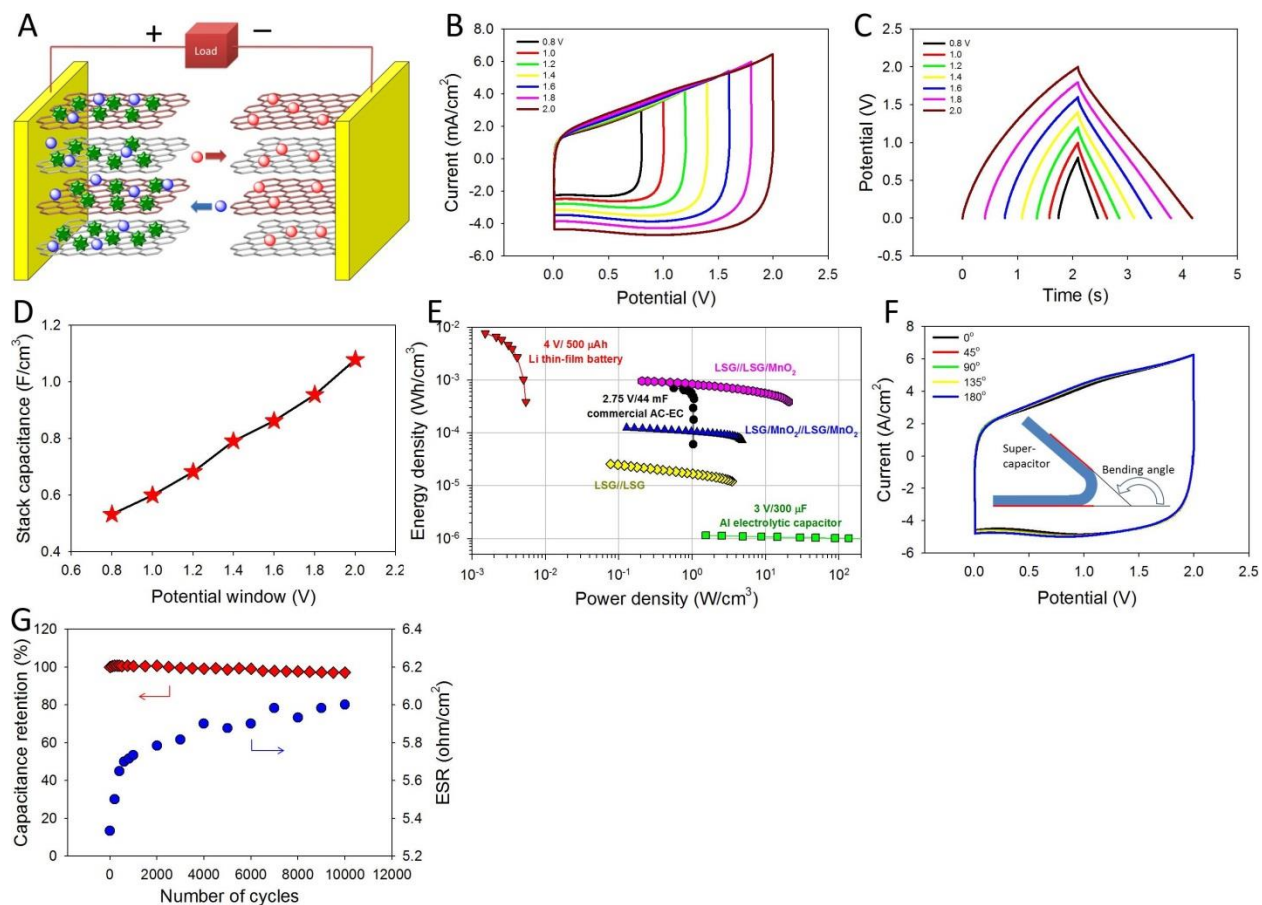
Figure 5.5: Asymmetric supercapacitor based on graphene/MnO$_2$ as positive electrode and LSG as negative electrode. (A) Schematic showing the structure of the assembled supercapacitor in 1.0 M Na$_2$SO$_4$ electrolyte. (B-C) The electrochemical performance of the asymmetric supercapacitor with the increase of the potential window from 0.8 to 2.0 V. (D) Change of the stack capacitance as a function of potential window. (E) Cancel. (F) Electrochemical performance of the device under different bending angles. (G) Cycling stability of the device tested over 10,000 cycles at a scan rate of 1000 mV/s. Change of the ESR during cycling is also shown.

In fact, ASCs based on carbon and NiOOH electrodes and aqueous electrolyte are now commercially available from ESMA-ELTON. However, while this configuration ensures high capacitance, it has a low cell voltage (<1.5 V) that is detrimental to its energy and power performance (44). Considering the high pseudo-capacitance of the LSG/MnO$_2$ electrode and the fast charge/discharge of the double layer capacitance of the LSG electrode, an asymmetric supercapacitor was assembled using LSG/MnO$_2$ and LSG as the positive and negative electrodes, respectively, as schematically illustrated in Fig. 5.5A. Here, the asymmetric cell used LSG/MnO$_2$ with 13% MnO$_2$ mass loading (3 min deposition time) for the positive electrode. The asymmetric supercapacitor exhibits an ideal capacitive behavior with nearly rectangular CV profiles and highly triangular CC curves, Fig. 5.5B-C. The CV profile retains its rectangular shape without apparent distortions with increasing scan rates up to an ultrahigh rate of 10,000 mV/s, indicating the high rate capability of this asymmetric supercapacitor. Interestingly, the asymmetric cell presents a wide and stable operating potential window up to 2.0 V in aqueous electrolyte that should afford high energy density. Furthermore, as the operating potential window is increased from 0.8 to 2.0 V, the stack capacitance increases significantly from 0.53 – 1.08 F/cm^3, meaning that the stored energy and power can be greatly improved at this wider potential window, Fig. 5.5D. Compared to that of LSG and LSG/MnO$_2$ symmetric supercapacitors, the asymmetric device shows remarkably enhanced energy density and power density; 0.96 mWh/cm^3 and 20.8 W/cm^3, respectively (Fig. 5.5E). In addition, not only the energy density of this supercapacitor is comparable to organic-based commercial AC supercapacitors, but its power density is ~20 times higher. The as-fabricated supercapacitor is highly flexible and can be folded and twisted without affecting the structural integrity of the device, Fig. 5.5A. In addition, the supercapacitor delivers almost the same capacity even when

placed under high bending conditions, holding promise as a practical energy storage system for flexible electronics, Fig. 5.5F.

Long cycle life is another important feature for commercially viable supercapacitors. Indeed, the asymmetric supercapacitor is very stable as it maintains over 97% of its original capacity after 10,000 charge/discharge cycles tested at a high scan rate of 1000 mV/s. The ESR of the supercapacitor was monitored during cycling using a Nyquist plot. The device demonstrates a slight increase of ESR in the first 1000 cycles with only subtle changes over the remaining cycles.

Three-dimensional interdigitated micro-supercapacitors. The development of miniaturized electronic systems such as smart sensors, implantable medical devices and micro-electromechanical systems (MEMS) has led to an increasing demand for microscale supercapacitors with high energy density in a limited space. Hence, this characteristic is crucial in the miniaturization of energy storage devices for modern electronic applications. Previous research has focused on increasing the micro-supercapacitor energy density by using different active materials such as activated carbon, graphene, carbon nanotubes, polymers and metal oxides. Since the capacitance of LSG/MnO$_2$ is generally higher than that of activated carbon, graphene or carbon nanotubes, it is more suitable for micro-supercapacitors where high capacity in a small footprint is required. Interestingly, a variety of supercapacitors with asymmetric electrodes can provide excellent overall performance; however, they are rarely reported as solutions for microscale supercapacitors. Taking the scalability and extensibility of the structure into consideration, a new device was designed as illustrated in Fig. 5.6, in which the positive and negative electrodes are separated into a 3D interdigitated structure.
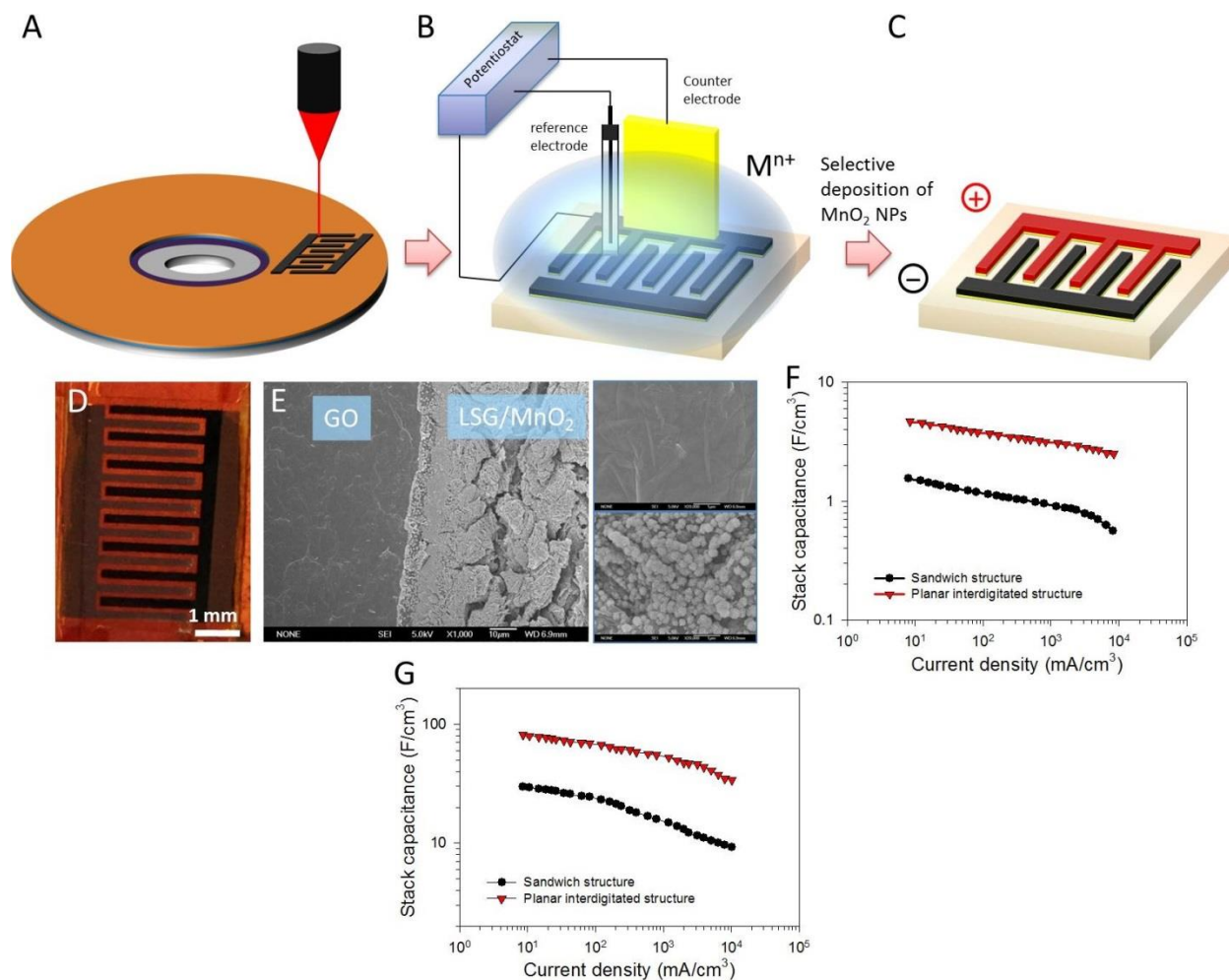
Figure 5.6: Engineering of 3D interdigitated micro-supercapacitors with high energy density. (A-C) Illustration of the fabrication process of an asymmetric micro-supercapacitor based on LSG/MnO$_2$ as the positive electrode and LSG as the negative electrode. (D) A photograph showing the asymmetric micro-supercapacitor. (E) An SEM image at the interface between GO and LSG showing the selective electro-deposition of MnO$_2$ on LSG only. A magnified view of the GO and LSG area are provided in the inset. (F-G) Comparing the stack capacitance of the supercapacitor in the sandwich and planar interdigitated structure for (F) asymmetric and (G) symmetric devices.

This structure was achieved by combining the techniques of "top down" LightScribe lithography with "bottom up" selective electro-deposition. First, 3D interdigitated LSG microelectrodes were produced by the direct writing of graphene patterns on GO films using a consumer grade LightScribe DVD burner as described in our previous report [45]. The device consists of 16 in-plane microelectrodes (8 positive and 8 negative) separated by nearly insulating GO and the distance between the microelectrodes is close enough to keep the ion-transport pathway short. Subsequently, MnO_2 nanoflowers were selectively electrodeposited on one set of the LSG micro-electrodes using the cell setup described in the schematic diagram (see methods). Fig. 5.6D shows a digital photograph of the asymmetric micro-supercapacitor that consists of alternating positive and negative electrodes. The lighter microelectrodes correspond to bare graphene (negative electrodes), whereas the other side turns darker in color after the electrodeposition of MnO_2 (positive electrodes). The optical microscope image shows a well-defined pattern and sharp boundaries between the microelectrodes (figure not shown). SEM further confirmed the conformal structure of this asymmetric micro-supercapacitor. A magnified view at the interface between GO and graphene shows the selective electro-deposition of MnO_2 on the graphene area only, Fig. 5.6E.

Electrochemical characterization shows that the asymmetric micro-supercapacitor provides enhanced volumetric capacitance and rate capability compared to a conventional sandwich-type asymmetric supercapacitor, Fig. 5.6F. This is likely due to the planar structure of the microdevices that results in better volumetric packaging efficiency by eliminating the need for the polymer separator typically used in the sandwich structure to avoid short circuiting between electrodes. Moreover, the micro-scale architecture of the devices results in a significant reduction of the mean ionic diffusion pathway between the two microelectrodes. This is

consistent with our previous results with all-graphene micro-supercapacitors [45]. Symmetric hybrid micro-supercapacitors showed a similar behavior, Fig. 5.6G. The stack capacity has now significantly improved to be around 80 F/cm^3, which is much higher than values previously reported for EDLC micro-supercapacitors: 1.3 F/cm^3 for carbon onions [46], 2.35-3.05 F/cm^3 for graphene [45], 1.08 F/cm^3 for CNT [47] and 3.1 F/cm^3 for graphene/CNT [48]

The energy and power density of the LSG/MnO_2-based supercapacitors are presented in Figure 5.7 (not shown). In order to put these results in perspective with current technology, we characterized a number of commercially available carbon-based supercapacitors, pseudo-capacitors, hybrid supercapacitors, and Li ion capacitors and the results are presented in the same plot. These devices were tested under the same dynamic conditions as LSG/MnO_2. For all devices, the calculations were made based on the volume of the full cell that includes the current collector, active material, separator and electrolyte. The energy density of the hybrid LSG/MnO_2 varies between 0.1 to 16.2 mWh/cm^3 depending on the configuration (symmetric, asymmetric and sandwich, interdigitated) and the mass loading of MnO_2. This is superior to EDLC carbon-based supercapacitors, pseudo-capacitors, hybrid supercapacitors and is comparable to or higher than Li ion capacitors (9.5-18.7 mWh/cm^3 depending the manufacturer and electrode composition). Furthermore, LSG/MnO_2 supercapacitors can provide up to 74 W/cm^3, which is about one order of magnitude higher than commercially available systems.

5.4 CONCLUSIONS

In summary, we have developed a simple and scalable approach for the fabrication of hybrid LSG/MnO_2 three-dimensional electrodes. The LSG with its high electrical conductivity and porous structure is shown to be an excellent scaffold for MnO_2 nanoparticles. The unique structure of these hybrid electrodes allow efficient use of the pseudo-capacitive properties of MnO_2, while providing facilitated transport of both electrolyte ions and electrons. As a result, these supercapacitors exhibit high specific capacitance, ultrafast charge/discharge rate, excellent cycling stability and high power density. Given that MnO_2 is widely used in alkaline batteries (selling approximately 60 billion pieces per year) and the scalability of graphene based materials, we believe the graphene/MnO_2 hybrid electrodes offer promise for applications such as grid scale energy storage.

5.5 MATERIALS AND METHODS

Synthesis of LSG/MnO$_2$, Au/MnO$_2$ and CCG/MnO$_2$ electrodes. The LSG framework was prepared following our previously reported method (35). This was followed by the electro-deposition of MnO_2 from 0.02 M $Mn(NO_3)_2$ in 0.1 M $NaNO_3$ aqueous solution using a standard three electrode setup, where a piece of LSG (1 cm^2) is used as the working electrode, Ag/AgCl as the reference electrode (BASi, Indiana, USA) and a platinum foil (2 cm^2, Sigma-Aldrich) as the counter-electrode. The deposition was achieved by applying a constant current of 50 $\mu A/cm^2$ for different periods of time between 3 min and 120 min. After electro-deposition, the working electrode was thoroughly washed with DI water to remove the excess electrolyte and dried in oven at 60 °C for 1 h. The amount of MnO_2 deposited on the LSG framework was determined

from the difference in weight of the electrode before and after electro-deposition using a high precision microbalance with a readability of 1 μg (Mettler Toledo, MX5).

For comparison, MnO_2 was electrodeposited on other substrates such as gold-coated polyimide and graphene (CCG) paper. The gold-coated polyimide was obtained from Astral Technology Unlimited, Inc. (Minnesota, USA) and used without further treatment. The graphene paper was produced following our previously reported method (49). The gold-coated polyimide and graphene paper were cut into rectangular strips of 1 cm^2 for further electro-deposition of MnO_2 under the same conditions as described above.

Assembly of sandwich-type hybrid supercapacitors. Hybrid supercapacitors with the conventional sandwich structure were assembled using electrodes prepared in the previous section. Both symmetric and asymmetric supercapacitors were constructed. Symmetric supercapacitors were assembled by sandwiching a Celgard 2501 (Celgard, NC) separator between two identical electrodes using 1.0 M Na_2SO_4 aqueous solution as electrolyte. In the asymmetric structure, LSG/MnO_2 was used as the positive electrode and LSG as the negative electrode. For the LSG- and CCG-based supercapacitors, stainless steel tape was attached to the electrodes, using silver paint, as the current collector. Before assembly, the electrodes were soaked in the electrolyte for 1 h to ensure proper wetting.

Fabrication of interdigitated hybrid micro-supercapacitors. The fabrication process of a micro-supercapacitor is illustrated in Figure 5.6 and described below. First, LSG interdigitated microelectrodes were printed directly on a GO film supported on a polyethylene terephthalate substrate using a consumer grade DVD burner (45). Second, MnO_2 nanoflowers were grown on one set of the interdigitated electrodes using the electro-deposition setup described above. The

160

applied current was normalized to the active LSG deposition area at a current density of 250 μA/cm^2 and the mass loading was controlled by adjusting the deposition time. Likewise, symmetric micro-supercapacitors based on LSG/MnO$_2$ as both the positive and the negative electrodes were prepared as well. Here, the fabrication process is the same except that the two sides (instead of one side) of the bare interdigitated LSG electrodes were connected together using copper tape and used as the working electrode during electro-deposition.

Characterization and measurements. The morphology and microstructure of the different electrodes were investigated by means of field emission scanning electron microscopy (JEOL 6700) equipped with energy dispersive spectroscopy (EDS) and optical microscopy (Zeiss Axiotech 100). XPS analysis was performed using a Kratos Axis Ultra DLD spectrometer. The thicknesses of the different components of the device were measured using cross-sectional scanning electron microscopy and a Dektak 6 profilometer. The electrochemical performances of the LSG-MSC supercapacitors were investigated by CV, galvanostatic charge/discharge tests and EIS. CV and charge/discharge testing were performed on a VersaSTAT3 electrochemical workstation (Princeton Applied Research, USA). EIS measurements were recorded on a VMP3 workstation (Bio-Logic Inc., Knoxville, TN) over a frequency range of 1 MHz to 10 mHz with an amplitude of 10 mV at the open-circuit potential. Calculations of the specific capacitance and the energy and power densities are discussed in detail in the Supporting Information.

BIBLIOGRAPHY

[1] Dr Peter Harrop and Dr Victor Zhitomirsky, Electrochemical Double Layer Capacitors: Supercapacitors 2013-2023, Business Report IDTechEx, July 2013. http://www.idtechex.com/research/reports/electrochemical-double-layer-capacitors-supercapacitors-2013-2023-000318.asp

[2] P. Simon, Y. Gogotsi, Materials for electrochemical capacitors, Nature Materials 7, 845-854 (2008).

[3] Li Li Zhang and X. S. Zhao, Carbon-based materials as supercapacitor electrodes, Chem. Soc. Rev., 2009, 38, 2520–2531.

[4] Guoping Wang, Lei Zhang and Jiujun Zhang, A review of electrode materials for electrochemical supercapacitors, Chem. Soc. Rev., 2012, 41, 797–828.

[5] P. Simon, Y. Gogotsi, Capacitive Energy Storage in Nanostructured Carbon-Electrolyte Systems, Accounts of Chemical Research 45, 1094–1103 (2013).

[6] Jeffrey W. Long, Daniel Bélanger, Thierry Brousse,Wataru Sugimoto, Megan B. Sassin, and Olivier Crosnier, MRS Bulletin 36, 513-522 (2011).

[7] Katsuhiko Naoi, Syuichi Ishimoto, Jun-ichi Miyamoto and Wako Naoi, Energy Environ. Sci., 2012, 5, 9363–9373.

[8] Jintao Zhang, Jianwen Jiang, Hongliang Li and X. S. Zhao, Energy Environ. Sci., 2011, 4, 4009–4015.

[9] Jing Xu, Qiufan Wang, Xiaowei Wang, Qingyi Xiang, Bo Liang, Di Chen, and Guozhen Shen, ACS Nano 7, 5453–5462 (2013).

162

[10] Huanlei Wang, Chris M. B. Holt, Zhi Li, Xuehai Tan, Babak Shalchi Amirkhiz, Zhanwei Xu, Brian C. Olsen, Tyler Stephenson, and David Mitlin, Nano Res. 2012, 5(9): 605–617.

[11] Zheng Chen, Veronica Augustyn, Jing Wen, Yuewei Zhang, Meiqing Shen, Bruce Dunn, and Yunfeng Lu, Adv. Mater. 2011, 23, 791–795.

[12] Junyi Ji, Li Li Zhang, Hengxing Ji, Yang Li, Xin Zhao, Xin Bai, Xiaobin Fan, Fengbao Zhang, and Rodney S. Ruoff, *ACS Nano*, **2013**, *7*, pp 6237–6243.

[13] Jintao Zhang, Jianwen Jiang, Hongliang Li and X. S. Zhao, Adv. Funct. Mater. 2011, 21, 2366–2375.

[14] Bélanger, D., Brousse, T. & Long, J. W. Manganese oxides: battery materials make the leap to electrochemical capacitors. *Electrochem. Soc. Interface* **17**, 49–52 (2008)

[15] Xingyou Lang, Akihiko Hirata, Takeshi Fujita and Mingwei Chen, *Nature Nanotechnology* 11, 232-236 (2011).

[16] Hongcai Gao, Fei Xiao, Chi Bun Ching, and Hongwei Duan, ACS Appl. Mater. Interfaces 2012, 4, 2801−2810.

[17] V. Khomenko, E. Raymundo-Pinero, F. Beguin, Journal of Power Sources 153 (2006) 183–190.

[18] Fischer, A. E.; Pettigrew, K. A.; Rolison, D. R.; Stroud, R. M.; Long, J. W. Nano Lett. 2007, 7 (2), 281−286.

[19] Yuan, L. Y.; Lu, X. H.; Xiao, X.; Zhai, T.; Dai, J. J.; Zhang, F. C.; Hu, B.; Wang, X.; Gong, L.; Chen, J.; Hu, C. G.; Tong, Y. X.; Zhou, J.; Wang, Z. L. ACS Nano 2012, 6 (1), 656−661.

[20] G.P. Pandeya, A.C. Rastogi, ECS Transactions, 50 (43) 71-78 (2013).

[21] Wei Chen, R. B. Rakhi, Liangbing Hu, Xing Xie, Yi Cui, and H. N. Alshareef

Nano Lett. 2011, 11, 5165–5172.

[22] Liangbing Hu, Wei Chen, Xing Xie, Nian Liu, Yuan Yang, Hui Wu, Yan Yao, Mauro Pasta, Husam N. Alshareef, and Yi Cui, ACS Nano 5, 8904-8913 (2011).

[23] Guihua Yu, Liangbing Hu, Michael Vosgueritchian, Huiliang Wang, Xing Xie, James R. McDonough, Xu Cui, Yi Cui, and Zhenan Bao, Nano Lett. 2011, 11, 2905–2911.

[24] Bong Gill Choi, MinHo Yang, Won Hi Hong, Jang Wook Choi, and Yun Suk Huh, ACS Nano 6, 4020-4028 (2012).

[25] Afriyanti Sumboja , Ce Yao Foo , Xu Wang , and Pooi See Lee. *Adv. Mater.* 2013, 25, 2809–2815.

[26] Xin Zhao, Lili Zhang, Shanthi Murali, Meryl D. Stoller, Qinghua Zhang, Yanwu Zhu, and Rodney S. Ruoff, ACS Nano 6, 5404-5412 (2012).

[27] Y. Gogotsi, P. Simon. *Science* 334, 917-918 (2011).

[28] Wei Lai, Can K. Erdonmez, Thomas F. Marinis, Caroline K. Bjune, Nancy J. Dudney, Fan Xu, Ryan Wartena, and Yet-Ming Chiang, Adv. Mater. 2010, 22, E139–E144.

[29] John Chmiola, Celine Largeot, Pierre-Louis Taberna, Patrice Simon, Yury Gogotsi. *Science* 328, 480 (2010).

[30] Majid Beidaghi, Chunlei Wang. Proc. of SPIE Vol. 8377, 837708-1.

[31] Timothy S. Arthur, Daniel J. Bates, Nicolas Cirigliano, Derek C. Johnson, Peter Malati, James M. Mosby, Emilie Perre, Matthew T. Rawls, Amy yL. Prieto, and Bruce Dunn, MRS Bulletin 36, 523-531 (2011).

[32] Caiwei Shen, Xiaohong Wang, Siwei Li, Jiangan Wang, Wenfeng Zhang, Feiyu Kang, Journal of Power Sources 234, 302-309 (2013).

[33] Wenwen Liu, Xingbin Yan, Jiangtao Chen, Yaqiang Feng and Qunji Xue, Nanoscale, 2013, 5, 6053–6062.

[34] Wen-Wen Liu, Ya-Qiang Feng, Xing-Bin Yan, Jiang-Tao Chen, and Qun-Ji Xue, Adv. Funct. Mater. 2013, DOI: 10.1002/adfm.201203771

[35] Maher F. El-Kady, Veronica Strong, Sergey Dubin and Richard B. Kaner. *Science* 335, 1326-1330 (2012).

[36] S. Devaraj and N. Munichandraiah, Journal of The Electrochemical Society 154, A80-A88 (2007).

[37] Jian Yan, Eugene Khoo, Afriyanti Sumboja, and Pooi See Lee, ACS Nano 4, 4247-4255 (2010).

[38] Zhi M, Xiang C, Li J, Li M, Wu N. Energy Environ Sci 5, 72-78 (2013).

[39] Mathieu Toupin, Thierry Brousse,, and Daniel Belanger, *Chem. Mater.* **2004,** *16,* 3184-3190.

[40] Cheng, Y, Lu, S, Zhang, H, Varanasi, CV, Liu, J. Nano Letters 12, 4206-4211 (2012).

[41] Lee, SW, Kim, J, Chen, S, Hammond, PT, Shao-Horn, Y. ACS Nano 4, 3889-3896 (2010).

[42] Patel, MN, Wang, X, Wilson, B, Ferrer, DA, Dai, S, Stevenson, KJ, Johnston, KP. J. Mater. Chem. 20, 390–398 (2010).

[43] Yi Huang , Jiajie Liang , and Yongsheng Chen, *Small* 8, 1805–1834 (2012).

[44] http://www.elton-cap.com/

[45] Maher F. El-Kady, Richard B. Kaner. Nature Communications 4:1475 (2013).

[46] David Pech, Magali Brunet, Hugo Durou, Peihua Huang, Vadym Mochalin, Yury Gogotsi, Pierre-Louis Taberna, Patrice Simon, Nature Nanotechnology 5, 651-654 (2010).

[47] Jian Lin, Chenguang Zhang, Zheng Yan, Yu Zhu, Zhiwei Peng, Robert H. Hauge, Douglas Natelson, and James M. Tour, Nano Lett. 2013, 13, 72−78.

[48] Majid Beidaghi and Chunlei Wang. *Adv. Funct. Mater.* 22, 4501-4510 (2012).

[49] Dan Li, Marc B. Muller, Scott Gilje, Richard B. Kaner and Gordon G. Wallace. Nature Nanotechnology 3, 101-105 (2008).

Large Scale Fabrication of Polyaniline and Graphene/Polyaniline Micro-Supercapacitors Using a LightScribe DVD Burner

6.1 ABSTRACT

Progress in micro-fabrication technology has enabled increasingly compact autonomous microsystems for applications ranging from distributed sensing and communications networks to implantable medical devices [1,2]. Yet, power sources to enable their widespread adoption have not advanced nearly as rapidly. This is mainly due to the lack of energy dense materials and current fabrication techniques that rely on complicated and time consuming processes. Here, we use a consumer grade LightScribe DVD burner for the direct fabrication of polyaniline micro-supercapacitors on a large scale. The configuration of the device is based on polyaniline microelectrodes and welded polyaniline as a separator. This new design represents an important advance from current state-of-the-art micro-supercapacitors. The structure of the device enables the full utilization of the surface area of polyaniline and demonstrates ultrahigh specific capacitance in excess of 1000 F/g, which is much higher than previously reported for conventional sandwich-type supercapacitors. Furthermore, by combining graphene with nanostructured polyaniline to produce hybrid micro-supercapacitors, the areal energy density and power density is further enhanced which should enable the reduction of the footprint of the entire system. Considering the ease of fabrication, flexibility and scalability, this technique could lead to the utilization of micro-supercapacitors as energy storage devices in future portable electronic and micro-electronic devices.

6.2 INTRODUCTION

The rapid development of portable electronics, wireless sensor networks and multifunctional microsystems drives an increasing demand for miniaturized energy storage (1-2). At the same time, the desire to further miniaturize existing on-chip systems makes it attractive to develop power devices integrated with other elements (3). Today, micro-power sources are essential for micro-electronics, such as non-volatile memory, smart sensors, radio frequency identification tags, implantable medical devices and micro-electromechanical systems (MEMS) (4). While thin-film batteries have been considered as the prime candidates for these applications, they suffer from many limitations including limited cycle life, abrupt failure, poor low-temperature kinetics, and safety concerns associated with using lithium (5). Supercapacitors can solve these issues and provide a higher power density with maintenance-free operation (5,6). The high surface-to-volume ratio of the active material creates the high energy and power densities of supercapacitors; this is even further enhanced in micro-supercapacitors (7,8).

Recently, notable advances have been achieved in the micro-supercapacitor field with most efforts focused on improving energy and power densities by investigating different electrode materials (6). Generally, electric double layer capacitors (EDLC), which store charge on the surface of conductive and high-surface carbon materials, have been widely explored in the fabrication of micro-supercapacitors. Various nanostructured carbon materials have been utilized including activated carbons (7), carbon nanotubes (9), carbide-derived carbons (5,10), onion-like carbon (8) and graphene (11). Alternatively, pseudo-capacitive materials store charge through fast and reversible redox reactions and can offer higher specific capacitance than EDLCs. This is particularly interesting because energy dense materials should enable further miniaturization of existing micro-supercapacitors and reduce the size of their footprint. Transition metal oxides

such as ruthenium oxide (12) and manganese oxide (13), and conducting polymers such as polypyrrole (14) and polyaniline (15-18) have been used as materials for pseudo-capacitive micro-supercapacitors.

Polyaniline can be considered as one of the most promising electrode materials, due to its unique ability to be doped/dedoped through acid/base interactions, and oxidation/reduction chemistry (19). The conductivity of polyaniline increases reversibly with doping from the undoped insulating base form ($\sigma \leq 10^{-10}$ S/cm) to the fully doped, conducting salt form ($\sigma \geq 1$ S/cm). Conductivity can also be controlled either chemically or electrochemically by changing the oxidation state. These characteristics makes polyaniline a promising material for many applications including sensors (20), actuators (21), electrochromic devices (22), plastic non-volatile memory (23), water filtration membranes (24) and batteries (25). Because of its high theoretical specific capacitance of around 2000 F/g, polyaniline is an ideal candidate for supercapacitors (26,27). However, supercapacitors with conducting polymer electrodes generally suffer from limited stability during cycling. Previous research suggested that coupling nanostructured polyaniline to carbonaceous materials can improve the utilization of the pseudo-capacitive properties of polyaniline and provide short transport pathways for ions and electrons (28-32). It is believed that the excellent electrical and mechanical properties of graphene relieve the volume change of expansion and contraction of polyaniline during long-term charge/discharge processes (33-36).

While most efforts have focused on performance improvements in micro-supercapacitors, they have ignored cost, ease of preparation and device integration, which are likely the main driving forces for industry. In fact, on-chip integrated micro-supercapacitors are still produced on the lab-scale only and have not yet found their way into commercial uses. Therefore, it remains a

challenge to develop an inexpensive and scalable technique that enables the manufacturing of micro-supercapacitors on a large scale. In particular, the development of high-energy density polyaniline micro-supercapacitors is highly desirable.

6.3 RESULTS AND DISCUSSION

Recently, we have developed a simple technique for the patterning of polyaniline nanofiber films using a near infrared laser available in consumer grade LightScribe DVD burners (37). Basically, a DVD disc is coated with a film of polyaniline nanofibers and then inserted into the drive for laser treatment. When light from the laser is absorbed by the nanostructured polyaniline, a photothermal effect occurs in which the absorbed light is converted into heat, leading to cross-linking of the molecular chains of polyaniline. This phenomenon is termed "laser welding" and is associated with a significant change in the electrical and optical properties of polyaniline. Since polyaniline nanofibers are poor heat conductors, the heat does not spread beyond the laser lines, resulting in a well-defined separation between the welded and the non-welded areas.

The high-resolution patterning along with a huge difference in electrical conductivity between pristine polyaniline (~1 S/cm) and welded polyaniline (10^{-8} S/cm) enables the direct fabrication of a new generation of polyaniline micro-pseudo-capacitors. These micro-pseudo-capacitors employ the insulating properties of the welded polyaniline as a separator between pristine polyaniline microelectrodes as shown in Figure 6.1.
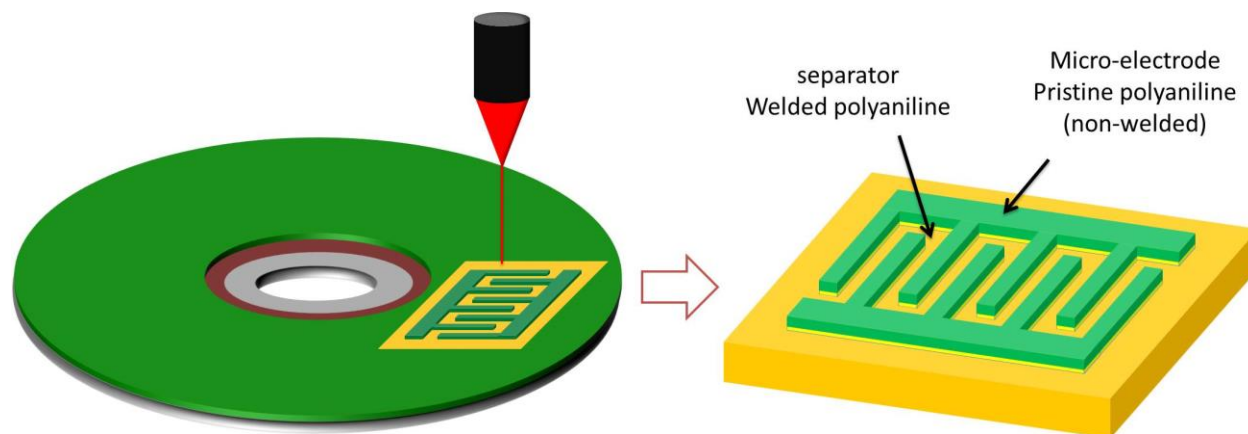
Figure 6.1: Fabrication of polyaniline micro-pseudo-capacitors. Polyaniline film is coated on a DVD followed by laser patterning using a LightScribe DVD burner.

This new and simplified architecture represents an important leap forward from current state-of-the-art micro-supercapacitors.

In previous work, we showed that a LightScribe DVD burner can also be used for the direct writing of graphene micro-supercapacitors from graphite oxide films (11). Thus, it is important to clarify the differences between the laser scribing of graphene and the laser welding of polyaniline, Figure 6.2. In the former process, wherever the laser hits the film, it turns electrically conducting. For example, in Figure 6.2a, a computerized image of an interdigitated pattern is printed on a graphite oxide film to produce graphene micro-supercapacitors. The inverse effect occurs during laser welding of polyaniline, i.e. wherever the laser hits the surface, it becomes electrically insulating. Hence, for producing polyaniline micro-pseudo-capacitors, the inverted image of the interdigitated pattern should be used instead, Figure 6.2b.
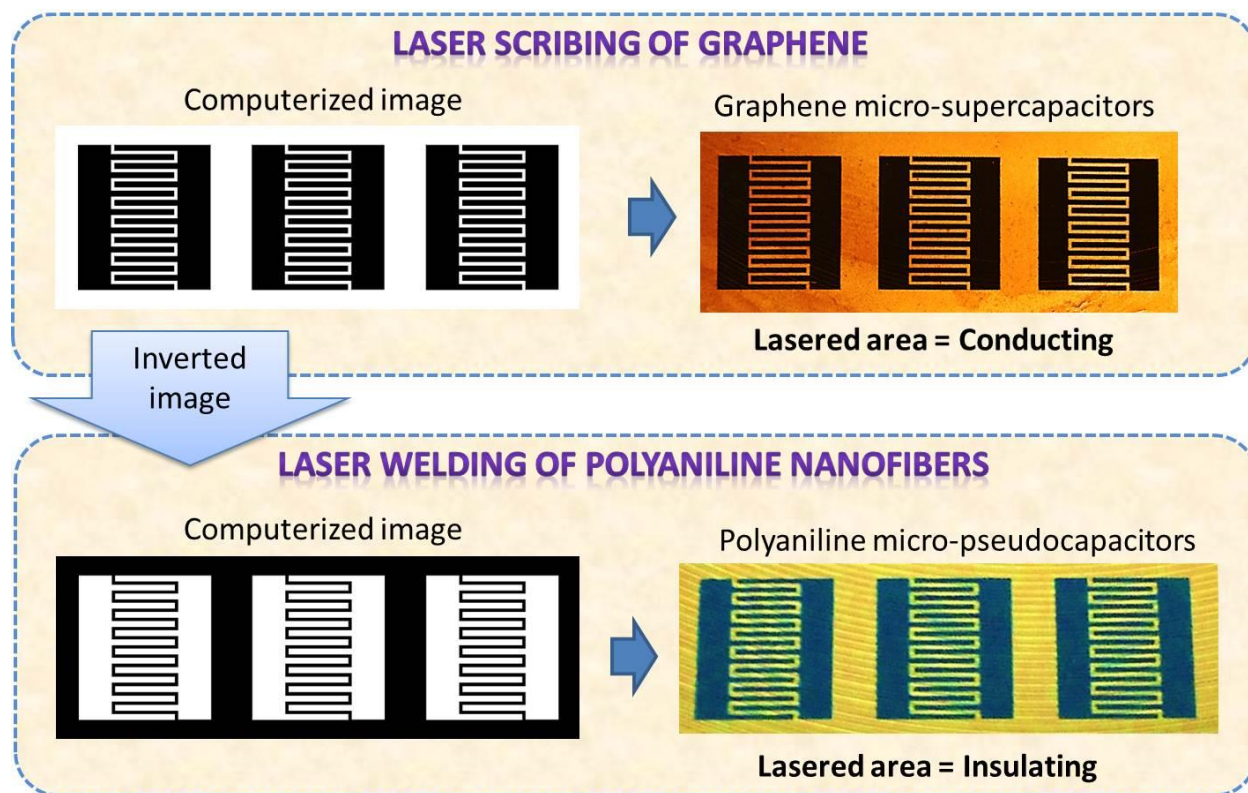
Figure 6.2: Explanation of the differences between the laser scribing of graphite oxide and the laser welding of polyaniline. The laser scribing process turns an electrically insulating graphite oxide film from golden brown to black electrically conducting 3D graphene. In the laser welding process, the green area is pristine (non-welded) doped polyaniline nanofibers, whereas the yellow area is polyaniline after it has been laser welded.

Although conventional microlithography processes are most commonly used in micro-supercapacitor fabrication, they are expensive and time consuming and have thus limited the wide adoption of microscale supercapacitors. The present techniques avoid the difficulties associated with current lithographic processes: i.e. no need for templates, stamps, masks, thermal annealing, photoresists, clean rooms, and/or post processing treatment of the polymer (37). Furthermore, this technique can be used for the fabrication of planar polyaniline micro-pseudo-capacitors on a large scale. Figure 6.3 shows that over 100 well-defined micro-pseudo-capacitors can be produced on one DVD disc and in less than 30 minutes.

172
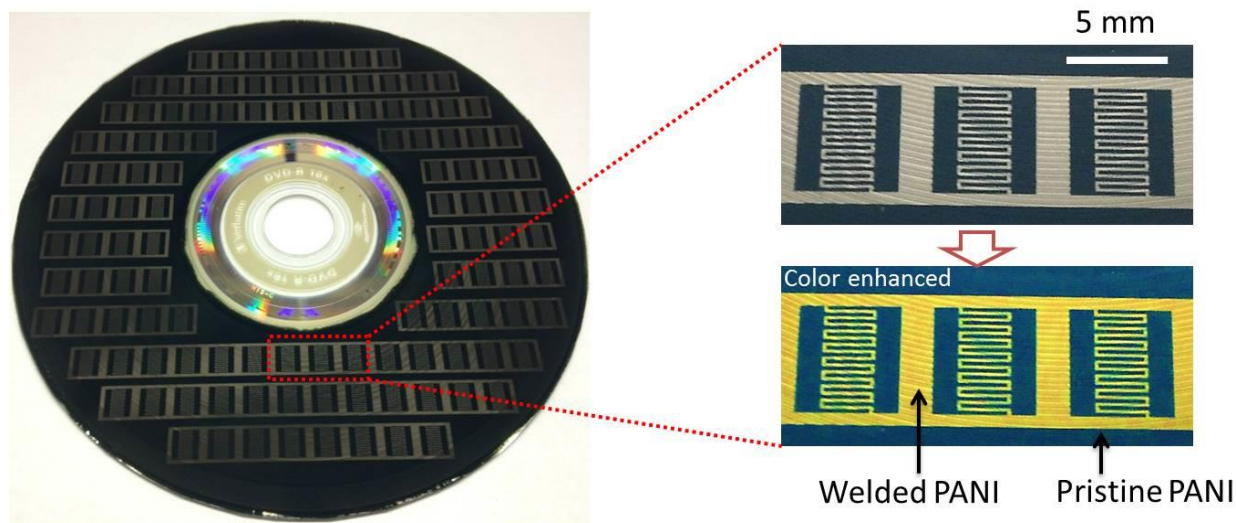
Figure 6.3: The laser welding of polyaniline inside a DVD burner can used for the fabrication of polyaniline micro-pseudo-capacitors on a large scale.

A flexible polyaniline micro-pseudo-capacitor made according to the method described above is shown in Figure 6.4. A droplet of gel-like PVA-H_2SO_4 is used as the electrolyte. The size of the device can be arbitrarily reduced to the micron scale because of the high resolution of the technique. The device shown in Figure 6.4a has an active area of 4.7 mm $\times$ 5 mm and can be folded without affecting its structural integrity or electrochemical performance.

Capacitive properties of a typical PANI micro-supercapacitor are shown in Figure 4b. Two pairs of distinct peaks are observed at slow scan rates due to the redox transitions in PANI. The first pair can be ascribed to the redox transition of PANI between its leucoemeraldine form (semiconducting state) and its emeraldine (conducting) state, while the second pair is attributed to the emeraldine-pernigraniline transformation (15). However, as the scan rate is increased to 100 mV/s, the CV curve of the device becomes distorted due to the large diffusion resistance.

173
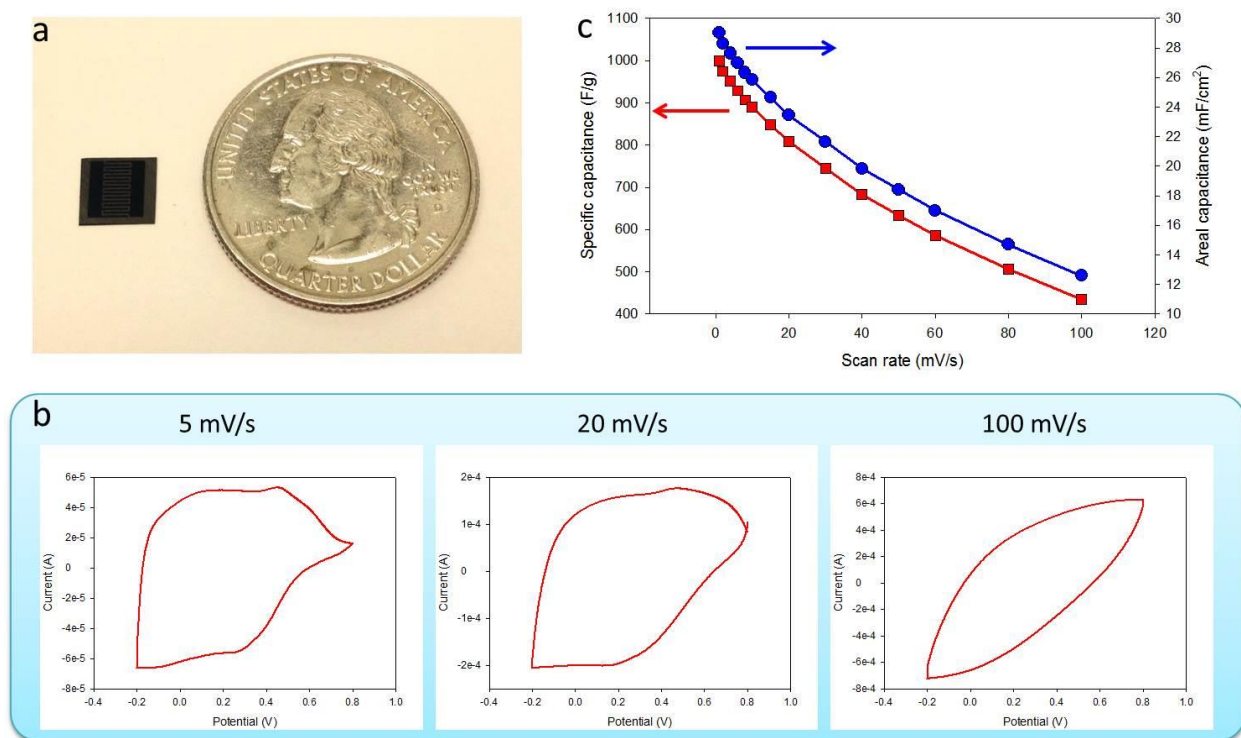
Figure 6.4: The electrochemical performance of a PANI-micro-pseudo-capacitor. (a) A digital photograph shows the device after the addition of the electrolyte, PVA-H$_2$SO$_4$. (b) CV profiles of the device at 5, 20, 100 mV/s. (c) specific capacitance and areal capacitance of the device shown as a function of scan rate.

The capacitance of the cell can be calculated by integrating the discharge current (*i*) vs. potential (*E*) of the CV curves over the whole potential window according to the following equation:

$$C = \frac{4 \int i\,dE}{vM\Delta E}$$

Where *v* is the scan rate (V/s), *M* is the total mass of the micro-device (g) and *ΔE* is the operating potential window.

The PANI micro-pseudo-capacitor exhibits extremely high specific capacitance of 1003 F/g which is about 50% of the theoretical specific capacitance of PANI (27), indicating superior

174

performance. This is a direct result from the high surface area and electrochemical activity of the polyaniline nanofibers. The size reduction of the nanostructured PANI increases the contact surface area between the electrode and electrolyte, and decreases the transport path length for both ions and electrons (26). This effect is even more pronounced when using a microstructured planar configuration. The microstructure of the electrodes optimizes the diffusion of the electrolyte ions, resulting in more efficient charge/discharge processes, Figure 6.5 (11).
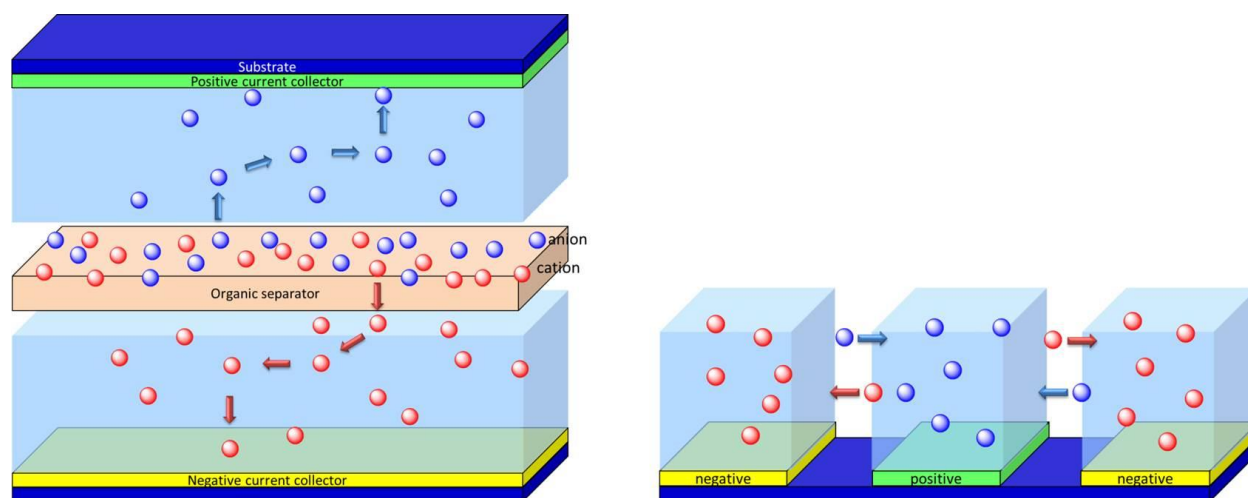
Figure 6.5: Schematic diagram showing the optimized and short diffusion pathway of electrolyte ions in the planar PANI-micro-pseudo-capacitor (right) compared to the conventional stacked structure (left).

Another interesting aspect of these PANI micro-pseudo-capacitors is the high areal capacitance of up to ~30 mF/cm^2 which is much higher than the corresponding values for state-of-the-art EDLC micro-supercapacitors which ranges from 0.4 to 6 mF/cm^2 (7-8,11,38-40). This high energy density per area is important for autonomous microsystems whose sizes are often determined by the size of the power supply. Increasing the areal capacity of the power source would reduce the size of the whole system, thus improving the efficiency of the design (41).

High specific capacitance per area is a critical requirement for practical supercapacitor electrodes and can be further improved by increasing the mass-loading of the active material. However, pursuing high mass-loading on conventional electrodes usually increases the ion and electron transport distance/resistance in the electrodes, thus preventing the full utilization of the active material and lower specific capacitances are often observed (42-44). Interestingly, the areal capacitance of a PANI micro-pseudo-capacitor scales linearly with mass loading, Figure 6.6. More importantly, the specific capacitance of PANI was not affected. The aggregation-resistant properties of PANI nanofibers allow them to maintain high accessible surface area and maintain their specific capacitance even upon increasing the film thickness. However, electrochemical impedance spectroscopy (EIS) (not shown) shows a relatively high equivalent series resistance (ESR) of 475 Ω/cm^2. This is possibly due to the relatively low electrical conductivity of polyaniline. The ESR can be reduced by using metallic current collectors (work in progress).
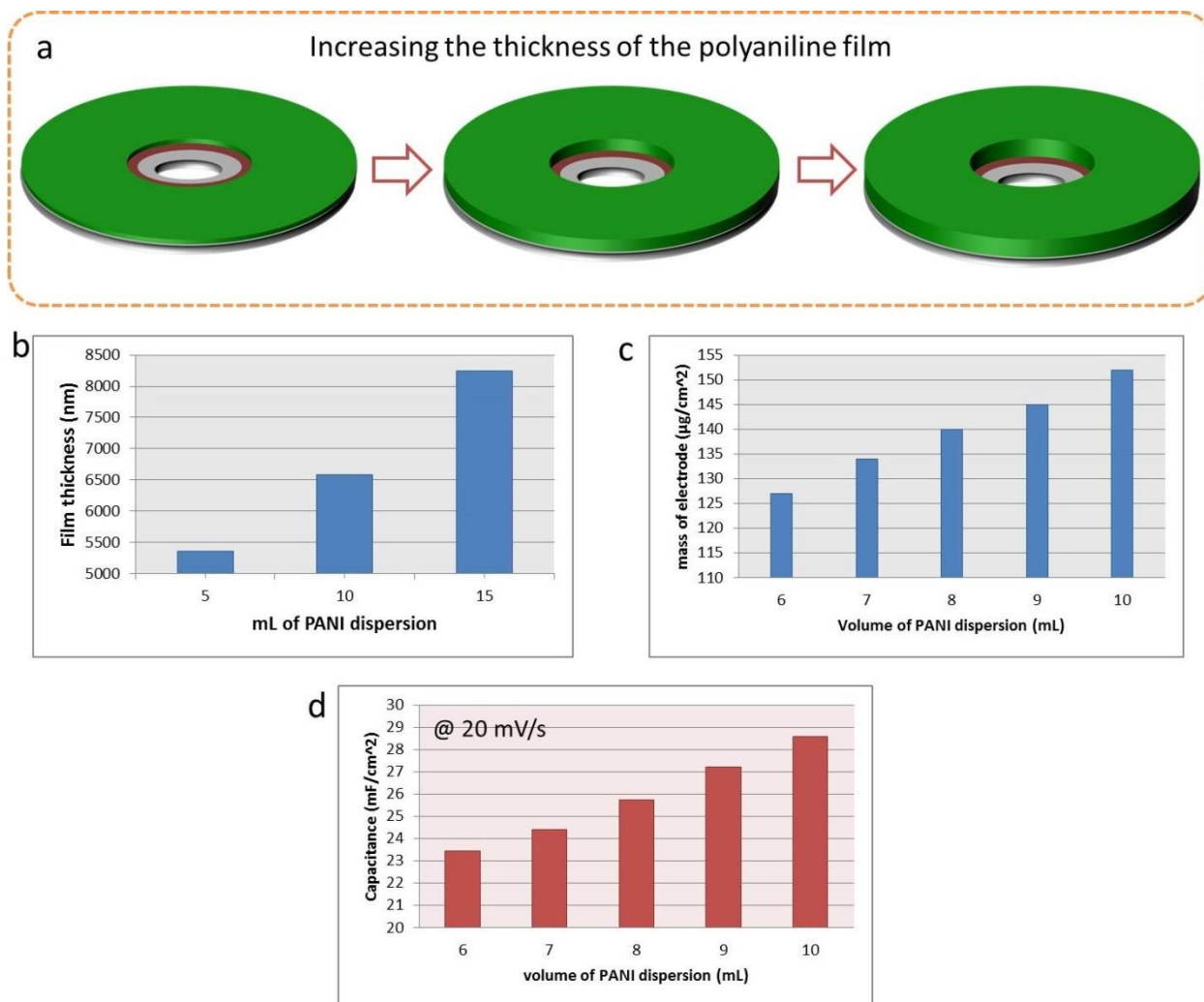
Figure 6.6: Boosting the areal capacitance of PANI micro-pseudo-capacitors by increasing the mass loading of PANI. (a) Schematic diagram showing increased thickness of the PANI film. (b) The thickness of the PANI film as a function of the volume of the PANI nanofiber dispersion. (c) The mass loading of PANI versus the volume of the cast PANI dispersion. (d) Areal capacitance of the PANI micro-pseudo-capacitor calculated at 20 mV/s as a function of the mass loading (represented by the volume of the dispersion).

Making a hybrid capacitor by combing the pseudo-capacitive polyaniline with the electric double layer capacitance of graphene is a proven solution that results in hybrid electrodes with lower ESR and improved capacity (30-36). The high conductivity of LSG, its high electron transfer rate as well as its high surface area makes it an excellent substrate for growing

polyaniline nanostructures (37). Here, LSG interdigitated microelectrodes were produced directly on a graphite oxide coated DVD disc as we described earlier (11). The LSG microelectrodes can be doped with polyaniline using the set up shown in Figure 6.7. Polyaniline is selectively electrodeposited on graphene using a three-electrode cell with graphene acting as the working electrode, a Ag/Ag reference electrode and a platinum foil counter-electrode.
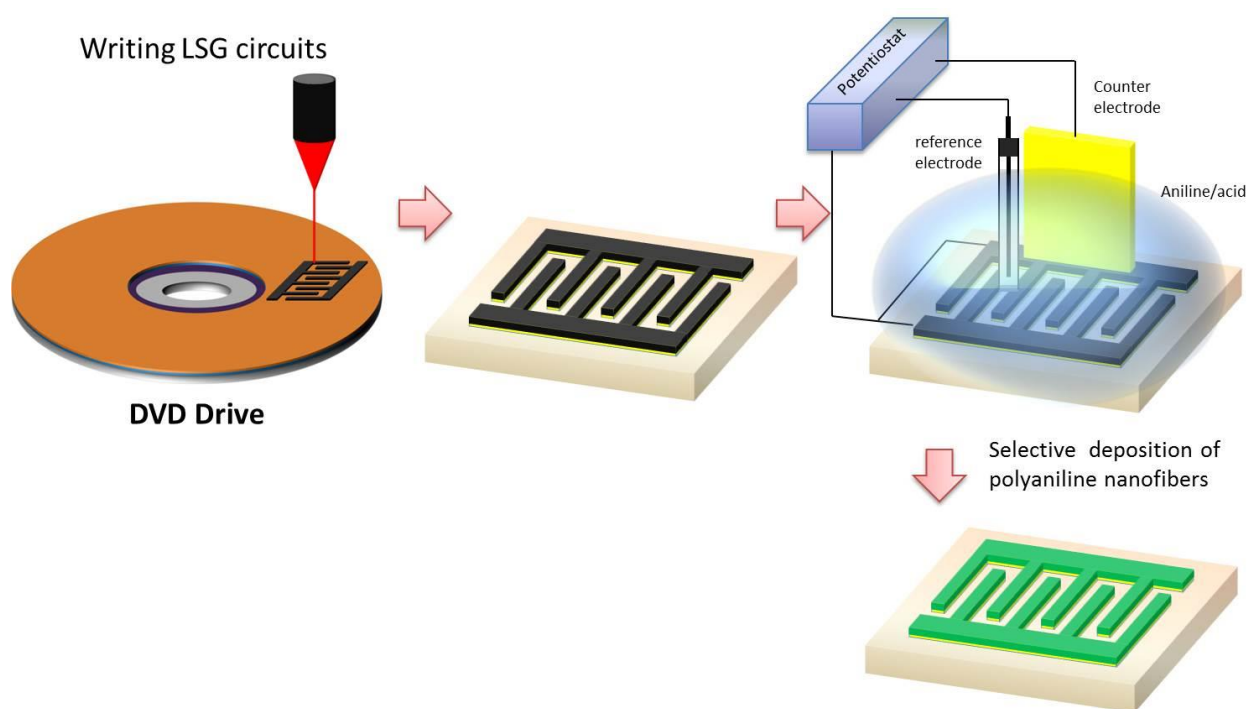
Figure 6.7: The fabrication process for LSG/PANI micro-supercapacitors: (a) First LSG micro-electrodes are printed on graphite oxide film. (b) The interdigitated micro-electrodes are then separated for the next steps. (c) Selective electro-deposition of PANI. (d) The produced LSG/PANI device.

Nanostructured polyaniline (mainly nanofibers) appears to form no matter what acid dopant is used in the polymerization. However, the aspect ratio and the diameter of the formed nanofibers depend strongly on the type of dopant, Figure 6.8. For example, very uniform and long nanofibers are observed in the SEM images after electro-polymerization from mineral acids: H_2SO_4 and HCl. The average diameter of the nanofibers is 500 nm when formed from H_2SO_4 and 100 nm for HCl. However, low aspect ratio nanofibers are produced when using organic acids dopants such as p-toluene sulfonic acid (p-TSA) or camphorsulfonic acid (CSA).
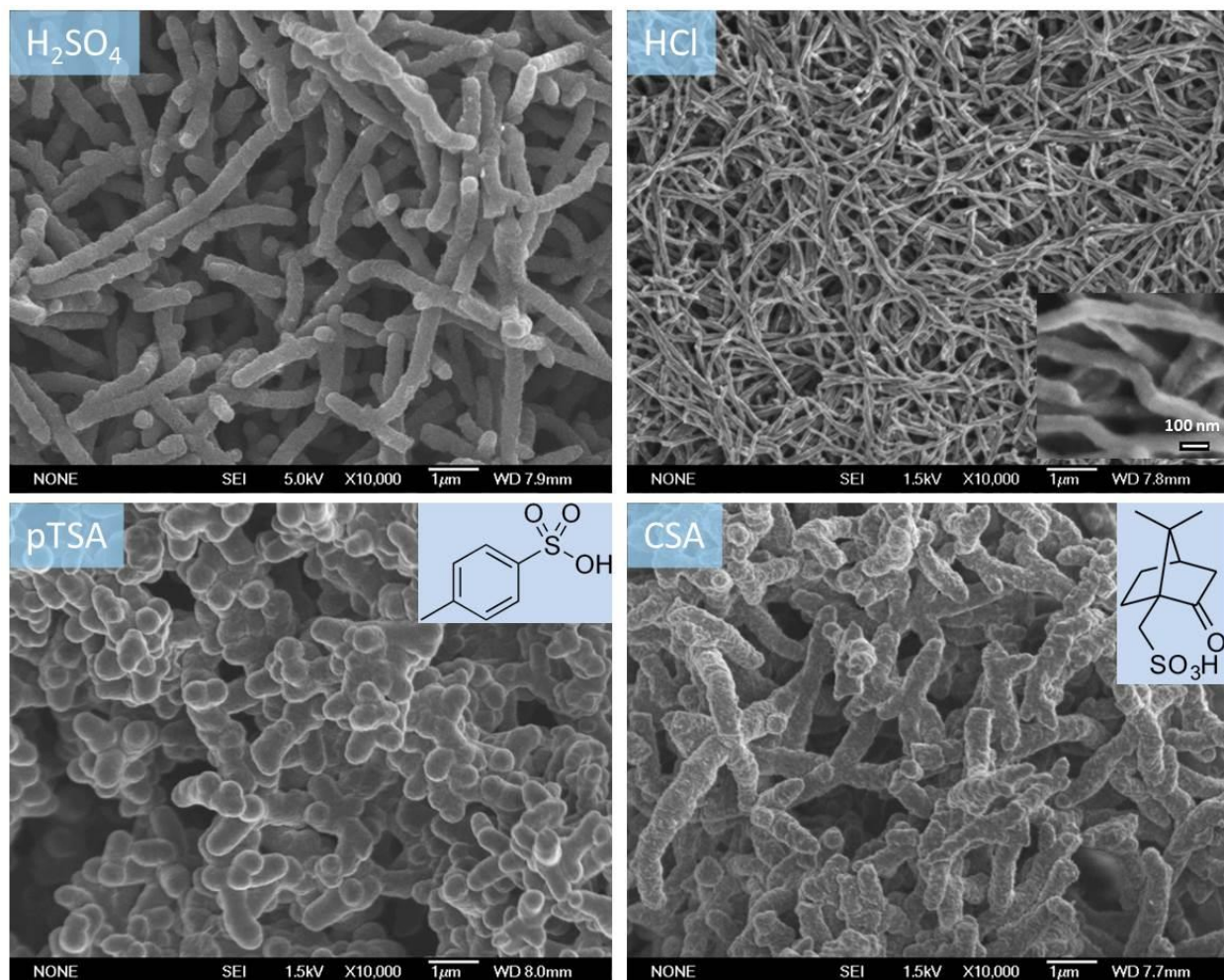
Figure 6.8: Morphology of polyaniline films grown electrochemically on LSG from (a) H_2SO_4, (b) HCl, (c) p-toluene sulfonic acid, p-TSA and (d) camphorsulfonic acid, CSA.
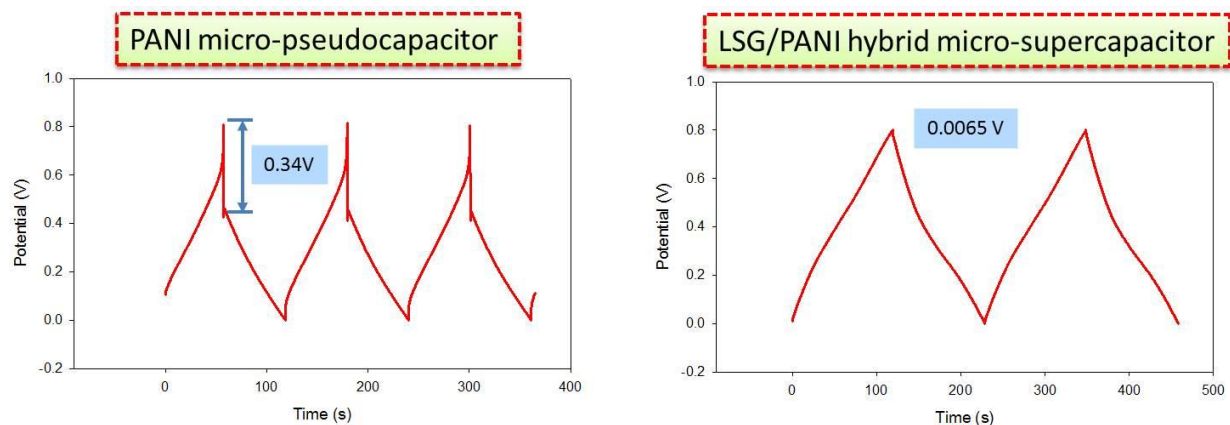
Figure 6.9: Charge/discharge curves of a PANI micro-pseudo-capacitor and LSG/PANI micro-supercapacitor tested at the same current density (mA/cm^2).

The representative charge/discharge curves for the LSG/PANI micro-supercapacitor is shown in Figure 6.9, the results for a PANI micro-pseudo-capacitor are also shown for comparison. The IR drop due to the internal resistance of the LSG/PANI micro-supercapacitor is hardly observed (even at high charge/discharge rates), which can be attributed to the improvement of conductivity of the device by incorporating graphene. The discharge behavior of a PANI micro-pseudo-capacitor is nearly linear from 0.46 V to 0 V; however, the large IR drop of 0.34 V limits the power of this capacitor. The LSG/PANI micro-supercapacitor, on the other hand, shows two voltage ranges in the discharge curve: 0.8-0.46 V and 0.46-0 V. The former stage with a relatively short discharging duration is ascribed to EDL capacitance; whereas, the latter stage with a much longer discharging duration is associated with the combination of EDL and Faradaic capacitances of the PANI component (30,45).

Cyclic voltammetry measurements were performed to explore the advantage of bare LSG and the LSG/PANI hybrid electrodes made at different loadings of PANI. The mass loading of PANI to LSG is controlled by adjusting the deposition time. The current increases with PANI deposition time, leading to an increase in areal capacitance to ~50 mF/cm^2 obtained at a

180

deposition time of 5 minutes, which is approximately 25 times higher than the value of bare LSG. Moreover, the LSG/PANI micro-supercapacitor exhibits fast charge/discharge kinetics and high rate capability compared to the PANI micro-pseudo-capacitor. For example, the LSG/PANI micro-supercapacitor (3 min) has a capacitance value of 25.9 mF/cm^2 at as scan rate of 1 mV/s. This device maintains 87% of this value as the scan rate is increased to 100 mV/s, while the PANI micro-supercapacitor retains only 45% of the capacitance when tested under the same conditions.
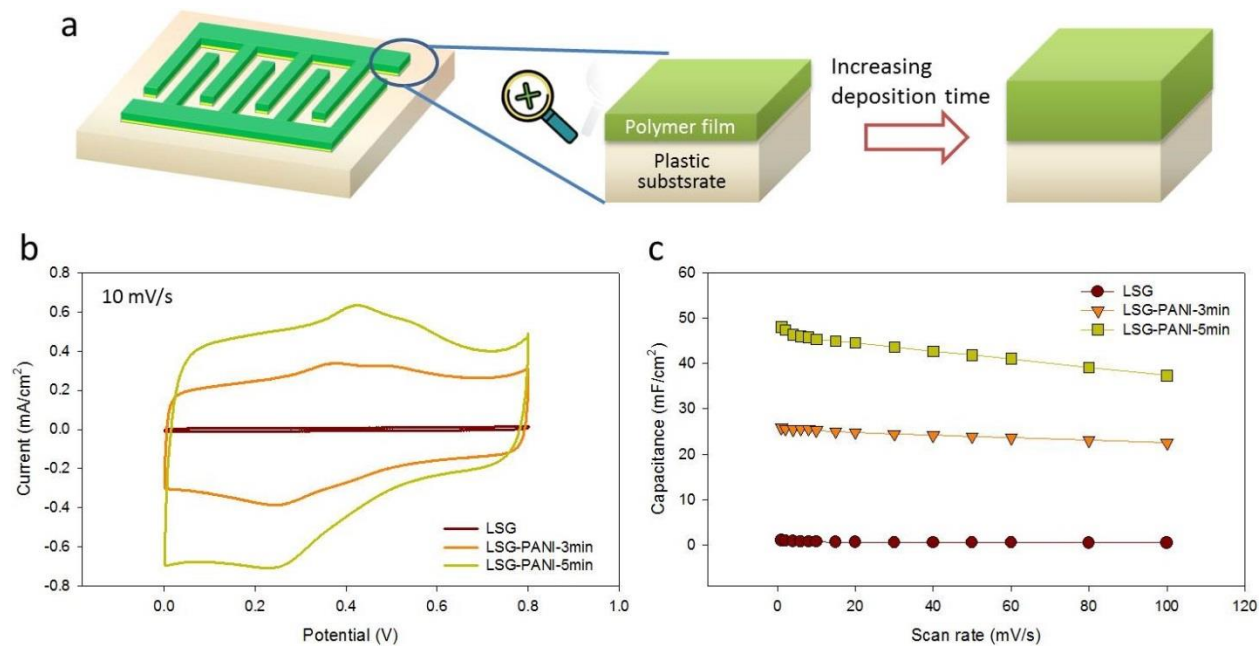
Figure 6.10: The electrochemical performance of LSG/PANI micro-supercapacitor with different electro-polymerization times. (a) Schematic diagram showing the control of the loading level of PANI by adjusting the deposition time. (b) CV profiles for LSG, LSG/PANI for 3 and 5 min depositions, tested at a scan rate of 10 mV/s. (c) Areal capacitances of the different devices as a function of scan rate.

Further understanding of the fast ion diffusion/transfer kinetics of the LSG/PANI micro-supercapacitor was further confirmed by electrochemical impedance spectroscopy (EIS). The

Nyquist Plot shows a nearly vertical line at low frequencies which reflect excellent capacitive behavior of the LSG/PANI micro-supercapacitor. From the extrapolation of the vertical portion of the Nyquist plot to the real axis, the equivalent series resistance (ESR) was estimated to be 10.3 ohm/cm^2, which falls within the same region for high power micro-supercapacitors (7-8,11,38-40). A phase angle of about −86.3⁰ has been achieved which again confirms good capacitive behavior of the LSG/PANI micro-supercapacitor. The device is characterized by a relatively good relaxation time constant, τ_0 of 3.3 s with τ_0 being the minimum time needed to discharge all the energy from the device with an efficiency of greater than 50% (ref. 46).
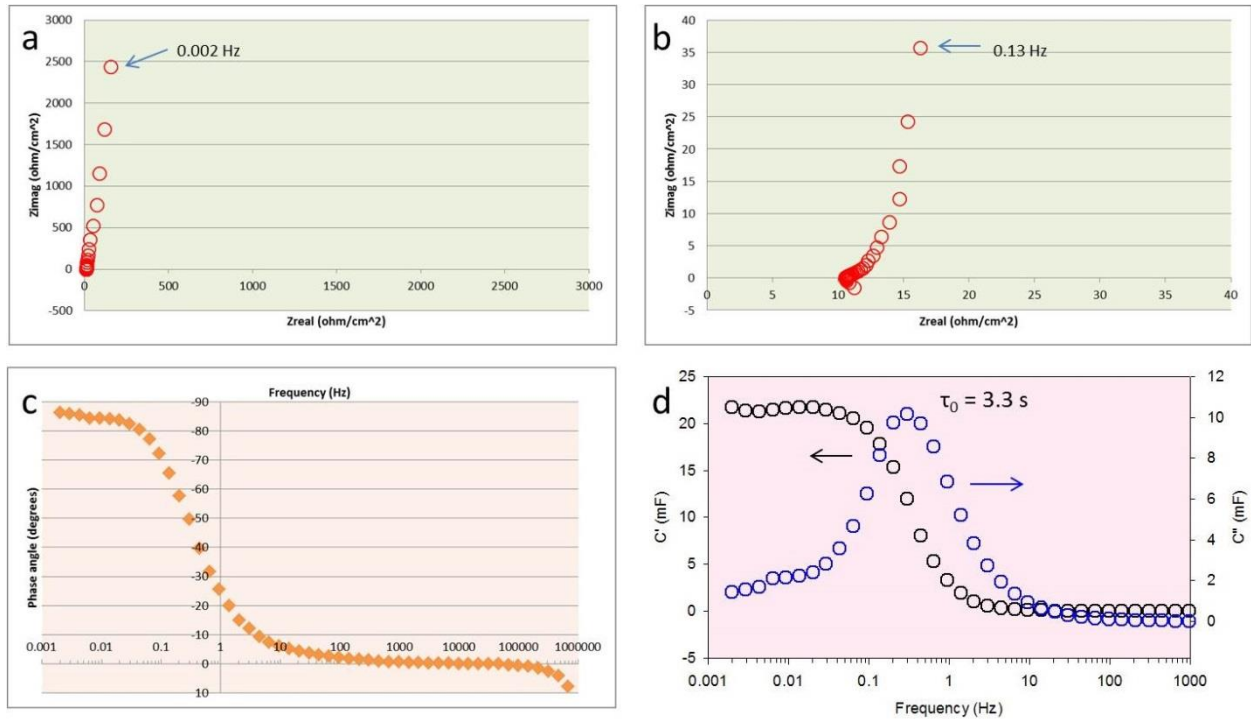
Figure 6.11: Electrochemical impedance spectroscopy of an LSG/PANI micro-supercapacitor. (a) Nyquist Plot over a frequency range of 1 MHz to 0.002 Hz. (b) Magnified view of the high frequency region of the Nyquist Plot. (c) Bode Plot showing the phase angle versus frequency. (d) Evolution of the real and imaginary part (C' and C'') of the areal capacitance.

The superior electrochemical performance of the LSG/PANI micro-supercapacitor can be attributed to the favorable structure of the LSG/PANI for energy storage. Specifically, the high surface area along with extremely high electron transfer rates on the surface of the LSG speeds up the charge/discharge kinetics. Also, the nanofiber structure of PANI provides a large number of electrochemically active sites that allows for fast and reversible surface redox reactions with high capacitance.

6.4 CONCLUSIONS

In summary, we have demonstrated a simple and scalable approach to fabricate interdigitated micro-supercapacitors via coating a polyaniline nanofiber film and subsequent laser patterning. The device shows outstanding electrochemical performance with a specific capacitance of around 1000 F/g and areal capacitance of 30 mF/cm^2 which is much higher than current state-of-the-art EDL micro-supercapacitors. Such an efficient approach can drastically increase the density of micro-supercapacitors on a chip and reduce their complexity by removing intricate interconnects to bulky energy storage devices (47); paving the way for efficient miniaturized flexible and portable electronic devices.

BIBLIOGRAPHY

[1] J. F. M. Oudenhoven, R. J. M. Vullers and R. van Schaijk, Int. J. Energy Res. 2012; 36:1139–1150.

[2] J. H. Prescott, S. Lipka, S. Baldwin, N. F. Sheppard, J. M. Maloney, J. Coppeta, B. Yomtov, M. A. Staples, J. T. Santini, Nat. Biotechnol. 2006, 24, 437.

[3] Caiwei Shen, Xiaohong Wang, Wenfeng Zhang, Feiyu Kang, Journal of Power Sources 196 (2011) 10465– 10471.

[4] Wei Lai, Can K. Erdonmez, Thomas F. Marinis, Caroline K. Bjune, Nancy J. Dudney, Fan Xu, Ryan Wartena, and Yet-Ming Chiang, Adv. Mater. 2010, 22, E139–E144.

[5] John Chmiola, Celine Largeot, Pierre-Louis Taberna, Patrice Simon, Yury Gogotsi. *Science* 328, 480 (2010).

[6] Majid Beidaghi, Chunlei Wang. Proc. of SPIE Vol. 8377, 837708-1.

[7] David Pech, Magali Brunet, Pierre-Louis Taberna, Patrice Simon, Norbert Fabre, Fabien Mesnilgrente, Véronique Conédéra, Hugo Durou, *J. Power Sources* 195, 1266-1269 (2010).

[8] David Pech, Magali Brunet, Hugo Durou, Peihua Huang, VadymMochalin, Yury Gogotsi, Pierre-Louis Taberna and Patrice Simon, *Nature Nanotech 5, 651-654* (2010).

[9] Chen, W. et al. Integration of carbon nanotube to C-MEMS for on-chip supercapacitors. IEEE Trans. Nanotech. 9, 734–740 (2010).

[10] Heon, M. et al. Continuous carbide-derived carbon films with high volumetric capacitance. Energy Environ. Sci. 4, 135–138 (2011).

[11] Maher F. El-Kady, Richard B. Kaner, Nature Communications 4:1475, 2013 | DOI: 10.1038/ncomms2446.

[12] Liu, C. -C. et al. Planar ultracapacitors of miniature interdigital electrode loaded with hydrous RuO_2 and RuO_2 nanorods. Electrochim. Acta 55, 5768–5774 (2010).

[13] Xue, M. et al. Microfluidic etching for fabrication of flexible and all-solid-state micro supercapacitor based on MnO_2 nanoparticles. Nanoscale 3, 2703–2708 (2011).

[14] Beidaghi, M. & Wang, C. Micro-supercapacitors based on three dimensiona interdigital polypyrrole/C-MEMS electrodes. Electrochim. Acta 56, 9508–9514 (2011).

[15] Wang, K. et al. An all-solid-state flexible micro-supercapacitor on a chip. Adv. Energy Mater. 1, 1068–1072 (2011).

[16] Mianqi Xue, Fengwang Li, Juan Zhu, Hang Song, Meining Zhang, and Tingbing Cao, *Adv. Funct. Mater.* 2012, 22, 1284–1290.

[17] Xu Wang, Afriyanti Sumboja, Wan Ling Foo, Chao Yi Yan,Kazuhito Tsukagoshi, and Pooi See Lee, RSC Adv., 2013, 3, 15827–15833.

[18] Wenwen Liu, Xingbin Yan, Jiangtao Chen, Yaqiang Feng and Qunji Xue, Nanoscale, 2013, 5, 6053–6062.

[19] Dan Li, Jiaxing Huang, Richard B. Kaner, *Acc. Chem. Res.*, **2009**, *42* (1), pp 135–145.

[20] Huang, J.; Virji, S.; Weiller, B. H.; Kaner, R. B. J. Am. Chem. Soc. 2003, 125, 314–415.

[21] Baker, C. O.; Shedd, B.; Innis, P. C.; Whitten, P. G.; Spinks, G. M.; Wallace, G. G.; Kaner, R. B. Adv. Mater. 2008, 20, 155–158.

[22] Julio M. D'Arcy, Henry D. Tran, Vincent C. Tung, Alexander K. Tucker-Schwartz, Rain P. Wong, Yang Yang, and Richard B. Kaner, Proceedings of the National Academy of Sciences, USA. 107, 19673-78 (2010).

[23] Tseng, R. J.; Huang, J.; Ouyang, J.; Kaner, R. B.; Yang, Y. Nano Lett. 2005, 5, 1077–1080.

[24] Gregory R. Guillen, Thomas P. Farrell, Richard B. Kaner and Eric M. V. Hoek. *J. Mater. Chem.* , 2010, **20**, 4621-4628.

[25] T. Nakajima, T. Kawagoe, Synthetic Metals 28, 629-638 (1989).

[26] Kai Wang , Haiping Wu , Yuena Meng , Zhixiang and Wei, *Small, 2013,* DOI: 10.1002/smll.201301991.

[27] Hanlu Li, JixiaoWang, Qingxian Chu, ZhiWang, Fengbao Zhang, ShichangWang, Journal of Power Sources 190 (2009) 578–586.

[28] Wang, Y. G.; Li, H. Q.; Xia, Y. Y. *Adv. Mater.* **2006**, 18, 2619– 2623.

[29] Yufei Wang, Xiaowei Yang, Ling Qiu and Dan Li, *Energy Environ. Sci.*, 2013,**6**, 477-481.

[30] Qiong Wu, Yuxi Xu, Zhiyi Yao, Anran Liu, and Gaoquan Shi, ACS Nano 4, 1963-1970 (2010).

[31] Da-Wei Wang, Feng Li, Jinping Zhao, Wencai Ren, Zhi-Gang Chen, Jun Tan, Zhong-Shuai Wu, Ian Gentle, Gao Qing Lu, and Hui-Ming Cheng. ACS Nano 3, 1745-1752 (2009).

[32] Hualan Wang, Qingli Hao, Xujie Yang, Lude Lu and Xin Wang, Nanoscale, 2010, 2, 2164–2170.

[33] Shuiping Zhou, Hongming Zhang, Xianhong Wang, Ji Li and Fosong Wang, *RSC Adv.* **, 2013, 3, 1797-1807.**

[34] F. Huang, F. Lou and D. Chen, *ChemSusChem*, 2012, **5**, 888–895.

[35] J. Yan, T. Wei, B. Shao, Z. Fan, W. Qian, M. Zhang and F. Wei, *Carbon*, 2010, **48**, 487–493.

[36] C. Peng, S. Zhang, D. Jewell and G. Z. Chen, *Prog. Nat. Sci.*, 2008, **18**, 777–788.

[37] Veronica Strong, Yue Wang, Ani Patatanyan, Philip G. Whitten, Geoffrey M. Spinks, Gordon G. Wallace, and Richard B. Kaner. Nano Lett. 2011, 11, 3128–3135.

[38] (a) John R. Miller, R. A. Outlaw, B. C. Holloway, *Science* 329, 1637 (2010); (b) John R. Miller, R.A. Outlaw, B.C. Holloway, Electrochimica Acta 56, 10443 (2011); (c) John R. Miller, *ECS Meet. Abstr. 2012 MA2012-02 595.*

[39] Majid Beidaghi, Chunlei Wang, *Adv. Funct. Mat.* 22, 4501 (2012).

[40] Wei Gao, Neelam Singh, Li Song, Zheng Liu, Arava Leela Mohana Reddy, Lijie Ci, Robert Vajtai, Qing Zhang, Bingqing Wei and Pulickel M. Ajayan, Nature Nanotech 6, 496-500, 2011.

[41] Timothy S. Arthur, Daniel J. Bates, Nicolas Cirigliano, Derek C. Johnson, Peter Malati, James M. Mosby, Emilie Perre, Matthew T. Rawls, Amy yL. Prieto, and Bruce Dunn, MRS Bulletin 36, 523-531 (2011).

[42] John Chmiola, Celine Largeot, Pierre-Louis Taberna, Patrice Simon, Yury Gogotsi, Science 328, 480-483 (2010).

[43] Jiayan Luo, Hee Dong Jang, and Jiaxing Huang, *ACS Nano* 7, 1464-1471 (2013).

[44] Zhiyi Lu, Qiu Yang, Wei Zhu, Zheng Chang, Junfeng Liu, Xiaoming Sun, David G. Evans, and Xue Duan, *Nano Res.* 2012, 5(5): 369–378.

[45] Lixia Li, Huaihe Song, Qincang Zhang, Jingyuan Yao, Xiaohong Chen, *Journal of Power Sources* 187 (2009) 268–274.

[46] Taberna, P. L.; Simon, P.; Fauvarque, J. F. J. Electrochem. Soc. 2003, 150, A292.

[47] Zhiqiang, Niu, Li Zhang, Lili Liu, Bowen Zhu, Haibo Dong, and Xiaodong Chen. *Advanced Materials* 25, 4035-4042 (2013).

CHAPTER 7

Scaling up production of graphene supercapacitors

7.1 ABSTRACT

In this chapter, the efforts we have made in the Kaner Lab to move our graphene supercapacitors from the laboratory to the industrial level are discussed. A research team from the Kaner Lab is working with industry partners with the goal of turning this technology into a product. This work is driven by our goal as scientists which has always been to contribute to the discovery of new technologies to the well-being of mankind.

7.2 INTRODUCTION

Energy storage devices are some of the most promising and important environmental technologies that are highly influential in advancing our civilization's abilities and standard of living (1-2). Energy storage has, thus, become a primary focus of the major world powers and scientific community. Both the government and industry are funding innovation in the energy storage technology in an effort to develop more efficient energy storage devices (3-6).

Although critical improvements have been achieved over the past few years, the progress is marginal compared with the vast advancements in microelectronics. Hence, we need to improve performance substantially to meet the higher requirements of future systems by developing new materials and advancing our understanding of the electrochemical interfaces at the nanoscale (3). Although great efforts have gone into developing high-performance Li-ion batteries, there have only been fractional improvements since they were discovered.

Supercapacitors are proven energy storage devices that play an important role in complementing or replacing batteries in the energy storage field as discussed in Chapter 2.

Basically, almost everywhere you see next generation electronic and power technology you see supercapacitors being fitted or planned because of superior performance, cost-over-life and fit-and-forget (7). There is a rapidly growing market for supercapacitors with over 66 supercapacitors manufacturers worldwide. Among them, Maxwell Technologies is a pioneering global leader in developing, manufacturing and marketing supercapacitors, with millions of units now performing reliably around the clock worldwide. Maxwell Technologies has grown to become the leading global supplier of supercapacitors, Figure 7.1 (ref. 8). The average market growth rate of supercapacitors over the past 10 years is 25% and most analysts predict growth rates for the market for next 10 years at greater than 30% year over year. The primary area of growth will be in mass customization of power modules and systems for automotive applications, such as micro/mild hybrid vehicle and board net stabilization, and green technology applications, such as windmill blade pitch control and smart utility meters (9).
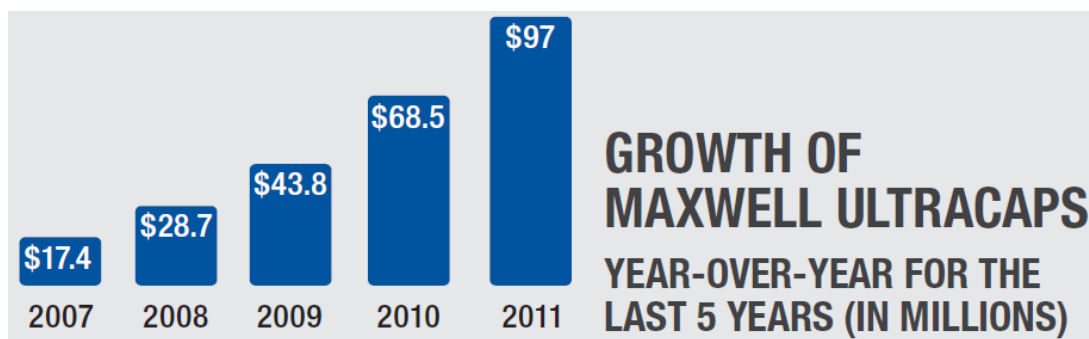
Figure 7.1: Growth of Maxwell ultracapacitors, year-over-year for the last 5 years (in millions), adapted from reference (8).

Research and development efforts into EDLC supercapacitors have been steadily gathering momentum since the 1970's. This rate of progress is likely to continue as concerns about energy efficiency and sustainable development increase (10). The available energy and power of supercapacitors greatly depends upon the materials used, and significant research is directed at ways of improving the electrode and electrolyte materials (3). Greater availability and more competitive prices combined with improved energy and power performance will lead to widespread adoption of supercapacitors as energy storage devices (10). Laser scribed graphene (LSG) may have an advantage compared to activated carbons, the most widely used material in the current EDLC supercapacitors. Basically, LSG shows enhanced energy density and power density compared to activated carbons. Also, given the facile fabrication process of LSG, this may set the basis for a new generation of supercapacitors.

7.3 RESULTS AND DISCUSSION

To achieve industrial-scale production of graphene supercapacitors, various design and operational strategies need to be investigated and optimized. This process of taking a laboratory-developed technique and modifying it to achieve high volume production is known as "scale-up", see Figure 7.2. It is should be understood that scaling up a chemistry experiment is not a simple linear process. When a laboratory process is modified for high-volume production, factors like time, temperature, concentration and mixing velocity can all change (11).

Supercapacitor design and construction requires the participation of different scientific and engineering disciplines. We have been working with experts from Maxwell Technologies for over the past year and have figured out the important factors that influence our process which are summarized in the next sections.
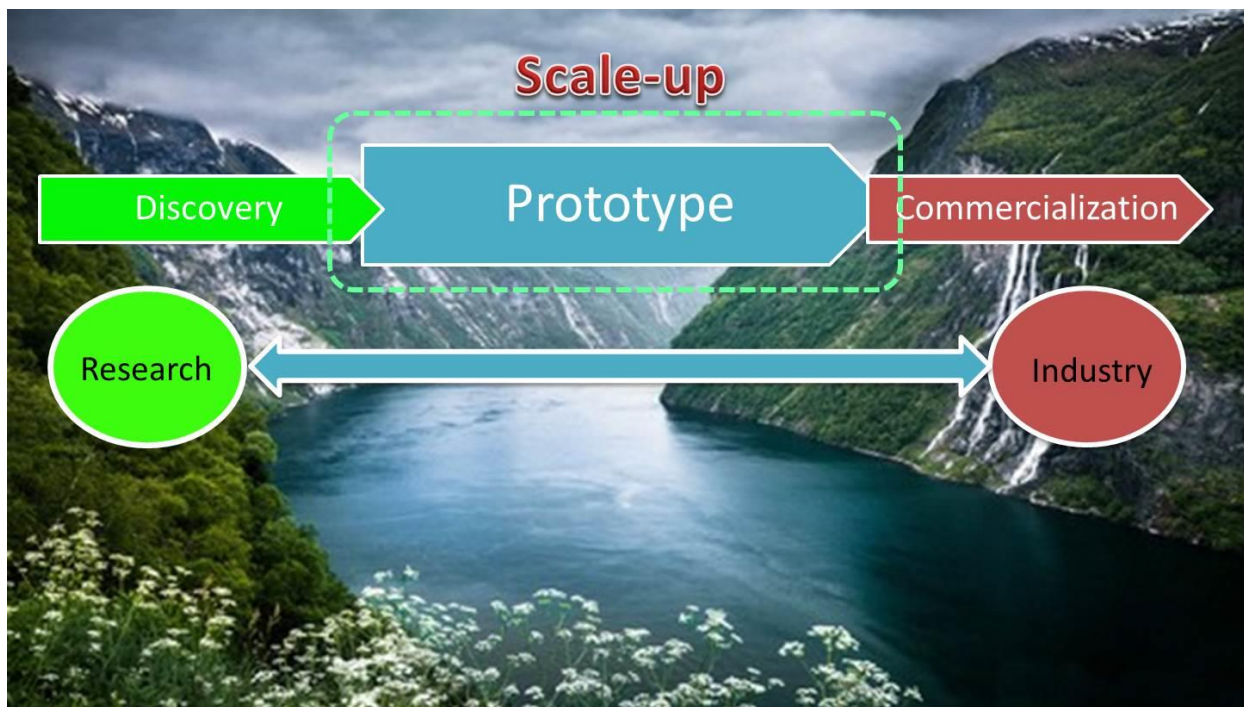
Figure 7.2: Moving a laboratory process to commercialization through a scale-up process.

A working program between UCLA and Maxwell Technologies is defined in two fundamental phases. First, a joint development agreement for technology development to advance the fundamental technology beyond the laboratory to the point of a prototype part that could be envisioned as the foundation for a production component based on graphene electrode technology. Second, is a commercialization phase which takes the lab technology and moves it to a production ready state including the buildup of infrastructure to make the technology at scale. Inside this phase is the demonstration of scale up capability of the fundamental background technology to illustrate high volume production capability at cost.

When scaling-up a new technology, the objective is to find the most efficient and at the same time cost-effective methods for producing materials at an industrial scale. This project helped us gain a greater understanding of the crucial factors that must be addressed by electrode and electrolyte materials to achieve the required performance. Since some of the details of this

work is proprietary, I am going to shed some light on the most important factors without giving away any proprietary information.

The most important part of a supercapacitor is the electrode. The performance of a supercapacitor is highly dependent on the details of the design, particularly the thickness of the electrode. It is thus important that the electrodes used for testing be of a similar thickness used in commercial cells. This depends on whether a supercapacitor is constructed to optimize energy density or power density. Commercial electrode thicknesses range from about 20 µm for high power density cells to several hundred microns for high energy density cells (12). It is important that the performance of the electrode material is demonstrated on a more "device-suitable" substrate such as a metallic current collector.

The one problem that has been limiting the development of high performance carbon-based supercapacitors is the high contact resistance between carbon particles. This gives rise to high equivalent series resistance, thus reducing the supercapacitor performance (13). Although, this resistance can be partially reduced by the addition of conducting additives, most commercially available carbon-based supercapacitors still suffer from high internal resistance. What is really nice about the LSG electrode is that it is a highly conducting interconnected porous network that demonstrates low internal resistance.

The second vital component that allows a supercapacitor to function is the electrolyte. The choice of electrolyte often depends on the intended application. Most supercapacitors available today use organic electrolytes that consist of a quaternary ammonium salt (typically, tetraethylammonium tetrafluoroborate) dissolved in acetonitrile or propylene carbonate. These supercapacitors deliver high energy densities due to the high operating voltage of organic

electrolytes, typically 2.3-2.7 V. High power density is achieved with aqueous electrolytes, but at the cost is lower energy density. It is important that the LSG supercapacitors have demonstrated excellent performance in various electrolytes, including aqueous, organic and even ionic liquids (Chapter 3). This opens the possibility to engineer supercapacitor electrodes based on this form of graphene in order to target a wide range of applications, such as high energy, high power, or low cost (14).

It is the cell composition—electrodes, electrolyte and separator—that makes a supercapacitor work. However, the design and construction of a supercapacitor makes it more efficient or safer or more reliable or more convenient to use. Supercapacitors, like batteries, come in an astounding array of shapes and sizes and have identification codes defined by the International Electrochemical Commission (IEC) and the American National Standards Institute (ANSI) (15). It is, thus, important to select the appropriate form factor for testing the performance of newly developed electrode materials.

Typically, the performance of both batteries and supercapacitors is presented using Ragone plots that show a relationship between the energy density and the power density. Figure 7.3 shows the Ragone plot for the LSG supercapacitors, compared with a number of commercially available capacitors, supercapacitors and batteries. The plot shows the performance of the assembled cells taking into account all the device components including the electrode materials, current collector, electrolyte, separator and packaging. Depending on the design, LSG supercapacitors can be used to target high energy or high power applications. It is important to point out the performance of LSG electrodes is demonstrated using commercial current collectors, separators and electrolytes; opening the door for a new generation of low cost high-performance supercapacitors.
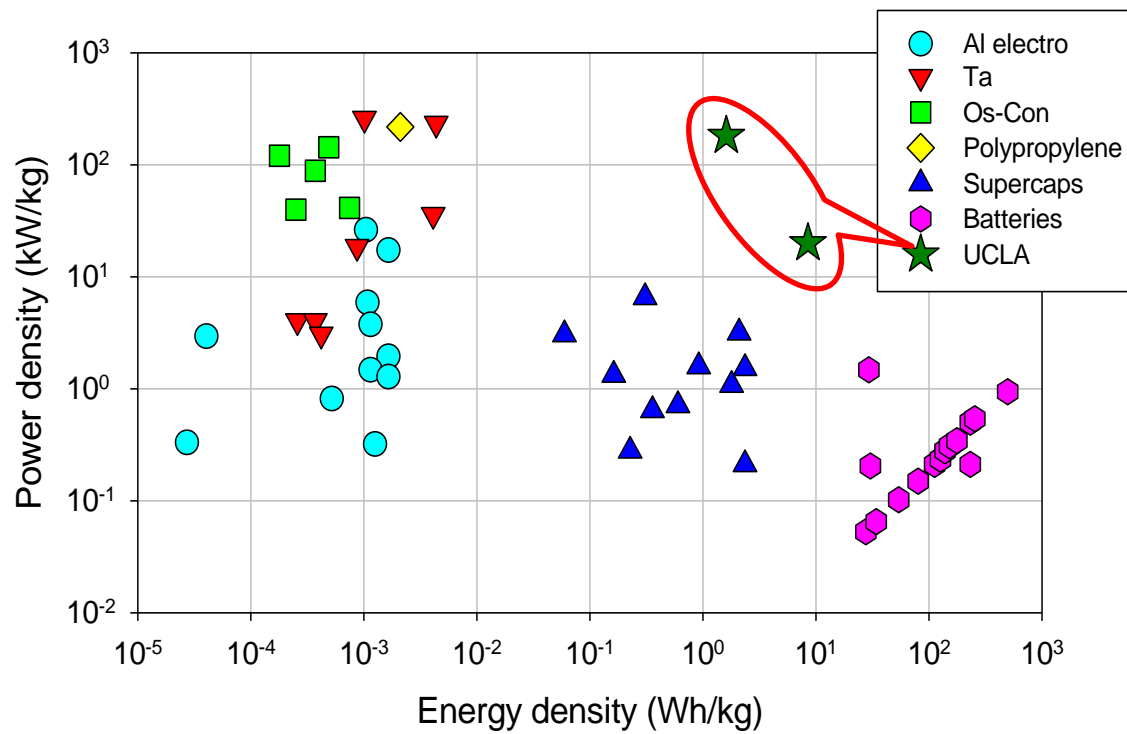
Figure 7.3: Ragone plot showing the energy density and power density of graphene supercapacitors developed at UCLA compared to a number of commercially available capacitors, supercapacitors and batteries.

BIBLIOGRAPHY

[1] Yang, Z.; Zhang, J.; Kintner-Meyer, M. C. W.; Lu, X.; Choi, D.; Lemmon, J. P.; Liu, J. Chem. Rev. 2011, 111 (5), 3577–3613.

[2] Katsuhiko Naoi, Wako Naoi, Shintaro Aoyagi, Jun-Ichi Miyamoto, and Takeo Kamino. Accounts of Chemical Research 46, 1075-1083 (2013).

[3] Simon, P.; Gogotsi, Y. Nat. Mater. 2008, 7, 845

[4] US Department of Energy. *Basic Research Needs for Electrical Energy Storage* <www.sc.doe.gov/bes/reports/abstracts.html#EES2007> (2007)

[5] David LaGesse, Supercapacitors Amp Up as an Alternative to Batteries, National Geographic, August 20, 2013.

http://news.nationalgeographic.com/news/energy/2013/08/130821-supercapacitors/

[6] Tyler Wells Lynch, Reviewed.com: In search of a better battery, USA TODAY July 17, 2013.

http://www.usatoday.com/story/tech/2013/07/17/reviewed-better-battery-column/2509507/

[7] Dr Peter Harrop and Dr Victor Zhitomirsky, Electrochemical Double Layer Capacitors: Supercapacitors 2013-2023, Business Report IDTechEx, July 2013.

http://www.idtechex.com/research/reports/electrochemical-double-layer-capacitors-supercapacitors-2013-2023-000318.asp

[8] http://www.maxwell.com/

[9] http://www.nesscap.com/images/news/Nesscapcatalogue_2012.pdf

[10]

http://www.aacmicrotec.com/index.php?option=com_content&view=article&id=34&Itemid=171

[11] http://web.anl.gov/eesa/publications/success_stories/battery_scaleup.html

[12] Meryl D. Stoller and Rodney S. Ruoff, *Energy Environ. Sci.*, 2010, 3, 1294-1301.

[13] A. Burke, J. Power Souces 91, 37 (2000).

[14] Yanwu Zhu, Shanthi Murali, Meryl D. Stoller, K. J. Ganesh, Weiwei Cai, Paulo J. Ferreira, Adam Pirkle, Robert M. Wallace, Katie A. Cychosz, Matthias Thommes, Dong Su, Eric A. Stach, Rodney S. Ruoff, Science 332, 1537-1541 (2011).

[15] David Linden, Thomas B. Reddy (ed). *Handbook of Batteries*, 3rd edition, McGraw-Hill, New York, 2002 ISBN 0-07-135978-8

CHAPTER 8

Conclusions and Future Work

8.1 Conclusions

The goal of this study has been the development of new energy storage technology providing devices that are reliable, lightweight and energy dense, charge quickly, have long cycle life and calendar life. During this journey in search for the perfect supercapacitor, this research has explored a large number of alternative electrode materials and fabrication techniques to improve the performance of the current supercapacitors and to meet the higher requirements of future systems.

From a materials perspective, graphene has been considered to be the ideal material for supercapacitor electrodes due to its extremely high surface area, high electrical conductivity, and mechanical strength (1,2). Conventional approaches to making graphene electrodes start with a particles and use roll-coating, screen printing, or ink-jet printing. Unfortunately, these wet coating processes tend to produce graphene in agglomerates that provide little performance advantage over traditional particulate-activated carbon electrodes (3). To solve this problem, we demonstrated thin and highly flexible graphene supercapacitors by converting graphite oxide film to graphene using a near infrared laser inside a consumer grade LightScribe DVD burner. This technique produces a three-dimensional network of interconnected graphene sheets with extremely high surface area (1520 m^2/g) and electrical conductivity (1780 S/cm) without the need for binders or conductive additives. These electrodes demonstrate supercapacitors with

ultrahigh power density while providing high energy density approaching those of thin film batteries. These graphene supercapacitors are safe, flexible and can be produced on a large scale and at low cost.

One of the main advantages of the laser scribing process is the ability to do patterning at precise locations. This offers the flexibility to design graphene supercapacitors in various designs and architectures. This is especially important considering that the continuous miniaturization of portable electronics poses more challenges for the development of microscale energy storage. Conventional methods for the fabrication of micro-supercapacitors involve labor-intensive lithographic techniques that have proven difficult to produce cost-effective micro-devices, thus limiting their commercial application. Instead, we used LightScribe lithography to produce graphene micro-supercapacitors over large areas at a fraction of the cost of traditional devices. For example, more than 100 micro-supercapacitors can be produced on a single disc in 30 min or less. The devices are built on flexible substrates for flexible electronics and on-chip uses that can be integrated with MEMS or CMOS in a single chip. Mminiaturization of the electrodes to the microscale results in enhanced charge-storage capacity and rate capability, an important finding of this study.

In another approach in this dissertation, the LSG network with its high electrical conductivity and porous structure is shown to be an excellent scaffold for nanostructured pseudo-capacitive materials such as MnO_2. The unique structure of these hybrid electrodes allow efficient use of the pseudo-capacitive properties of MnO_2, while providing facilitated transport of both electrolyte ions and electrons, thus solving the fundamental problems that have limited the realization of the full capacity of MnO_2 electrodes. These hybrid electrodes achieve ultrahigh volumetric capacitance of over 300 F/cm^3 which is considerably higher than pure graphene and

is considered among the highest values achieved for hybrid electrodes. The specific capacitance of the constituent MnO_2 is 1029 F/g, which is close to the theoretical value of 1380 F/g. The energy density of the full device varies between 0.1-16.2 mWh/cm^3 depending on the configuration, which is superior to those of commercially available double layer capacitors, pseudo-capacitors and hybrid supercapacitors tested under the same conditions. Given the ease of fabrication of the electrodes and the abundance of MnO_2 which is widely used in traditional alkaline batteries, these graphene/MnO_2 hybrid electrodes are promising for various applications such as large scale energy storage.

While great efforts have been made for the fabrication of macro-scale hybrid supercapacitors, there are only a few studies on the design and integration of hybrid materials into micro-supercapacitors (4-5). This is likely due to complicated micro-fabrication techniques that are often involved in building 3D micro-electrodes with micro-meter separations (4). The current work presents a simple, yet versatile technique for the fabrication of a variety of hybrid micro-supercapacitors. By selecting the appropriate design parameters and combination of materials, it is possible to tune the properties of the micro-supercapacitor to target high power or high energy applications. This opens up new opportunities for micro-supercapacitors to be integrated into consumer electronics and miniaturized electronics.

Another type of supercapacitor with a high amount of pseudo-capacitance uses conducting polymers such as polyaniline. This work demonstrated a simple and scalable approach to fabricate interdigitated micro-supercapacitors via coating a polyaniline nanofiber film and subsequent laser patterning. The configuration of the device is based on polyaniline microelectrodes and welded polyaniline as a separator. This new design is an important finding of this work and represents an advance from current state-of-the-art micro-supercapacitors.

Furthermore, combining graphene with nanostructured polyaniline to produce hybrid micro-supercapacitors results in enhancement of the areal energy density and power density and cycling stability which has so far limited the commercial applications of polyaniline-based supercapacitors.

Considering the ease of fabrication, flexibility and scalability, the laser scribing technique could lead to the utilization of supercapacitors as energy storage devices in future portable electronic and micro-electronic devices. So turning the research results of this work to real products should be the next step. This requires a combination of efforts from researchers, industry and investors as described in Chapter 7 of this dissertation.

8.2 Future Work

Future research in graphene supercapacitors should focus on the development of cost-effective and environmentally benign methods for the production of high quality graphene at large scale. This requires a complete understanding of the chemistry and physics of graphene under different processing conditions (2). A number of critical issues, such as complete exfoliation of graphite, stabilization of single or few-layer graphene sheets in various solvents, and retaining the intrinsic properties of 2D graphene must be addressed before the chemical exfoliation method can be commercially used to mass produce graphene for a plethora of applications awaiting this promising material (2).

In an attempt to address some of these problems and to build on the current work, we are investigating alternative methods for producing high quality graphene that can be easily processed into supercapacitors on a large scale. We and others (6) originally found that the flash of a camera can spontaneously trigger the de-oxygenation of graphene oxide to graphene. This

process has similarities to the laser scribing in that it uses photo-thermal energy for the conversion of graphite oxide to graphene (7). High performance supercapacitor electrodes can be produced *in situ* by coating graphite oxide onto the required substrate and then flashing to produced graphene in less than a second as shown in Figure 8.1a. Supercapacitors built from these electrodes demonstrate high energy density and high power density.

Lithium ion batteries with high energy density and long cycle life are in demand to address the ever increasing energy storage needs for consumer electronics, electric drive vehicles and grid-scale stationary energy storage. Si is of great interest since it has 10 times higher specific capacity than traditional carbon anodes. However, Si suffers from poor cycling stability owing to large volume changes during charge and discharge which has been an impediments to realizing this technology (8-10). Much research has focused on solving this stability issue mostly through nanostructured material design. It has been shown that the uniform deposition of silicon on a graphene substrate improves tolerance to structural deformation and results in better cycling stability (11,12). Taking advantage of the three-dimensional network structure of LSG with its high surface area and facilitated ion and electron transport within this substrate, it is likely to produce graphene/Si Li-ion battery anodes with high energy and high power. Shown in Figure 8.1b is a silicon thin film grown on an LSG network. The energy-dispersive X-ray spectroscopic (EDL) elemental maps show the homogeneous deposition of Si on graphene.

In addition to the large scale applications, such as grid scale batteries, micro-scale batteries must also be developed to satisfy the rapid improvements occurring in microelectronics (13). The current technology uses flat, two-dimensional solid-state lithium-ion micro-batteries (14). To enhance the energy and power of these systems, new materials and battery architectures are highly researched nowadays (14). We are currently exploring a new design for a Li-ion

202

micro-battery based on an LSG network as the negative electrode and LSG/PANI as the positive electrode, Figure 8.1c. Unlike current methods which often involve complicated fabrication techniques, this process is straightforward as it combines LightScribe lithography with simple electrochemical deposition technique.

The high electrical conductivity and extremely high surface of LSG could impact other research areas such as catalysis and fuel cells. For example, metal nanoparticle-based catalysts are widely used in many important chemical processes and automobile industries (15,16). Since the catalytic activity of these metals is a function of the surface area, the incorporation of metal nanoparticles into anLSG network may provide a solution to high efficiency nanocatalysts. The LSG network was successfully functionalized with noble metals such as Pt, Au and Pd using a simple electro-deposition technique as shown in Figure 8.1d. It is possible to adjust the particle size, distribution and density of the nanoparticles by controlling the deposition time and applied current. This is likely to produce advanced electrodes with tunable properties for various catalytic applications.

The unique properties of graphene have resulted in new applications such as practical chemical sensors and biosensors (17-18). Surface area was found have a significant impact on the sensitivity of graphene-based sensors (18). As a continuation of the present study, we are investigating alternative methods for producing three-dimensional graphene electrodes that maintain the intrinsic properties of the individual sheets and provide high catalytic activity at the same time. By adjusting the pH, zeta potential and dynamic conditions of GO solution, it is possible to directly deposit a graphene hydrogel on virtually any conductive substrate and in one step, see Figure 8.1e. This form of graphene is capable of detecting up to three bio-compounds at the same time with high selectivity and sensitivity levels.
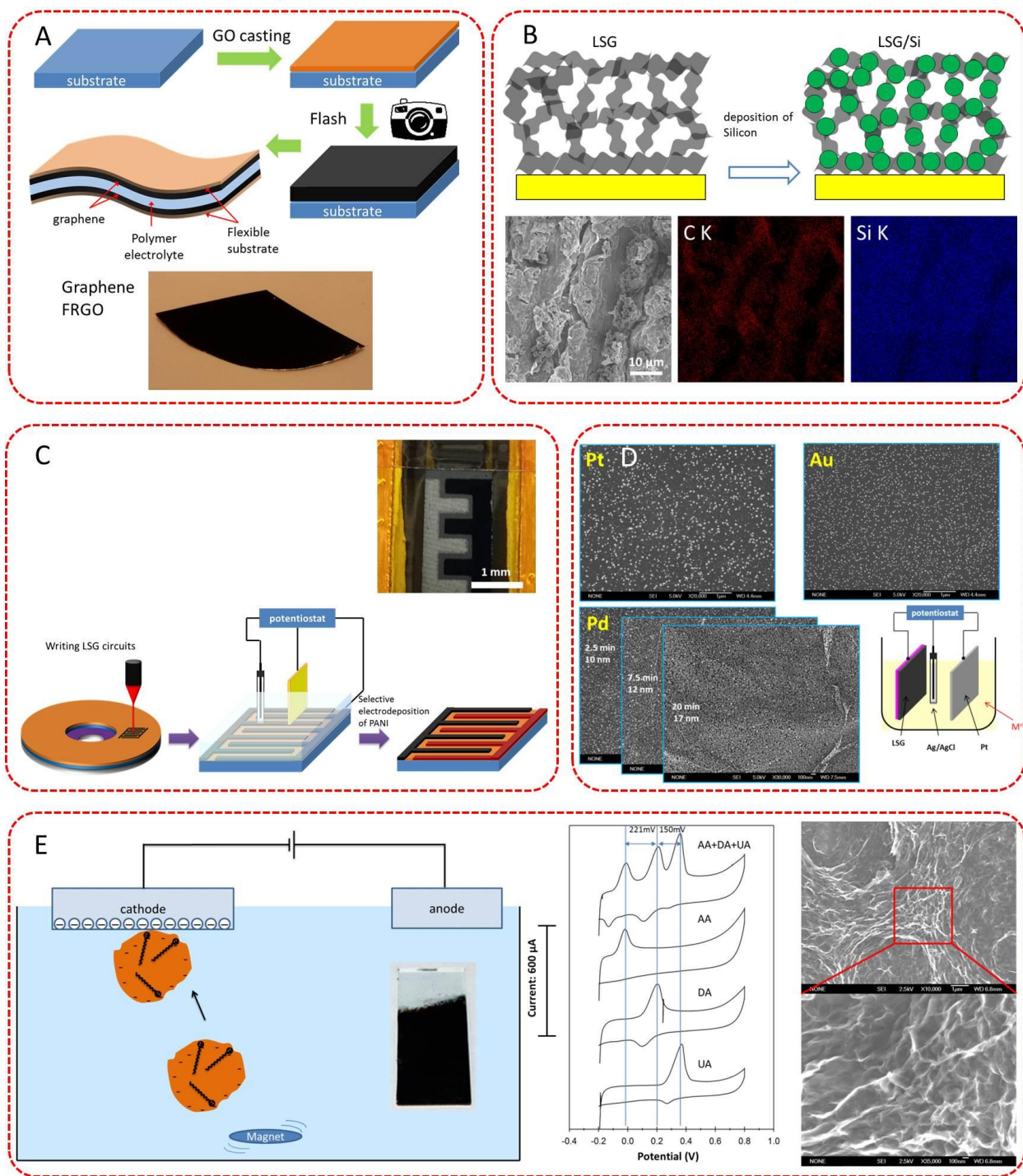
203

Figure 8.1: Other ongoing research projects on graphene based-electronics: (a) Making graphene supercapacitors in a flash; (b) Silicon anode for Li-ion batteries; (c) Li-ion micro-battery; (d) Graphene-metal nanocomposites for catalysis; (e) Graphene sensors.

8.3 Future of Graphene Supercapacitors

The number of diverse electronic device applications is driving the need for further improvements in energy storage. Government and industry funding is fueling this growth in recognition of the need for better ways to store energy. This is inspiring scientists from all over the world to search for new electrode materials, device architectures and new ways to assemble the materials into practical energy storage devices. This trend is unlikely to change any time soon. Future research in supercapacitors/batteries should address the following issues:

1. New Carbons: The viability of the current supercapacitor technology is demonstrated using symmetric carbon EDLCs with an ever-expanding range of applications. It is believed that future research areas in carbon materials are development of new carbon electrodes with higher specific surface area, higher electronic conductivity and rational pore distribution to optimize overall capacitance without compromising the rate of charge and discharge (19). Although various high surface area carbon materials are currently being researched, they suffer from low volumetric density and large pore volume meaning that a huge amount of electrolyte is needed to build the device which adds to the mass of the device without adding any capacitance (20). Accordingly, the energy density and power density of these systems struggle on the device level. Future research should focus on ways to produce high surface area carbons without compromising the volumetric density.

2. New Supercapacitor Designs: About 90% of the supercapacitors currently available (EDLCs) have the same basic structure as those carbon supercapacitors first commercialized by NEC 35 years ago. If we want the supercapacitor technology to move further a lot faster, new design concepts and device architectures should be developed.

3. Asymmetric Supercapacitors: It is likely that aqueous asymmetric supercapacitors will be the logical choice for large-scale energy storage because of higher energy and reduced costs compared to the current EDLCs. The progress of these hybrid supercapacitors depends on further understanding of the electrochemical reactions that support higher energy density and long term cycling stability (21). The development of new battery electrode materials with high charge storage capacity would boost the market opportunities of asymmetric supercapacitors. For example, the present asymmetric supercapacitors are composed of a carbon negative electrode and PbO_2 or NiOOH as the positive electrode and an aqueous electrolyte (22). While this configuration is functional, it suffers from poor cycling stability and the capacity is still far below what's theoretically possible. Here, the unique structure of LSG could allow efficient use of the pseudo-capacitive properties of PbO_2 or NiOOH. Moreover, the excellent mechanical properties of LSG could improve the cycling stability of these oxides by relieving any volume changes during charge and discharge and by providing electron "superhighways" for charge collection. Since $PbO_2 \parallel$ carbon and NiOOH $\parallel$ carbon asymmetric supercapacitor technology is already in production, a slight modification to the process that promises significant improvement could be industrially viable.

4. New Hybrid Electrode Materials: Most of the ongoing research on hybrid electrodes focus on the combination of carbons with transition metal oxides. Although transition metal oxides have high theoretical specific capacitance, their poor electronic and proton conductivity have been limiting the realization of high-performance hybrid supercapacitors. In recent years, transition metal nitrides appeared as an alternative because of their decent electronic conductivity (23). Furthermore, their low cost, high molar density, superior chemical resistance and good electrochemical stability are desirable in energy storage applications (23-24). Nanostructured

metal nitrides such as titanium nitride (TiN), vanadium nitride (VN), molybdenum nitride (MoN) are promising candidates (23-25). The combination of these nitrides with graphene may pave the way to the next generation of high-performance supercapacitors.

5. Textile-Based Supercapacitors for Wearable Electronics: Smart textiles, also known as electronic textiles or *e*-textiles, are fabrics that enable digital components and electronics to be embedded in them. Smart garments can be found commercially, but they typically require bulky battery packs or have to be plugged into the wall, so energy storage is the bottle-neck that prevents the widespread adoption of these smart garments (26,27). Researchers at Drexel University suggested smart garments outfitted with energy harvesters that captures energy from environmental sources such as sunlight or body movement and flexible supercapacitors to store the energy (26-28). If successful, these self-powered garments can work completely off the grid without the need for heavy battery packs. Here, LSG supercapacitors can be directly integrated onto smart garments by coating aqueous graphite oxide dispersion onto the appropriate textile structures that are widely used, then focusing a laser beam to convert graphite oxide to graphene. Unlike other methods which often use particulate activated carbon with poor mechanical properties, the LSG films are robust and can be bent or twisted without affecting their integrity.

6. Stretchable: The microelectronics industry has long relied on rigid and brittle silicon wafers. Research progress is moving forward to enable stretchable electronics which have the capacity to accommodate large levels of strain without significant degradation in their electronic performance (29). Stretchable electronics often make use of circuits built- or completely embedded-in stretchable substrates such as polydimethoxysiloxanes (PDMS) or polyurethanes. The widespread use of these electronics is still limited by energy storage units that should be capable of accommodating large strain while retaining their electrochemical performance.

Current research with stretchable supercapacitors often use buckled carbon nanotubes as the active electrode material (29-31). LSG can be a promising alternative with its excellent mechanical properties, high electronic conductivity and ease of fabrication. To demonstrate LSG stretchable supercapacitors, one needs to replace the polyethylene terephthalate substrate that was used to demonstrate the performance of LSG supercapacitors in this work with stretchable ones, such as PDMS. Also, combining carbon nanotubes with LSG might result in new composite electrodes with even better mechanical properties.

7. Transparency: Transparent electronics is growing so fast nowadays with applications ranging from liquid crystal displays, organic light emitting diodes, transistors, optical sensors, touch screens to solar cells. However, to realize fully transparent electronics, one may also consider making transparent energy storage units with appropriate capacity (32-35). Conventional supercapacitors consist of a current collector, electrode material, electrolyte, separator and packaging. Unfortunately, none of these components is transparent except for the electrolyte. Since these components are stacked together, all of them must be transparent in order to make the whole device transparent (32). This can be achieved via the development of new transparent materials with high charge storage capacity and electronic conductivity that would allow them to act as both active electrode material and current collector at the same time. One way to make these electrodes is by the deposition of transparent conducting metal oxides such as SnO_2 and In_2O_3 on single or few layer CVD graphene film supported on transparent PET plastic. Combining these new materials together with transparent gel electrolytes and plastic packaging could realize fully transparent supercapacitors that are also flexible.

8. Long Lifespan: One of the main advantages of the current carbon supercapacitors is a lifespan of up to a million cycles. This was made possible through synthetic strategies that

produce carbon materials with low impurities and oxygen content which was found to have a significant impact on the cycling stability. Nowadays, graphene electrodes are mainly produced from a graphite oxide precursor which contain high amounts of oxygen bonded to the edge and basal planes of graphene sheets. It is evident that new synthetic routes that enable effective de-oxygenation are highly demanding. On the other hand, hybrid electrodes that integrate graphene with pseudo-capacitive materials, such as conducting polymers and transition metal oxides and nitrides, show promise for high energy supercapacitors. Although poor cycling stability affects their chances for commericalizaiton. Future research efforts should focus on enhancing the interactions between graphene and the pseudo-capacitive material and understanding the underlying reaction mechanims of performance degradation upon cycling.

9. Low Self-Discharge: Significant progress has been made in the design of supercapacitors capable of delivering high energy and high power. Suprisingly, less attention has been paid to the well-known self-discharge problem (36). Understanding the mechanisms of self-discharge would enable us to better control or even prevent the self-discharge of supercapacitors, thus extending their life and practical applications.

10. Lithium-Ion Capacitors (LIC): LICs have garnered a lot of attention as they offer energy density of 15 Wh/kg which is more than twice the energy density of EDLCs. LICs consist of a lithium insertion battery-type negative electrode and an activated carbon positive electrode. Because of the slow diffusion of Li ions in the layered structure of the negative electrode, LICs deliver generally much lower power density (~1 kW/kg) than EDLCs. To solve this critical issue, future research should focus on producing negative electrodes with faster charge and discharge characteristics. An example of a fast negative electrode based on nanocrytalline $Li_4Ti_5O_{12}$ was developed recently by a Japanese group (38-39). An ultrafast negative electrode can be obtained

by loading nanocrystalline $Li_4Ti_5O_{12}$ onto the three-dimensional LSG network. By combining this negative electrode with an LSG positive electrode which offers 20 times more power than any form of activated carbon, this is likely to generate LICs with ultrahigh energy density and power density.

BIBLIOGRAPHY

[1] Yi Huang , Jiajie Liang , and Yongsheng Chen, *Small* 8,1805–1834 (2012).

[2] Li Li Zhang, Rui Zhou and X. S. Zhao, *J. Mater. Chem.*, 20, 5983–5992 (2010).

[3] John R. Miller, *Science* 335, 1312-1313 (2012).

[4] Caiwei Shen, Xiaohong Wang, Siwei Li, Jiangan Wang, Wenfeng Zhang, Feiyu Kang, *Journal of Power Sources* 234, 302-309 (2013).

[5] Wen-Wen Liu, Ya-Qiang Feng, Xing-Bin Yan, Jiang-Tao Chen, and Qun-Ji Xue, Adv. Funct. Mater. 2013, DOI: 10.1002/adfm.201203771.

[6] Scott Gilje, Sergey Dubin, Alireza Badakhshan, Jabari Farrar, Stephen. A. Danczyk, and Richard B. Kaner, *Adv. Mater.* 22, 419–423 (2010); Cote, L. J., Cruz-Silva, R. & Huang, J. J. Am. Chem. Soc. 131, 11027–11032 (2009).

[7] Veronica Strong, Sergey Dubin, Maher F. El-Kady, Andrew Lech, Yue Wang, Bruce H. Weiller, and Richard B. Kaner, ACS Nano 6, 1395-1403 (2012).

[8] Hui Wu, Yi Cui, *Nano Today* 7, 414-429 (2012).

[9] Robert A. Huggins & Yi Cui et al. Nature Nanotech 3, 31-35 (2008).

[10] Matthew T. McDowell , Seok Woo Lee , William D. Nix , and Yi Cui, Adv. Mater. **2013**, DOI: 10.1002/adma.201301795.

[11] Harold Kung et al. Adv. Energy Mater. 1, 1079-1084 (2011).

[12] Gleb Yushin et al., Adv. Energy Mater. 1, 495-498 (2011).

[13] M. Armand & J.-M. Tarascon. *Nature* 451, 652-657 (2008).

[14] Jos F. M. Oudenhoven , Loïc. Baggetto , and Peter H. L. Notten, *Adv. Energy Mater.* 1, 10–33 (2011).

[15] Sirilak Sattayasamitsathit *et al. J. Mater. Chem. A* , **1**, 1639-1645 (2013).

[16] Shuhui Sun *et al. Scientific Reports* 3:1775 (2013).

[17] (a) Fowler, J. D.; Allen, M. J.; Tung, V. C.; Yang, Y.; Kaner, R. B.; Weiller, B. H. ACS Nano 2009, 3, 301–306; (b) Xue, T.; Jiang, S.; Qu, Y.; Su, Q.; Cheng, R.; Dubin, S.; Chiu, C.-Y.; Kaner, R.; Huang, Y.; Duan, X. Angew. Chem., Int. Ed. 2012, 51, 3822–3825.

[18] Martin Pumera, Adriano Ambrosi, Alessandra Bonanni, Elaine Lay Khim Chng, Hwee Ling Poh, *Trends in Analytical Chemistry*, 29, 954-965 (2010).

[19] Guoping Wang, Lei Zhang and Jiujun Zhang, *Chem. Soc. Rev.,* 2012, **41**, 797–828

[20] Y. Gogotsi, P. Simon. *Science* 334, 917-918 (2011).

[21] Jeffrey W. Long, Daniel Bélanger, Thierry Brousse, Wataru Sugimoto, Megan B. Sassin, and Olivier Crosnier, MRS Bulletin 36, 513-522 (2011).

[22] A. Burke, Journal of Power Sources 91, 37–50 (2000).

[23] Shanmu Dong *et al. Energy Environ. Sci.*, 4, 3502–3508 (2011).

[24] Minghui Yang, Francis J. Disalvo, *Chem. Mater.* 24, 4406-4409 (2012).

[25] X. Lu et al. *Nano Letters* 13, 2628-2633 (2013).

[26] Kristy Jost, Carlos R. Perez, John K. McDonough, Volker Presser, Min Heon, Genevieve Dion and Yury Gogotsi, Energy Environ. Sci., 4, 5060–5067 (2011).

[27] Kristy Jost, Daniel Stenger, Carlos R. Perez, John K. McDonough, Keryn Lian, Yury Gogotsi and Genevieve Dion, Energy Environ. Sci., 6, 2698–2705 (2013).

[28] John R. Miller, *Science* 335, 1312-1313 (2012).

[29] Zhiqiang Niu, Haibo Dong, Bowen Zhu, Jinzhu Li, Huey Hoon Hng, Weiya Zhou, Xiaodong Chen , and Sishen Xie, *Adv. Mater.* 25, 1058–1064 (2013).

[30] Daeil Kim, Gunchul Shin, Yu Jin Kang, Woong Kim, and Jeong Sook Ha, *ACS Nano* (2013), DOI:10.1021/nn403068d.

[31] Cunjiang Yu, Charan Masarapu, Jiepeng Rong, Bingqing Wei, and Hanqing Jiang, *Adv. Mater.* 21, 4793–4797 (2009).

[32] Yuan Yang, Sangmoo Jeong, Liangbing Hu, Hui Wu, Seok Woo Lee, and Yi Cui, PNAS 108, 13013-13018 (2011).

[33] Po-Chiang Chen, Guozhen Shen, Saowalak Sukcharoenchoke, and Chongwu Zhou, Applied Physics Letters 94, 043113 (2009).

[34] Y. Gao, Y. S. Zhou, W. Xiong, L. J. Jiang, M. Mahjouri-samani, P. Thirugnanam, X. Huang, M. M. Wang, L. Jiang, and Y. F. Lu, APL Materials 1, 012101 (2013).

[35] Jung, H.Y., Karimi, M.B., Hahm, M.G., Ajayan, P.M. & Jung, Y.J. *Scientific Reports* 2, 773; DOI:10.1038/srep00773 (2012).

[36] Leif Nyholm, Gustav Nyström, Albert Mihranyan, and Maria Strømme, *Adv. Mater. 23*, 3751–3769 (2011).

[37] Borges, R.S. et al. *Scientific Reports* 3, 2572; DOI:10.1038/srep02572 (2013).

[38] Katsuhiko Naoi, Syuichi Ishimoto, Jun-ichi Miyamoto and Wako Naoi, Energy Environ. Sci., 5, 9363 (2012).

[39] K. Naoi, W Naoi, S. Aoyag, J.-I. Miyamoto, T. Kamino, Accounts of Chemical Research 46, 1075-1083 (2013).

Supercapacitor Calculations

A.1 Charge/Discharge Curves

Supercapacitors are often charged and discharged under constant current or galvanostatic conditions. A typical charge/discharge protocol for a supercapacitor is shown in Figure 1. The supercapacitor is charged at a constant current (i_{app}) until the voltage changes from the discharged state (E_1) to its maximum operating voltage (E_2). The current is then reversed to discharge the supercapacitor back to the discharged state (E_1). The typical charge/discharge (CC) profile of a symmetric carbon double-layer supercapacitor is shown on the right.
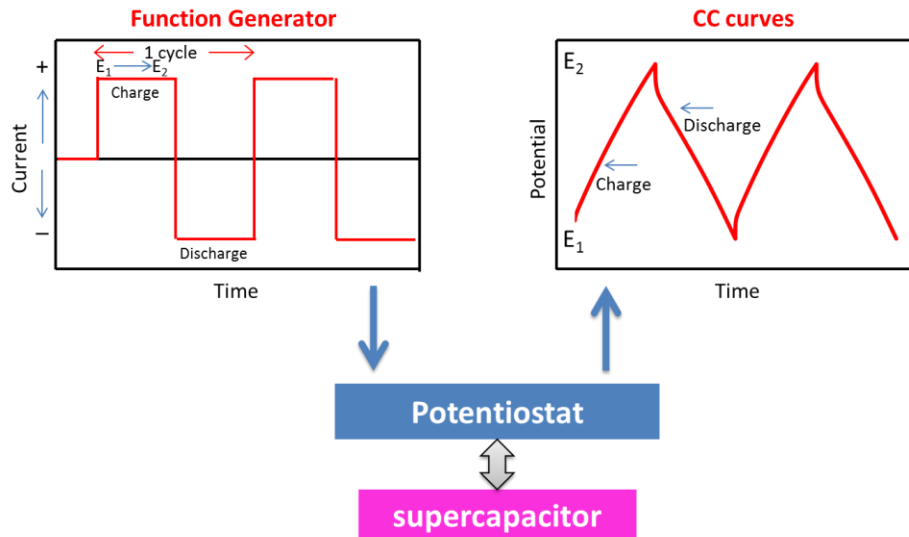

Figure 1: Galvanostatic charge/discharge protocol for supercapacitors.

The charge/discharge (CC) profile can be used to do all the performance analysis of the supercapacitor. Basically, the CC profile consists of two parts; capacitive and resistive as illustrated in Figure 2. The capacitive part represents the voltage change due to the change in

energy within the supercapacitor. The resistive part represents the voltage change due to the equivalent series resistance (ESR) of the supercapacitor (ref. 1).
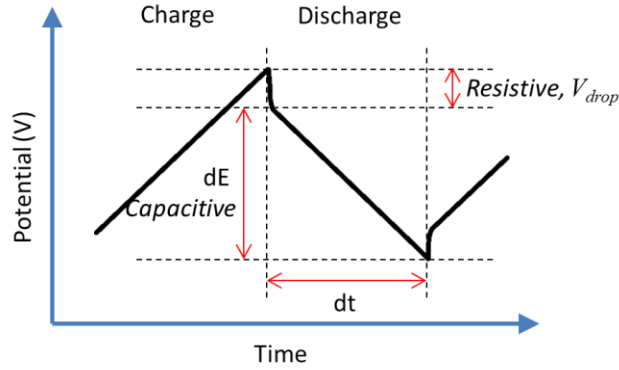

Figure 2: Constant current charge/discharge profile.

Where V_{drop}: the voltage drop due to ESR of the capacitor, $i_{app} = V_{drop} \times ESR$

dE: the voltage change during the discharge of the capacitor, in Volts

dt: discharge time, in seconds

Calculations

A.1.1 Capacitance of the device, $C_{device} = \dfrac{i_{app}}{-dE/dt}$;

Where i_{app} is the discharge current, and $-dE/dt$ is the slope of the discharge curve

A.1.2 Specific capacitance of the device, $C_{s(device)} = \dfrac{C_{device}}{M}$

Where M is the total mass of the active material on both electrodes

A.1.3 Specific capacitance per electrode, $C_{s(electrode)} = 4 \times C_{s(device)}$

A.1.4 Volumetric capacitance of the device, $C_{v(device)} = \dfrac{C_{device}}{V}$

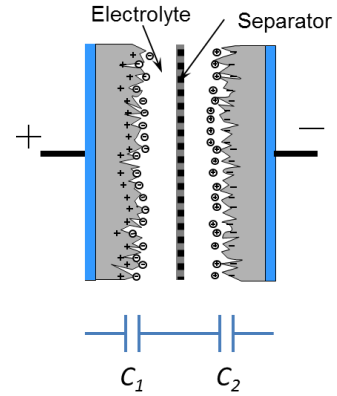Where V is the volume of the active material on both electrodes

A.1.5 Volumetric capacitance per electrode, $C_{v(electrode)} = 4 \times C_{v(device)}$

215

Note: Origin of factor 4 in equations 3 and 5:

$$C_{device} = \frac{C_1 \times C_2}{C_1 + C_2}$$

Since $C_1 = C_2$

$$C_{device} = \frac{C_1}{2}$$

$$C_{(electrode)} = 2 \times C_{(device)}$$

$$M_{(device)} = 2 \times m_{(electrode)}$$

$$C_{s(electrode)} = 4 \times C_{s(device)}$$

A.1.6 Energy Density & Specific Energy

$$Specific\ energy = \frac{1}{2} \times C_{s(device)} \times V^2 = \frac{1}{8} \times C_{s(electrode)} \times V^2$$

$$Energy\ density = \frac{1}{2} \times C_{v(device)} \times V^2 = \frac{1}{8} \times C_{v(electrode)} \times V^2$$

a. To get specific energy in *Wh/kg*

$$Specific\ energy = \frac{1}{2} \times C_{s(device)} \times V^2 = \frac{1}{2} \times \frac{F}{g} \times V^2$$

$$= \frac{1}{2} \times \frac{Coul}{g \times V} \times V^2$$

$$= \frac{1}{2} \times \frac{A.s}{g} \times V$$

$$= \frac{1}{2} \times \frac{W.s}{g} \times V = \frac{1}{2} \times W \times \frac{1000\ g}{1\ kg} \times \frac{1\ h}{3600\ s}$$

$$= \frac{1000}{2 \times 3600} C_{s(device)} \left(\frac{F}{g}\right) \times V^2\ (volt^2)$$

b. To get energy density in *Wh/l*

$$Energy\ density = \frac{1}{2} \times C_{v(device)} \times V^2 = \frac{1}{2} \times \frac{F}{cm^3} \times V^2$$

$$= \frac{1}{2} \times \frac{Coul}{V \times cm^3} \times V^2$$

$$= \frac{1}{2} \times \frac{A.s}{cm^3} \times V$$

$$= \frac{1}{2} \times \frac{W.s}{cm^3} \times V = \frac{1}{2} \times W \times \frac{1000\ cm^3}{1\ l} \times \frac{1h}{3600\ s}$$

$$= \frac{1000}{2 \times 3600} C_{v(device)} \left(\frac{F}{cm^3}\right) \times V^2\ (volt^2)$$

c. The energy density of micro-supercapacitors is often calculated in *Wh/cm³* or *mWh/cm³*.

For *Wh/cm³*

$$E = \frac{1}{2 \times 3600} C_{v(device)} \left(\frac{F}{cm^3}\right) \times V^2\ (volt^2)$$

For *mWh/cm³*

$$E = \frac{1000}{2 \times 3600} C_{v(device)} \left(\frac{F}{cm^3}\right) \times V^2\ (volt^2)$$

A.1.7 Power Density & Specific Power

a. Specific power: the power normalized to the mass of the device

$$Specific\ power = \frac{(\Delta E)^2}{4 \times ESR \times M}$$

$$ESR = \frac{V_{drop}}{2 \times i_{app}}$$

Where ΔE, V_{drop} have the same definition as in Figure 2; M is the total mass of the active material on both electrodes in grams; *ESR* is the equivalent series resistance of the supercapacitors in ohms; i_{app} is the discharge current in Amperes.

To get the specific power in *W/kg*

$$P = \frac{V^2}{4 \times \Omega \times g} = \frac{V^2}{4 \times \frac{V}{A} \times g} = \frac{A \times V}{4 \times g}$$

$$= \frac{W}{4 \times g} = \frac{W}{4 \times g} \times \frac{1000g}{1kg}$$

$$\therefore Specific\ power = \frac{1000 \times \Delta E^2(volt^2)}{4 \times ESR\ (ohm) \times M(g)}$$

b. Power density: the power normalized to the volume of the device

For traditional supercapacitors, the power density is calculated in *W/l*

$$Power\ density = \frac{1000 \times (\Delta E)^2(volt^2)}{4 \times ESR(ohm) \times V(cm^3)}$$

For micro-supercapacitors, the power density is calculated in *W/cm³*

$$Power\ density = \frac{(\Delta E)^2(volt^2)}{4 \times ESR(ohm) \times V(cm^3)}$$

Where ΔE and *ESR* have the same definition presented in the previous section, *V* is the volume of the active material on both electrodes.

A.2 Cyclic Voltammetry

Cyclic voltammetry (CV) is another widely used technique for testing the performance of supercapacitors. It consists of scanning linearly the potential of the supercapacitor between two potential limits (E_1 and E_2) using a triangular waveform as shown in Figure 3. During the potential scan, the potentiostat measures the current resulting from the applied potential (ref. 2). A typical CV profile of a symmetric carbon double layer supercapacitor is shown in Figure 3.
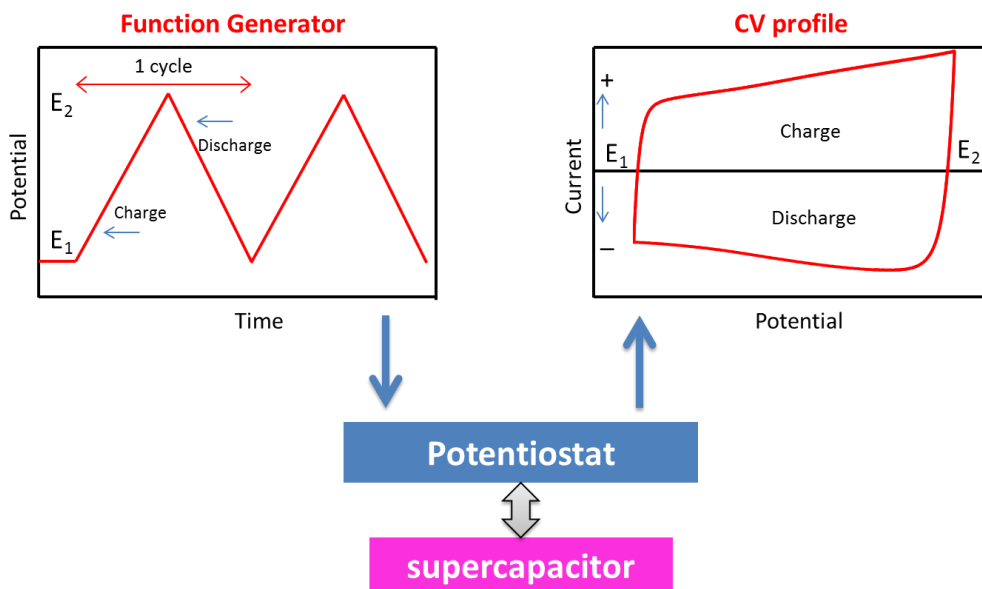

Figure 3: Cyclic voltammetry protocol for supercapacitors.

A.2.1 Capacitance of the device, F

$$C_{device} = \frac{\int_{v1}^{vn} i dV}{v \times \Delta E}$$

This integral can be made using Microsoft Excel as follows:

E (volt)	I (Amp)	dV	idV	$\int_{v1}^{vn} idV$	$v \times \Delta E$	C_{device}
V_1	I_1	$V_2 - V_1$	$I_1 \times dV_1$	=SUM($I_1 \times dV_1$: $I_n \times dV_n$)	v: scan rate, V/s	$= \dfrac{\int_{v1}^{vn} idV}{v \times \Delta E}$
V_2	I_2	$V_3 - V_2$	$I_2 \times dV_2$		ΔE: voltage window, V	
V_3	I_3	$V_4 - V_3$	$I_3 \times dV_3$			
...	...	...	...			
...	...	...	...			
V_n	I_n	$V_n - V_{n-1}$	$I_n \times dV_n$			

A.2.2—A.2.5 The specific capacitance and volumetric capacitance can be calculated in the same way as in Equations A.1.2 to A.1.5 in the charge/discharge curves.

A.2.6 Power Density & Specific Power

a. The power of the supercapacitor, W

$$power = \int_{V1}^{Vn} I \, dV$$

b. Power density, W/cm^3 or W/l

$$= \frac{power \, (W)}{V}$$

where V is the volume of the active material on both electrodes, in cm^3 or liter (l)

c. Specific power, in W/kg

$$= \frac{power \, (W)}{M}$$

where M is the mass of the active material on both electrodes, in kg

A.2.7 Energy Density & Specific Energy

$$Energy = power \times time$$

For cyclic voltammetry, the discharge time can be calculated from scan rate (*V/s*) and the voltage

window (*V*)

$$disc\square arge\ time = \frac{\Delta E\ (V)}{v\ \left(\frac{V}{s}\right)}; \ in\ seconds$$

$$= \frac{\Delta E\ (V)}{v\ \left(\frac{V}{s}\right)} \times \frac{1\ h}{3600\ s}; \ in\ hours$$

$$\therefore Energy = \frac{\Delta E}{v \times 3600} \times \int_{V1}^{Vn} I \times V\ dV\ ; \ in\ Wh$$

b. Energy density, *Wh/l or Wh/cm^3*

$$= \frac{Energy\ (Wh)}{V}$$

c. Specific energy, *Wh/kg*

$$= \frac{Energy\ (Wh)}{M}$$

Where *V* and *M* have the same definition as in Equations B.6

A.3. **General Comments** on charge/discharge curves and cyclic voltammetry: All the previous calculations were made based on the mass/volume of the active materials only. For more accurate calculations one should account for the other components of the device as well: current collector, active materials, separator, electrolyte and packaging. The capacitance calculated using this method is called stack capacitance (C_{stack}) or capacitance of the packaged device. The cross-sectional view of a packaged supercapacitor is shown in Figure 4.
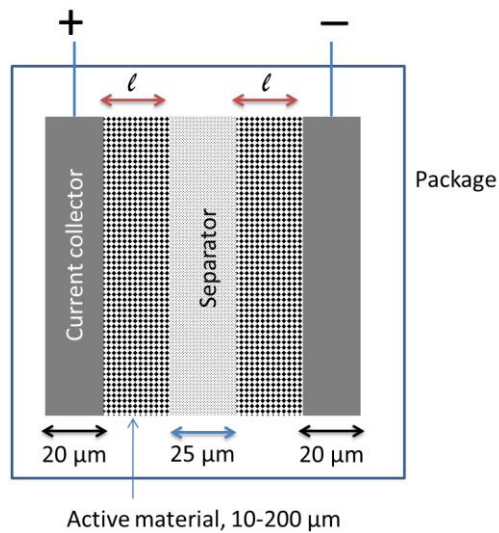

Figure 4: Schematic diagram showing the components of a supercapacitor, the cross-sectional thicknesses of the different components typical of commercial supercapacitors are also shown.

A.4. The capacitance of a supercapacitor depends on how fast the supercapacitor is operated; i.e. it is a function of the charge/discharge rate. The charge/discharge rate can be adjusted by controlling by the current density in CC curves and scan rate in CV profiles. Hence, the capacitance is often presented as shown in Figure 5.
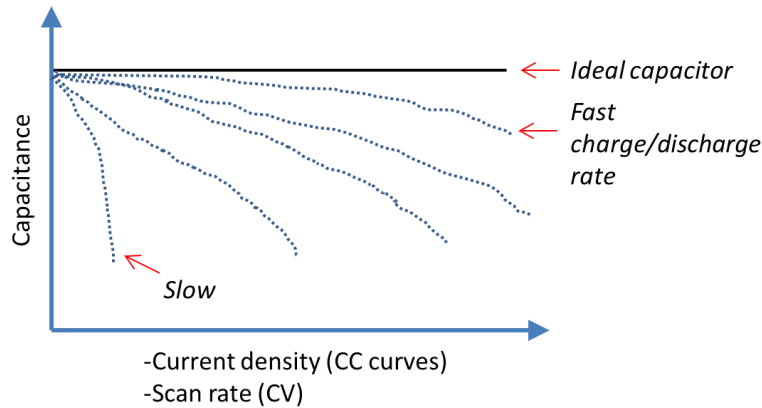

Figure 5: evolution of the capacitance of a supercapacitor as a function of the charge/discharge rate.

Some notes on Figure 5,

1. *Capacitance: it can be C_{device}, $C_{s(device)}$, $C_{s(electrode)}$, $C_{V(device)}$, $C_{V(electrode)}$ or the areal capacitance of the device ($C_{A(device)}$) which is defined as*

$$C_{A(device)} = \frac{C_{device}}{footprint\ area\ of\ the\ device, cm^2}$$

2. Current density $= \dfrac{applied\ current}{mass, volume, area\ (of\ of\ the\ electrode\ or\ device)}$, A/g, A/cm^3, or mA/cm^2

3. Scan rate is the slope of the triangular wave function used to acquire the CV profile, *V/s*.

4. Since capacitance is a function of charge/discharge rate, the specific capacitance of a new material is typically reported at a current density of 1 A/g.

A.5. Ragone Plot

The energy density and power density of supercapacitors are often presented in a Ragone plot, an example is shown in Figure 6.
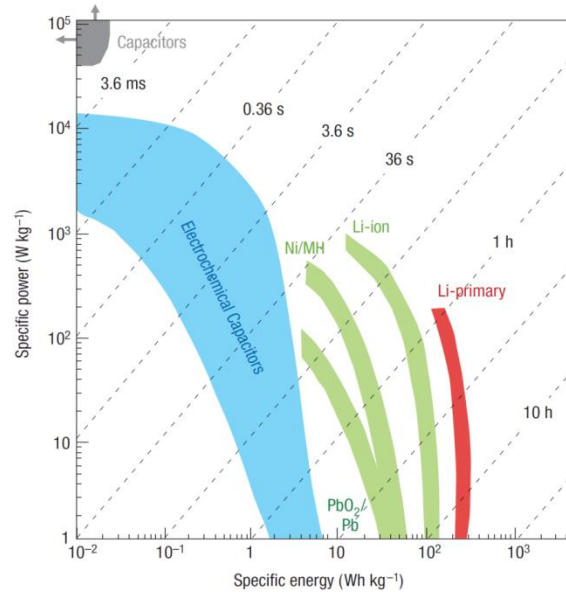

Figure 6: A Ragone plot showing the specific energy and specific power for various electrical energy storage devices, adapted from ref. 3.

In this plot, the times shown are the time constants of the devices, obtained by dividing the energy density by the power (ref. 3). Note that the values presented in Figure 6 are for the packaged devices. To compare a new supercapacitor/battery technology on this plot, the calculation should be made for the whole package and not just the active materials as described in Section A.3.

An alternative method for calculating the energy and power from CC curves and from CV:

1. Calculate the capacitance of the cell as shown previously

2. Calculate the energy using the formula $E = \frac{1}{2} CV^2$

3. Calculate the power, $P = E/t$

A.6. Additional Calculations

1. The capacity of conventional batteries is presented in (Ah rating); how is this related to supercapacitors?

    a. Calculate the energy of the supercapacitor in Wh

    b. Divide by the voltage window of the device

$$\frac{W.h}{V} = A.h$$

2. Depending on the size of the device, a supercapacitor can provide currents from milliamps for a few minutes to several amps current for much shorter periods. The time (t) a supercapacitor can deliver a constant current (I) can be calculated as (ref. 4):

$$t = \frac{C \times (V_{max} - V_{min})}{I}$$

3. The cycle life: The industry definition of the cycle life or the lifespan of a supercapacitor is the time duration from the first use of the device in the application until it reaches one of the following criteria: (a) A reduction in the capacitance of 20%, (b) an increase in the ESR of 100% (ref. 5).

4. Coulombic efficiency: measures the efficiency of the storage device and is calculated using the following formula:

$$\eta = \frac{\Delta Q_d}{\Delta Q_c} \times 100$$

where ΔQ_c and ΔQ_d are the amount of charge involved in the charging and discharging, respectively. This formula can be simplified for the CC curves to be

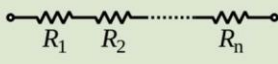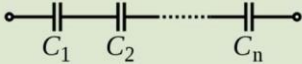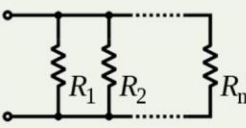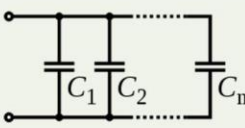$$\eta = \frac{\Delta t_d}{\Delta t_c} \times 100$$

where *Δtc* and *Δtd* are charging and discharging times, respectively.

Unlike batteries that typically have higher losses during charge than during discharge, supercapacitors can be totally charged and discharged very quickly with high efficiency of up to 99% (refs. 6,7).

5. Leakage current and self-discharge: see Chapter 4 and reference 4.

6. Tandem Supercapacitors: Portable equipment often requires cells packaged either in series, in parallel, or in combinations of the two in order to meet energy and power requirements. For example, laptop batteries commonly have four 3.6 V lithium ion cells connected in series to achieve a voltage of 14.4 V, and two in parallel to increase the capacity from 2400 mAh to 4800 mAh. Another application for a series circuit in consumer electronics is the 9 volt block battery which is internally built from six 1.5 V batteries. The following table summarizes the calculation of the capacitance and ESR of the stack in both series and parallel combinations.

	Resistors	Capacitors
Series	$$R_{total} = R_1 + R_2 + \cdots + R_n$$	$$\frac{1}{C_{total}} = \frac{1}{C_1} + \frac{1}{C_2} + \cdots + \frac{1}{C_n}$$
Parallel	$$\frac{1}{R_{total}} = \frac{1}{R_1} + \frac{1}{R_2} + \cdots + \frac{1}{R_n}$$	$$C_{total} = C_1 + C_2 + \cdots + C_n.$$

BIBLIOGRAPHY

[1] Maxwell Ultracapacitor, Boostcap, cell sizing,

http://www.maxwell.com/products/ultracapacitors/docs/10073627.3_how_to_determine_the_app ropriate_size.pdf

[2] Joseph Wang, Analytical Electrochemistry, 2nd edition, Wiley-VCH, USA, 2000.

[3] Patrice Simon, Yury Gogotsi. *Nature Materials* 7, 845-854 (2008)

[4] Maxwell Technologies' Test Procedures for Capacitance, ESR, Leakage Current and Self-Discharge Characterizations of Ultracapacitors**.**

http://www.maxwell.com/products/ultracapacitors/docs/applicationnote_maxwelltestprocedures. pdf

[5] Maxwell Technologies BOOSTCAP Energy Storage Modules Life Duration Estimation

http://www.maxwell.com/products/ultracapacitors/docs/applicationnote1012839_1.pdf

[6] John R. Miller, *Science* 335, 1312-1313 (2012).

[7] S.Mallika, Dr. R.Saravana Kumar, International Journal of Engineering and Technology 3, 37-43 (2011).